Available online at www.sciencedirect.com

ScienceDirect

Nuclear Physics B 914 (2017) 461–552

NUCLEAR PHYSICS B

www.elsevier.com/locate/nuclphysb

One-electron singular spectral features of the 1D Hubbard model at finite magnetic field

J.M.P. Carmelo [a,b,c,d,*], T. Čadež [c,b]

[a] *Department of Physics, University of Minho, Campus Gualtar, P-4710-057 Braga, Portugal*
[b] *Center of Physics of University of Minho and University of Porto, P-4169-007 Oporto, Portugal*
[c] *Beijing Computational Science Research Center, Beijing 100193, China*
[d] *University of Gothenburg, Department of Physics, SE-41296 Gothenburg, Sweden*

Received 25 May 2016; received in revised form 28 September 2016; accepted 12 November 2016

Available online 18 November 2016

Editor: Hubert Saleur

Abstract

The momentum, electronic density, spin density, and interaction dependences of the exponents that control the (k,ω)-plane singular features of the $\sigma =\uparrow,\downarrow$ one-electron spectral functions of the 1D Hubbard model at finite magnetic field are studied. The usual half-filling concepts of one-electron lower Hubbard band and upper Hubbard band are defined in terms of the rotated electrons associated with the model Bethe-ansatz solution for all electronic density and spin density values and the whole finite repulsion range. Such rotated electrons are the link of the non-perturbative relation between the electrons and the pseudofermions. Our results further clarify the microscopic processes through which the pseudofermion dynamical theory accounts for the one-electron matrix elements between the ground state and excited energy eigenstates.

1. Introduction

The Hubbard model with nearest-neighbor hopping integral t and on-site repulsion U is possibly the most studied lattice system of correlated electrons. It was originally introduced as a toy model to study d-electrons in transition metals [1,2]. The Hubbard model on a one-dimensional

* Corresponding author.
E-mail addresses: carmelo@fisica.uminho.pt, carmelo@MIT.EDU (J.M.P. Carmelo).

http://dx.doi.org/10.1016/j.nuclphysb.2016.11.009

(1D) lattice is exactly solvable by the Bethe ansatz (BA). Such a solution was first achieved by the coordinate BA [3,4]. This has followed a similar solution for a related continuous model with repulsive δ-function interaction [5]. For the 1D Hubbard model, the BA solution is also reachable by the inverse-scattering method [6]. In the thermodynamic limit (TL) the imaginary part of its BA complex rapidities simplifies [7].

On the one hand, static properties such as the charge and spin stiffnesses of the 1D Hubbard model under periodic boundary conditions can be determined from the use of the response of the energy eigenvalues to an external flux piercing the ring [8,9]. On the other hand, one of the main challenges in the study of the 1D Hubbard model properties is the calculation of dynamical correlation functions. Its BA solution provides the exact spectrum of the energy eigenstates. However, it has been difficult to apply to the derivation of high-energy dynamical correlation functions. (In this paper we use the designation *high energy* for all energy scales larger than the model low-energy limit associated with the Tomonaga–Luttinger-liquid regime [10–18].) The high-energy dynamical correlation functions of both some integrable models with spectral gap [19–25] and spin lattice systems [26–31] can be studied by the form-factor approach. Form factors of the 1D Hubbard model $\sigma =\uparrow, \downarrow$ electron creation and annihilation operators involved in the spectral functions studied in this paper remains though an unsolved problem.

The low-energy behavior of the correlation functions of the 1D Hubbard model at finite magnetic field was addressed in Refs. [14–16,32]. In what high-energy behavior of dynamical correlation functions is concerned, the method used in Refs. [33,34] has been a breakthrough to address it for one-electron removal and addition spectral functions at zero magnetic field in the $u \rightarrow \infty$ limit. In that limit they have been derived over the whole (k, ω) plane. That method relies on the spinless-fermion phase shifts imposed by Heisenberg spins $1/2$. Such elementary objects naturally arise from the zero spin density and $u \rightarrow \infty$ electron wave-function factorization [35–38].

A related pseudofermion dynamical theory (PDT) was introduced in Refs. [39,40]. It relies on a representation of the model BA solution in terms of pseudofermions. Those are generated by a unitary transformation from corresponding pseudoparticles [41,42]. It is an extension of the $u \rightarrow \infty$ method of Refs. [33,34] to the whole $u \equiv U/4t > 0$ range of the 1D Hubbard model. A key property is that the pseudofermions are inherently constructed to their energy spectrum having no interaction terms. This allows the expression of the one-electron spectral functions in terms of convolutions of pseudofermion spectral functions. The price to pay for the lack of pseudofermion energy spectrum interaction terms is that creation or annihilation of pseudofermions under transitions to excited states imposes phase shifts to the remaining pseudofermions. Within the PDT such phase shifts fully control the one- and two-electron spectral-weight distributions over the (k, ω) plane. That approach has been the first breakthrough for the derivation of analytical expressions of the zero-magnetic-field 1D Hubbard model high-energy dynamical correlation functions for the whole finite $u > 0$ range. Recently a modified form of the PDT was used to study the high-energy spin dynamical correlation functions of the 1D Hubbard model electronic density $n_e = 1$ Mott–Hubbard insulator phase [42].

After the PDT of the 1D Hubbard model was introduced in Refs. [39,40], a set of novel methods have been developed to also tackle the high-energy physics of 1D correlated quantum problems, beyond the low-energy Tomonaga–Luttinger-liquid limit [43]. In the case of the 1D Hubbard model at zero magnetic field, such methods reach the same results as the PDT. For instance, the momentum, electronic density, and on-site repulsion $u = U/4t > 0$ dependence of the exponents that control the line shape of the one-electron spectral function of the model at zero magnetic field calculated in Refs. [44,45] in the framework of a mobile impurity model

using input from the BA solution is exactly the same as that obtained previously by the use of the PDT.

However, the applications to the study of the repulsive 1D Hubbard model one-electron spectral functions of both such methods [44,45], those of the PDT [46–49], and the time-dependent density-matrix renormalization group (tDMRG) method [50,51] have been limited to zero magnetic field. The tDMRG studies of Ref. [52] studied the one-electron spectral-weight distributions of the attractive 1D Hubbard model at finite magnetic field. Under the canonical transformation that maps that model into the repulsive 1D Hubbard model, the one-electron spectral-weight distributions plotted in Figs. 1 (c) and 2 of that reference correspond to electronic densities $n_e = 1$ and $n_e = 0.9$, respectively, and spin density $m = 1/2$. The results refer to a finite system with 40 electrons. While they provide some information on the one-electron spectral-weight distributions, it is not possible to extract from them the momentum dependence of the exponents that *in the TL* control the line shapes near the σ one-electron spectral functions singularities.

The main goal of this paper is to extend the PDT applications to the study of the σ one-electron spectral functions of the repulsive 1D Hubbard model at finite magnetic field h in the TL near their singularities. The corresponding line shapes are controlled by exponents whose momentum, on-site repulsion $u = U/4t$, electronic density n, and spin density m dependences we study for $u > 0$, $n \in [0, 1[$, and $m \in [0, n_e]$. In addition, the issue of how the σ one-electron creation and annihilation operators matrix elements between the ground state and excited energy eigenstates are accounted for by the PDT introduced in Refs. [39,40] is further clarified in this paper. Beyond the preliminary analysis of these references, the corresponding microscopic processes are shown to involve the rotated electrons as a needed link of the non-perturbative relation between the electrons and PDT pseudofermions.

Our studies refer to the TL of the Hubbard model under periodic boundary conditions on a 1D lattice with an even number $L \rightarrow \infty$ of sites and in a chemical potential μ and magnetic field h,

$$\begin{aligned}
\hat{H} &= \hat{H}_u + 2\mu\,\hat{S}^z_\eta + 2\mu_B h\,\hat{S}^z_s\,, \\
\hat{H}_u &= -t\sum_{\sigma=\uparrow,\downarrow}\sum_{j=1}^{L}\left(c^\dagger_{j,\sigma}\,c_{j+1,\sigma} + c^\dagger_{j+1,\sigma}\,c_{j,\sigma}\right) \\
&\quad + U\sum_{j=1}^{L}\left(c^\dagger_{j,\uparrow}\,c_{j,\sigma} - 1/2\right)\left(c^\dagger_{j,\downarrow}\,c_{j,\sigma} - 1/2\right), \\
\hat{S}^z_\eta &= -\frac{1}{2}(L - \hat{N})\,; \qquad \hat{S}^z_s = -\frac{1}{2}(\hat{N}_\uparrow - \hat{N}_\downarrow)\,. \qquad (1)
\end{aligned}$$

Here the first and second terms of $\hat{H}_u$ are the kinetic-energy operator and the electron on-site repulsion operator, respectively, the operator $c^\dagger_{j,\sigma}$ (and $c_{j,\sigma}$) creates (and annihilates) one spin-projection σ electron at lattice site $j = 1, ..., L$, and the electron number operators read $\hat{N} = \sum_{\sigma=\uparrow,\downarrow}\hat{N}_\sigma$ and $\hat{N}_\sigma = \sum_{j=1}^{L}\hat{n}_{j,\sigma} = \sum_{j=1}^{L}c^\dagger_{j,\sigma}\,c_{j,\sigma}$. Moreover, μ_B is the Bohr magneton and $\hat{S}^z_\eta$ and $\hat{S}^z_s$ are the diagonal generators of the Hamiltonian $\hat{H}_u$ global η-spin and spin $SU(2)$ symmetry algebras, respectively. We use in general units of lattice constant one, so that the number of lattice sites N_a equals the lattice length L. The model properties depend on the ratio U/t. In this paper the corresponding parameter $u = U/4t$ is often used.

The lowest weight states (LWSs) and highest weight states (HWSs) of the η-spin ($\alpha = \eta$) and spin ($\alpha = s$) $SU(2)$ symmetry algebras have numbers $S_\alpha = -S^z_\alpha$ and $S_\alpha = S^z_\alpha$, respectively.

Here S_η is the states η-spin, S_s their spin, and S^z_η and S^z_s are the corresponding projections, respectively. The latter are the eigenvalues of the spin operators given in Eq. (1).

Let $\{|l_{\rm r}, l_{\eta s}, u\rangle\}$ be the complete set of 4^L energy eigenstates of the Hamiltonian $\hat{H}$, Eq. (1), associated with the BA solution for $u > 0$. The LWSs of both $SU(2)$ symmetry algebras are here denoted by $|l_{\rm r}, l^0_{\eta s}, u\rangle$. The u-independent label $l_{\eta s}$ is a short notation for the set of quantum numbers,

$$l_{\eta s} = S_\eta, S_s, n_\eta, n_s\,; \qquad n_\alpha = S_\alpha + S^z_\alpha = 0, 1, ..., 2S_\alpha\,, \qquad \alpha = \eta, s\,. \tag{2}$$

Furthermore, the label $l_{\rm r}$ refers to the set of all remaining u-independent quantum numbers needed to uniquely specify an energy eigenstate $|l_{\rm r}, l_{\eta s}, u\rangle$. This refers to occupancy configurations of BA momentum quantum numbers $q_j = \frac{2\pi}{L} I^\beta_j$. Here I^β_j are successive integers, $I^\beta_j = 0, \pm 1, \pm 2, ...$, or half-odd integers, $I^\beta_j = \pm 1/2, \pm 3/2, \pm 5/2, ...$, according to well-defined boundary conditions. Their allowed occupancies are zero and one. The index β denotes several BA branches of quantum numbers defined below in Section 2.2.

We call a *Bethe state* an energy eigenstate that is a LWS of both $SU(2)$ symmetry algebras. For a Bethe state one then has that $n_\eta = n_s = 0$ in Eq. (2), so that $l^0_{\eta s}$ stands for $S_\eta, S_s, 0, 0$. The non-LWSs $|l_{\rm r}, l_{\eta s}, u\rangle$ can be generated from the corresponding Bethe states $|l_{\rm r}, l^0_{\eta s}, u\rangle$ as [53],

$$\begin{aligned}
&|l_{\rm r}, l_{\eta s}, u\rangle = \prod_{\alpha=\eta,s} \left(\frac{1}{\sqrt{\mathcal{C}_\alpha}} (\hat{S}^+_\alpha)^{n_\alpha} \right) |l_{\rm r}, l^0_{\eta s}, u\rangle\,; \\
&\mathcal{C}_\alpha = (n_\alpha!) \prod_{j=1}^{n_\alpha} (2S_\alpha + 1 - j)\,, \qquad n_\alpha = 1, ..., 2S_\alpha\,, \\
&\hat{S}^+_\eta = \sum_{j=1}^{L} (-1)^j\, c^\dagger_{j,\downarrow}\, c^\dagger_{j,\uparrow}\,; \qquad \hat{S}^+_s = \sum_{j=1}^{L} c^\dagger_{j,\downarrow}\, c_{j,\uparrow}\,.
\end{aligned} \tag{3}$$

Here $\mathcal{C}_\alpha$ where $\alpha = \eta, s$ are normalization constants. The model in its full Hilbert space can be described either directly within the BA solution [36,54] or by application onto the Bethe states of the η-spin and spin $SU(2)$ symmetry algebras off-diagonal generators, as given in Eq. (3).

Relying on the model symmetries, for simplicity and without loss in generality the studies of this paper refer to electronic densities and spin densities in the ranges $n_e \in [0, 1[$ and $m \in [0, n_e]$, respectively. For such electronic densities and spin densities, the model ground states are LWSs of both the η-spin and spin $SU(2)$ symmetry algebras. Hence we use the LWS formulation of 1D Hubbard model BA solution.

The PDT is used in this paper to clarify one of the unresolved questions concerning the physics of the 1D Hubbard model at finite magnetic field, Eq. (1): The dependence of the exponents that control the singularities at the σ one-electron spectral functions on the momentum, repulsive interaction $u = U/4t$, electron-density n_e, and spin-density m. We derive the (k, ω)-plane line shape near the singularities of the following σ one-electron spectral function $B_{\sigma,\gamma}(k, \omega)$ such that $\gamma = -1$ (and $\gamma = +1$) for one-electron removal (and addition),

$$\begin{aligned}
B_{\sigma,-1}(k, \omega) &= \sum_{\nu^-} |\langle \nu^-|\, c_{k,\sigma}\, |GS\rangle|^2\, \delta(\omega + (E^{N_\sigma - 1}_{\nu^-} - E^{N_\sigma}_{GS})) \qquad \omega \leq 0\,, \\
B_{\sigma,+1}(k, \omega) &= \sum_{\nu^+} |\langle \nu^+|\, c^\dagger_{k,\sigma}\, |GS\rangle|^2\, \delta(\omega - (E^{N_\sigma + 1}_{\nu^+} - E^{N_\sigma}_{GS})) \qquad \omega \geq 0\,.
\end{aligned} \tag{4}$$

Here $c_{k,\sigma}$ and $c^{\dagger}_{k,\sigma}$ are electron annihilation and creation operators, respectively, of momentum k. $|GS\rangle$ denotes the initial N_σ-electron ground state of energy $E^{N_\sigma}_{GS}$. The ν^- and ν^+ summations run over the $N_\sigma - 1$ and $N_\sigma + 1$-electron excited energy eigenstates, respectively, and $E^{N_\sigma-1}_{\nu^-}$ and $E^{N_\sigma+1}_{\nu^+}$ are the corresponding energies.

The remainder of the paper is organized as follows. In Section 2 the σ one-electron lower-Hubbard band (LHB) and upper-Hubbard band (UHB) are defined for $u > 0$ and all densities in terms of quantum numbers associated with the rotated-electron energy eigenstates occupancies. Moreover, the relation of the β pseudoparticle representation to such rotated electrons is an issue also addressed in that section. The electron–rotated-electron unitary operator is uniquely defined in terms of its matrix elements between all model 4^L energy and momentum eigenstates. The PDT suitable for the study of the σ one-electron spectral weights is the topic addressed in Section 3. This includes extracting further information beyond that provided in Refs. [39,40] on how the PDT accounts for the matrix elements of the electron operators between the ground state and the excited energy eigenstates. In Section 4 the (k,ω)-plane line shape near the singular spectral features of the σ one-electron spectral functions, Eq. (4), is studied. Finally, the concluding remarks are presented in Section 5.

The complexity of the problems studied in this paper requires that some general concepts and theoretical tools used in our analysis are suitably revisited within the specific context of the one-electron problem in a finite magnetic field. Concerning which results are new, the most important such results refer to the expressions of the one-electron spectral functions of the 1D Hubbard model at finite magnetic field near the corresponding (k,ω)-plane high-energy singular features derived in Section 4. The exact relation defined in Section 2 of the c pseudoparticles, rotated spins $1/2$, and rotated η-spins $1/2$ to the electrons is also new. (The composite sn pseudofermions and composite ηn pseudofermions internal degrees of freedom refer to $n = 1, ..., \infty$ neutral pairs of such rotated spins $1/2$ and rotated η-spins $1/2$, respectively.) That relation involves the extension of the unique definition of the electron–rotated-electron unitary operator given in Ref. [42] for a specific subspace of the Mott–Hubbard insulator phase to the model full Hilbert space. The PDT expressions of the leading-order operators that at finite magnetic field contribute to the one-electron spectral functions near high-energy singular features and the precise description of the corresponding microscopic processes reported in Section 3 are new as well. The same applies to the definition in Section 2 of lower- and upper-Hubbard bands for $u > 0$ and electronic densities away from half filling in terms of rotated-electron occupancies.

2. Lower- and upper-Hubbard bands and the pseudoparticle representation emerging from the rotated electrons associated with the BA solution

Important concepts for one-electron addition are those of a LHB and a UHB. Such bands are defined in Section 2.1 for the whole $u > 0$ range and all densities in terms of rotated-electron quantum numbers associated with the one-electron addition excited energy eigenstates. In Section 2.2 the corresponding electron–rotated-electron unitary transformation performed by the BA solution is uniquely defined. The separation of the rotated-electron occupancy configurations that generate the exact $u > 0$ energy eigenstates into occupancy configurations of three types of fractionalized particles is an issue also addressed in that section. The latter are the c pseudoparticles without internal degrees of freedom, the rotated spins $1/2$, and the rotated η-spins $1/2$. The electron–rotated-electron unitary operator definition allows the introduction and expression in Section 2.3 of operators for the c pseudoparticles, rotated spins $1/2$, and rotated η-spins $1/2$

in terms of the σ rotated-electron creation and annihilation operators. In Section 2.4 the pseudoparticle energy dispersions and other quantities that emerge from the pseudoparticle quantum liquid are introduced. Such quantities are needed for our study. They appear in the expressions of the $\sigma = \uparrow, \downarrow$ one-electron spectral functions, Eq. (4), near their (k, ω)-plane singular features derived in Section 4.

2.1. Definition of σ one-electron lower- and upper-Hubbard bands

The concept of σ one-electron UHB addition is well established at electronic density $n_e = 1$ for $u > 0$ [3,4,55]. Below we define the concepts of a LHB and a UHB for $n_e \neq 1$ and $u > 0$. At the $n_e = 1$ Mott–Hubbard insulator quantum phase there is only σ one-electron UHB addition. For $n_e \neq 1$ there is both σ one-electron LHB and UHB addition. The Hamiltonian $\hat{H}$, Eq. (1), quantum phases are associated with different ranges of electronic density n_e and spin density m and are marked by important energy scales. Those correspond to limiting values of the charge energy scale $2\mu = 2\mu(n_e)$ and magnetic energy scale $2\mu_B\, h = 2\mu_B\, h(m)$ involving the chemical potential μ and magnetic field h, respectively.

The energy scales $2\mu = 2\mu(n_e)$ and $2\mu_B\, h = 2\mu_B\, h(m)$ are odd functions of the hole concentration $(1 - n_e)$ and spin density m, respectively. They are defined below in Section 2.5 in terms of BA energy dispersions. We consider the ranges $n_e \in [0, 1[$ and $m \in [0, n_e]$ for which they are positive. The interval $n_e \in]0, 1[$ refers for $m < n_e$ to a metallic quantum phase. For it $2\mu = 2\mu(n_e)$ is a continuous function of n_e. It smoothly decreases from $2\mu = (U + 4t)$ for $n_e \to 0$ to $2\mu = 2\mu_u$ for $n_e \to 1$ where $2\mu_u < (U + 4t)$ is the Mott–Hubbard gap. At $n_e = 1$ the chemical potential varies in the range $\mu \in [-\mu_u, \mu_u]$. This is in spite of the electronic density remaining constant, which is a property of the corresponding $n_e = 1$ and $u > 0$ Mott–Hubbard insulator quantum phase. The $n_e = 1$ Mott–Hubbard gap $2\mu_u$ is the energy scale associated with the phase transition between the two above mentioned quantum phases. For $u > 0$ it remains finite for all spin densities, $m \in [0, 1[$.

For the metallic quantum phase corresponding to the spin density interval $m \in [0, n_e[$ for $n_e \in [0, 1[$ the magnetic energy scale $2\mu_B\, h$ is a continuous function of m. It smoothly increases from zero at $m = 0$ to $2\mu_B\, h_c$ for $m \to n_e$. Here h_c is the critical field for the fully polarized ferromagnetism quantum phase transition. Indeed, for $h > h_c$ there is no electron double occupancy, so that the on-site repulsive interaction term in the Hamiltonian, Eq. (1), has no effects and the system is driven into a non-interactive quantum phase. The magnetic energy scale $2\mu_B\, h_c$ associated with such a quantum phase transition is an even function of the hole concentration $(1 - n_e)$. Its analytical expression is given below in Section 2.5.

The definition of the σ one-electron LHB and UHB addition for the whole $u > 0$ range, electronic densities $n_e \in [0, 1]$, and spin densities $m \in [0, n_e]$ relies on the occupancy configurations of uniquely defined *rotated electrons*. This involves selecting out of the many choices of $u \to \infty$ degenerate 4^L energy eigenstates, those obtained from the $u > 0$ Bethe states and corresponding non-LWSs, Eq. (3), as $|l_r, l_{\eta s}, \infty\rangle = \lim_{u\to\infty} |l_r, l_{\eta s}, u\rangle$.

The wave function amplitudes of the $u \to \infty$ energy eigenstates $|l_r, l_{\eta s}, \infty\rangle$ is an interesting issue discussed below in Section 2.2. As further discussed in that section, an important property is that σ electron single occupancy, double occupancy, and unoccupancy are good quantum numbers for such $u \to \infty$ energy eigenstates. Hence the numbers of electron $\uparrow$ and $\downarrow$ singly occupied sites, doubly occupied sites, and unoccupied sites are eigenvalues of corresponding number operators. We call V *tower* the set of energy eigenstates $|l_r, l_{\eta s}, u\rangle$ with exactly the same u-independent quantum numbers l_r and $l_{\eta s}$ and different u values in the range $u > 0$. σ electron

single occupancy, electron double occupancy, and electron non-occupancy are not good quantum numbers for the finite-u energy eigenstates $|l_r, l_{\eta s}, u\rangle$ belonging to the same V tower. This means that for finite u the numbers of electron $\uparrow$ and $\downarrow$ singly occupied sites, doubly occupied sites, and unoccupied sites are u-dependent expectation values rather than integer eigenvalues. Consider, for instance, ground states with densities $n_e \in [0, 1]$ and $m \in [0, n_e]$. In the $u \rightarrow \infty$ limit they have zero electron double occupancy. Upon decreasing u, there emerges for such ground states belonging to the same V tower a finite electron double occupancy expectation value. For densities $n_e \in [0, 1]$ and $m = 0$ it reads $D_0 = L\,(n_e/2)^2\, f(n_e, u)$. Here $f(n_e, u)$ is a continuous function of n_e and u with limiting behaviors $\lim_{u\rightarrow 0} f(n_e, u) = 1$ and $f(n_e, u) = \frac{\ln 2}{u^2}\left(1 - \frac{\sin(2\pi n_e)}{2\pi n_e}\right)$ for $u \gg 1$, respectively [58].

For any $u > 0$ value the set of energy eigenstates $|l_r, l_{\eta s}, u\rangle$ that belong to the same V tower are generated by exactly the same occupancy configurations of the u-independent quantum numbers l_r and $l_{\eta s}$ given in Eq. (2) and below in Section 2.2, respectively. Hence the Hilbert space is the same for the whole $u > 0$ range. It follows that for any $u > 0$ there is a uniquely defined unitary operator $\hat{V} = \hat{V}(u)$ such that $|l_r, l_{\eta s}, u\rangle = \hat{V}^\dagger |l_r, l_{\eta s}, \infty\rangle$. This operator $\hat{V}$ is the σ electron–rotated-electron unitary operator such that,

$$\tilde{c}^\dagger_{j,\sigma} = \hat{V}^\dagger\, c^\dagger_{j,\sigma}\, \hat{V}\,; \qquad \tilde{c}_{j,\sigma} = \hat{V}^\dagger\, c_{j,\sigma}\, \hat{V}\,; \qquad \tilde{n}_{j,\sigma} = \tilde{c}^\dagger_{j,\sigma}\, \tilde{c}_{j,\sigma}\,,$$
$$j = 1, ..., L\,, \qquad \sigma = \uparrow, \downarrow\,, \tag{5}$$

are the operators that create and annihilate, respectively, the σ rotated electrons as defined here. Moreover, $|l_r, l_{\eta s}, \infty\rangle = \hat{G}^\dagger_{l_r, l_{\eta s}}\, |0\rangle$ where $|0\rangle$ is the electron and rotated-electron vacuum and $\hat{G}^\dagger_{l_r, l_{\eta s}}$ a uniquely defined operator. Hence $|l_r, l_{\eta s}, u\rangle = \tilde{G}^\dagger_{l_r, l_{\eta s}}\, |0\rangle$. The generator $\tilde{G}^\dagger_{l_r, l_{\eta s}} = \hat{V}^\dagger\, \hat{G}^\dagger_{l_r, l_{\eta s}}\, \hat{V}$ has the same expression in terms of the σ rotated-electron creation and annihilation operators as $\hat{G}^\dagger_{l_r, l_{\eta s}}$ in terms of σ electron creation and annihilation operators, respectively.

Further useful information on the emergence of the rotated electrons associated with the operators, Eq. (5), is provided below in Section 2.2. This includes the unique definition of the electron–rotated-electron unitary operator $\hat{V}$ for the whole $u > 0$ range. This is done in terms of its matrix elements between all 4^L energy and momentum eigenstates, Eq. (3). The properties of the rotated electrons are found in that section to result from those of the electrons in the $u \rightarrow \infty$ limit. An important example is that, as reported above, σ electron single occupancy, electron double occupancy, and electron unoccupancy are good quantum numbers for a $u \rightarrow \infty$ energy eigenstate $|l_r, l_{\eta s}, \infty\rangle$. This then implies that for all the finite-u energy eigenstates $|l_r, l_{\eta s}, u\rangle$ belonging to the same V tower σ rotated-electron single occupancy, rotated-electron double occupancy, and rotated-electron unoccupancy are also good quantum numbers for $u > 0$. This applies to *all* 4^L energy and momentum eigenstates provided that $u > 0$.

Ground states with densities $n_e \in [0, 1]$ and $m \in [0, n_e]$ have zero rotated-electron double occupancy for the whole $u > 0$ range. This is a direct consequence of ground states belonging to the same V towers having in $u \rightarrow \infty$ limit zero electron double occupancy. As confirmed in Section 2.2, the BA quantum numbers are directly related to the numbers of sites singly occupied, doubly occupied, and unoccupied by σ rotated electrons. The σ one-electron LHB addition spectral function $B^{\rm LHB}_{\sigma,+1}(k,\, \omega)$ and UHB addition spectral function $B^{\rm UHB}_{\sigma,+1}(k,\, \omega)$ are uniquely defined for $u > 0$ as follows,

$$B_{\sigma,+1}(k,\, \omega) = B^{\rm LHB}_{\sigma,+1}(k,\, \omega) + B^{\rm UHB}_{\sigma,+1}(k,\, \omega)\,,$$

$$B^{\rm LHB}_{\sigma,+1}(k,\,\omega) = \sum_{\nu_0^+} |\langle \nu_0^+ |\, c^\dagger_{k,\sigma}\,|\, GS\rangle|^2\, \delta(\omega - (E^{N_\sigma+1}_{\nu_0^+} - E^{N_\sigma}_{GS})) \qquad \omega \geq 0\,,$$

$$B^{\rm UHB}_{\sigma,+1}(k,\,\omega) = \sum_{\nu_D^+} |\langle \nu_D^+ |\, c^\dagger_{k,\sigma}\,|\, GS\rangle|^2\, \delta(\omega - (E^{N_\sigma+1}_{\nu_D^+} - E^{N_\sigma}_{GS})) \qquad \omega \geq 0\,. \tag{6}$$

Here the ν_0^+ and ν_D^+ summations run over the $N_\sigma + 1$-electron excited energy eigenstates with zero and $D > 0$, respectively, rotated-electron double occupancy and $E^{N_\sigma-1}_{\nu_0^+}$ and $E^{N_\sigma+1}_{\nu_D^+}$ are the corresponding energy eigenvalues.

The σ one-electron spectral functions obey the following sum rules,

$$\sum_k \int_{-\infty}^{\infty} d\omega\, B_{\sigma,-1}(k,\,\omega) = N_\sigma\,; \qquad \sum_k \int_{-\infty}^{\infty} d\omega\, B_{\sigma,+1}(k,\,\omega) = L - N_\sigma\,,$$

$$\sum_k \int_{-\infty}^{\infty} d\omega\, B^{\rm LHB}_{\sigma,+1}(k,\,\omega) = L - N\,; \qquad \sum_k \int_{-\infty}^{\infty} d\omega\, B^{\rm UHB}_{\sigma,+1}(k,\,\omega) = N - N_\sigma\,. \tag{7}$$

The first two sum rules are well known and exact for all u values. The $B^{\rm LHB}_{\sigma,+1}(k,\,\omega)$ and $B^{\rm UHB}_{\sigma,+1}(k,\,\omega)$ sum rules are found to be exact both in the $n_e \rightarrow 0$ and $n_e \rightarrow 1$ limits for $u > 0$. Both in the $u \ll 1$ and $u \gg 1$ limits they are exact as well for electronic densities $n_e \in [0,\,1[$ and spin densities $m \in [0, n_e]$. They are likely exact also for intermediate u values yet we could not prove it. If otherwise, they are a very good approximation. Fortunately, clarification of this issue is not needed for our studies. Indeed, it focuses on the line shapes in the vicinity of the singularities of the σ one-electron spectral functions. This does not include the detailed weight distribution over the whole $(k,\,\omega)$ plane. The line shape near the singularities is actually that observed in experiments on actual condensed matter systems and spin $1/2$ ultra-cold atom systems. The important point for the present study is rather the definition of σ one-electron LHB and UHB for $u > 0$, $n_e \in [0,\,1]$, and $m \in [0, n_e]$, Eq. (6), which follows from the corresponding unique definition of rotated electrons in Section 2.2 in terms of quantities of the exact BA solution.

The present definition for $u > 0$ and all densities of the concepts of a LHB and a UHB is directly associated with a global lattice $U(1)$ symmetry of the Hamiltonian $\hat{H}_u$, Eq. (1), beyond its well-known $SO(4) = [SU(2) \otimes SU(2)]/Z_2$ symmetry. The latter contains the η-spin and spin $SU(2)$ symmetries [59–61]. Such a global lattice $U(1)$ symmetry exists for the model on the 1D lattice and on any other bipartite lattice [62]. It is behind its global symmetry being actually larger than $SO(4)$ and given by $[SO(4) \otimes U(1)]/Z_2 = [SU(2) \otimes SU(2) \otimes U(1)]/Z_2^2$, which is equivalent to $SO(3) \otimes SO(3) \otimes U(1)$. (The factor $1/Z_2^2$ follows from the total number 4^L of independent representations of the group $[SU(2) \otimes SU(2) \otimes U(1)]/Z_2^2$ being four times smaller than the dimension 4^{L+1} of the group $SU(2) \otimes SU(2) \otimes U(1)$.)

That the Hamiltonian $\hat{H}_u$, Eq. (1), global symmetry is $[SO(4) \otimes U(1)]/Z_2$ has direct effects on the 4^L energy and momentum eigenstates of the Hamiltonian $\hat{H}$ in the presence of a chemical potential and magnetic field also given in Eq. (1). Indeed, these states refer to 4^L state representations of the group $[SO(4) \otimes U(1)]/Z_2$ in the model full Hilbert space. In the present 1D case, the occurrence of the global lattice $U(1)$ symmetry justifies, for instance, that the spin and charge monodromy matrices of the BA inverse-scattering method have different ABCD and ABCDF forms associated with the spin $SU(2)$ and charge $U(2) = SU(2) \otimes U(1)$ symmetries, respectively. (See the definition of such forms in Ref. [6].) Consistently, the latter

matrix is larger than the former and involves more fields [6]. If the model global symmetry was $SO(4) = [SU(2) \otimes SU(2)]/Z_2$, the charge and spin monodromy matrices would have the same traditional ABCD form, which is that of the spin-1/2 XXX Heisenberg chain [63].

What is the relation of the global lattice $U(1)$ symmetry beyond $SO(4)$ to the LHB and UHB as defined here for $u > 0$ and all densities results? The generator of such a symmetry is the operator that counts the number N_s^R of rotated-electron singly occupied sites. Alternatively, that generator may be chosen to be the operator that counts the number $N_\eta^R = L - N_s^R$ of rotated-electron unoccupied sites plus doubly occupied sites. The relation under consideration is that the UHB exactly originates from transitions to energy eigenstates with a finite number of (i) rotated-electron doubly occupied sites and (ii) rotated-electron unoccupied sites for the electronic density ranges (i) $n_e \in [0, 1]$ and (ii) $n_e \in [1, 2]$, respectively.

2.2. *Rotated-electron separation in terms of c pseudoparticles, rotated spins* 1/2*, and rotated* η*-spins* 1/2

The charge-only and spin-only fractionalized particles that emerge in 1D correlated electronic systems are usually identified with holons and spinons, respectively [64]. In 1D integrable correlated electronic models, such holons and spinons are associated with excited-state occupancies of specific quantum numbers of the exact solutions. The use of holon and spinon representations provides a suitable description of these models low-energy physics. Some of such quantum liquids exotic properties survive at higher energies. However, the exponents characterizing the dynamical correlation functions singularities are functions of the momentum. They differ significantly from the predictions of the linear Tomonaga–Luttinger liquid theory [39,43–45]. This applies to the 1D Hubbard model.

Furthermore, a careful analysis of the high-energy dynamical correlation functions reveals that their spectral weights are controlled by the scattering of both fractionalized particles without internal degrees of freedom and neutral composite objects. The constituents of the latter are spin-1/2 or η-spin 1/2 fractionalized particles. Both the fractionalized particles without internal degrees of freedom and the composite elementary objects refer to the pseudofermions of the PDT representation used in this paper to study the σ one-electron spectral functions, Eq. (4). Such pseudofermions are identical to the pseudoparticles of Ref. [41] except that their momentum values are slightly shifted by a well defined unitary transformation. The direct relation of the corresponding c pseudoparticles without internal degrees of freedom and spin-1/2 or η-spin 1/2 fractionalized particles within the neutral composite pseudoparticles to the rotated electrons whose operators are given in Eq. (5) encodes important physical information. Such a direct relation is actually the needed missing link of the corresponding non-perturbative relation between the electrons and PDT pseudofermions.

It is useful for the understanding of the physics behind such relations to revisit some interesting properties of the 1D Hubbard model in the $u \rightarrow \infty$ limit. As mentioned above, in that limit the number of sites singly occupied by electrons, which we denote by N_c, is a good quantum number. The following related numbers are thus also conserved: The number $M_{s,\pm 1/2}$ of sites singly occupied by electrons of spin projection $\pm 1/2$, the number $M_{\eta,+1/2}$ of sites unoccupied by electrons, and the number $M_{\eta,-1/2}$ of sites doubly occupied by electrons. These $u \rightarrow \infty$ electron conserved numbers are such that,

$$M_s = M_{s,+1/2} + M_{s,-1/2} = N_c \,,$$
$$M_\eta = M_{\eta,+1/2} + M_{\eta,-1/2} = L - N_c = N_c^h \,,$$

$$M_{s,+1/2} - M_{s,-1/2} = -2S^z_s = N_\uparrow - N_\downarrow \, ,$$
$$M_{\eta,+1/2} - M_{\eta,-1/2} = -2S^z_\eta = L - N \, . \quad (8)$$

In $u \to \infty$ limit the model wave function amplitudes provided in Eqs. (2.5)–(2.10) of Ref. [35] are found to be given by Eq. (2.23) of Ref. [36]. The latter are of the general form,

$$(-1)^Q \left[e^{i\pi M_{\eta,-1/2}} \, \psi_1(y^d_1, y^d_2, ..., y^d_{M_{\eta,-1/2}}) \right]$$
$$\times \left[\left(\sum_P (-1)^P \, e^{\left(i \sum_{j=1}^{N_c} k_{Pj} x^s_{Qj} \right)} \right) \psi_2(y^s_1, y^s_2, ..., y^s_{M_{s,-1/2}}) \right] . \quad (9)$$

Here $y^d_1, y^d_2, ..., y^d_{M_{\eta,-1/2}}$ are the spatial coordinates of the doubly occupied sites and $y^s_1, y^s_2, ..., y^s_{M_{s,-1/2}}$ those of the down-spin singly occupied sites. Moreover, Q stands for a permutation that arranges the spatial coordinates $x^s_1, x^s_2, ..., x^s_{N_c}$ of the singly occupied sites that multiply $k_{P1}, k_{P2}, ..., k_{PN_c}$, respectively, into non-decreasing order. There is an additional restriction in the case of two equal spatial coordinates. The Pauli exclusion principle implies that they refer to electrons with different spin projection. The restriction is that the spatial coordinate of the electron with down spin projection must come first in $x^s_1, x^s_2, ..., x^s_{N_c}$. The sum $\sum_P$ in Eq. (9) runs over all permutations of the $j = 1, ..., N_c$ BA real momentum rapidity numbers k_j [36].

Furthermore, the factor $\sum_P (-1)^P \, e^{\left(i \sum_{j=1}^{N_c} k_{Pj} x^s_{Qj} \right)}$ in that equation is a Slater determinant of $u \to \infty$ spinless fermions [34,37]. They live on a lattice similar to that of the model. They occupy the N_c sites of spatial coordinates $x^s_1, x^s_2, ..., x^s_{N_c}$. The remaining $L - N_c$ sites correspond to spinless fermion holes. The quantity $\psi_1(y^d_1, y^d_2, ..., y^d_{M_{\eta,-1/2}})$ is in Eq. (9) the wave function of a $u \to \infty$ η-spin 1/2 XXX Heisenberg chain. Within the $u \to \infty$ limit, the η-spin $SU(2)$ symmetry is associated with η-spins 1/2 of projection $+1/2$ and $-1/2$ that describe the η-spin degrees of freedom of the unoccupied and doubly occupied sites, respectively. The quantity $\psi_2(y^s_1, y^s_2, ..., y^s_{M_{s,-1/2}})$ in that equation is in turn the wave function of a $u \to \infty$ spin 1/2 XXX Heisenberg chain. The corresponding N_c spins 1/2 are those of the electrons that singly occupy sites. The charges of these electrons are carried by the N_c spinless fermions. We call these two XXX chains, Heisenberg chains 1 and 2, respectively.

On the one hand, the $M_\eta = L - N_c$ η-spins 1/2 of the $u \to \infty$ Heisenberg chain 1 only "see" the $L - N_c$ sites unoccupied and doubly occupied by electrons. Their spatial coordinates are those left over by the N_c spatial coordinates $x^s_1, x^s_2, ..., x^s_{N_c}$ of the electron singly occupied sites. On the other hand, the $M_s = N_c$ spins 1/2 of the $u \to \infty$ Heisenberg chain 2 only "see" the latter N_c sites. Hence for the $u \to \infty$ 1D Hubbard model in fixed-N_c subspaces one can define within the TL a squeezed η-spin effective lattice with $M_\eta = L - N_c$ sites for the η-spins 1/2 and a corresponding squeezed spin effective lattice with $M_s = N_c$ sites on which the singly-occupied sites spins 1/2 live. Such squeezed spaces are well known from studies of the 1D Hubbard model in that limit [33–38]. The order of the $M_s = N_c$ Heisenberg chain 2 spins 1/2 in the squeezed spin effective lattice is the same as their order in the model lattice [36]. The same applies to the order of the $M_\eta = L - N_c$ Heisenberg chain 1 η-spins 1/2 in the squeezed η-spin effective lattice.

The form of the wave function amplitude, Eq. (9), follows from in the $u \to \infty$ limit the degrees of freedom of each 1D Hubbard model lattice site occupancy separating into two degrees of freedom. On the one hand, those of the N_c singly occupied sites separate into lattice/charge degrees of freedom described by the N_c spinless fermions and spin degrees of freedom associated

with the $M_s = M_{s,+1/2} + M_{s,-1/2} = N_c$ spins 1/2 of the Heisenberg chain 2, respectively. On the other hand, the degrees of freedom of the remaining $L - N_c$ sites separate into lattice/charge degrees of freedom described by the $L - N_c$ spinless fermion holes and η-spin/charge degrees of freedom associated with the $M_\eta = M_{\eta,+1/2} + M_{\eta,-1/2} = L - N_c$ η-spins 1/2 of the Heisenberg chain 1, respectively.

The electron occupancy configurations that generate the exact energy eigenstates $|l_r, l_{\eta s}, \infty\rangle$ remain complex even in the corresponding $u \rightarrow \infty$ limit. It is easiest to express them in terms of spatial lattice occupancy configurations of the N_c spinless fermions, $M_\eta = L - N_c$ Heisenberg chain 1 η-spins 1/2, and $M_s = N_c$ Heisenberg chain 2 spins 1/2 that naturally emerge from the wave function amplitude, Eq. (9), degrees of freedom separation.

The spatial lattice occupancies of the N_c spinless fermions that generate the exact energy eigenstates $|l_r, l_{\eta s}, \infty\rangle$ can be expressed in terms of occupancy configurations of the BA momentum quantum numbers $q_j = \frac{2\pi}{L} I_j^c$ introduced below. Here I_j^c are successive integers $I_j^c = 0, \pm 1, \pm 2, ...$ or half-odd integers $I_j^c = \pm 1/2, \pm 3/2, \pm 5/2, ...$ according to well-defined boundary conditions. Similarly, the η-spins 1/2 ($\alpha = \eta$) and spins 1/2 ($\alpha = s$) spatial occupancies of their corresponding squeezed effective lattices, respectively, that generate such energy eigenstates can be expressed in terms of occupancy configurations of the BA momentum quantum numbers $q_j = \frac{2\pi}{L} I_j^{\alpha n}$ also considered below. Here $I_j^{\alpha n}$ are again successive integers $I_j^{\alpha n} = 0, \pm 1, \pm 2, ...$ or half-odd integers $I_j^{\alpha n} = \pm 1/2, \pm 3/2, \pm 5/2, ...$ according to well-defined boundary conditions. Furthermore, $n = 1, ..., \infty$ is the number of neutral η-spin 1/2 pairs ($\alpha = \eta$) and spin 1/2 pairs ($\alpha = s$) associated with the corresponding αn branches of BA quantum number configurations. Out of the $M_s = N_c$ spins 1/2, an even number $N_c - 2S_s$ of them are paired within such spin-singlet configurations. The remaining $2S_s$ spins 1/2 remain unpaired, contributing to the spin $SU(2)$ multiplet configurations. Similarly, out of the $M_\eta = L - N_c$ η-spins 1/2, an even number $L - N_c - 2S_\eta$ of them are paired within the above ηn branches η-spin-singlet configurations. The $2S_\eta$ η-spins 1/2 left over remain unpaired, contributing to the η-spin $SU(2)$ multiplet configurations. For a LWS, all $2S_s$ unpaired spins 1/2 have up spin projection and all $2S_\eta$ unpaired η-spins 1/2 have up η-spin projection, *i.e.* correspond to unoccupied sites.

An important BA solution property is that for the whole $u = U/4t > 0$ range the exact energy eigenstates $|l_r, l_{\eta s}, u\rangle$ remain being generated by occupancy configurations of *exactly* the same u-independent BA momentum quantum numbers $q_j = \frac{2\pi}{L} I_j^c$ and $q_j = \frac{2\pi}{L} I_j^{\alpha n}$ where $\alpha = \eta, s$ and $n = 1, ..., \infty$. Furthermore, also the spin and η-spin multiplet configurations are exactly the same for the whole $u = U/4t > 0$ interval. For finite U the relation of the occupancy configurations of BA momentum quantum numbers $q_j = \frac{2\pi}{L} I_j^c$ and $q_j = \frac{2\pi}{L} I_j^{\alpha n}$ to lattice occupancy configurations becomes though much more complex. This is because at finite U electron single occupancy and double occupancy are not good quantum numbers anymore. This is reflected in the much more involved form of the wave function amplitudes. Rather than the simpler form, Eq. (9), for general finite u values they are given by Eqs. (2.5)–(2.10) of Ref. [35].

Interestingly, though, there is a uniquely defined unitary transformation under which such $u > 0$ wave function amplitudes become of the simpler form, Eq. (9). That unitary transformation only changes the lattice electron occupancies that generate the exact energy eigenstates. It preserves their individual spins and charges. It actually maps the electrons and their operators into rotated electrons and their operators, as given in Eq. (5). The resulting rotated electrons have the same charge and spin as the corresponding electrons. For them single occupancy and double occupancy are good quantum numbers for the whole $u > 0$ range. As mentioned in Section 2.1, the importance of such rotated electrons is that they are the link between the electrons and the

pseudofermions of the PDT representation used in this paper to study the σ one-electron spectral functions, Eq. (4).

For the 1D Hubbard model there is an infinite number of transformations that generate rotated electrons from the electrons such that rotated-electron single occupancy is a good quantum number for $u > 0$ [62]. The pseudoparticle representation and corresponding pseudofermion representation refer though to the specific choice of rotated electrons under which the wave function amplitudes provided in Eqs. (2.5)–(2.10) of Ref. [35] become of the simpler form, Eq. (9). Those are thus generated from the electrons by a uniquely defined unitary transformation. Actually, the BA solution performs such a transformation. It is behind the exact energy eigenstates belonging to the same V tower being generated by *exactly the same* occupancy configurations of u-independent BA momentum quantum numbers for the whole $u = U/4t > 0$ range.

The electron–rotated-electron unitary operator $\hat{V}$ in Eq. (5) can be defined by its matrix elements between the model 4^L energy and momentum eigenstates $|l_{\rm r}, l_{\eta s}, u\rangle$. Fortunately, such matrix elements can be expressed in terms of the well known $u > 0$ BA wave function amplitudes of the Bethe states $|l_{\rm r}, l^0_{\eta s}, u\rangle$,

$$f_{l_{\rm r},l^0_{\eta s},u}(x_1\sigma_1, ..., x_{N^0}\sigma_{N^0}) = \langle x_1\sigma_1, ..., x_{N^0}\sigma_{N^0}|l_{\rm r}, l^0_{\eta s}, u\rangle\,. \tag{10}$$

Those are uniquely defined in Eqs. (2.5)–(2.10) of Ref. [35]. In them, $|x_1\sigma_1, ..., x_{N^0}\sigma_{N^0}\rangle$ denotes a local state in which the $N^0 = L - 2S_\eta$ electrons with spin projection $\sigma_1, ..., \sigma_{N^0}$ are located at sites of spatial coordinates $x_1, ..., x_{N^0}$, respectively. For a LWS their numbers are $N^0_\uparrow = L/2 - S_\eta + S_s$ and $N^0_\downarrow = L/2 - S_\eta - S_s$. Due to symmetry, the amplitudes of the non-LWSs $|l_{\rm r}, l_{\eta s}, u\rangle$ generated from each Bethe state as given in Eq. (3) differ from it by the trivial phase factor $(-1)^{n_\eta}$. Here $n_\eta = S_\eta + S^z_\eta$ is the non-LWS number given in Eq. (2).

The amplitudes $\langle n_\eta; n_s; x_1\sigma_1, ..., x_{N^0}\sigma_{N^0}|l_{\rm r}, l_{\eta s}, u\rangle$ of a non-LWS are given in terms of those of the corresponding Bethe state merely by $(-1)^{n_\eta}\langle x_1\sigma_1, ..., x_{N^0}\sigma_{N^0}|l_{\rm r}, l^0_{\eta s}, u\rangle$ and thus by $(-1)^{n_\eta} f_{l_{\rm r},l^0_{\eta s},u}(x_1\sigma_1, ..., x_{N^0}\sigma_{N^0})$. Here the local states $|x'_1\sigma_{1'}, ..., x'_{N^0+2n_\eta}\sigma_{(N^0+2n_\eta)'}\rangle$ in which the $N^0 + 2n_\eta$ electrons with spin projection $\sigma_{1'}, ..., \sigma_{(N^0+2n_\eta)'}$ are located at sites of spatial coordinates $x'_1, ..., x'_{N^0+2n_\eta}$ have been denoted by $|n_\eta; n_s; x_1\sigma_1, ..., x_{N^0}\sigma_{N^0}\rangle$. Except for the phase factor $(-1)^{n_\eta}$, this equality follows from the non-LWS amplitudes being insensitive to the n_η created electrons pairs and their spatial coordinates. These electrons pairs emerge as a result of the application onto the Bethe state of the η-spin off-diagonal generator $\hat{S}^+_\eta$ a number of times n_η, as given in Eq. (3). Moreover, such amplitudes are insensitive to the spatial coordinates of the n_s electrons whose spin has been flipped by the n_s spin off-diagonal generators $(\hat{S}^+_s)^{n_s}$, Eq. (3). Such insensitivities are behind denoting the local states $|x'_1\sigma_{1'}, ..., x'_{N^0+2n_\eta}\sigma_{(N^0+2n_\eta)'}\rangle$ by $|n_\eta; n_s; x_1\sigma_1, ..., x_{N^0}\sigma_{N^0}\rangle$. They also imply that, as for the Bethe states, for the set of any energy eigenstates corresponding to different finite u values and belonging to the same V tower the general amplitudes $f_{l_{\rm r},l_{\eta s},u}(x_1\sigma_1, ..., x_{N^0}\sigma_{N^0}) = \langle n_\eta; n_s; x_1\sigma_1, ..., x_{N^0}\sigma_{N^0}|l_{\rm r}, l_{\eta s}, u\rangle$ smoothly and continuously behave as a function of u.

One then straightforwardly finds that the electron–rotated-electron unitary operator $\hat{V}$ in Eq. (5) is uniquely defined by the set of the following matrix elements between the energy eigenstates,

$$\begin{aligned}\langle l_{\rm r}, l_{\eta s}, u|\hat{V}|l'_{\rm r}, l'_{\eta s}, u\rangle &= \langle l_{\rm r}, l_{\eta s}, u|l'_{\rm r}, l'_{\eta s}, \infty\rangle = \delta_{l_{\eta s},l'_{\eta s}}\,\langle l_{\rm r}, l_{\eta s}, u|l'_{\rm r}, l_{\eta s}, \infty\rangle \\ &= \delta_{l_{\eta s},l'_{\eta s}}\sum_{x=1}^{L}\cdots\sum_{x_{N^0}=1}^{L} f^*_{l_{\rm r},l^0_{\eta s},u}(x\sigma_1, ..., x_{N^0}\sigma_{N^0})\, f_{l'_{\rm r},l^0_{\eta s},\infty}(x\sigma_1, ..., x_{N^0}\sigma_{N^0})\,.\end{aligned} \tag{11}$$

To arrive to the last expression of $\langle l_{\rm r}, l_{\eta s}, u|\hat{V}|l'_{\rm r}, l'_{\eta s}, u\rangle$ given here, we accounted for the relations $\hat{V}^{\dagger}|l'_{\rm r}, l'_{\eta s}, \infty\rangle = |l'_{\rm r}, l'_{\eta s}, u\rangle$ and thus $\hat{V}|l'_{\rm r}, l'_{\eta s}, u\rangle = |l'_{\rm r}, l'_{\eta s}, \infty\rangle$. Moreover, we introduced in the resulting amplitude $\langle l_{\rm r}, l_{\eta s}, u|l'_{\rm r}, l'_{\eta s}, \infty\rangle$ a decomposition of unity in terms of the complete basis of local states $|n_{\eta}; n_s; x_1\sigma_1, ..., x_{N^0}\sigma_{N^0}\rangle$.

The quantity $\delta_{l,l'}$ in Eq. (11) is the usual Kronecker symbol such that $\delta_{l,l'} = 1$ for $l = l' = 0, 1, 2, ...$ and $\delta_{l,l'} = 0$ for $l \neq l'$. The factor $\delta_{l_{\eta s}, l'_{\eta s}}$ in that equation then implies that the phase factors $(-1)^{n_{\eta}}$ always occur in pairs. This gives rise to an overall phase factor $(-1)^{2n_{\eta}} = 1$. Moreover, $f_{l_{\rm r}, l^0_{\eta s}, u}(x_1\sigma_1, ..., x_{N^0}\sigma_{N^0})$ and $f_{l'_{\rm r}, l^0_{\eta s}, \infty}(x_1\sigma_1, ..., x_{N^0}\sigma_{N^0})$ are in Eq. (11) the amplitude, Eq. (10), for the finite u value under consideration and $u \rightarrow \infty$, respectively. They are defined by Eqs. (2.5)–(2.10) of Ref. [35] for $u > 0$ and Eq. (2.23) of Ref. [36] for $u \rightarrow \infty$, respectively. That the latter amplitude is that given in Eq. (9) and thus in Eq. (2.23) of Ref. [36] can be confirmed by expressing $\lim_{u\rightarrow\infty} f_{l'_{\rm r}, l^0_{\eta s}, u}(x_1\sigma_1, ..., x_{N^0}\sigma_{N^0})$, Eqs. (2.5)–(2.10) of Ref. [35], in terms of the $u \rightarrow \infty$ spatial coordinates $x^s_1, x^s_2, ..., x^s_{N_c}$ of the singly occupied sites, $y^s_1, y^s_2, ..., y^s_{M_{s,-1/2}}$ of the down-spin singly occupied sites, and $y^d_1, y^d_2, ..., y^d_{M_{\eta,-1/2}}$ of the doubly occupied sites.

The set of $4^L \times 4^L = 4^{2L}$ matrix elements of form, Eq. (11), are between all 4^L energy and momentum eigenstates that span the model full Hilbert space. This is why they uniquely define the electron–rotated-electron unitary operator $\hat{V}$. That because of symmetries behind the factor $\delta_{l_{\eta s}, l'_{\eta s}}$ many of the matrix elements vanish simplifies the quantum problem under consideration. Specifically, the electron–rotated-electron unitary operator $\hat{V}$ commutes with the three generators of both the global η-spin and spin $SU(2)$ symmetry algebras and the charge density operator. This ensures that the σ rotated electrons have the same charge and spin $1/2$ as the σ electrons.

From analysis of the relation between (i) the BA quantum numbers and (ii) rotated-electron occupancy configurations, respectively, that generate the finite-u exact energy eigenstates $|l_{\rm r}, l_{\eta s}, u\rangle = \hat{V}^{\dagger}|l_{\rm r}, l_{\eta s}, \infty\rangle$ of any V tower one reaches important physical information. First, the σ rotated-electron spatial occupancy configurations that generate the finite-u energy eigenstates $|l_{\rm r}, l_{\eta s}, u\rangle = \hat{V}^{\dagger}|l_{\rm r}, l_{\eta s}, \infty\rangle$ of any V tower are exactly the same as the σ electron spatial occupancy configurations of the tower $u \rightarrow \infty$ energy eigenstate $|l_{\rm r}, l_{\eta s}, \infty\rangle$. Hence for $u > 0$ the number $N^R_{s,\pm 1/2}$ of spin-projection $\pm 1/2$ rotated-electron singly occupied sites, $N^R_{\eta,+1/2}$ of rotated-electron unoccupied sites, and $N^R_{\eta,-1/2}$ of rotated-electron doubly occupied sites are conserved. Such numbers obey the sum rules $N^R_{s,\pm 1/2} + N^R_{\eta,-1/2} = N_{\pm 1/2}$, $N^R_s + 2N^R_{\eta,-1/2} = N$, and $N^R_s + N^R_{\eta} = L$. The σ rotated-electron numbers values equal those of the σ electrons. Hence here $N_{\pm 1/2}$ denotes the number of electrons and rotated electrons of spin projection $\pm 1/2$. For finite u values the numbers $N^R_s = N^R_{s,+1/2} + N^R_{s,-1/2}$ of rotated-electron singly occupied sites and $N^R_{\eta} = N^R_{\eta,+1/2} + N^R_{\eta,-1/2}$ of rotated-electron doubly occupied plus unoccupied sites are only conserved for rotated electrons.

Second, for $u > 0$ a non-perturbative three degrees of freedom lattice–η-spin–spin separation occurs at all energy scales. Here the lattice–η-spin degrees of freedom separation may be considered as a separation of the charge degrees of freedom. At energy scales lower than $2|\mu|$, one has that $D = N^R_{\eta,-1/2} = 0$ (and $N^R_{\eta,+1/2} = 0$) for $n_e \in [0, 1[$ (and $n_e \in]1, 2]$). Therefore, the η-spin degrees of freedom are hidden. Hence the three degrees of freedom non-perturbative lattice–η-spin–spin separation is seen as the usual two degrees of freedom charge–spin separation. Within the former general separation the (i) lattice global $U(1)$ symmetry, (ii) η-spin global $SU(2)$ symmetry, and (iii) spin global $SU(2)$ symmetry state representations are in each fixed number N^R_s of rotated-electron singly occupied sites subspace generated by well-defined oc-

cupancy configurations: (i) Those of the $N_c = N_s^R$ *c pseudoparticles* without internal degrees of freedom and corresponding $N_c^h = N_\eta^R$ c pseudoparticle holes whose c effective lattice is identical to the original lattice and thus has $N_s^R + N_\eta^R = L$ sites; (ii) Configurations involving $M_{s,\pm 1/2} = N_{s,\pm 1/2}^R$ spin-1/2 fractionalized particles of spin projection $\pm 1/2$ that we call *rotated spins* 1/2; (iii) Those involving $M_{\eta,\pm 1/2} = N_{\eta,+1/2}^R$ η-spin-1/2 fractionalized particles of η-spin projection $\pm 1/2$ that we call *rotated η-spins* 1/2. ($+1/2$ and $-1/2$ η-spin projections refer to η-spin degrees of freedom of rotated-electron unoccupied and doubly occupied sites, respectively.)

Third, the properties of the rotated electrons stem for $u > 0$ from those of the electrons in the $u \to \infty$ limit. Hence their above numbers equal for $u > 0$ those of the $M_\eta = M_{\eta,+1/2} + M_{\eta,-1/2}$ $u \to \infty$ Heisenberg chain 1 η-spins 1/2, $M_s = M_{s,+1/2} + M_{s,-1/2}$ $u \to \infty$ Heisenberg chain 2 spins 1/2, and N_c $u \to \infty$ spinless fermions given in Eq. (8). As confirmed below in Section 2.3 in terms of operators, the N_c c pseudoparticles, $M_{\eta,\pm 1/2}$ rotated η-spins of η-spin projection $\pm 1/2$, and $M_{s,\pm 1/2}$ rotated spins of spin projection $\pm 1/2$ stem from rotated-electron occupancy configurations degrees of freedom separation. Hence their numbers are fully controlled by those of rotated electrons as follows,

$$
\begin{aligned}
&N_c = N_R^s\,; \qquad N_c^h = N_R^\eta\,; \qquad N_c + N_c^h = N_R^s + N_R^\eta = L\,, \\
&M_{\alpha,\pm 1/2} = N_{R,\pm 1/2}^\alpha\,; \qquad M_\alpha = M_{\alpha,+1/2} + M_{\alpha,-1/2} = N_R^\alpha\,, \qquad \alpha = \eta, s\,.
\end{aligned}
\tag{12}
$$

The following rotated-electron properties valid for $u > 0$ also stem from those in terms of electrons in the $u \to \infty$ limit. On the one hand, the degrees of freedom of each rotated-electron occupied site decouple into one c pseudoparticle without internal degrees of freedom that carries the rotated-electron charge and one rotated spin 1/2 that carries its spin. On the other hand, the degrees of freedom of each rotated-electron unoccupied and doubly occupied site decouple into one c pseudoparticle hole and one rotated η-spin 1/2 of projection $+1/2$ and $-1/2$, respectively. Hence the rotated-electron on-site separation refers to two degrees of freedom associated with the lattice global $U(1)$ symmetry and one of the two global $SU(2)$ symmetries, respectively. That the rotated-electron occupancy configurations give rise to the independent occupancy configurations of the c pseudoparticles, rotated spins 1/2, and rotated η-spins 1/2 is behind the exotic properties of the corresponding quantum liquid.

Fourth, from the further analysis of the relation between the BA quantum numbers and the three degrees of freedom separation of the rotated-electron occupancy configurations one finds that such quantum numbers are directly associated with the occupancy configurations of the three types of fractionalized particles that generate all 4^L energy eigenstates, Eq. (3). For the densities ranges $n_e \in [0, 1]$ and $m \in [0, n_e]$ one has that $N_{s,+1/2}^R \geq N_{s,-1/2}^R$ and $N_{\eta,+1/2}^R \geq N_{\eta,-1/2}^R$. For the corresponding exact Bethe states, there is a number $M_{s\,\mathrm{sp}} = N_{s,-1/2}^R$ of spin-singlet pairs ($\alpha = s$) and $M_{\eta\,\mathrm{sp}} = N_{\eta,-1/2}^R$ of η-spin-singlet pairs ($\alpha = \eta$). All $N_{s,-1/2}^R$ rotated spins of projection $-1/2$ are paired with an equal number of rotated spins of projection $+1/2$. Similarly, all $N_{\eta,-1/2}^R$ rotated η-spins of projection $-1/2$ are paired with an equal number of rotated η-spins of projection $+1/2$. Such $M_{\alpha\,\mathrm{sp}}$ spin-singlet ($\alpha = s$) and η-spin-singlet ($\alpha = \eta$) pairs are found to correspond to the internal structure of a set of composite αn pseudoparticles. Here $n = 1, ..., \infty$ gives the number of pairs that refer to such an internal structure. One denotes by $N_{\alpha n}$ the number of such αn pseudoparticles in each energy and momentum eigenstate. The sum rule $M_{\alpha\,\mathrm{sp}} = \sum_{n=1}^\infty n\, N_{\alpha n}$ is then obeyed.

The remaining $M^{un}_{\alpha} = N^{R}_{\alpha,+1/2} - N^{R}_{\alpha,-1/2} = 2S_{\alpha}$ unpaired rotated spins ($\alpha = s$) and rotated η-spins ($\alpha = \eta$) have for a Bethe state spin and η-spin projection $+1/2$. For general energy eigenstates, the multiplet configurations of these $2S_s$ unpaired rotated spins and $2S_\eta$ unpaired rotated η-spins generate the spin and η-spin, respectively, towers of non-LWSs. Specifically, the $2S_s$ unpaired rotated spins and $2S_\eta$ unpaired rotated η-spins of the Bethe states are flipped upon the application of the corresponding $SU(2)$ algebras off-diagonal generators, as given in Eq. (3). Application of such generators leaves the spin ($\alpha = s$) and η-spin ($\alpha = \eta$) singlet configurations of the $M_{\alpha\,\mathrm{sp}} = \sum_{n=1}^{\infty} n\, N_{\alpha n}$ pairs in αn pseudoparticles unchanged. Hence for general $u > 0$ energy eigenstates one finds that the number $M^{un}_{s,\pm 1/2}$ of unpaired rotated spins of projection $\pm 1/2$ and $M^{un}_{\eta,\pm 1/2}$ of unpaired rotated η-spins of projection $\pm 1/2$ are good quantum numbers. They read,

$$M^{un}_{\alpha,\pm 1/2} = (S_{\alpha} \mp S^{z}_{\alpha})\,; \qquad M^{un}_{\alpha} = M^{un}_{\alpha,-1/2} + M^{un}_{\alpha,+1/2} = 2S_{\alpha}\,, \qquad \alpha = \eta, s\,. \tag{13}$$

For the $\alpha = \eta, s$ LWSs one has that $M^{un}_{\alpha,+1/2} = M^{un}_{\alpha} = 2S_{\alpha}$ and $M^{un}_{\alpha,-1/2} = 0$ for both $\alpha = \eta, s$. The set of $M_{\eta\,\mathrm{sp}}$ η-spin-singlet pairs and $M_{s\,\mathrm{sp}}$ spin-singlet pairs of an energy eigenstate contains an equal number of rotated η-spins and rotated spins, respectively, of opposite projection. Hence the total numbers $M_{\eta,\pm 1/2}$ of rotated η-spins of projection $\pm 1/2$ and $M_{s,\pm 1/2}$ of rotated spins of projection $\pm 1/2$ are given by,

$$M_{\alpha,\pm 1/2} = M_{\alpha\,\mathrm{sp}} + M^{un}_{\alpha,\pm 1/2}\,, \qquad \alpha = \eta, s\,. \tag{14}$$

Moreover, by combining the above equations one finds that the set of numbers $\{N_{\alpha n}\}$ of composite αn pseudoparticles of any $u > 0$ energy eigenstate obey the following exact sum rules concerning the number of $M_{\alpha\,\mathrm{sp}}$ of spin ($\alpha = s$) and η-spin ($\alpha = \eta$) singlet pairs,

$$\begin{aligned} M_{\alpha\,\mathrm{sp}} &= \sum_{n=1}^{\infty} n\, N_{\alpha n} = \frac{1}{2}(L_{\alpha} - 2S_{\alpha})\,, \qquad \alpha = s, \eta\,, \\ M^{SU(2)}_{\mathrm{sp}} &\equiv \sum_{\alpha=\eta,s} \sum_{n=1}^{\infty} n\, N_{\alpha n} = \frac{1}{2}(L - 2S_s - 2S_{\eta})\,. \end{aligned} \tag{15}$$

Here $M^{SU(2)}_{\mathrm{sp}}$ denotes the total number of both rotated spins and rotated η-spins pairs.

The BA solution contains different types of quantum numbers. Their occupancy configurations are within the pseudoparticle representation described by corresponding occupancy configurations of c pseudoparticles without internal degrees of freedom and composite αn pseudoparticles. Complete information on the microscopic details of the latter pseudoparticles internal η-spin ($\alpha = \eta$) and spin ($\alpha = s$) n-pair configurations is encoded within the BA solution. It is not needed for the studies of this paper. Indeed, within the present TL the problem concerning an αn pseudoparticle internal degrees of freedom and that associated with its translational degrees of freedom center of mass motion separate.

Here we merely provide some general information on the internal degrees of freedom issue. As further discussed below, in the TL a composite αn pseudoparticle internal degrees of freedom are described by the imaginary part of a set of $l = 1, ..., n$ BA complex rapidities with the same real part [7],

$$\Lambda^{\alpha n,l}(q_j) = \Lambda^{\alpha n}(q_j) + i\,(n + 1 - 2l)\,u\,, \qquad l = 1, ..., n\,. \tag{16}$$

Here $\alpha = \eta, s$ and $n = 1, ..., \infty$. The real part $\Lambda^{\alpha n}(q_j)$ of these rapidities depends on the αn pseudoparticle momentum q_j defined in the following. It associated with the pseudoparticle translational degrees of freedom and may have $j = 1, ..., L_{\alpha n}$ different values.

The number $L_{\alpha n}$ of the set $j = 1, ..., L_{\alpha n}$ of the αn branch BA quantum numbers $\{q_j\}$ and that L_c of the related set $j = 1, ..., L_c$ of the c branch BA quantum numbers $\{q_j\}$ are given by,

$$L_{\alpha n} = N_{\alpha n} + N^h_{\alpha n}\,; \qquad N^h_{\alpha n} = 2S_\alpha + \sum_{n'=n+1}^{\infty} 2(n'-n)N_{\alpha n'}\,, \qquad \alpha = \eta, s\,, \qquad n = 1, ..., \infty\,,$$
$$L_c = N_c + N^h_c = N^R_s + N^R_\eta = L\,, \tag{17}$$

respectively. The real part $\Lambda^{\alpha n}(q_j)$ of the complex rapidities, Eq. (16), is the rapidity function that for each $u > 0$ energy eigenstate is the solution of the BA equations introduced in Ref. [7] for the TL. Within the pseudoparticle momentum distribution functional notation [41], these equations have the form given in Eqs. (A.1) and (A.2) of Appendix A. The sets of $j = 1, ..., L_c$ and $j = 1, ..., L_{\alpha n}$ of quantum numbers q_j, respectively, in these equations read,

$$q_j = \frac{2\pi}{L} I^\beta_j\,, \qquad j = 1, ..., L_\beta\,, \qquad \beta = c, \eta n, sn\,, \qquad n = 1, ..., \infty\,. \tag{18}$$

Here the $j = 1, ..., L_\beta$ quantum numbers I^β_j are either integers or half-odd integers according to the following boundary conditions [7],

$$I^\beta_j = 0, \pm 1, \pm 2, ... \quad \text{for } I_\beta \text{ even}\,,$$
$$= \pm 1/2, \pm 3/2, \pm 5/2, ... \quad \text{for } I_\beta \text{ odd}\,, \tag{19}$$

where the numbers I_β are given by,

$$I_c = N^{SU(2)}_{\rm ps} \equiv \sum_{\alpha=\eta,s}\sum_{n=1}^{\infty} N_{\alpha n}\,,$$
$$I_{\alpha n} = L_{\alpha n} - 1\,, \qquad \alpha = \eta, s\,, \qquad n = 1, ..., \infty\,. \tag{20}$$

The $\beta = c, \alpha n$ band successive set $j = 1, ..., L_\beta$ of momentum values q_j, Eq. (18), have only β pseudoparticle occupancies zero and one and the usual separation, $q_{j+1} - q_j = 2\pi/L$. They play the role of $\beta = c, \alpha n$ band momentum values. Consistently, within our functional representation the momentum eigenvalues of all $u > 0$ energy and momentum eigenstates are additive in q_j. They read,

$$P = \sum_{j=1}^{L} q_j\, N_c(q_j) + \sum_{n=1}^{\infty}\sum_{j=1}^{L_{sn}} q_j\, N_{sn}(q_j) + \sum_{n=1}^{\infty}\sum_{j=1}^{L_{\eta n}} (\pi - q_j)\, N_{\eta n}(q_j) + \pi\, M_{\eta,-1/2}\,. \tag{21}$$

The β-band momentum distribution functions $N_\beta(q_j)$ in this equation and BA equations, Eqs. (A.1) and (A.2) of Appendix A, read $N_\beta(q_j) = 1$ and $N_\beta(q_j) = 0$ for occupied and unoccupied discrete momentum values, respectively. One finds from the use of Eq. (14) that the momentum contribution $\pi M_{\eta,-1/2}$ can be written as $\pi(M_{\eta\,\rm sp} + M^{un}_{\eta,-1/2})$. It results from both the paired and unpaired rotated spins 1/2 and rotated η-spins 1/2 of projection $\pm 1/2$ having an intrinsic momentum given by,

$$q_{s,\pm 1/2} = q_{\eta,+1/2} = 0\,; \qquad q_{\eta,-1/2} = \pi\,. \tag{22}$$

Furthermore, the ηn pseudoparticle contribution $(\pi - q_j)$ to the momentum eigenvalue, Eq. (21), refers to its translational degrees of freedom. It is associated with the center of mass motion of that composite n-pair object as a whole. That such a contribution to the momentum eigenvalue

reads $(\pi - q_j)$ rather than q_j is related to each of the $M_{\eta\,\mathrm{sp}}$ η-spin singlet pairs having an anti-binding character, as confirmed below in Section 2.5.

On the one hand, the c pseudoparticles have no internal structure. On the other hand, the imaginary part $i\,(n+1-2l)\,u$ of the set of $l = 1, ..., n$ complex rapidities, Eq. (16), with the same real part $\Lambda^{\alpha n}(q_j)$ refers to the internal degrees of freedom of one composite αn pseudoparticle with $n > 1$ pairs whose center of mass carries αn band momentum q_j. Specifically, for $\alpha = s$ the imaginary part of such $l = 1, ..., n$ rapidities refers to the set $l = 1, ..., n$ of spin-singlet pairs of rotated spins $1/2$. It is associated with a corresponding binding of these pairs within the composite sn pseudoparticle. For $\alpha = \eta$ it is rather associated with a set $l = 1, ..., n$ of η-spin-singlet pairs of rotated η-spins $1/2$ and the binding of these pairs within the composite ηn pseudoparticle. (The anti-binding character found in Section 2.5 rather refers to the η-spin singlet configuration of a single pair.) Each such $l = 1, ..., n$ rapidities thus refers to one of the $l = 1, ..., n$ singlet pairs bound within the composite αn pseudoparticle. For $n = 1$ the rapidity imaginary part vanishes. Indeed, the $\alpha 1$ pseudoparticle internal degrees of freedom correspond to a single singlet pair of rotated spins $1/2$ ($\alpha = s$) or rotated η-spins $1/2$ ($\alpha = \eta$).

By combining the $M_{\alpha\,\mathrm{sp}}$ sum rule, Eq. (15), with the $N^h_{\alpha 1}$ expression, Eq. (17) for $n = 1$, one finds after some straightforward algebra that the following sum rules involving the number $N_{\alpha\,\mathrm{ps}} = \sum_{n=1}^{\infty} N_{\alpha n}$ of composite αn pseudoparticles of all $n = 1, ..., \infty$ branches and the related number $N^{SU(2)}_{\mathrm{ps}} = \sum_{\alpha=\eta,s} N_{\alpha\,\mathrm{ps}}$ in Eq. (20) are also obeyed,

$$
\begin{aligned}
N_{s\,\mathrm{ps}} &= \sum_{n=1}^{\infty} N_{sn} = \frac{1}{2}(N_c - N^h_{s1})\,, \\
N_{\eta\,\mathrm{ps}} &= \sum_{n=1}^{\infty} N_{\eta n} = \frac{1}{2}(N^h_c - N^h_{\eta 1})\,, \\
N^{SU(2)}_{\mathrm{ps}} &= \sum_{\alpha=\eta,s}\sum_{n=1}^{\infty} N_{\alpha n} = \frac{1}{2}(L - N^h_{s1} - N^h_{\eta 1})\,.
\end{aligned}
\tag{23}
$$

Hence for given fixed N_c and $N^h_c = L - N_c$ values, that of $N_{\alpha\,\mathrm{ps}}$ is determined by the corresponding value of the number $N^h_{\alpha 1}$ of $\alpha 1$-band holes.

The c band is populated by $N_c = N^R_s$ c pseudoparticles. They occupy N_c discrete momentum values out of the c band $j = 1, ..., L_c$ such momentum values, where $L_c = L$. Hence the number of c pseudoparticle holes indeed reads $N^h_c = N^R_\eta = L - N^R_s$. The number $L_{\alpha n}$ in Eq. (17) refers in turn to that of αn band $j = 1, ..., L_{\alpha n}$ momentum values q_j in Eq. (18). For an energy and momentum eigenstate each such a band is populated by a well defined number $N_{\alpha n}$ of αn pseudoparticles. The corresponding number $N^h_{\alpha n}$ of αn pseudoparticle holes is also a conserved number given in Eq. (17).

The set $j = 1, ..., L_\beta$ of $\beta = c, \alpha n$ bands discrete momentum values q_j whose different occupancy configurations generate the energy and momentum eigenstates and determine the corresponding momentum eigenvalues, Eq. (21), belong to well-defined domains, $q_j \in [q^-_\beta, q^+_\beta]$. The corresponding limiting momentum values $q^\pm_\beta$ read,

$$
\begin{aligned}
q^\pm_c &= \pm\frac{\pi}{L}(L-1) \approx \pm\pi \ \text{ for } \ N^{SU(2)}_{\mathrm{ps}} \ \text{ odd}\,; \\
q^\pm_c &= \pm\frac{\pi}{L}(L-1\pm 1) \approx \pm\pi \ \text{ for } \ N^{SU(2)}_{\mathrm{ps}} \ \text{ even}\,, \\
q^\pm_{\alpha n} &= \pm\frac{\pi}{L}(L_{\alpha n}-1)\,.
\end{aligned}
\tag{24}
$$

The label $l_{\rm r}$ in an energy eigenstate $|l_{\rm r}, l_{\eta s}, u\rangle$, Eq. (3), refers to the specific β bands occupancy configurations of the u-independent momentum values q_j that generate the state,

$$l_{\rm r} = \{I_j^\beta\} \text{ such that } N_\beta(q_j) = 1 \text{ where } q_j = \frac{2\pi}{L} I_j^\beta \quad \text{for } j = 1, ..., L_\beta\,, \;\; \beta = c, \eta n, sn\,, \;\; n = 1, ..., \infty\,. \tag{25}$$

All the energy eigenstates $|l_{\rm r}, l_{\eta s}, u\rangle$ corresponding to different $u > 0$ values and belonging to the same V tower are generated by *exactly* the same occupancy configurations of u-independent quantum numbers. The latter are associated with the labels $l_{\eta s}$, Eq. (2), and $l_{\rm r}$, Eq. (25).

Ground states are neither populated by composite sn pseudoparticles with $n > 1$ spin-singlet pairs nor by composite ηn pseudoparticles with any number $n = 1, ..., \infty$ of η-spin-singlet pairs. For electronic densities $n_e \in [0, 1]$ and spin densities $m \in [0, n_e]$, ground states are LWSs. Hence they have no unpaired rotated spins of projection $-1/2$ and no unpaired rotated η-spins of projection $-1/2$. For them the number $M_s^{un} = N_s^R = 2S_s$ of unpaired rotated spins of projection $+1/2$ and the number $M_\eta^{un} = N_\eta^R = 2S_\eta$ of unpaired rotated η-spins of projection $+1/2$ equal those $N_{s1}^h = N_s^R = 2S_s$ of $s1$ pseudoparticle holes and $N_c^h = N_\eta^R = 2S_\eta$ of c pseudoparticle holes, respectively. Within the pseudoparticle representation of the one-electron excitations that contribute to the singularities of the spectral functions, Eq. (4), the unpaired rotated spins play the role of empty sites of the squeezed $s1$ effective lattice considered below in Section 2.3. Moreover, the unpaired rotated η-spins play the role of empty sites of the c effective lattice. Hence their translational degrees of freedom are accounted for by that representation.

The ground-state β band pseudoparticle momentum distribution functions are given by,

$$N_c^0(q_j) = \theta(q_j - q_{Fc}^-)\,\theta(q_{Fc}^+ - q_j)\,; \qquad N_{s1}^0(q_j) = \theta(q_j - q_{Fs1}^-)\,\theta(q_{Fs1}^+ - q_j)\,;$$
$$N_{\alpha n}^0(q_j) = 0\,, \qquad \alpha n \neq s1\,, \tag{26}$$

where the distribution $\theta(x)$ reads $\theta(x) = 1$ for $x > 0$ and $\theta(x) = 0$ for $x \leq 0$. For the c and $s1$ bands the momentum distribution functions, Eq. (26), refer to compact and symmetrical occupancy configurations. The corresponding $\beta = c, s1$ Fermi points are associated with the Fermi momentum values $q_{F\beta}^\pm$ in Eq. (26). Accounting for $\mathcal{O}(1/L)$ corrections, they are given in Eqs. (C.4)–(C.11) of Ref. [41]. If within the TL we ignore such corrections, one finds that $N_\beta^0(q_j) = \theta(q_{F\beta} - |q_j|)$ for $\beta = c, s1$ where the Fermi momentum values are given by,

$$q_{Fc} = 2k_F = \pi\, n_e\,; \qquad q_{Fs1} = k_{F\downarrow} = \pi\, n_{e\downarrow}\,. \tag{27}$$

2.3. The c pseudoparticle, rotated spin, and rotated η-spin operators in terms of σ rotated-electron operators

The c pseudoparticles, rotated spins $1/2$, and rotated η-spins $1/2$ naturally emerge from the σ rotated-electron onsite occupancy configurations separation. This allows the introduction of local operators for these fractionalized particles in terms of the local rotated-electron creation and annihilation operators, Eq. (5).

The simplest case refers to the following $l = z, \pm$ local operators associated with the rotated spins $1/2$ ($\alpha = s$) and rotated η-spins $1/2$ ($\alpha = \eta$),

$$\tilde{S}_{j,\alpha}^l = \hat{V}^\dagger\, \hat{S}_{j,\alpha}^l\, \hat{V}\,, \qquad l = z, \pm\,, \qquad \alpha = \eta, s\,,$$
$$\tilde{S}_{j,\alpha}^\pm = \tilde{S}_{j,\alpha}^x \pm i\, \tilde{S}_{j,\alpha}^y\,, \qquad \alpha = \eta, s\,. \tag{28}$$

Here $\hat{S}_{j,\alpha}^l$ are the usual unrotated $l = z, \pm$ local spin ($\alpha = s$) and η-spin ($\alpha = \eta$) operators.

The $l = z, \pm$ local operators $\tilde{S}^{l}_{j,\alpha}$, Eq. (28), have in terms of creation and annihilation rotated-electron operators, Eq. (5), exactly the same expressions as the corresponding unrotated $l = z, \pm$ local operators $\hat{S}^{l}_{j,\alpha}$ in terms of creation and annihilation σ electron operators. The spin operators $\tilde{S}^{l}_{j,s}$ act onto sites singly occupied by σ rotated electrons. They read $\tilde{S}^{-}_{j,s} = (\tilde{S}^{+}_{j,s})^{\dagger} = \tilde{c}^{\dagger}_{j,\uparrow}\tilde{c}_{j,\downarrow}$ and $\tilde{S}^{z}_{j,s} = (\tilde{n}_{j,\downarrow} - 1/2)$. The η-spin operators $\tilde{S}^{l}_{j,\eta}$ act onto sites unoccupied by rotated electrons and sites doubly occupied by rotated electrons. They are given by $\tilde{S}^{-}_{j,\eta} = (\tilde{S}^{+}_{j,\eta})^{\dagger} = (-1)^{j}\,\tilde{c}_{j,\uparrow}\tilde{c}_{j,\downarrow}$ and $\tilde{S}^{z}_{j,\eta} = (\tilde{n}_{j,\downarrow} - 1/2)$.

Below the c pseudoparticle creation operator $f^{\dagger}_{j,c}$ and annihilation operator $f_{j,c}$ on the lattice site $j = 1, ..., L$ are uniquely defined in terms of the local rotated-electron creation and annihilation operators, Eq. (5). (Their c effective lattice is identical to the original lattice.) The c pseudoparticles have inherently emerged from the rotated electrons to the sites singly occupied by the latter being occupied by c pseudoparticles and those unoccupied and doubly occupied by rotated electrons being unoccupied by c pseudoparticles. Hence the c pseudoparticle local density operator $\tilde{n}_{j,c} \equiv f^{\dagger}_{j,c} f_{j,c}$ and the corresponding operator $(1 - \tilde{n}_{j,c})$ are the natural projectors onto the subset of $N^{s}_{R} = N_c$ original-lattice sites singly occupied by rotated electrons and onto the subset of $N^{\eta}_{R} = N^{h}_{c} = L - N_c$ original-lattice sites unoccupied and doubly occupied by rotated electrons, respectively. It then follows that the $\alpha = s, \eta$ and $l = z, \pm$ local operators $\tilde{S}^{l}_{j,\alpha}$, Eq. (28), can be written as,

$$\tilde{S}^{l}_{j,s} = \tilde{n}_{j,c}\,\tilde{q}^{l}_{j}\,; \qquad \tilde{S}^{l}_{j,\eta} = (1 - \tilde{n}_{j,c})\,\tilde{q}^{l}_{j}\,, \qquad l = z, \pm\,, \tag{29}$$

respectively. The $l = z, \pm$ local ηs *quasi-spin* operators,

$$\tilde{q}^{l}_{j} = \tilde{S}^{l}_{j,s} + \tilde{S}^{l}_{j,\eta}\,, \qquad l = \pm, z\,, \tag{30}$$

appearing here, such that $\tilde{q}^{\pm}_{j} = \tilde{q}^{x}_{j} \pm i\,\tilde{q}^{y}_{j}$, have the following expression in terms of rotated-electron creation and annihilation operators,

$$\tilde{q}^{-}_{j} = (\tilde{q}^{+}_{j})^{\dagger} = (\tilde{c}^{\dagger}_{j,\uparrow} + (-1)^{j}\,\tilde{c}_{j,\uparrow})\,\tilde{c}_{j,\downarrow}\,; \qquad \tilde{q}^{z}_{j} = (\tilde{n}_{j,\downarrow} - 1/2)\,. \tag{31}$$

The N_c c pseudoparticles live on the $N^{s}_{R} = N_c$ sites singly occupied by the rotated electrons. Hence their occupancy configurations refer to the lattice degrees of freedom associated with the relative positions of the $M_s = N^{s}_{R} = N_c$ sites occupied by rotated spins 1/2 and $M_{\eta} = N^{\eta}_{R} = N^{h}_{c} = L - N_c$ sites occupied by rotated η-spins 1/2. The corresponding three degrees of freedom separation of the rotated-electron occupancy configurations then implies that the rotated-electron operators, Eq. (5), can be written as,

$$\begin{aligned}
&\tilde{c}^{\dagger}_{j,\uparrow} = \left(\frac{1}{2} - \tilde{S}^{z}_{j,s} - \tilde{S}^{z}_{j,\eta}\right) f^{\dagger}_{j,c} + (-1)^{j}\left(\frac{1}{2} + \tilde{S}^{z}_{j,s} + \tilde{S}^{z}_{j,\eta}\right) f_{j,c}\,; \qquad \tilde{c}_{j,\uparrow} = (\tilde{c}^{\dagger}_{j,\uparrow})^{\dagger}\,, \\
&\tilde{c}^{\dagger}_{j,\downarrow} = (\tilde{S}^{+}_{j,s} + \tilde{S}^{+}_{j,\eta})(f^{\dagger}_{j,c} + (-1)^{j}\,f_{j,c})\,, \qquad \tilde{c}_{j,\downarrow} = (\tilde{c}^{\dagger}_{j,\downarrow})^{\dagger}\,.
\end{aligned} \tag{32}$$

The local c pseudoparticle operators $f^{\dagger}_{j,c}$ and $f_{j,c}$ appearing here are then *uniquely* defined for $u > 0$ in terms of σ rotated-electron creation and annihilation operators, Eq. (5). This is achieved by combining the inversion of the relations, Eq. (32), with the expressions of the $l = z, \pm$ local operators $\tilde{S}^{l}_{j,\alpha}$, Eq. (28), provided in Eqs. (29)–(31). These operators are associated with the rotated spins 1/2 ($\alpha = s$) and rotated η-spins 1/2 ($\alpha = \eta$). This uniquely gives,

$$f^{\dagger}_{j,c} = (f_{j,c})^{\dagger} = \tilde{c}^{\dagger}_{j,\uparrow}\,(1-\tilde{n}_{j,\downarrow}) + (-1)^{j}\,\tilde{c}_{j,\uparrow}\,\tilde{n}_{j,\downarrow}\,;$$
$$\tilde{n}_{j,c} = f^{\dagger}_{j,c}\,f_{j,c}\,, \qquad j = 1,...,L\,, \tag{33}$$

where $\tilde{n}_{j,\sigma}$ is the σ rotated-electron local density operator in Eq. (5).

The unitarity of the electron–rotated-electron transformation implies that the rotated-electron operators $\tilde{c}^{\dagger}_{j,\sigma}$ and $\tilde{c}_{j,\sigma}$, Eqs. (5) and (32), have the same anticommutation relations as the corresponding electron operators $c^{\dagger}_{j,\sigma}$ and $c_{j,\sigma}$, respectively. Straightforward manipulations based on Eqs. (28)–(33) then lead to the following algebra for the local c pseudoparticle creation and annihilation operators,

$$\{f^{\dagger}_{j,c}\,,f_{j',c}\} = \delta_{j,j'}; \qquad \{f^{\dagger}_{j,c}\,,f^{\dagger}_{j',c}\} = \{f_{j,c}\,,f_{j',c}\} = 0\,. \tag{34}$$

Furthermore, the local c pseudoparticle operators and the $l = z,\pm$ local rotated quasi-spin operators $\tilde{q}^{l}_{j}$, Eq. (31), commute with each other. The latter $l = z,\pm$ operators and corresponding rotated η-spin ($\alpha = \eta$) and rotated spin ($\alpha = s$) operators $\tilde{S}^{l}_{j,\alpha}$, Eqs. (28) and (29), obey the usual $SU(2)$ operator algebra.

On the one hand, the c pseudoparticle and ηs quasi-spin operator algebras refer to the whole Hilbert space. On the other hand, those of the rotated η-spin and rotated spin operators correspond to well-defined subspaces spanned by energy eigenstates whose value of the number $N^{R}_{s} = N_{c}$ of rotated-electron singly occupied sites and thus of c pseudoparticles is fixed. This ensures that the value of the corresponding rotated η-spin number $M_{\eta} = N^{R}_{\eta} = L - N_{c}$ and rotated spin number $M_{s} = N^{R}_{s} = N_{c}$ is fixed as well.

The degrees of freedom separation, Eq. (32), is such that the c pseudoparticle operators, Eq. (33), rotated-spin $1/2$ and rotated-η-spin $1/2$ operators, Eq. (29), and the related ηs quasi-spin operators, Eqs. (30) and (31), emerge from the rotated-electron operators by an exact local transformation that *does not* introduce constraints.

That, as given in Eq. (26), ground states are only populated by c and $s1$ pseudoparticles plays an important role in the PDT. On the one hand and as mentioned above, for $u > 0$ the c pseudoparticles live on a c effective lattice identical to the original lattice. It thus has $j = 1,...,L$ sites and length L. On the other hand, the $s1$ pseudoparticles live on a squeezed $s1$ effective lattice [34,37,38]. Its $j = 1,...,L_{s1}$ sites number L_{s1} equals that of $s1$ band discrete momentum values, Eq. (17) for $\alpha n = s1$. The squeezed $s1$ effective lattice has length L. Hence its spacing is in general larger than a. In the TL considered in this paper it is given by,

$$a_{s1} = \frac{N_a}{L_{s1}}\,a\,. \tag{35}$$

This ensures that indeed $L = L_{s1}\,a_{s1}$. (Except in Eq. (35), in this paper we use units of lattice spacing a one.)

The $s1$ pseudoparticle translational degrees of freedom center of mass motion are described by operators $f^{\dagger}_{j,s1}$ (and $f_{j,s1}$) that create (and annihilate) one $s1$ pseudoparticle at the $s1$ effective lattice site $x_j = a_{s1}\,j$ where $j = 1,...,L_{s1}$. Such local $s1$ pseudoparticle creation and annihilation operators obey a fermionic algebra. This is consistent with the $\beta = c, s1$ band momentum value q_j having only occupancies zero and one.

The $s1$ pseudoparticle operator representation is valid for the 1D Hubbard model in subspaces spanned by energy eigenstates with fixed L_{s1} value, Eq. (17) for $\alpha n = s1$. That in such subspaces the local $s1$ pseudoparticle operators obey a fermionic algebra, can be confirmed in terms of

their statistical interactions [65]. This is a problem that we address here very briefly. The local $s1$ pseudoparticle creation and annihilation operators may be written as,

$$f^{\dagger}_{j,s1} = e^{i\phi_{j,s1}}\, g^{\dagger}_{j,s1}\,; \qquad f_{j,s1} = (f^{\dagger}_{j,s1})^{\dagger}\,, \qquad j = 1, ..., L_{s1}\,. \tag{36}$$

Here $\phi_{j,s1} = \sum_{j'\neq j} f^{\dagger}_{j',s1}$ and the operator $g^{\dagger}_{j,s1}$ obeys a hard-core bosonic algebra. This algebra is justified by the corresponding statistical interaction vanishing for the model in subspaces spanned by energy eigenstates with fixed L_{s1} value. The $s1$ effective lattice has been constructed inherently to that algebra being of hard-core type for the operators $g^{\dagger}_{j,s1}$ and $g_{j,s1}$. Therefore, through a Jordan–Wigner transformation, $f^{\dagger}_{j,s1} = e^{i\phi_{j,s1}}\, g^{\dagger}_{j,s1}$ [66], the operators $f^{\dagger}_{j,s1}$ and $f_{j,s1} = (f^{\dagger}_{j,s1})^{\dagger}$ in Eq. (36) obey indeed a fermionic algebra,

$$\{f^{\dagger}_{j,s1}\,, f_{j',s1}\} = \delta_{j,j'}; \qquad \{f^{\dagger}_{j,s1}\,, f^{\dagger}_{j',s1}\} = \{f_{j,s1}\,, f_{j',s1}\} = 0\,. \tag{37}$$

Each of the N_{s1} occupied $s1$ effective lattice sites corresponds to a spin-singlet pair. It thus involves two model lattice sites occupied by rotated spins $1/2$ of opposite spin projection. For the densities $n_e \in [0, 1[$ and $m \in [0, n_e]$, the line shape in the vicinity of the singular features of the σ one-electron spectral functions, Eq. (4), studied in Sections 3 and 4 is controlled by ground state transitions to excited energy eigenstates for which $N_{sn} = 0$ for $n > 1$. For both the ground states and such excited states, the number N^{h}_{s1} of unoccupied $s1$ effective lattice sites, Eq. (17) for $\alpha n = s1$, reads $N^{h}_{s1} = 2S_s$. For such states the $s1$ effective lattice unoccupied sites refer to the $M^{un}_{s} = M^{un}_{s,+1/2} = 2S_s$ sites occupied in the original lattice by the unpaired rotated spins $1/2$. Such unpaired rotated spins $1/2$ are used within the $s1$ pseudoparticle motion as unoccupied sites with which they interchange position.

The $\beta = c, s1$ pseudoparticle operators labeled by the $\beta = c, s1$ band momentum values defined in Eqs. (18) and (19) play a key role in these studies. They read,

$$f^{\dagger}_{q_j,\beta} = \frac{1}{\sqrt{L}} \sum_{j'=1}^{L_\beta} e^{i\, q_j\, x_{j'}}\, f^{\dagger}_{j',\beta}\,; \qquad f_{q_j,\beta} = (f^{\dagger}_{q_j,\beta})^{\dagger}\,, \qquad j = 1, ..., L_\beta\,, \qquad \beta = c, s1\,. \tag{38}$$

The $j' = 1, ..., L_\beta$ local operators $f^{\dagger}_{j',\beta}$ appearing in this expression are those given in Eqs. (33) and (36) for $\beta = c$ and $\beta = s1$, respectively.

The $s1$ pseudofermion operators labeled by momentum q_j, Eq. (38) for $\beta = s1$, act within subspaces spanned by energy eigenstates with fixed L_{s1} values. In addition, they also appear in the expressions of the shakeup effects generators that transform such subspaces quantum number values into each other.

The expressions of the σ one-electron LHB and UHB addition spectral functions, Eq. (6), near their singularities studied in Sections 3 and 4 are controlled by transitions to excited energy eigenstates with $N_{\eta 1} = 0$ and $N_{\eta 1} = 1$, respectively. Such states are not populated by composite αn pseudoparticles with $n > 1$ pairs. Moreover, they have no unpaired rotated spins of projection $-1/2$ and no unpaired rotated η-spins of projection $-1/2$.

As for the $s1$ pseudoparticles, one introduces anti-commuting operators $f^{\dagger}_{q_j,\eta 1}$ and $f_{q_j,\eta 1}$ for the $\eta 1$ pseudoparticles. Such $\eta 1$ pseudofermion operators appear in the one-electron expressions derived below in Section 3.2. As justified in Section 3, their explicit use is not though required in what the computation of the corresponding UHB one-electron matrix elements involving creation of one $\eta 1$ pseudofermion with momentum values $\pm(\pi - 2k_F)$ is concerned.

Only the c and $s1$ pseudofermion operators generated from the $\beta = c, s1$ pseudoparticle operators, Eq. (38), are needed for the computation of the one-electron matrix elements considered in our study.

2.4. Needed quantities associated with the β pseudoparticle quantum liquid

The quantities associated with the β pseudoparticle quantum liquid briefly revisited in this section are needed for the σ one-electron spectral functions expressions studied in Sections 3 and 4.

A *particle subspace* (PS) is spanned by one ground state and the set of excited energy eigenstates generated from it by a finite number of β pseudoparticle processes. For the densities $n_e \in [0, 1[$ and $m \in [0, n_e]$ considered in this paper, ground states are LWSs of both the spin and η-spin $SU(2)$ symmetry algebras. The deviation densities $\delta N_\beta/L$, $\delta S_s/L$, and $\delta S_\eta/L$ of their PS excited energy eigenstates vanish in the TL as $L \rightarrow \infty$. For a PS there are though no restrictions on the value of the excitation energy and excitation momentum.

The β pseudoparticle quantum liquid shortly reported here refers to general PSs whose finite occupancies may correspond to more $\beta = c, \alpha n$ bands than those of the PSs directly involved in our study. It is often convenient within the TL to replace the $\beta = c, \alpha n$ band discrete momentum values q_j, Eq. (18), such that $q_{j+1} - q_j = 2\pi/L$, by a corresponding continuous momentum variable, q. It belongs to a domain $q \in [q_\beta^-, q_\beta^+]$ whose limiting momentum values $q_\beta^\pm$ are given in Eq. (24). For the $\beta = \alpha n$ bands the relation $q_{\alpha n}^- = -q_{\alpha n}^+$ is exact, as given in that equation. Ignoring $1/L$ corrections as $L \rightarrow \infty$, one finds $q_\beta^\pm \approx \pm q_\beta$ where for all $\beta = c, \alpha n$ bands q_β has simple expressions for the ground states and their PS excited energy eigenstates. For the present densities ranges they read [41],

$$q_c = \pi\,; \quad q_{s1} = k_{F\uparrow}\,; \quad q_{sn} = (k_{F\uparrow} - k_{F\downarrow}) = \pi\, m\,, \quad n > 1\,;$$
$$q_{\eta n} = (\pi - 2k_F) = \pi\,(1 - n_e)\,. \tag{39}$$

The $\beta = c, \alpha n$ momentum band distribution functions of the PS excited energy eigenstates are of the general form $N_\beta(q_j) = N_\beta^0(q_j) + \delta N_\beta(q_j)$. The ground-state β band pseudoparticle momentum distribution functions $N_\beta^0(q_j)$ appearing here are given in Eq. (26). Several physical quantities are then expressed as functionals of the corresponding $\beta = c, \alpha n$ momentum band distribution function deviations,

$$\delta N_\beta(q_j) = N_\beta(q_j) - N_\beta^0(q_j)\,, \quad j = 1, ..., L_\beta\,, \quad \beta = c, \alpha n\,, \quad n = 1, ..., \infty\,. \tag{40}$$

For transitions to an excited energy eigenstate for which the number L_{s1} of BA $s1$ band momentum values changes, their removal or addition occurs in the vicinity of the $s1$ band edges $q_{s1}^- = -q_{s1}^+$, Eq. (24) for $\alpha n = s1$. Those are zero-momentum and zero-energy processes.

Under transitions from a ground state to its PS excited energy eigenstates, there may occur a β band momentum q_j shakeup effect. It is an overall β-band discrete momentum shift, $q_j \rightarrow q_j + 2\pi\,\Phi_\beta^0/L$, where Φ_β^0 reads,

$$\Phi_c^0 = 0\,; \quad \delta N_{\rm ps}^{SU(2)} \quad \text{even}\,; \quad \Phi_c^0 = \pm\frac{1}{2}\,; \quad \delta N_{\rm ps}^{SU(2)} \quad \text{odd}\,;$$
$$\Phi_{\alpha n}^0 = 0\,; \quad \delta N_c + \delta N_{\alpha n} \quad \text{even}\,; \quad \Phi_{\alpha n}^0 = \pm\frac{1}{2}\,; \quad \delta N_c + \delta N_{\alpha n} \quad \text{odd}\,,$$
$$\alpha = \eta, s\,, \quad n = 1, ..., \infty\,. \tag{41}$$

Here $\delta N_{\rm ps}^{SU(2)}$ is the deviation in the number $N_{\rm ps}^{SU(2)}$, Eq. (23). The shakeup effect results from a collective shift, $(2\pi/L)\,\Phi_\beta^0 = \pm\pi/L$, that all β band discrete momentum values $q_j = (2\pi/L)\,I_j^\beta$ may undergo due to a change in the boundary conditions that determine the q_j values, Eqs. (18) and (19).

Within the continuum q representation, the deviation values $\delta N_\beta(q_j) = -1$ and $\delta N_\beta(q_j) = +1$, Eq. (40), become $\delta N_\beta(q) = -(2\pi/L)\delta(q-q_j)$ and $\delta N_\beta(q) = +(2\pi/L)\delta(q-q_j)$, respectively. Here and throughout this paper, $\delta(x)$ denotes the usual Dirac delta-function distribution. Within such a representation the ground state occupancy $q \in [-q_{F\beta}, q_{F\beta}]$ becomes a continuum compact distribution. Hence a β band shakeup effect is felt mostly by q values at the four $\beta = c, s1$ and $\iota = \pm 1$ Fermi points, $\iota\, q_{F\beta}$. This effect is captured within that representation by additional deviations, $\pm(\pi/L)\delta(q - \iota\, q_{F\beta})$. Their signs $\pm$ are those of $(2\pi/L)\,\Phi_\beta^0 = \pm\pi/L$.

The PS energy functionals are derived from the use in the TBA equations, Eqs. (A.1)–(A.2) of Appendix A, and general energy spectra, Eq. (A.4) of that Appendix, of distribution functions of general form $N_\beta(q_j) = N_\beta^0(q_j) + \delta N_\beta(q_j)$ for the excited energy eigenstates. The combined and consistent solution of such equations and spectra up to second order in the deviations, Eq. (40), leads to [57],

$$\delta E = \sum_\beta \sum_{j=1}^{L_\beta} \varepsilon_\beta(q_j)\delta N_\beta(q_j) + \frac{1}{L}\sum_\beta\sum_{\beta'}\sum_{j=1}^{L_\beta}\sum_{j'=1}^{L_{\beta'}} \frac{1}{2}\, f_{\beta\,\beta'}(q_j, q_{j'})\,\delta N_\beta(q_j)\delta N_{\beta'}(q_{j'}) + \sum_{\alpha=\eta,s} \varepsilon_{\alpha,-1/2}\, M^{un}_{\alpha,-1/2}\,. \tag{42}$$

For the present densities ranges, the unpaired rotated η-spin ($\alpha = \eta$) and unpaired rotated spin ($\alpha = s$) energies in this expression read,

$$\varepsilon_{\alpha,-1/2} = 2\mu_\alpha\,; \qquad \varepsilon_{\alpha,+1/2} = 0\,, \qquad \alpha = \eta, s\,, \tag{43}$$

where the energy scales $2\mu_\alpha$ are given by,

$$2\mu_\eta = 2|\mu|\,; \qquad 2\mu_s = 2\mu_B\,|h|\,. \tag{44}$$

The latter expression applies to general electronic and spin densities. It reads $2\mu_\eta = 2\mu$ and $2\mu_s = 2\mu_B\, h$ for the densities ranges $n_e \in [0, 1[$ and $m \in [0, n_e]$ which Eq. (43) refers to. For the $n_e = 1$ Mott–Hubbard insulator phase, the unpaired rotated η-spin energy rather is given by $\varepsilon_{\eta,\mp 1/2} = (\mu_u \pm \mu)$ for $\mu \in [-\mu_u, \mu_u]$. The $n_e = 1$ Mott–Hubbard gap $2\mu_u$ appearing in that range is behind the spectra of the one-electron and charge excitations of the half-filled 1D Hubbard model being gapped [3,4,56].

The $\beta = c, \alpha n$ band energy dispersions $\varepsilon_\beta(q_j)$ in Eq. (42) are given by,

$$\varepsilon_\beta(q_j) = E_\beta(q_j) + \frac{t}{\pi}\int_{-Q}^{Q} dk\, 2\pi\, \bar{\Phi}_{c,\beta}\left(\frac{\sin k}{u}, \frac{\Lambda_0^\beta(q_j)}{u}\right)\sin k\,, \qquad j = 1, ..., L_\beta\,. \tag{45}$$

Here $E_\beta(q_j)$ stands for the $\beta = c, \eta n, sn$ energy spectra, Eq. (A.5) of Appendix A, with the rapidity functions in their expressions given by the ground-state rapidity functions $k_0^c(q_j)$ and $\Lambda_0^\beta(q_j)$. These functions are the solution of Eqs. (A.1) and (A.2) of that Appendix for the β-band ground-state distribution function distributions, Eq. (26). The parameter Q also appearing in Eq. (45) and related parameters B, r_c^0, and r_0^s read,

$$Q \equiv k_c^0(2k_F)\,; \qquad B \equiv \Lambda_0^{s1}(k_{F\downarrow})\,; \qquad r_c^0 = \frac{\sin Q}{u}\,; \qquad r_s^0 = \frac{B}{u}\,. \tag{46}$$

Furthermore, the rapidity dressed phase shift $2\pi\,\bar{\Phi}_{c,\beta}(r,r')$ in Eq. (45) is a particular case of the more general rapidity dressed phase shifts $2\pi\,\bar{\Phi}_{\beta,\beta'}(r,r')$ uniquely defined by the set of integral equations given in Eqs. (A.8)–(A.22) of Appendix A. The general expression of the f functions in the second-order terms of the energy functional, Eq. (42), is provided in Eq. (A.24) of that Appendix. It involves the related momentum dressed phase shifts,

$$2\pi\,\Phi_{\beta,\beta'}(q_j,q_{j'}) = 2\pi\,\bar{\Phi}_{\beta,\beta'}\left(r,r'\right)\,; \quad r = \Lambda_0^{\beta}(q_j)/u\,; \quad r' = \Lambda_0^{\beta'}(q_{j'})/u\,. \tag{47}$$

Such a f function expression also involves the β band group velocities $v_\beta(q_j)$. Within the TL continuum q representation, they read,

$$\begin{aligned} &v_\beta(q) = \frac{\partial\varepsilon_\beta(q)}{\partial q}\,, \qquad \beta = c,\eta n,sn\,, \qquad n = 1,...,\infty\,; \\ &v_\beta \equiv v_\beta(q_{F\beta})\,, \qquad \beta = c,s1\,. \end{aligned} \tag{48}$$

The β band energy dispersions appearing here are given in Eq. (45).

The following overall dressed phase shift functional,

$$2\pi\,\Phi_\beta(q_j) = \sum_{\beta'}\sum_{j'=1}^{N_{a_{\beta'}}} 2\pi\,\Phi_{\beta,\beta'}(q_j,q_{j'})\,\delta N_{\beta'}(q_{j'})\,, \qquad j = 1,...,L_\beta\,, \qquad \beta = c,s1\,, \tag{49}$$

plays a key role in the PDT dynamical correlation functions expressions. It involves the momentum dressed phase shifts, Eq. (47). The summation $\sum_{\beta'}$ in Eq. (49) refers to $\beta' = c,s1$ for σ one-electron removal and LHB addition and to $\beta' = c,s1,\eta 1$ for σ one-electron UHB addition. The deviation $\delta N_{\beta'}(q_{j'})$ is defined in Eq. (40).

The functional energy spectrum, Eq. (42), describes the 1D Hubbard model as a quantum liquid of c, ηn, and sn pseudoparticles. They have residual interactions associated with the f functions, Eqs. (A.24). On the one hand, the general energy spectrum, Eq. (A.4) of Appendix A, gives the energy eigenvalues. On the other hand, that given in Eq. (42) provides the excitation energies. Those are given by the excited-state energy eigenvalues minus the ground state energy. The second term of the energy dispersion, Eq. (45), and the f-function terms in Eq. (42) are absent from Eq. (A.4) of Appendix A. Indeed, they stem from the latter energies difference. This justifies why that energy dispersion term and the f-function expressions involve dressed phase shifts, Eq. (47): Those emerge under the transitions from the ground state to energy eigenstates of excitation energy, Eq. (42).

The spectra of the σ one-electron spectral functions near their singular features are expressed in Sections 3 and 4 in terms of the c and $s1$ band energy dispersions, Eq. (45) for $\beta = c,s1$. The spectrum of a particular type of such features involves as well the β pseudoparticle group velocities, Eq. (48). The exponents that control the line shape in the vicinity of singular features called branch lines also considered in these sections are expressed in terms of momentum dressed phase shifts, Eq. (47). Hence in Appendix B useful limiting behaviors of these quantum-liquid quantities are provided.

2.5. Binding and anti-binding character of the rotated spins $1/2$ ($\alpha = s$) and rotated η-spins $1/2$ ($\alpha = \eta$) pairing, respectively, and important energy scales

On the one hand, for general electronic densities $n_e \neq 1$ and all spin densities m the energy of two unpaired rotated η-spins ($\alpha = \eta$) and two unpaired rotated spins ($\alpha = s$) of opposite projection reads,

$$2\mu_\alpha = \varepsilon_{\alpha,-1/2} + \varepsilon_{\alpha,+1/2}\,, \qquad \alpha = \eta, s\,, \tag{50}$$

where the energy scale $2\mu_\alpha$ is given in Eq. (44). For $n_e = 1$ and $m \in [-1, 1]$ this expression remains valid for $\alpha = s$. For $\alpha = \eta$ it is replaced by $2\mu_u = \varepsilon_{\eta,-1/2} + \varepsilon_{\eta,+1/2}$ and thus rather involves the $n_e = 1$ Mott–Hubbard gap $2\mu_u$.

On the other hand, the αn pseudoparticle energy dispersion, Eq. (45) for $\beta = \alpha n$, may be written as,

$$\varepsilon_{\alpha n}(q_j) = n\,2\mu_\alpha + \varepsilon^0_{\alpha n}(q_j)\,, \qquad \alpha = \eta, s\,, \qquad n = 1, ..., \infty\,. \tag{51}$$

The term $n\,2\mu_\alpha$ in this energy dispersion is merely additive in the bare energy $2\mu_\alpha$, Eq. (50). Indeed, that bare η-spin-triplet ($\alpha = \eta$) and spin-triplet ($\alpha = s$) pair energy also applies to an η-spin-singlet ($\alpha = \eta$) and spin-singlet ($\alpha = s$) pair, respectively. This requires that $\varepsilon_{\alpha n}(q_j) = n\,2\mu_\alpha$ and thus $\varepsilon^0_{\alpha n}(q_j) = 0$ in Eq. (51). This occurs when each single pair configuration has no binding or anti-binding character.

The internal degrees of freedom of an $\alpha 1$ pseudoparticle correspond to a single pair. The energy $\varepsilon^0_{\alpha 1}(q_j)$ in its energy dispersion $\varepsilon_{\alpha 1}(q_j) = 2\mu_\alpha + \varepsilon^0_{\alpha 1}(q_j)$, Eq. (51) for $n = 1$, refers to a binding or anti-binding character if $\varepsilon^0_{\alpha 1}(q_j) < 0$ or $\varepsilon^0_{\alpha 1}(q_j) > 0$, respectively. One finds that $\varepsilon^0_{s1}(q_j) < 0$ for $|q_j| < q_{s1}$ and $\varepsilon^0_{\eta 1}(q_j) > 0$ for $|q_j| < q_{\eta 1}$. This reveals that the spin-singlet $s1$-pair configuration and the η-spin-singlet $\eta 1$-pair configuration have a binding and an anti-binding character, respectively. Interestingly, though, one finds that $\varepsilon^0_{\alpha 1}(\pm q_{\alpha 1}) = 0$ at the $\alpha = s, \eta$ limiting momenta $q_j = \pm q_{\alpha 1}$. Hence at these two band edge momenta the two spins 1/2 ($\alpha = s$) or two η-spins 1/2 ($\alpha = \eta$) remain in a singlet configuration, yet become unbound. The energy $\varepsilon_{\alpha 1}(\pm q_{\alpha 1}) = 2\mu_\alpha$ then reduces to the intrinsic pair energy, Eq. (50).

In the case of a composite αn pseudoparticle with $n > 1$ pairs bound within it, one finds as well that $\varepsilon^0_{sn}(q_j) < 0$ for $|q_j| < q_{sn}$ and $\varepsilon^0_{\eta n}(q_j) > 0$ for $|q_j| < q_{\eta n}$. However, the maximum absolute value of the αn-pair configuration binding ($\alpha = s$) and anti-binding ($\alpha = \eta$) energy per pair, $|\varepsilon^0_{\alpha n}(0)|/n$, is found to strongly decrease upon increasing n. This reveals that the binding of the $n > 1$ pairs within the composite αn pseudoparticle tends to suppress the single-pair binding ($\alpha = s$) and anti-binding ($\alpha = \eta$) energy of each such pairs.

Moreover, one finds that $\varepsilon^0_{\alpha n}(\pm q_{\alpha n}) = 0$ and thus $\varepsilon_{\alpha n}(\pm q_{\alpha n}) = n\,2\mu_\alpha$, as for the $\alpha 1$ pseudoparticles. Hence at the αn band limiting values $q_j = \pm q_{\alpha n}$ given in Eq. (39) the energy, Eq. (51), becomes additive in the intrinsic energy $2\mu_\alpha$, Eq. (50). As discussed below in Section 4.3, this is due to a symmetry that is behind the σ one-electron UHB addition singular spectral features being for $n_e \in [0, 1[$ and under the transformations $k \rightarrow \pi - k$ and $\omega \rightarrow 2\mu - \omega$ similar to those of the corresponding $\bar{\sigma}$ one-electron removal singular spectral features. (Here $\bar{\sigma}$ denotes the spin projection opposite to σ.)

The magnetic-field energy scale $2\mu_B\,h = 2\mu_B\,h(m)$ and the energy scale $2\mu = 2\mu(n_e)$ associated with the chemical potential μ are given by [57],

$$\begin{aligned}
2\mu_B\,h(m) &= -\varepsilon^0_{s1}(q_{Fs1}) \in [0, 2\mu_B\,h_c] \\
&\quad \text{for } q_{Fs1} = k_{F\downarrow} = \frac{\pi}{2}(n_e - m) \text{ where } m \in [0, n_e] \text{ at fixed } n_e\,, \\
2\mu(n_e) &= -2\varepsilon^0_c(q_{Fc}) - \varepsilon^0_{s1}(q_{Fs1}) \in [2\mu_u, (U + 4t)] \\
&\quad \text{for } q_{Fc} = 2k_F = \pi\,n_e \text{ and } q_{Fs1} = \frac{\pi}{2}(n_e - m) \text{ where } n_e \in [0, 1[\\
&\quad \text{at fixed } m < n_e\,.
\end{aligned} \tag{52}$$

Here $\varepsilon^0_{s1}(q_j) = \varepsilon_{s1}(q_j) - 2\mu_s$ is the $s1$ band binding energy in Eq. (51) and,

$$\varepsilon^0_c(q_j) = \varepsilon_c(q_j) - \frac{1}{2}(2\mu_\eta - 2\mu_s)\,. \tag{53}$$

In some limits the energy scales $2\mu_B\, h = 2\mu_B\, h(m)$ and $2\mu = 2\mu(n_e)$, Eq. (52), are associated with the quantum phase transitions considered in Section 2.1.

On the one hand, the $n_e = 1$ Mott–Hubbard gap $2\mu_u$ associated with the phase transition between the metallic and Mott–Hubbard insulator quantum phases reads $2\mu_u = \lim_{n_e\to 1} 2\mu(n_e)$. For $u > 0$ it remains finite for all spin densities, $m \in [0, 1[$. In the limits $m \to 0$ [3,4,56] and $m \to 1$ it is found to read,

$$\begin{aligned} 2\mu_u &= U - 4t + 8t\int_0^\infty d\omega \frac{J_1(\omega)}{\omega\,(1+e^{2\omega u})} = \frac{16\,t^2}{U}\int_1^\infty d\omega \frac{\sqrt{\omega^2-1}}{\sinh\left(\frac{2\pi t\omega}{U}\right)}\,, \qquad m \to 0\,, \\ &= \sqrt{(4t)^2 + U^2} - 4t\,, \qquad m \to 1\,, \end{aligned} \tag{54}$$

respectively. Its $u \ll 1$ limiting behaviors are $2\mu_u \approx (8/\pi)\sqrt{t\,U}\, e^{-2\pi\left(\frac{t}{U}\right)}$ for $m \to 0$ [56] and $2\mu_u \approx U^2/8t$ for $m \to 1$. For $u \gg 1$ it behaves as $2\mu_u \approx (U - 4t)$ for the whole spin density range $m \in [0, 1]$.

On the other hand, the magnetic energy scale $2\mu_B\, h_c$ associated with the quantum phase transition to fully polarized ferromagnetism is given by $2\mu_B\, h_c = 2\mu_B\, h(m)|_{m=n_e} = 2\mu_B\, h(n_e)$. It is found to have the following closed-form expression in terms of $u = U/4t$ and the electronic density n_e valid for the whole range $n_e \in [0, 1[$ [57],

$$\begin{aligned} 2\mu_B\, h_c = 2t\Big[\sqrt{1+u^2}\left(1 - \frac{2}{\pi}\,\mathrm{arccot}\left(\frac{\sqrt{1+u^2}}{u}\tan(\pi n_e)\right)\right) \\ - 2u\,n_e - \frac{2}{\pi}\cos(\pi n_e)\arctan\left(\frac{\sin(\pi n_e)}{u}\right)\Big]\,. \end{aligned} \tag{55}$$

In the $n_e \to 0$ and $n_e \to 1$ limits this gives,

$$\begin{aligned} 2\mu_B\, h_c &= 0\,, \qquad n_e \to 0\,, \\ &= \sqrt{(4t)^2 + U^2} - U\,, \qquad n_e \to 1\,, \end{aligned} \tag{56}$$

respectively. It behaves as $2\mu_B\, h_c = 4t\sin^2(\pi\, n_e/2)$ for $u \to 0$ whereas for $u \gg 1$ its behavior is $2\mu_B\, h_c = (2t\, n_e/u)[1 - \sin(2\pi n_e)/(2\pi n_e)]$.

At fixed electronic density $n_e < 1$, the magnetic-field energy scale $2\mu_B\, h = 2\mu_B\, h(m)$, Eq. (52), is an increasing continuous function of the spin density $m \in [0, n_e]$. It smoothly increases from $2\mu_B\, h(0) = 0$ for $m \to 0$ to $2\mu_B\, h(n_e) = 2\mu_B\, h_c$ for $m \to n_e$. Here $2\mu_B\, h_c$ is the magnetic energy scale, Eq. (55). At fixed spin density $m < n_e$, the chemical potential energy scale $2\mu = 2\mu(n_e)$, Eq. (52), is a decreasing continuous function of the electronic density $n_e \in [0, 1]$. It smoothly decreases from $2\mu(0) = U + 4t$ for $n_e \to 0$ to $2\mu(1^-) = 2\mu_u$ for $n_e \to 1$. Here $2\mu_u$ is the Mott–Hubbard gap, Eq. (54).

3. The pseudofermion dynamical theory microscopic processes that account for the σ one-electron spectral weights

Here the PDT quantities and concepts needed for our study on the one-electron spectral functions, Eq. (4), are introduced. This involves new needed information beyond that provided in

Refs. [39,40] on the specific microscopic processes that control the σ one-electron spectral weights at finite magnetic field. This includes how the PDT accounts through such processes for the matrix elements of the σ electron creation or annihilation operators between the initial ground state and the excited energy eigenstates.

Specifically, in Section 3.1 we briefly revisit the pseudofermion representation. The σ one-electron operators used in our study are expressed in terms of pseudofermion operators in Section 3.2. Section 3.3 addresses issues related to the matrix elements of these operators. In addition, the σ one-electron spectral functions are expressed in terms of $\beta = c, s1$ pseudofermion spectral functions. The effects of the small higher-order pseudofermion contributions to the σ one-electron spectral weight are discussed in Section 3.4. In Section 3.5 the involved state summations problem is addressed. Analytical expressions of the σ one-electron spectral functions are obtained by partially performing such state summations for (k,ω)-plane regions near these functions singular features. The relation of the PDT to conformal-field theory and finite-size scaling is the issue discussed in Section 3.6. In Section 3.7 the validity of the expressions for the line shape near σ one-electron singular spectral features is discussed. Finally, the general effects of symmetry on the one-electron spectral functions is the issue addressed in Section 3.8.

3.1. Pseudofermion representation to be used for the σ electron operators matrix elements

Here we consider the 1D Hubbard model at a finite magnetic field in a PS as defined in Section 2.4. For that quantum problem the c and $s1$ rapidity functions of the excited energy eigenstates can be expressed in terms of those of the corresponding initial ground state. This is given in Eq. (A.7) of Appendix A. The set of $j = 1, ..., L_\beta$ values $\bar{q}_j = \bar{q}(q_j)$ in such excited energy eigenstates rapidity expressions $\Lambda^c(q_j) = \Lambda^c_0(\bar{q}(q_j))$ and $\Lambda^{s1}(q_j) = \Lambda^{s1}_0(\bar{q}(q_j))$ are the $\beta = c, s1$ band discrete *canonical momentum* values. They read,

$$\bar{q}_j = \bar{q}(q_j) = q_j + \frac{2\pi\,\Phi_\beta(q_j)}{L} = \frac{2\pi}{L}\left(I^\beta_j + \Phi_\beta(q_j)\right), \qquad j = 1, ..., L_\beta\,, \qquad \beta = c, s1\,. \tag{57}$$

Here $\Phi_\beta(q_j)$ stands for the dressed phase-shift functional, Eq. (49), in units of 2π. The discrete canonical momentum values, Eq. (57), have spacing $\bar{q}_{j+1} - \bar{q}_j = 2\pi/L + \text{h.o.}$ where h.o. stands for contributions of second order in $1/L$.

We call a $\beta = c, s1$ *pseudofermion* each of the N_β occupied β-band discrete canonical momentum values $\bar{q}_j$ [39,40]. We call a β *pseudofermion hole* the remaining N^h_β unoccupied β-band discrete canonical momentum values $\bar{q}_j$ of a PS energy eigenstate. There is a pseudofermion representation for each initial ground state and its PS. This holds for all electronic and spin densities.

The $\beta = c, s1$ pseudofermion creation and annihilation operators are generated from the corresponding $\beta = c, s1$ pseudoparticle creation and annihilation operators, Eq. (38), as follows,

$$\bar{f}^\dagger_{\bar{q}_j,\beta} = f^\dagger_{q_j+2\pi\,\Phi_\beta(q_j)/L,\beta} = \left(\hat{S}^\Phi_\beta\right)^\dagger f^\dagger_{q_j,\beta}\,\hat{S}^\Phi_\beta\,; \qquad \bar{f}_{\bar{q}_j,\beta} = (\bar{f}^\dagger_{\bar{q}_j,\beta})^\dagger\,,$$
$$\hat{S}^\Phi_\beta = e^{\sum_{j=1}^{L_\beta} f^\dagger_{q_j+2\pi\,\Phi_\beta(q_j)/L,\beta} f_{q_j,\beta}}\,; \qquad \left(\hat{S}^\Phi_\beta\right)^\dagger = e^{\sum_{j=1}^{L_\beta} f^\dagger_{q_j-2\pi\,\Phi_\beta(q_j)/L,\beta} f_{q_j,\beta}}\,. \tag{58}$$

In these expressions $\hat{S}^\Phi_\beta$ is the β pseudoparticle–β pseudofermion unitary operator.

The c and $s1$ pseudofermions live on exactly the same c and $s1$ effective lattices, respectively, as the corresponding pseudoparticles. The canonical-momentum $\beta = c, s1$ pseudofermion operators, Eq. (58), are related to local $\beta = c, s1$ pseudofermion operators $\bar{f}^\dagger_{j',\beta}$ and $\bar{f}_{j',\beta}$. Those

create and annihilate, respectively, one $\beta = c, s1$ pseudofermion at the $\beta = c, s1$ effective lattice site $x_{j'} = a_\beta\, j'$. Here $j' = 1, ..., L_\beta$. The relation reads,

$$\bar{f}^{\dagger}_{\bar{q}_j,\beta} = \frac{1}{\sqrt{L}}\sum_{j'=1}^{L_{s1}} e^{i\,\bar{q}_j\,x_{j'}}\,\bar{f}^{\dagger}_{j',\beta}\,; \qquad \bar{f}_{\bar{q}_j,\beta} = \frac{1}{\sqrt{L}}\sum_{j'=1}^{L_{s1}} e^{-i\,\bar{q}_j\,x_{j'}}\,\bar{f}_{j',\beta}\,,$$
$$j = 1, ..., L_\beta\,, \qquad \beta = c, s1\,. \tag{59}$$

By combining Eq. (33) with Eq. (59) for $\beta = c$, the c pseudofermion operator, Eq. (58), can be formally expressed in terms of rotated-electron operators as,

$$\bar{f}^{\dagger}_{\bar{q}_j,c} = \frac{1}{\sqrt{L}}\sum_{j'=1}^{L} e^{+i\bar{q}_j\,j'}\left(\tilde{c}^{\dagger}_{j',\uparrow}\,(1-\tilde{n}_{j',\downarrow}) + (-1)^{j'}\,\tilde{c}_{j',\uparrow}\,\tilde{n}_{j',\downarrow}\right); \qquad \bar{f}_{\bar{q}_j,c} = (\bar{f}^{\dagger}_{\bar{q}_j,c})^{\dagger}\,. \tag{60}$$

On the one hand, the c pseudofermions have no internal structure. On the other hand, the $s1$ pseudofermions have exactly the same internal structure as the corresponding $s1$ pseudoparticles. They only differ in their discrete momentum values. Those rather refer to the translational degrees of freedom associated with their center of mass motion.

In the present pseudofermion operator representation, a PS ground state has the simple form,

$$|GS\rangle = \prod_{\bar{q}=-k_{F\downarrow}}^{k_{F\downarrow}}\prod_{\bar{q}'=-\pi}^{\pi}\bar{f}^{\dagger}_{\bar{q},\,s1}\,\bar{f}^{\dagger}_{\bar{q}',\,c}|0\rangle = \prod_{j=1}^{N_\downarrow}\prod_{j'=1}^{L}\bar{f}^{\dagger}_{\bar{q}_j,\,s1}\,\bar{f}^{\dagger}_{\bar{q}_{j'},\,c}|0\rangle\,. \tag{61}$$

That representation has been inherently constructed to $\bar{q} = q$ for a PS ground state. Indeed, for it the dressed phase-shift functional $2\pi\,\Phi_\beta(q_j)$, Eq. (49), vanishes. Hence here the $s1$ and c band momentum values $\bar{q} = q = \bar{q}_j = q_j$ and $\bar{q}' = q' = \bar{q}_{j'} = q_{j'}$, respectively, are those of the corresponding $s1$ and c pseudoparticle occupied ground-state Fermi seas. Moreover, $|0\rangle$ stands in Eq. (61) for the electron and rotated-electron vacuum. The ground-state generator onto that vacuum has been written in terms of $s1$ and c pseudofermion creation operators, Eqs. (58) and (59).

The c pseudofermions as defined here refer to an extension to finite u of the usual $u \to \infty$ spinless fermions [33,34,37] considered in the discussions of Section 2.2. Indeed, in the $u \to \infty$ limit the momentum rapidity function of the ground state $k^c_0(q_j)$ simplifies to $k^c_0(q_j) = q_j$. The use of the exact relation, Eq. (A.7) of Appendix A, then leads to $k^c(q_j) = \bar{q}_j$ for the PS excited energy eigenstates generated from the initial ground state under consideration. The $u \to \infty$ spinless fermions of Refs. [33,34] have been constructed inherently to carry such a momentum rapidity, $k_j = k^c(q_j) = \bar{q}_j$. This confirms that the spinless fermions are the c pseudofermions as defined here in the $u \to \infty$ limit. The relations $\bar{f}^{\dagger}_{\bar{q}_j,c} = \hat{V}^{\dagger}\,b^{\dagger}_{k_j}\,\hat{V}$ and $\bar{f}_{\bar{q}_j,c} = \hat{V}^{\dagger}\,b_{k_j}\,\hat{V}$ then hold. Here $\hat{V}$ is the electron–rotated-electron unitary operator defined in terms of its matrix elements in Eq. (11). Moreover, $b^{\dagger}_{k_j}$ and b_{k_j} stand for the $u \to \infty$ spinless fermions creation and annihilation operators that appear in the anti-commutators given in the first equation of Section IV of Ref. [34].

There is a one-to-one correspondence defined by Eq. (57) between a canonical momentum value $\bar{q}_j$ and the corresponding bare momentum value q_j. It enables the expression of several $\bar{q}_j$-dependent pseudofermion quantities in terms of the corresponding bare momentum q_j. This applies to the dressed phase shift $2\pi\,\Phi_{\beta,\beta'}(q_j, q_{j'})$, Eq. (47). Actually such a phase shift has a precise physical meaning within the pseudofermion representation: $2\pi\,\Phi_{\beta,\beta'}(q_j, q_{j'})$ (and

$-2\pi\,\Phi_{\beta,\beta'}(q_j,q_{j'}))$ is the phase shift acquired by a β pseudofermion or β pseudofermion hole of canonical momentum $\bar{q}_j=\bar{q}(q_j)$ upon scattering off a β' pseudofermion (and β' pseudofermion hole) of canonical momentum value $\bar{q}_{j'}=\bar{q}(q_{j'})$ created under a transition from the ground state to a PS excited energy eigenstate.

It then follows that the important functional $2\pi\,\Phi_\beta(q_j)$, Eq. (49), in the $\beta=c,s1$ canonical momentum expression $\bar{q}_j=q_j+\frac{2\pi}{L}\Phi_\beta(q_j)$, Eq. (57), is the phase shift acquired by a β pseudofermion or β pseudofermion hole of canonical momentum value $\bar{q}_j=\bar{q}(q_j)$ upon scattering off the set of β' pseudofermions and β' pseudofermion holes created under such a transition. Hence the β pseudofermion phase shift $2\pi\,\Phi_\beta(q_j)$ has a specific value for each ground-state–excited-state transition.

The expression of the σ one-electron UHB addition spectral function near its singular features has a contribution from the creation of a single $\eta1$ pseudoparticle at one of the $\eta1$ band limiting momentum values $q_j=\pm q_{\eta1}=\pm(\pi-2k_F)$, Eq. (39). $\eta1$ band canonical momentum values $\bar{q}_j=q_j+2\pi\,\Phi_{\eta1}(q_j)/L$ can be introduced, as in Eq. (57) for the $\beta=c,s1$ bands. Interestingly, one finds that $2\pi\,\Phi_{\eta1}(q_j)=0$ at the $\eta1$ band limiting momentum values $q_j=\pm(\pi-2k_F)$, so that $\bar{q}_j=q_j$. This reveals that an $\eta1$ pseudofermion with canonical momentum values $\bar{q}_j=\pm(\pi-2k_F)$ does not acquire phase shifts under transitions from the ground state to the PS excited energy eigenstates. This is as for the unpaired rotated spins $1/2$ and unpaired rotated η-spins $1/2$. This behavior follows from a symmetry associated with the invariance under the $\eta1$ pseudoparticle–$\eta1$ pseudofermion unitary transformation of an $\eta1$ pseudoparticle with momentum values $q_j=\pm(\pi-2k_F)$. An $\eta1$ pseudoparticle and an $\eta1$ pseudofermion of momenta $\pm(\pi-2k_F)$ are indeed the same quantum object. Such a symmetry is behind the vanishing at $q_j=\pm q_{\eta1}=\pm(\pi-2k_F)$ of the $\eta1$ pseudoparticle anti-binding energy $\varepsilon^0_{\eta1}(q_j)$ on the right-hand side of Eq. (51) for $\alpha n=\eta1$. The same applies to the corresponding $\eta1$ pseudofermion anti-binding energy $\varepsilon^0_{\eta1}(\bar{q}_j)$, which also vanishes at $\bar{q}_j=\pm(\pi-2k_F)$.

One can introduce a creation operator $f^\dagger_{q_j,\eta1}$ for the $\eta1$ pseudoparticles. At $q_j=\iota(\pi-2k_F)$ where $\iota=\pm1$ it is identical to the corresponding $\eta1$ pseudofermion creation operator,

$$\bar{f}^\dagger_{\bar{q}_j,\eta1}=f^\dagger_{q_j,\eta1}\ \text{at}\ \bar{q}_j=q_j=\iota(\pi-2k_F)\,,\qquad \iota=\pm1\,. \tag{62}$$

In the present case, $\bar{f}^\dagger_{\bar{q}_j,\eta1}$ creates one $\eta1$ pseudofermion at the canonical momentum values $\bar{q}_j=\pm(\pi-2k_F)$.

Such an $\eta1$ pseudofermion does not acquire phase shifts of its own. However, the $\beta=c,s1$ pseudofermions of canonical momentum $\bar{q}_j$ acquire a phase shift $2\pi\,\Phi_{\beta,\eta1}(q_j,\pm(\pi-2k_F))$, Eq. (47) for $\beta'=\eta1$ and $q_{j'}=\pm(\pi-2k_F)$. This occurs under that $\eta1$ pseudofermion creation within a transition from the ground state to a PS excited energy eigenstate. After some manipulations relying on the use of Eqs. (A.9) and (A.15) of Appendix A for $\eta n=\eta1$, one finds that it can be written as,

$$2\pi\,\Phi_{\beta,\eta1}(q_j,\pm(\pi-2k_F))=\pm\frac{1}{2}\left(\delta_{\beta,c}\,2\pi+2\pi\,\Phi_{\beta,c}(q_j,2k_F)-2\pi\,\Phi_{\beta,c}(q_j,-2k_F)\right),\quad \beta=c,s1\,,\qquad \iota=\pm1\,. \tag{63}$$

Except for the factor $1/2$, creation of one $\eta1$ pseudofermion at the canonical momentum values $\pm(\pi-2k_F)$ is thus felt by a $\beta=c,s1$ pseudofermion as the creation and annihilation of two c pseudofermions at opposite c band Fermi points, respectively.

The momentum dependent exponents that control the σ one-electron spectral weight in the (k,ω)-plane vicinity of a type of singular features called branch lines play an important role in the

PDT. As reported below in Section 3.3, the expression of these exponents involves pseudofermion phase shifts $2\pi\,\Phi_{c,\beta}(\pm 2k_F, q_j)$ and $2\pi\,\Phi_{s1,\beta}(\pm k_{F\downarrow}, q_j)$ where $\beta = c, s1$. Such phase shifts are acquired by c and $s1$ pseudofermions, respectively, at the corresponding Fermi points. They result though from high-energy processes within which one c or $s1$ pseudofermion is created or annihilated at a canonical momentum $\bar{q}_j = \bar{q}(q_j)$ associated with a momentum q_j outside the c or $s1$ Fermi points, respectively. Furthermore, such exponents expression also involves the following related $\gamma = 0, 1$ Fermi-points phase-shift parameters,

$$\xi^{\gamma}_{\beta\,\beta'} = \delta_{\beta,\beta'} + \sum_{\iota=\pm 1} (\iota)^{\gamma}\,\Phi_{\beta,\beta'}\left(q_{F\beta}, \iota q_{F\beta'}\right)\,, \qquad \beta,\beta' = c, s1\,, \qquad \gamma = 0, 1\,. \tag{64}$$

(For the particular case of $\beta = \beta'$ and $\iota = 1$ in Eq. (64), the present notation assumes that the two $\beta = c, s1$ Fermi momenta in the argument of the β pseudofermion phase shift, $2\pi\,\Phi_{\beta,\beta}(q_{F\beta}, q_{F\beta})$, differ by $2\pi/L$; For identical momentum values one has that $2\pi\,\Phi_{\beta,\beta}(q_j, q_j) = 0$.)

In the particular case of $\beta = c, s1$ pseudofermions with momentum $q_j = \iota q_{F\beta}$ at the $\iota = \pm 1$ Fermi points, the phase shift $2\pi\,\Phi_{\beta,\eta 1}(q_j, \iota'(\pi - 2k_F))$, Eq. (63), can be expressed in terms of the $\gamma = 1$ parameters, Eq. (64), as follows,

$$\Phi_{\beta,\eta 1}(\iota q_{F\beta}, \iota'(\pi - 2k_F)) = \iota'\frac{\xi^{1}_{\beta\,c}}{2}\,, \qquad \beta = c, s1\,, \qquad \iota,\iota' = \pm 1\,. \tag{65}$$

The pseudofermion phase-shift related anti-symmetrical $\xi^{1}_{\beta\,\beta'}$ and symmetrical $\xi^{0}_{\beta\,\beta'}$ parameters, Eq. (64), emerge naturally from the pseudofermion representation. Their limiting behaviors are given in Appendix B. They are actually the entries of the low-energy conformal-field theory dressed-charge matrix and of the transposition of its inverse matrix [14,15,40,57],

$$Z^1 = \begin{bmatrix} \xi^{1}_{c\,c} & \xi^{1}_{c\,s1} \\ \xi^{1}_{s1\,c} & \xi^{1}_{s1\,s1} \end{bmatrix}; \qquad Z^0 = ((Z^1)^{-1})^T = \begin{bmatrix} \xi^{0}_{c\,c} & \xi^{0}_{c\,s1} \\ \xi^{0}_{s1\,c} & \xi^{0}_{s1\,s1} \end{bmatrix}, \tag{66}$$

respectively. (Here the dressed-charge matrix definition of Ref. [14] has been used, which is the transposition of that of Ref. [15].)

As mentioned previously, for densities $n_e \in [0, 1[$ and $m \in [0, n_e]$ the PS excited energy eigenstates that contribute to the σ one-electron spectral functions expressions near their singularities are populated only by c and $s1$ pseudofermions. In case of the UHB one-electron addition, they are populated as well by a single $\eta 1$ pseudofermion of canonical momentum $\pm(\pi - 2k_F)$. For such PSs, the pseudoparticle representation general energy functional, Eq. (42), simplifies to,

$$\begin{aligned}\delta E = &\sum_{\beta=c,s1}\sum_{j=1}^{L_\beta}\varepsilon_\beta(q_j)\delta N_\beta(q_j) \\ &+ \frac{1}{L}\sum_{\beta=c,s1}\sum_{\beta'=c,s1,\eta 1}\sum_{j=1}^{L_\beta}\sum_{j'=1}^{L_{\beta'}}\frac{1}{2}\,f_{\beta\,\beta'}(q_j, q_{j'})\,\delta N_\beta(q_j)\delta N_{\beta'}(q_{j'}) + 2\mu\,N_{\eta 1}\,.\end{aligned} \tag{67}$$

Expression of this functional in the pseudofermion representation involves the $\beta = c, s1$ bands discrete canonical momentum values $\bar{q}_j = \bar{q}(q_j)$, Eq. (57). One finds after some algebra that in such a representation it reads up to $\mathcal{O}(1/L)$ order,

$$\delta E = \sum_{\beta=c,s1}\sum_{j=1}^{L_\beta}\varepsilon_\beta(\bar{q}_j)\,\delta\mathcal{N}_\beta(\bar{q}_j) + 2\mu\,N_{\eta 1}\,. \tag{68}$$

Here $\delta\mathcal{N}_\beta(\bar{q}_j) = \delta N_\beta(q_j)$ and the $\beta = c, s1$ pseudofermion energy dispersions $\varepsilon_\beta(\bar{q}_j)$ have exactly the same form as those given in Eq. (45) with the momentum q_j replaced by the corresponding canonical momentum, $\bar{q}_j = \bar{q}(q_j)$.

The pseudofermion energy functional, Eq. (68), can be expressed in terms of the momentum q_j upon expanding the $\beta = c, s1$ band canonical momentum $\bar{q}_j = q_j + 2\pi\,\Phi_\beta(q_j)/L$ around q_j and considering all energy contributions up to $\mathcal{O}(1/L)$ order. Upon performing such an expansion, one arrives after some algebra to the energy functional, Eq. (67). It includes terms of second order in the deviations $\delta N_\beta(q_j)$. Their absence from the corresponding energy spectrum, Eq. (68), follows from the $\beta = c, s1$ pseudofermion phase shifts $2\pi\,\Phi_\beta(q_j)$, Eq. (49), being incorporated in the $\beta = c, s1$ band canonical momentum, Eq. (57).

That in contrast to the equivalent energy functional, Eq. (67), that in Eq. (68) has no energy interaction terms of second-order in the deviations $\delta\mathcal{N}_\beta(\bar{q}_j)$ has a deep physical meaning. It is that the $\beta = c, s1$ pseudofermions have no such interactions up to $\mathcal{O}(1/L)$ order. Within the present TL, only finite-size corrections up to that order are relevant for the spectral functions expressions. The property that the excitation energy spectrum, Eq. (68), has no pseudofermion energy interactions is found below to simplify the expression of the σ one-electron spectral functions. They can be expressed in terms of a sum of convolutions of c and $s1$ pseudofermion spectral functions. Moreover, the spectral weights of the latter spectral functions can be expressed as Slater determinants of pseudofermion operators.

3.2. Expression of the σ one-electron problem in terms of pseudofermion operators

Within the PDT of Refs. [39,40], the $\beta = c, s1$ pseudofermion phase shifts control the dynamical correlation functions spectral-weight distributions. Here we provide additional specific information relative to that given in these references about how that dynamical theory accounts for the matrix elements $\langle \nu^-|\, c_{k,\sigma}\,|GS\rangle$ and $\langle \nu^+|\, c^\dagger_{k,\sigma}\,|GS\rangle$ in the one-electron spectral functions, Eq. (4), for the model at finite magnetic field. For such spectral functions the elementary processes that generate the excited energy eigenstates from ground states with densities in the ranges $n_e \in [0, 1[$ and $m \in [0, n_e]$ can be classified into three classes (A)–(C):

(A) High-energy and finite-momentum elementary $\beta = c, s1$ pseudofermion processes. Specifically, creation or annihilation of one or a finite number of $\beta = c, s1$ pseudofermions with canonical momentum values $\bar{q}_j \neq \pm\bar{q}_{F\beta}$ outside the corresponding Fermi points;

(B) Finite-momentum processes of excitation energy zero that change the number of $\beta = c, s1$ pseudofermions at the $\iota = +1$ right and $\iota = -1$ left $\beta = c, s1$ Fermi points and finite-momentum processes of high energy 2μ that involve creation of one $\eta1$ pseudofermion at one of the limiting momenta $q^{\pm}_{\eta1} = \pm(\pi - 2k_F)$;

(C) Low-energy and small-momentum elementary pseudofermion particle–hole processes in the vicinity of the $\beta = c, s1$ bands right ($\iota = +1$) and left ($\iota = +1$) Fermi points, relative to the excited-state $\beta = c, s1$ pseudofermion momentum occupancy configurations generated by the above elementary processes (A) and (B).

The processes (B) of high energy 2μ contribute to the line shape near the σ one-electron UHB spectral function singular features. Their high excitation energy 2μ is the minimal energy for creation of one rotated-electron doubly occupied site. It stems from the first term of the spectrum $E_{\eta1}(q_j)$, Eq. (A.5) of Appendix A for $\alpha n = \eta1$. Such a spectrum is part of the $\eta1$ energy dispersion $\varepsilon_{\eta1}(q_j)$, Eq. (45) for $\beta = \eta1$. Such processes refer to transitions from ground

states with densities $n_e < 1$. For $n_e = 1$ initial ground states the σ one-electron UHB involves instead transitions to excited energy eigenstates populated by one unpaired rotated η-spin $1/2$ of η-spin projection $-1/2$. This also amounts for creation of one rotated-electron doubly occupied site.

The first two steps to express in the pseudofermion representation the matrix elements $\langle \nu^- | \, c_{k,\sigma} \, | GS \rangle$ and $\langle \nu^+ | \, c^\dagger_{k,\sigma} \, | GS \rangle$ in the spectral functions, Eq. (4), are: (i) To express the σ electron creation or annihilation operator in terms of σ rotated electron creation and annihilation operators, Eq. (5); (ii) To express the latter operators in terms of rotated spin $1/2$ operators, rotated η-spin $1/2$ operators, and c pseudofermion operators. This is accomplished by accounting for the relation between the c pseudoparticle and c pseudofermion operators, Eq. (58) for $\beta = c$. In addition one uses the σ rotated electron creation and annihilation operators expressions in terms of rotated spin $1/2$ operators, rotated η-spin $1/2$ operators, and c pseudoparticle operators, Eqs. (32) and (71).

The momentum k dependent σ electron operators in the spectral functions Lehmann representation, Eq. (4), are related to the corresponding local operators as,

$$c_{k,\sigma} = \frac{1}{\sqrt{L}} \sum_{j=1}^{L} e^{i\,k\,x_j} c_{j,\sigma} \, ; \qquad c^\dagger_{k,\sigma} = (c_{k,\sigma})^\dagger \, , \qquad \sigma = \uparrow, \downarrow \, . \tag{69}$$

To write the operators $c_{k,\sigma}$ and $c^\dagger_{k,\sigma}$ in terms of σ rotated electron creation and annihilation operators, Eq. (5), we use the Baker–Campbell–Hausdorff formula. This allows rewriting the relation, Eq. (5), as follows,

$$\begin{aligned}
c_{k,\sigma} &= \sum_{i=0}^{\infty} c_{k,\sigma,i} = \tilde{c}_{k,\sigma} + \frac{1}{1!}\,[\tilde{c}_{k,\sigma}, \tilde{S}\,] + \frac{1}{2!}\,[[\tilde{c}_{k,\sigma}, \tilde{S}\,], \tilde{S}\,] + \ldots \, ; \\
c^\dagger_{k,\sigma} &= (c_{k,\sigma})^\dagger \, , \qquad \sigma = \uparrow, \downarrow \, , \\
c_{k,\sigma,i} &= [\tilde{c}_{k,\sigma}, \tilde{S}\,]_i = \frac{1}{i!}[[\tilde{c}_{k,\sigma}, \tilde{S}\,]_{i-1}, \tilde{S}\,] \, , \qquad i = 1, \ldots, \infty \, ; \\
[\tilde{c}_{k,\sigma}, \tilde{S}\,]_0 &= \tilde{c}_{k,\sigma} = \hat{V}^\dagger \, c_{k,\sigma} \, \hat{V} \, , \\
\hat{V} &= e^{\hat{S}} = e^{\tilde{S}} \, .
\end{aligned} \tag{70}$$

Here the operator $\tilde{S} = \hat{S}$ commutes with $\hat{V}$ and thus has the same expression in terms of creation and annihilation rotated-electron operators and electron operators, respectively. Moreover, the momentum operators $\tilde{c}^\dagger_{k,\sigma} = \hat{V}^\dagger \, c^\dagger_{k,\sigma} \, \hat{V}$ and $\tilde{c}_{k,\sigma} = \hat{V}^\dagger \, c_{k,\sigma} \, \hat{V}$ can be written in terms of the local operators $\tilde{c}^\dagger_{j,\sigma}$ and $\tilde{c}_{j,\sigma}$, respectively, in Eqs. (5) and (32) as,

$$\tilde{c}^\dagger_{k,\sigma} = \frac{1}{\sqrt{L}} \sum_{j=1}^{L} e^{i\,k\,x_j} \tilde{c}^\dagger_{j,\sigma} \, ; \qquad \tilde{c}_{k,\sigma} = (\tilde{c}^\dagger_{k,\sigma})^\dagger \, , \qquad \sigma = \uparrow, \downarrow \, . \tag{71}$$

The next step of our program consists in rewriting the rotated-electron expression $c_{k,\sigma} = \sum_{i=0}^{\infty} c_{k,\sigma,i}$ within its uniquely defined β pseudofermion representation as,

$$c_{k,\sigma} = \sum_{i'=0}^{\infty} \hat{g}_{i'}(k) \, \hat{c}_{\odot} \, . \tag{72}$$

The new index $i' = 0, 1, ..., \infty$ refers here to β pseudofermions processes. Furthermore, $\hat{c}_{\odot}$ is a generator that transforms the initial ground state $|GS\rangle$ into a state with the same electron and rotated-electron numbers as the ground state of the final PS, which we call $|GS_f\rangle$. It has the same compact symmetrical c and $s1$ bands momentum occupancies as that ground state. The only difference between the states $\hat{c}_{\odot}|GS\rangle$ and $|GS_f\rangle$ lays in their c and $s1$ band discrete momentum values: They are those of the initial ground state, $\bar{q}' = q'$, and of the excited-energy eigenstate $\sum_{i'=0}^{\infty} \hat{g}_{i'}(k)|GS_f\rangle$, $\bar{q} \neq q$, respectively.

Each term of index $i' = 0, 1, ..., \infty$ in Eq. (72) may have contributions from several terms of different index $i = 0, 1, ..., \infty$ in $c_{k,\sigma} = \sum_{i=0}^{\infty} c_{k,\sigma,i}$, Eq. (70). Fortunately, one can compute the operational form in terms of β pseudofermion operators of the leading $i' = 0, 1, ..., \infty$ orders of $c_{k,\sigma} = \sum_{i'=0}^{\infty} \hat{g}_{i'}(k)\,\hat{c}_{\odot}$ from the transformation laws of the ground state $|GS\rangle$, Eq. (61). This is achieved upon action of the related operators $c_{k,\sigma,i}$ in the expression $c_{k,\sigma} = \sum_{i=0}^{\infty} c_{k,\sigma,i}$ onto that state.

The 1D Hubbard model is a non-perturbative quantum problem in terms of σ electron processes. This is behind the computation of the one-electron spectral functions, Eq. (4), being a very complex many-electron problem. A property that plays key role in our study follows from expressing the electron operator $c_{k,\sigma}$ in the terms of pseudofermion operators as $c_{k,\sigma} = \sum_{i'=0}^{\infty} \hat{g}_{i'}(k)\,\hat{c}_{\odot}$, Eq. (72). Indeed, this renders the computation of the σ one-electron spectral functions, Eq. (4), a perturbative problem.

Note that both the expressions $c_{k,\sigma} = \sum_{i=0}^{\infty} c_{k,\sigma,i}$ and $c_{k,\sigma} = \sum_{i'=0}^{\infty} \hat{g}_{i'}(k)\,\hat{c}_{\odot}$ are not small-parameter expansions. Consistently, the perturbative character of the β pseudofermions processes refers to the spectral weight contributing to the spectral functions being dramatically suppressed upon increasing the number of corresponding elementary processes of classes (A) and (B). Those are generated by application onto the ground state, Eq. (61), of operators in $\sum_{i'=0}^{\infty} \hat{g}_{i'}(k)\,\hat{c}_{\odot}$ with an increasingly large value of the index $i' = 0, 1, ..., \infty$.

The perturbative character of the 1D Hubbard model upon expressing the σ electron creation or annihilation operators in the spectral functions, Eq. (4), in terms of pseudofermion operators follows from the exact energy eigenstates being generated by occupancy configurations of such pseudofermions. The non-perturbative character of the problem in terms of electrons results from their relation to the pseudofermions having as well a non-perturbative nature. It is qualitatively different from that of the electrons to the quasiparticles of a Fermi liquid.

For simplicity, in the following we denote the $i' = 0$ operator $\hat{g}_0(k)$ associated with the σ one-electron operator $c_{k,\sigma}$ (or $c^{\dagger}_{k,\sigma}$) by $\hat{g}(k)$. Such an $i' = 0$ leading-order operator term in the one- or two-electron operator expression,

$$c_{k,\sigma} = \left(\hat{g}(k) + \sum_{i'=1}^{\infty} \hat{g}_{i'}(k)\right)\hat{c}_{\odot}\,, \tag{73}$$

plays a key role in our study.

In the present case, the leading-order operators $\hat{g}(k)\,\hat{c}_{\odot}$ are selected inherently to all the singular spectral features in the σ one-electron spectral functions, Eq. (4), being produced by their application onto the ground state. Here we list and define such leading-order pseudofermion processes (A) and (B). After being dressed by low-energy and small-momentum elementary $\beta = c, s1$ pseudofermion particle–hole processes (C) in the vicinity of their right ($\iota = +1$) and left ($\iota = +1$) Fermi points, they control the line shape near the singular features of the σ one-electron spectral functions, Eq. (4). Importantly, for the whole $u > 0$ range the creation or annihilation of one σ electron gives rise to the creation or annihilation, respectively, of *exactly*

one σ rotated electron. The leading-order pseudofermion processes (A) and (B) under consideration are the following:

(1) Removal of one $\uparrow$ electron is a process that involves the recombination of one c pseudofermion and one unpaired rotated spin $1/2$ of projection $\uparrow$. This leads to the emergence in the system of one $\uparrow$ rotated electron. It is annihilated under the $\uparrow$ electron removal. This process thus involves one c pseudofermion annihilation. It leads to a deviation $\delta N_c = -1$. The annihilation of the unpaired rotated spin $1/2$ of projection $\uparrow$ leaves the number N_{s1} $s1$ pseudofermions unchanged. It leads to a deviation $\delta N^h_{s1} = -1$ in the number of $s1$ band holes.

(2) LHB addition of one $\uparrow$ electron is a process that involves creation of one $\uparrow$ rotated electron. It separates into one c pseudofermion and one unpaired rotated spin $1/2$ of projection $\uparrow$. Hence $\delta N_c = 1$. The creation of the unpaired rotated spin $1/2$ leaves the number N_{s1} $s1$ pseudofermions unchanged. It gives rise to a deviation $\delta N^h_{s1} = 1$ in the number of $s1$ band holes.

(3) UHB addition of one $\uparrow$ electron is a process that involves combination of one c pseudofermion with one rotated spin $1/2$ of projection $\downarrow$. This gives rise to the emergence in the system of one $\downarrow$ rotated electron. The rotated spin $1/2$ originates from one $s1$ pseudofermion spin-singlet pair breaking. Such processes thus involve annihilation of one c pseudofermion and one $s1$ pseudofermion and creation of one unpaired rotated spin $1/2$ of projection $\uparrow$. As described below, one $\eta 1$ pseudofermion is also created. Hence $\delta N_c = -1$, $\delta N_{s1} = -1$, and $\delta N_{\eta 1} = 1$. The above emerging $\downarrow$ rotated electron pairs with the $\uparrow$ rotated electron that also emerges in the system under the $\uparrow$ electron creation. This gives rise to a rotated-electron doubly occupied site. The rotated η-spin $1/2$ of projection $-1/2$ that describes the η-spin degrees of freedom of such a doubly occupied site combines with one ground-state unpaired rotated η-spin $1/2$ of projection $+1/2$. This originates the $\eta 1$ pseudofermion and its η-spin-singlet pair. The creation of one unpaired rotated spin $1/2$ of projection $\uparrow$ leads to a deviation $\delta N^h_{s1} = 1$ in the number of $s1$ band holes.

(4) Removal of one $\downarrow$ electron is a process that involves the recombination of one c pseudofermion and one rotated spin $1/2$ of $\downarrow$ projection. This gives rise to the emergence in the system of one $\downarrow$ rotated electron. The rotated spin $1/2$ originates from one $s1$ pseudofermion spin-singlet pair breaking. Such processes thus involve annihilation of one c pseudofermion and one $s1$ pseudofermion and creation of one unpaired rotated spin $1/2$ of projection $\uparrow$. This leads to the deviations $\delta N_c = -1$ and $\delta N_{s1} = -1$. The annihilation of the emerging $\downarrow$ rotated electron gives rise to the $\downarrow$ electron removal. The creation of the rotated spin $1/2$ of projection $\uparrow$ leads to a deviation $\delta N^h_{s1} = 1$ in the number of $s1$ band holes.

(5) LHB addition of one $\downarrow$ electron is a process that involves the creation of one $\downarrow$ rotated electron. It separates into one c pseudofermion and one rotated spin $1/2$ of $\downarrow$ projection. The latter combines with one unpaired rotated spin $1/2$ of projection $\uparrow$. This gives rise to the formation of one $s1$ pseudofermion spin-singlet pair and annihilation of the unpaired rotated spin $1/2$ of projection $\uparrow$. The corresponding deviations thus read $\delta N_c = 1$ and $\delta N_{s1} = 1$. The annihilation of the unpaired rotated spin $1/2$ of projection $\uparrow$ leads to a deviation $\delta N^h_{s1} = -1$ in the number of $s1$ band holes.

(6) UHB addition of one $\downarrow$ electron is a process that involves the recombination of one c pseudofermion with one unpaired rotated spin $1/2$ of projection $\uparrow$. This gives rise to the emergence in the system of one $\uparrow$ rotated electron. That process thus involves the annihilation of one c pseudofermion and one unpaired rotated spin $1/2$ of projection $\uparrow$. As described in the following, it involves as well the creation of one $\eta 1$ pseudofermion. The corresponding deviations are

thus given by $\delta N_c = -1$ and $\delta N_{\eta 1} = 1$. The above emerging $\uparrow$ rotated electron pairs with the $\downarrow$ rotated electron that also emerges in the system as a result of the $\downarrow$ electron creation. This gives rise to a doubly occupied site. The rotated η-spin $1/2$ of projection $-1/2$ that describes the η-spin degrees of freedom of such a doubly occupied site combines with one ground-state unpaired rotated η-spin $1/2$ of projection $+1/2$. This originates the creation of one $\eta 1$ pseudofermion η-spin singlet pair. The annihilation of one unpaired rotated spin $1/2$ leaves the number N_{s1} $s1$ pseudofermions unchanged. It leads to a deviation $\delta N^h_{s1} = -1$ in the number of $s1$ band holes.

The above elementary processes involving $s1$ pseudofermion pair breaking and $s1$ pseudofermion pair formation are behind the squeezed $s1$ effective lattice and corresponding $s1$ momentum band being exotic. Their number of sites and discrete momentum values, respectively, both given by $L_{s1} = N_{s1} + N^h_{s1}$, have different values for different subspaces. Hence within the $s1$ pseudofermion operator algebra one distinguishes two types of variations in the number of $s1$-band holes: The $s1$-band holes created and annihilated by processes that conserve the number $L_{s1} = N_{s1} + N^h_{s1}$, under which one $s1$ pseudofermion is annihilated and created, respectively; The $s1$-band holes created and annihilated by processes that do not conserve the number $L_{s1} = N_{s1} + N^h_{s1}$. (For $S_s > 0$ states such exotic L_{s1} variations only lead to N^h_{s1} variations.)

The former processes are described by application of the operators $\bar{f}_{\bar{q},s1}$ and $\bar{f}^{\dagger}_{\bar{q},s1}$, respectively, onto the initial state. The processes leading to the latter N^h_{s1} variations that do not conserve $L_{s1} = N_{s1} + N^h_{s1}$ result from vanishing energy and vanishing momentum processes. Under such processes discrete momentum values are added to and removed from one of the $s1$ band limiting momentum values $q^{\pm}_{s1}$, Eq. (24) for $\alpha n = s1$. Whether such an addition or removal occurs at the left limiting momentum q^{-}_{s1} or at right limiting momentum q^{+}_{s1} is uniquely defined. Only one of these two choices leaves invariant the $s1$ band symmetrical relation $q^{+}_{s1} = -q^{-}_{s1}$ for the final state. Such a relation must hold for all energy eigenstates.

In the present cases of (i) $\uparrow$ one-electron removal processes (1) and $\downarrow$ one-electron UHB addition processes (6) and (ii) $\uparrow$ one-electron LHB addition processes (2) a single discrete momentum value is (i) removed from and (ii) added to, respectively, the $s1$ band limiting momentum values. Such vanishing energy and vanishing momentum processes are implicitly accounted for by the pseudofermion representation. This occurs through the $s1$ band discrete momentum values of the final states, which are uniquely defined.

In the following we derive the expression of the leading-order operators $\hat{g}(k)\,\hat{c}_{\odot}$, Eq. (73), in terms of c and $s1$ pseudofermion operators for the processes (1), (2), (4), and (5). In the case of the σ one-electron UHB addition processes (3) and (6), they are expressed in terms of c, $s1$, and $\eta 1$ pseudofermion operators. This is achieved by the use of the transformation laws of the ground state, Eq. (61), upon acting onto it with the $i = 0, 1, ..., \infty$ operators on the right-hand side of the equation, $c_{k,\sigma} = \sum_{i=0}^{\infty} c_{k,\sigma,i}$ (and $c^{\dagger}_{k,\sigma} = \sum_{i=0}^{\infty} c^{\dagger}_{k,\sigma,i}$), whose first terms are given in Eq. (70).

Within the PDT, the σ electron creation and annihilation operators are approximated by the corresponding pseudofermion representation leading-order terms, $\hat{g}(k)\,\hat{c}_{\odot}$. This is justified by the perturbative nature of that representation. It ensures that the use of such leading-order terms provides the correct expressions of the corresponding σ one-electron spectral functions near their singular features.

In the case of the $\uparrow$ one-electron removal processes (1), one finds the following leading-order operator expression,

$$
\begin{aligned}
&c_{k,\uparrow} \approx \hat{g}_\iota(k)\,\hat{c}_\odot\,, \\
&\hat{c}_\odot = \bar{f}_{\pm 2k_F,c}\,; \qquad \Phi_c^0 = 0\,; \qquad \Phi_{s1}^0 = \iota/2\,, \qquad \iota = \pm 1\,, \\
&\hat{g}_\iota(k) = \bar{f}^\dagger_{\bar{q}(\pm 2k_F),c}\,\bar{f}_{\bar{q}(\iota k_{F\downarrow}),s1} \sum_{q=-2k_F}^{2k_F} \Theta(k_{F\downarrow} - |k+q|)\,\bar{f}_{\bar{q}(q),c}\,\bar{f}^\dagger_{\bar{q}(k+q),s1}\,. \qquad (74)
\end{aligned}
$$

The shift parameters Φ_β^0 are here those in Eq. (41) for $\beta = c, s1$ and $\bar{q}(q) = q + 2\pi\,\Phi_\beta(q)/L$. The capital-$\Theta$ distribution $\Theta(x)$ is given in this expression and in the following by $\Theta(x) = 1$ for $x \geq 0$ and $\Theta(x) = 0$ for $x < 0$. A momentum $\mp k_{F\downarrow}$ results from the $s1$ pseudofermion annihilation at $\bar{q}(\pm k_{F\downarrow})$. It exactly cancels the momentum $\pm k_{F\downarrow}$ stemming from the overall $s1$ band momentum shift $q_j \rightarrow q_j \pm \pi/L$. The latter results from $\Phi_{s1}^0 = \pm 1/2$ in Eq. (74) for the transitions under consideration.

Within a k extended zone scheme, the $\omega < 0$ spectrum generated by application of the $\uparrow$ one-electron removal leading-order generator, Eq. (74), onto the ground state reads $-\omega = -\varepsilon_c(q) + \varepsilon_{s1}(k+q)$. It has two branches whose spectra are of the form,

$$
\begin{aligned}
&-\omega(k) = -\varepsilon_c(q) + \varepsilon_{s1}(q')\,; \qquad k = -q + q'\,, \\
&\quad k \in [-k_{F\uparrow}, (2k_F + k_{F\uparrow})]\,; \quad q \in [-2k_F, 2k_F]\,; \quad q' \in [k_{F\downarrow}, k_{F\uparrow}]\,, \quad \text{branch } A\,, \\
&\quad k \in [-(2k_F + k_{F\uparrow}), k_{F\uparrow}]\,; \quad q \in [-2k_F, 2k_F]\,; \quad q' \in [-k_{F\uparrow}, -k_{F\downarrow}]\,, \quad \text{branch } B\,. \qquad (75)
\end{aligned}
$$

In the case of the $\uparrow$ one-electron LHB addition processes (2), the leading-order operator is given by,

$$
\begin{aligned}
&c^\dagger_{k,\uparrow} \approx \hat{g}_\iota(k)\,\hat{c}_\odot\,, \\
&\hat{c}_\odot = \bar{f}^\dagger_{\pm 2k_F,c}\,; \qquad \Phi_c^0 = 0\,; \qquad \Phi_{s1}^0 = \iota/2\,, \qquad \iota = \pm 1\,, \\
&\hat{g}_\iota(k) = \bar{f}_{\bar{q}(\pm 2k_F),c}\,\bar{f}^\dagger_{\bar{q}(-\iota k_{F\downarrow}),s1} \Big(\sum_{q=-\pi}^{-2k_F} + \sum_{q=2k_F}^{\pi} \Big)\,\Theta(k_{F\downarrow} - |k-q|)\,\bar{f}^\dagger_{\bar{q}(q),c}\,\bar{f}_{\bar{q}(-k+q),s1}\,. \qquad (76)
\end{aligned}
$$

A momentum $\mp k_{F\downarrow}$ results from the $s1$ pseudofermion creation at $\bar{q}(\mp k_{F\downarrow})$. It exactly cancels again the momentum $\pm k_{F\downarrow}$ stemming from an overall $s1$ band momentum shift $q_j \rightarrow q_j \pm \pi/L$.

The $\omega > 0$ spectrum generated by application of the $\uparrow$ one-electron LHB addition leading-order generator, Eq. (76), onto the ground state reads $\omega = \varepsilon_c(q) - \varepsilon_{s1}(k-q)$. Within a k extended zone scheme, it has again two branches. Their spectra are of the form,

$$
\begin{aligned}
&\omega(k) = \varepsilon_c(q) - \varepsilon_{s1}(q')\,; \qquad k = q - q'\,, \\
&\quad k \in [k_{F\uparrow}, (\pi + k_{F\downarrow})]\,; \quad q \in [2k_F, \pi]\,; \quad q' \in [-k_{F\downarrow}, k_{F\downarrow}]\,, \quad \text{branch } A\,, \\
&\quad k \in [-(\pi + k_{F\downarrow}), -k_{F\uparrow}]\,; \quad q \in [-\pi, -2k_F]\,; \quad q' \in [-k_{F\downarrow}, k_{F\downarrow}]\,, \quad \text{branch } B\,. \qquad (77)
\end{aligned}
$$

In the case of the $\uparrow$ one-electron UHB addition processes (3), the leading-order operator reads,

$$
\begin{aligned}
&c^\dagger_{k,\uparrow} \approx \hat{g}_\iota(k)\,\hat{c}_\odot\,, \\
&\hat{c}_\odot = \bar{f}_{\iota 2k_F,c}\,\bar{f}_{\pm k_{F\downarrow},s1}\,\bar{f}^\dagger_{-\iota(\pi - 2k_F),\eta 1}\,; \qquad \Phi_c^0 = \Phi_{s1}^0 = 0\,, \qquad \iota = \pm 1\,,
\end{aligned}
$$

$$\hat{g}_{\iota}(k) = \bar{f}^{\dagger}_{\bar{q}(\iota 2k_F),c}\, \bar{f}^{\dagger}_{\bar{q}(\pm k_{F\downarrow}),s1} \sum_{q=-2k_F}^{2k_F} \Theta(k_{F\downarrow} - |k - \iota\,(\pi - 2k_F) + q|) \times \bar{f}_{\bar{q}(q),c}\, \bar{f}_{\bar{q}(-k+\iota\,(\pi-2k_F)-q),s1}\,. \quad (78)$$

In this case one has $N_{\eta 1}(q_j) = 1$ where $q_j = -\iota(\pi - 2k_F)$ and $M_{\eta,-1/2} = 1$ for the excited energy eigenstates in the general momentum expression, Eq. (21). The momentum $\pi\, M_{\eta,-1/2} = \pi$ then combines with $(\pi - q_j)\, N_{\eta 1}(q_j) = \pi - q_j$. This gives $2\pi - q_j = -q_j = \iota(\pi - 2k_F)$.

Within a k extended zone scheme, the $\omega > 0$ spectrum generated by application of the $\uparrow$ one-electron UHB addition leading-order generator, Eq. (78), onto the ground state reads $\omega = 2\mu - \varepsilon_c(q) - \varepsilon_{s1}(k - \iota\,(\pi - 2k_F) + q)$. It has two branches associated with the two values of the index $\iota = \pm 1$. Their spectra are of the form,

$$\begin{aligned}
&\omega(k) = 2\mu - \varepsilon_c(q) - \varepsilon_{s1}(q')\,; \\
&\quad k = \iota(\pi - 2k_F) - q - q'\,; \quad q \in [-2k_F, 2k_F]\,; \quad q' \in [-k_{F\downarrow}, k_{F\downarrow}]\,, \\
&\quad k = (\pi - 2k_F) - q - q' \in [(\pi - 4k_F - k_{F\downarrow}), (\pi + k_{F\uparrow})]\,, \quad \text{branch } A\,, \\
&\quad k = -(\pi - 2k_F) - q - q' \in [-(\pi + k_{F\uparrow}), -(\pi - 4k_F - k_{F\downarrow})]\,, \quad \text{branch } B\,. \quad (79)
\end{aligned}$$

In the case of the $\downarrow$ one-electron removal processes (4), the leading-order operator is given by,

$$\begin{aligned}
&c_{k,\downarrow} \approx \hat{g}_{\iota}(k)\, \hat{c}_{\odot}\,, \\
&\hat{c}_{\odot} = \bar{f}_{\iota\, 2k_F,c}\, \bar{f}_{-\iota k_{F\downarrow},s1}\,; \quad \Phi^0_c = \iota/2\,; \quad \Phi^0_{s1} = 0\,, \quad \iota = \pm 1\,, \\
&\hat{g}_{\iota}(k) = \bar{f}^{\dagger}_{\bar{q}(\iota\, 2k_F),c}\, \bar{f}^{\dagger}_{\bar{q}(-\iota k_{F\downarrow}),s1} \sum_{q=-2k_F}^{2k_F} \Theta(k_{F\downarrow} - |k - \iota\, 2k_F + q|) \\
&\qquad \times \bar{f}_{\bar{q}(q),c}\, \bar{f}_{\bar{q}(-k+\iota\, 2k_F - q),s1}\,. \quad (80)
\end{aligned}$$

The operator $\bar{f}_{\iota\, 2k_F,c}$ in $\hat{c}_{\odot}$ leads to a momentum $-\iota 2k_F$. On the one hand, it exactly cancels the momentum $\iota 2k_F$ stemming from the overall c band momentum shift associated with $\Phi^0_c = \iota/2$. On the other hand, the operator $\bar{f}^{\dagger}_{\bar{q}(\iota\, 2k_F),c}$ in $\hat{g}_{\iota}(k)$ leads to a momentum contribution that restores such a momentum $\iota 2k_F$.

The $\omega < 0$ spectrum generated by application of the $\downarrow$ one-electron removal leading-order generator, Eq. (80), onto the ground state reads $-\omega = -\varepsilon_c(q) - \varepsilon_{s1}(k - \iota\, 2k_F + q)$. It has two branches associated with the two values of the index $\iota = \pm 1$ whose spectra are of the form,

$$\begin{aligned}
&\omega(k) = -\varepsilon_c(q) - \varepsilon_{s1}(q')\,; \quad k = \iota\, 2k_F - q - q'\,; \\
&\quad q \in [-2k_F, 2k_F]\,; \quad q' \in [-k_{F\downarrow}, k_{F\downarrow}]\,, \\
&\quad k = 2k_F - q - q' \in [-k_{F\downarrow}, (4k_F + k_{F\uparrow})]\,, \quad \text{branch } A\,, \\
&\quad k = -2k_F - q - q' \in [-(4k_F + k_{F\uparrow}), k_{F\downarrow}]\,, \quad \text{branch } B\,. \quad (81)
\end{aligned}$$

In the case of the $\downarrow$ one-electron LHB addition processes (5), the leading-order operator reads,

$$\begin{aligned}
&c^{\dagger}_{k,\downarrow} \approx \hat{g}_{\iota}(k)\, \hat{c}_{\odot}\,, \\
&\hat{c}_{\odot} = \bar{f}^{\dagger}_{-\iota\, 2k_F,c}\, \bar{f}^{\dagger}_{\iota k_{F\downarrow},s1}\,; \quad \Phi^0_c = \iota/2\,; \quad \Phi^0_{s1} = 0\,, \quad \iota = \pm 1\,,
\end{aligned}$$

$$\hat{g}_\iota(k) = \bar{f}_{\bar{q}(-\iota\,2k_F),c}\,\bar{f}_{\bar{q}(\iota k_{F\downarrow}),s1}$$
$$\times \Big(\sum_{q=-\pi}^{-2k_F} + \sum_{q=2k_F}^{\pi}\Big)\,\delta_{-\iota,\mathrm{sgn}\{k-\iota\,2k_F-q\}}\,\Theta(k_{F\uparrow} - |k-\iota\,2k_F-q|)$$
$$\times\,\Theta(|k-\iota\,2k_F-q| - k_{F\downarrow})\,\bar{f}^{\dagger}_{\bar{q}(q),c}\,\bar{f}^{\dagger}_{\bar{q}(k-\iota\,2k_F-q),s1}\,. \qquad (82)$$

Here and throughout this paper the sign distribution reads $\mathrm{sgn}\{x\} = 1$ for $x > 0$, $\mathrm{sgn}\{x\} = -1$ for $x < 0$, and $\mathrm{sgn}\{x\} = 0$ for $x = 0$. The operator $\bar{f}^{\dagger}_{-\iota\,2k_F,c}$ in the expression of the operator $\hat{c}_\odot$ leads to a momentum $-\iota 2k_F$. It exactly cancels the momentum $\iota 2k_F$ stemming from the c band overall momentum shift. The operator $\bar{f}_{\bar{q}(-\iota\,2k_F),c}$ in $\hat{g}_\iota(k)$ leads to a momentum contribution that restores such a momentum $\iota 2k_F$.

Within a k extended zone scheme, the $\omega > 0$ spectrum generated by application of the $\downarrow$ one-electron LHB addition leading-order generator, Eq. (82), onto the ground state reads $\omega = \varepsilon_c(q) + \varepsilon_{s1}(k-\iota\,2k_F-q)$. It has four branches. Their spectra are of the form,

$$\omega(k) = \varepsilon_c(q) + \varepsilon_{s1}(q')\,; \qquad k = \iota\,2k_F + q + q'\,; \qquad \mathrm{sgn}\{q'\} = -\iota \text{ for } q' \neq 0\,,$$
$$k = 2k_F + q + q' \in [(4k_F + k_{F\uparrow}), (\pi + 2k_F + k_{F\uparrow})]\,, \quad \text{branch } A\,,$$
$$q \in [2k_F, \pi]\,; \quad q' \in [k_{F\downarrow}, k_{F\uparrow}]\,,$$
$$k = 2k_F + q + q' \in [-(\pi - 2k_F - k_{F\downarrow}), k_{F\uparrow}]\,, \quad \text{branch } B\,,$$
$$q \in [-\pi, -2k_F]\,; \quad q' \in [k_{F\downarrow}, k_{F\uparrow}]\,,$$
$$k = -2k_F + q + q' \in [-(\pi + 2k_F + k_{F\uparrow}), -(4k_F + k_{F\uparrow})]\,, \quad \text{branch } A'\,,$$
$$q \in [-\pi, -2k_F]\,; \quad q' \in [-k_{F\uparrow}, -k_{F\downarrow}]\,,$$
$$k = -2k_F + q + q' \in [-k_{F\uparrow}, (\pi - 2k_F - k_{F\downarrow})]\,, \quad \text{branch } B'\,,$$
$$q \in [2k_F, \pi]\,; \quad q' \in [-k_{F\uparrow}, -k_{F\downarrow}]\,. \qquad (83)$$

In the case of the UHB addition of one $\downarrow$ electron processes (6), the leading-order operator is given by,

$$\hat{c}^{\dagger}_{k,\downarrow} \approx \hat{g}(k)\,\hat{c}_\odot\,,$$
$$\hat{c}_\odot = \bar{f}_{\iota\,2k_F,c}\,\bar{f}^{\dagger}_{-\iota(\pi-2k_F),\eta 1}\,; \qquad \Phi^0_c = \iota/2\,; \qquad \Phi^0_{s1} = \pm 1/2\,, \qquad \iota = \pm 1\,,$$
$$\hat{g}(k) = \bar{f}^{\dagger}_{\bar{q}(\iota\,2k_F),c}\,\bar{f}_{\bar{q}(\pm k_{F\downarrow}),s1}\sum_{q=-2k_F}^{2k_F}\Theta(k_{F\downarrow} - |k-\iota\,\pi+q|)\,\bar{f}_{\bar{q}(q),c}\,\bar{f}^{\dagger}_{\bar{q}(k-\iota\,\pi+q),s1}\,. \qquad (84)$$

The operator $\bar{f}_{\iota\,2k_F,c}$ in $\hat{c}_\odot$ leads to a momentum $-\iota 2k_F$. It exactly cancels the momentum $\iota 2k_F$ stemming from the c band overall momentum shift. The operator $\bar{f}^{\dagger}_{\bar{q}(\iota\,2k_F),c}$ in $\hat{g}_\iota(k)$ leads to a momentum contribution that restores such a momentum $\iota 2k_F$. The latter momentum is finally canceled by the momentum $-\iota 2k_F$ from the second term of the momentum $\iota(\pi - 2k_F)$. It stems from the operator $\bar{f}^{\dagger}_{-\iota(\pi-2k_F),\eta 1}$. As in the case of the $\uparrow$ one-electron UHB addition processes (3), Eq. (78), one has $N_{\eta 1}(q_j) = 1$ where $q_j = -\iota(\pi - 2k_F)$ and $M_{\eta,-1/2} = 1$ for the excited energy eigenstates in the general momentum expression, Eq. (21). The momentum $\pi\,M_{\eta,-1/2} = \pi$ then combines with $(\pi - q_j)\,N_{\eta 1}(q_j) = \pi - q_j$. This gives $2\pi - q_j = -q_j = \iota(\pi - 2k_F)$. Moreover, the momentum $\mp k_{F\downarrow}$ resulting from the $s1$ pseudofermion annihilation at $\bar{q}(\pm k_{F\downarrow})$ exactly cancels the momentum $\pm k_{F\downarrow}$ stemming from the $s1$ band overall momentum shift.

The $\omega > 0$ spectrum generated by application of the $\downarrow$ one-electron UHB addition leading-order generator, Eq. (84), onto the ground state reads $\omega = 2\mu - \varepsilon_c(q) + \varepsilon_{s1}(k - \iota\pi + q)$. Within a k extended zone scheme, it has two branches whose spectra are of the form,

$$\begin{aligned}
&\omega(k) = 2\mu - \varepsilon_c(q) + \varepsilon_{s1}(q')\,; \qquad k = \iota\pi - q + q' = \pi - q + q'\,, \\
&\quad k \in [(\pi - k_{F\uparrow}), (\pi + 2k_F + k_{F\uparrow})]\,; \\
&\qquad q \in [-2k_F, 2k_F]\,; \qquad q' \in [k_{F\downarrow}, k_{F\uparrow}]\,, \qquad \text{branch } A\,, \\
&\quad k \in [(\pi - 2k_F - k_{F\uparrow}), (\pi + k_{F\uparrow})]\,; \\
&\qquad q \in [-2k_F, 2k_F]\,; \qquad q' \in [-k_{F\uparrow}, -k_{F\downarrow}]\,, \qquad \text{branch } B\,.
\end{aligned} \tag{85}$$

On the one hand, the c and/or $s1$ pseudofermion momentum values $\pm 2k_F$ and $\pm k_{F\downarrow}$, respectively, in the operators $\hat{c}_{\odot}$ appearing in the above expressions belong to the initial ground state $\beta = c, s1$ band. On the other hand, the β pseudofermion momentum values $\bar{q}(q) = q + 2\pi\,\Phi_{\beta}(q)/L$ in the operators $\hat{g}(k)$ expressions belong to the excited energy eigenstates $\beta = c, s1$ bands.

3.3. The σ one-electron operators matrix elements between the ground state and the excited energy eigenstates and corresponding spectral functions in terms of $\beta = c, s1$ pseudofermion spectral functions

The σ one-electron spectral functions, Eq. (4), can be written in the pseudofermion representation as follows,

$$B_{\gamma}(k,\omega) = \sum_{i'=0}^{\infty}\sum_{\nu} |\langle\nu|\,\hat{g}_{i'}(k)\,\hat{c}_{\odot}|GS\rangle|^2\,\delta\Big(\omega - \gamma(E_{\nu} - E_{GS})\Big)\,, \qquad \gamma\,\omega > 0\,. \tag{86}$$

For simplicity, we have here omitted from $B_{\sigma,\gamma}(k,\omega)$ the label σ. The excited-state indices ν^- and ν^+ have been denoted generally by ν.

Following the properties reported in the previous section regarding the perturbative nature of the pseudofermion representation, one approximates the general spectral function, Eq. (86), by its pseudofermion leading-order term. It involves the operators given in Eqs. (74), (76), (78), (80), (82), and (84). This gives,

$$B_{\gamma}(k,\omega) \approx B^{\odot}_{\gamma}(k,\omega) = \sum_{\nu} |\langle\nu|\,\hat{g}(k)\,\hat{c}_{\odot}|GS\rangle|^2\,\delta\Big(\omega - \gamma(E_{\nu} - E_{GS})\Big)\,, \qquad \gamma\,\omega > 0\,. \tag{87}$$

Both the generator onto the electron vacuum of the initial ground state in Eq. (61) and the operator $\hat{c}_{\odot}$ in $\hat{c}_{\odot}|GS\rangle$ are written in terms of c and $s1$ pseudofermion creation and/or annihilation operators, Eqs. (58) and (59). Their discrete canonical momentum values equal the corresponding momentum values q_j, Eqs. (18) and (19), of that initial ground state. In the case of the σ one-electron UHB addition operators in Eqs. (78) and (84), the expression of the operator $\hat{c}_{\odot}$ includes as well an $\eta 1$ pseudofermion creation operator of canonical momentum $\pm(\pi - 2k_F)$.

Both the operator $\hat{g}(k)$ and the generators onto the electron vacuum of the excited energy eigenstates $|\nu\rangle$ are written in terms of c and $s1$ pseudofermion operators. Their discrete canonical momentum values $\bar{q}_j$, Eq. (57), are those of these excited energy eigenstates. A useful property is that there is *always* an exact excited energy eigenstate $|f_G\rangle$ of the final $N_{\sigma} \pm 1$ ground state $|GS_f\rangle$such that,

$$|f_G\rangle = \hat{g}(k)|GS_f\rangle\,. \tag{88}$$

In the case of the c and $s1$ bands, the two types of discrete canonical momentum values that correspond to the initial ground state and excited energy eigenstates, respectively, account for the Anderson orthogonality catastrophes [34,67]. They occur in these bands under the transitions to the excited energy eigenstates $|\nu\rangle$. On the one hand, such c and $s1$ bands Anderson orthogonality catastrophes are behind the exotic character of the quantum overlaps that control the one-electron spectral functions. On the other hand, the UHB one-electron operators matrix elements overlaps involving creation of one $\eta 1$ pseudofermion do not involve Anderson orthogonality catastrophes. Such overlaps are straightforwardly computed. This follows in part from the initial ground state not being populated by $\eta 1$ pseudofermions. A second reason is the symmetry behind the invariance of an $\eta 1$ pseudoparticle with band limiting momentum values $\pm(\pi - 2k_F)$ under the pseudoparticle–pseudofermion unitary transformation. Hence the corresponding $\eta 1$ pseudofermion canonical momentum has exactly the same values, $\pm(\pi - 2k_F)$. Indeed, such an $\eta 1$ pseudofermion does not acquire phase shifts under the transitions to the excited states.

The excitation $\hat{g}(k)\,\hat{c}_{\odot}|GS\rangle$ in the matrix elements of the spectral function expression, Eq. (87), has finite overlap with the corresponding specific energy eigenstate, Eq. (88). This gives,

$$\begin{aligned}\langle f_G|\,\hat{g}(k)\,\hat{c}_{\odot}|GS\rangle &= \langle GS_f^{\rm ex}|\hat{c}_{\odot}|GS\rangle \\ &= \langle 0|\prod_{\beta=c,s1}\bar{f}_{\bar{q}_{N_\beta^{\odot}},\beta}\ldots\bar{f}_{\bar{q}_2,\beta}\,\bar{f}_{\bar{q}_1,\beta}\,\bar{f}^{\dagger}_{q'_1,\beta}\,\bar{f}^{\dagger}_{q'_2,\beta}\ldots\bar{f}^{\dagger}_{q'_{N_\beta^{\odot}},\beta}|0\rangle \\ &= \langle 0|\prod_{\beta=c,s1}\bar{f}_{q'_{N_\beta^{\odot}},\beta}\ldots\bar{f}_{q'_2,\beta}\,\bar{f}_{q'_1,\beta}\,\bar{f}^{\dagger}_{\bar{q}_1,\beta}\,\bar{f}^{\dagger}_{\bar{q}_2,\beta}\ldots\bar{f}^{\dagger}_{\bar{q}_{N_\beta^{\odot}},\beta}|0\rangle^{*}\,. \end{aligned} \tag{89}$$

Here $1,...,N_\beta^{\odot}$ labels the occupied $\beta = c, s1$ band discrete canonical momentum values and $|GS_f^{\rm ex}\rangle$ is a state with the same c and $s1$ pseudofermion occupancy as $|GS_f\rangle$. Its $\beta = c, s1$ band discrete momentum values are though those of the excited energy eigenstate $|f_G\rangle = \hat{g}(k)|GS_f\rangle$.

On the one hand, the $\beta = c, s1$ bands discrete canonical momentum values $q'_1, q'_2, ..., q'_{N_\beta^{\odot}}$ in Eq. (89) equal the corresponding initial ground state discrete momentum values. On the other hand, $\bar{q}_1, \bar{q}_2, ..., \bar{q}_{N_\beta^{\odot}}$ are the discrete canonical momentum values of the excited energy eigenstate $|f_G\rangle$, Eq. (88). Since these two sets of discrete momenta have different values, an Anderson orthogonality catastrophe occurs. It is such that the excited energy eigenstates of general form,

$$\begin{aligned}|f_{G_C}\rangle &= \prod_{\beta=c,s1}\hat{g}_C(m_{\beta,+1},m_{\beta,-1})\,\hat{g}(k)|GS_f\rangle \\ &= \prod_{\beta=c,s1}\hat{g}_C(m_{\beta,+1},m_{\beta,-1})\,|f_G\rangle\,, \qquad \beta = c,s1\,, \qquad \iota = \pm 1\,, \end{aligned} \tag{90}$$

also have overlap with the excitation $\hat{g}(k)\,\hat{c}_{\odot}|GS\rangle$. These states are originated by the application onto the state $|f_G\rangle$, Eq. (88), of the $\beta = c, s1$ generators $\hat{g}_C(m_{\beta,+1}, m_{\beta,-1})$ of the low-energy and small-momentum processes (C).

One then finds,

$$\begin{aligned}&\langle f_G|\prod_{\beta=c,s1}\hat{g}^{\dagger}_C(m_{\beta,+1},m_{\beta,-1})\hat{g}(k)\,\hat{c}_{\odot}|GS\rangle = \langle GS_f^{\rm ex}|\prod_{\beta=c,s1}\hat{g}^{\dagger}_C(m_{\beta,+1},m_{\beta,-1})\hat{c}_{\odot}|GS\rangle \\ &= \langle 0|\prod_{\beta=c,s1}\bar{f}_{\bar{q}_{N_\beta^{\odot}},\beta}\ldots\bar{f}_{\bar{q}_2,\beta}\,\bar{f}_{\bar{q}_1,\beta}\,\hat{g}^{\dagger}_C(m_{\beta,+1},m_{\beta,-1})\,\bar{f}^{\dagger}_{q'_1,\beta}\,\bar{f}^{\dagger}_{q'_2,\beta}\ldots\bar{f}^{\dagger}_{q'_{N_\beta^{\odot}},\beta}|0\rangle \\ &= \langle 0|\prod_{\beta=c,s1}\bar{f}_{q'_{N_\beta^{\odot}},\beta}\ldots\bar{f}_{q'_2,\beta}\,\bar{f}_{q'_1,\beta}\,\hat{g}^{\dagger}_C(m_{\beta,+1},m_{\beta,-1})\,\bar{f}^{\dagger}_{\bar{q}_1,\beta}\,\bar{f}^{\dagger}_{\bar{q}_2,\beta}\ldots\bar{f}^{\dagger}_{\bar{q}_{N_\beta^{\odot}},s1}|0\rangle^{*}\,. \end{aligned} \tag{91}$$

The number of elementary $\beta = c, s1$ pseudofermion–pseudofermion-hole processes (C) of momentum $\pm 2\pi/L$ in the vicinity of the $\beta; \iota = \pm 1$ Fermi points of $|GS_f\rangle$ is denoted here and in the following by $m_{\beta,\iota} = 1, 2, 3, ...$ Such processes conserve the number $N^{\odot}_{\beta}$ of $\beta = c, s1$ pseudofermions. Hence the matrix elements, Eq. (91), have the same form as that in Eq. (89). Their excited-state occupied discrete canonical momentum values $\bar{q}_1, \bar{q}_2, ..., \bar{q}_{N^{\odot}_{\beta}}$ in the vicinity of the $\beta = c, s1$ bands Fermi points are though slightly different from those in that equation.

The function $B^{\odot}(k,\omega)$, Eq. (87), is below expressed in terms of a sum of terms. Each of them is a convolution of c and $s1$ pseudofermion spectral functions. The expression of such pseudofermion spectral functions involves sums that run over the processes (C) numbers $m_{\beta,\iota} = 1, 2, 3, ...$ It reads,

$$B_{Q_\beta}(k',\omega') = \frac{L}{2\pi} \sum_{m_{\beta,+1};m_{\beta,-1}} A^{(0,0)}_{\beta}\, a_\beta(m_{\beta,+1},\, m_{\beta,-1})\delta\Big(\omega' - \frac{2\pi}{L}\, v_\beta \sum_{\iota=\pm 1} (m_{\beta,\iota} + \Delta^{\iota}_{\beta})\Big)$$
$$\times\, \delta\Big(k' - \frac{2\pi}{L} \sum_{\iota=\pm 1} \iota\, (m_{\beta,\iota} + \Delta^{\iota}_{\beta})\Big)\,, \qquad \beta = c, s1\,. \tag{92}$$

The $\beta = c, s1$ *lowest peak weights* $A^{(0,0)}_{\beta}$ appearing here are associated with a transition from the ground state to a PS excited energy eigenstate generated by processes (A) and (B). The corresponding $\beta = c, s1$ relative weights $a_\beta = a_\beta(m_{\beta,+1},\, m_{\beta,-1})$ are generated by additional processes (C). Their $\beta = c, s1$ generators $\hat{g}_C(m_{\beta,+1}, m_{\beta,-1})$ are those in Eq. (90). The quantity Δ^{ι}_{β} in Eq. (92) refers to a functional given by $2\Delta^{\iota}_{\beta} = (\iota\delta N^{F}_{\beta,\iota} + \Phi_\beta(\iota q_{F\beta}))^2$. That functional involves the $\beta = c, s1$ pseudofermion number deviation $\delta N^{F}_{\beta,\iota}$ at the $\iota = \pm 1$ Fermi points and corresponding phase shift $2\pi\, \Phi_\beta(\iota q_{F\beta})$, Eq. (49), in units of 2π. These phase shifts are acquired by the $\beta = c, s1$ pseudofermions with momenta $\iota q_{F\beta} = \pm q_{F\beta}$ under the above transition. This functional plays a key role in the PDT. It is found below to emerge naturally in the $\beta = c, s1$ pseudofermion spectral weights.

In the case of σ one-electron UHB addition, the $\beta = c, s1$ weights $A^{(0,0)}_{\beta}\, a_\beta(m_{\beta,+1},\, m_{\beta,-1})$ in Eq. (92) are reached after the quantum overlap stemming from creation of the $\eta 1$ pseudofermion is trivially computed. For all the σ one-electron removal, LHB addition, and UHB addition processes that contribute to the spectral functions in the vicinity of their singular features the $\beta = c, s1$ weights $A_\beta = A^{(0,0)}_{\beta}\, a_\beta(m_{\beta,+1},\, m_{\beta,-1})$ have the general form,

$$A_\beta = |\langle 0|\bar{f}_{q'_{N^{\odot}_{\beta}},\beta} ... \bar{f}_{q'_2,\beta}\, \bar{f}_{q'_1,\beta}\, \bar{f}^{\dagger}_{\bar{q}_1,\beta}\, \bar{f}^{\dagger}_{\bar{q}_2,\beta} ... \bar{f}^{\dagger}_{\bar{q}_{N^{\odot}_{\beta}},\beta}|0\rangle|^2\,, \qquad \beta = c, s1\,. \tag{93}$$

Here $N^{\odot}_{\beta}$ stands for the number of $\beta = c, s1$ pseudofermions of the excited energy eigenstate generated by the processes (A) and (B). Such matrix element square can be expressed in terms of a Slater determinant of $\beta = c, s1$ pseudofermion operators, Eqs. (58) and (59), as follows,

$$A_\beta = \left|\left| \begin{array}{cccc} \{\bar{f}^{\dagger}_{\bar{q}_1,\beta}, \bar{f}_{q'_1,\beta}\} & \{\bar{f}^{\dagger}_{\bar{q}_1,\beta}, \bar{f}_{q'_2,\beta}\} & \cdots & \{\bar{f}^{\dagger}_{\bar{q}_1,\beta}, \bar{f}_{q'_{N^{\odot}_{\beta}},\beta}\} \\ \{\bar{f}^{\dagger}_{\bar{q}_2,\beta}, \bar{f}_{q'_1,\beta}\} & \{\bar{f}^{\dagger}_{\bar{q}_2,\beta}, \bar{f}_{q'_2,\beta}\} & \cdots & \{\bar{f}^{\dagger}_{\bar{q}_2,\beta}, \bar{f}_{q'_{N^{\odot}_{\beta}},\beta}\} \\ \cdots & \cdots & \cdots & \cdots \\ \{\bar{f}^{\dagger}_{\bar{q}_{N^{\odot}_{\beta}},\beta}, \bar{f}_{q'_1,\beta}\} & \{\bar{f}^{\dagger}_{\bar{q}_{N^{\odot}_{\beta}},\beta}, \bar{f}_{q'_2,\beta}\} & \cdots & \{\bar{f}^{\dagger}_{\bar{q}_{N^{\odot}_{\beta}},\beta}, \bar{f}_{q'_{N^{\odot}_{s1}},\beta}\} \end{array} \right|\right|^2, \qquad \beta = c, s1\,. \tag{94}$$

The matrix elements $\langle 0|\bar{f}_{q'_{N^{\odot}_{\beta}},\beta}\ldots\bar{f}_{q'_2,\beta}\,\bar{f}_{q'_1,\beta}\,\bar{f}^{\dagger}_{\bar{q}_1,\beta}\,\bar{f}^{\dagger}_{\bar{q}_2,\beta}\ldots\bar{f}^{\dagger}_{\bar{q}_{N^{\odot}_{\beta}},\beta}|0\rangle$ in Eq. (93) of the $\beta = c, s1$ pseudofermion operators are associated with the two factors of the product $\prod_{\beta=c,s1}$ in the matrix elements, Eq. (89).

The function $B^{\odot}_{\gamma}(k,\omega)$, Eq. (87), can be written as follows,

$$B^{\odot}_{\gamma}(k,\omega) = \sum_{\nu}\Theta\Big(\Omega-\delta\omega_{\nu}\Big)\,\Theta\Big(\delta\omega_{\nu}\Big)\,\Theta\left(|v_{\nu}|-v_{\bar{\beta}}\right)\breve{B}^{\odot}_{\nu}(\delta\omega_{\nu},v_{\nu})\,. \tag{95}$$

The summation $\sum_{\nu}$ runs here over excited energy eigenstates of the form given in Eq. (90), $|f_{GC}\rangle = \prod_{\beta=c,s1}\hat{g}_C(m_{\beta,+1},m_{\beta,-1})\,|f_G\rangle$, generated by processes (A), (B), and (C) with *exactly* the same values of the excitation momentum k and excitation energy ω.

The excitation energy and momentum of the corresponding excited energy eigenstates $|f_G\rangle$, Eq. (88), generated by processes (A) and (B) are given by,

$$\delta E^{\odot}_{\nu} = E^{\odot}_{\nu} - E_{GS} \geq 0\,; \qquad \delta P^{\odot}_{\nu} = P^{\odot}_{\nu} - P_{GS}\,, \tag{96}$$

respectively. Such states have finite quantum overlap with the excitation $\hat{g}(k)\,\hat{c}_{\odot}|GS\rangle$.

The spectra of the excited states $|f_{GC}\rangle$, Eq. (90), generated from those by processes (C), whose excitation momentum k and excitation energy ω are fixed under the summation $\sum_{\nu}$ in Eq. (95), read,

$$\begin{aligned}
&\delta E_{\nu} = \delta E^{\odot}_{\nu} + \delta\omega_{\nu} = \gamma\,\omega \geq 0\,; \qquad \delta P_{\nu} = \delta P^{\odot}_{\nu} + \delta k_{\nu} = k\,,\\
&\delta\omega_{\nu} = \gamma\,\omega - \delta E^{\odot}_{\nu} \in [0,\Omega]\,; \qquad \delta k_{\nu} = k - \delta P^{\odot}_{\nu} \in [0,\Omega/v_{\nu}]\,,\\
&\delta E^{\odot}_{\nu} = \gamma\,\omega - \delta\omega_{\nu} \in [\omega-\Omega,\Omega]\,; \qquad \delta P^{\odot}_{\nu} = k - \delta k_{\nu} \in [k-\Omega/v_{\nu},k]\,.
\end{aligned} \tag{97}$$

Here $\delta\omega_{\nu}$ and δk_{ν} are their excitation energy and momentum, respectively, relative to those of the corresponding states $|f_G\rangle$, Eq. (88). Their intervals given here are controlled by the processes (C) energy range Ω. Its value is self-consistently determined as that for which the corresponding velocity v_{ν},

$$v_{\nu} = \delta\omega_{\nu}/\delta k_{\nu}\,; \qquad v_{\bar{\beta}} = \min\{v_c, v_{s1}\}\,; \qquad v_{\beta} = \max\{v_c, v_{s1}\}\,, \tag{98}$$

remains nearly unchanged. The related $\beta = c, s1$ velocities $v_{\bar{\beta}}$ and v_{β} in Eq. (95) are also defined here in terms of the $\beta = c, s1$ Fermi velocities v_c and v_{s1}, Eq. (48). For each fixed values of k and ω, the summation $\sum_{\nu}$ in Eq. (95) runs over excited energy eigenstates $|f_G\rangle$, Eq. (88), generated by processes (A) and (B). Their excitation energy and momentum vary under such a summation in corresponding intervals $\delta E^{\odot}_{\nu} \in [\omega-\Omega,\Omega]$ and $\delta P^{\odot}_{\nu} \in [k-\Omega/v_{\nu},k]$, respectively, as given in Eq. (97).

The lack of c and $s1$ pseudofermion interaction terms in the PS finite-u energy spectrum, Eq. (68), enables the function $\breve{B}^{\odot}_{\nu}(\delta\omega_{\nu},v_{\nu})$ in Eq. (95) being expressed as the following convolution of c and $s1$ pseudofermion spectral functions, Eq. (92),

$$\breve{B}^{\odot}_{\nu}(\delta\omega_{\nu},v_{\nu}) = \frac{\mathrm{sgn}(v_{\nu})}{2\pi}\int_{0}^{\delta\omega_{\nu}}d\omega'\int_{-\mathrm{sgn}(v_{\nu})\delta\omega_{\nu}/v_{\beta}}^{+\mathrm{sgn}(v_{\nu})\delta\omega_{\nu}/v_{\beta}}dk'\,B_{Q_{\bar{\beta}}}(\delta\omega_{\nu}/v_{\nu}-k',\delta\omega_{\nu}-\omega')\,B_{Q_{\beta}}(k',\omega')\,. \tag{99}$$

Here $\bar{\beta} = c, s1$ and $\beta = s1, c$, respectively, are chosen according to the criterion, Eq. (98), concerning the relative magnitudes of the two c and $s1$ Fermi velocities, Eq. (48).

The spectral-function matrix-element overlap associated with the creation of one $\eta 1$ pseudofermion of canonical momentum $\pm(\pi - 2k_F)$ is non-interacting like. Its creation leads to contributions 2μ and $\mp(\pi - 2k_F)$ to the excitation energy and excitation momentum spectra $\delta E^{\odot}$ and $\delta P^{\odot}$, Eq. (96), respectively.

The Slater determinant of $\beta = c, s1$ pseudofermion operators, Eq. (94), involves the pseudofermion anti-commutators. The apparent simplicity of such a Slater determinant masks the complexity of the main technical problem of the PDT. It lays in performing the state summations in the spectral functions Lehmann representation, Eq. (4). As discussed in the following, that problem stems from the involved form of such anti-commutators and thus of the corresponding Slater determinants of $\beta = c, s1$ pseudofermion operators.

The unitarity of the pseudoparticle–pseudofermion transformation implies that the local $\beta = c, s1$ pseudofermion operators $\bar{f}^{\dagger}_{j',\beta}$ and $\bar{f}_{j',\beta}$ in Eq. (59) obey the following fermionic algebra,

$$\{\bar{f}^{\dagger}_{j,\beta}, \bar{f}_{j',\beta}\} = \delta_{j,j'}\,, \qquad \beta = c, s1\,. \tag{100}$$

It is similar to that in Eqs. (34) and (37) for the corresponding local $\beta = c, s1$ pseudoparticle operators.

Consider two $\beta = c, s1$ pseudofermions of canonical momentum $\bar{q}_j$ and $\bar{q}_{j'}$, respectively. Here $\bar{q}_j$ and $\bar{q}_{j'} = q_{j'}$ refer to the $\beta = c, s1$ bands of a PS excited energy eigenstate and the corresponding ground state, respectively. The $\beta = c, s1$ pseudofermion phase-shift functional $2\pi\,\Phi_\beta(q_j)$, Eq. (49), is incorporated in the canonical momentum, Eq. (57). One then straightforwardly finds from the use of Eqs. (59) and (100) that the anti-commutator of $\bar{f}^{\dagger}_{j',\beta}$ and $\bar{f}_{j',\beta}$ reads,

$$\{\bar{f}^{\dagger}_{\bar{q}_j,\beta}, \bar{f}_{\bar{q}_{j'},\beta}\} = \frac{1}{L_\beta}\, e^{-i(\bar{q}_j - \bar{q}_{j'})/2}\, e^{i\,2\pi\,\Phi^T_\beta(q_j)/2}\, \frac{\sin\left(2\pi\,\Phi^T_\beta(q_j)/2\right)}{\sin([\bar{q}_j - \bar{q}_{j'}]/2)}\,;$$
$$\Phi^T_\beta(q_j) = \Phi^0_\beta + \Phi_\beta(q_j)\,, \qquad \beta = c, s1\,, \tag{101}$$

whereas $\{\bar{f}^{\dagger}_{\bar{q}_j,\beta}, \bar{f}^{\dagger}_{\bar{q}_{j'},\beta}\} = \{\bar{f}_{\bar{q}_j,\beta}, \bar{f}_{\bar{q}_{j'},\beta}\} = 0$. Here $2\pi\,\Phi^T_\beta(q_j)$ is the overall phase shift acquired by a $\beta = c, s1$ pseudofermion of momentum q_j under the transition from the ground state to the PS excited energy eigenstate. The quantities $2\pi\,\Phi^0_\beta$, Eq. (41), and $2\pi\,\Phi_\beta(q_j)$, Eq. (49), are the corresponding non-scattering and scattering part, respectively, of that phase shift.

For $2\pi\,\Phi^T_\beta(q_j) \to 0$ the anti-commutator relation, Eq. (101), would be the usual one, $\{f^{\dagger}_{\bar{q}_j,\beta}, f_{q_{j'},\beta}\} = \delta_{\bar{q}_j,\bar{q}'_j}$. That such an anti-commutator relation has not that simple form is the price to pay to render the $\beta = c, s1$ pseudofermions without interaction terms in their energy spectrum, Eq. (68). This is achieved by incorporating the β pseudofermion scattering phase shift $2\pi\,\Phi_\beta(q_j)$, Eq. (49), in the $\beta = c, s1$ band canonical momentum, Eq. (57). As confirmed below, the unusual form, Eq. (101), of that anti-commutator relation is behind such a scattering phase shift controlling the spectral weight distributions of the σ one-electron spectral functions, Eq. (4).

The unitarity of the pseudoparticle–pseudofermion transformation would preserve the pseudoparticle operator algebra provided that the sets of $\beta = c, s1$ band $j = 1, ..., L_\beta$ and $j' = 1, ..., L_\beta$ canonical momentum values $\{\bar{q}_j\}$ and $\{\bar{q}_{j'}\}$, respectively, were the same. The exotic form of the anti-commutator, Eq. (101), follows from $\bar{q}_j$ and $\bar{q}_{j'}$ corresponding to different sets of slightly shifted canonical momentum values. This is due to the shakeup effects introduced by the state-dependent $\beta = c, s1$ pseudofermion phase-shift functional $2\pi\,\Phi^T_\beta(q_j)$, Eq. (101).

The derivation of the $\beta = c, s1$ spectral weights $A_\beta = A_\beta^{(0,0)}\, a_\beta(m_{\beta,+1}, m_{\beta,-1})$ in the $\beta = c, s1$ pseudofermion spectral functions, Eq. (92), proceeds much as for the corresponding $u \to \infty$ spinless fermion spectral function in Ref. [34]. Following the procedures of such a reference, after some algebra that involves the use of the pseudofermion operators anti-commutators, Eq. (101), in the pseudofermion operators Slater determinant representation of these weights, Eq. (94), one arrives to their expressions given in Eqs. (A.25)–(A.27) of Appendix A.

Also the corresponding computation of the one-electron spectral-weight (k, ω)-plane distributions follows steps similar to those used in Ref. [34]. The PDT is indeed an extension to finite u of the method used in that reference for $u \to \infty$ [39]. Note though that the mapping to a Heisenberg chain used in that reference to deal with the spin part of the problem is valid only at $m = 0$ and $u \gg 1$. In our case for which u is finite and $m \in [0, n_e]$, the alternative use of the $s1$ pseudofermion representation renders the treatment of the corresponding rotated spins $1/2$ formally similar to that of the related c pseudofermion representation.

For $m_{\beta,\iota} = 1$, the four $\beta = c, s1$ and $\iota = \pm 1$ relative weights given in Eq. (A.27) of Appendix A play a key role in the one-electron spectral-weight distributions. They are actually the four functionals $2\Delta_\beta^\iota$ that appear in the c and $s1$ pseudofermion spectral function expression, Eq. (92). They read,

$$2\Delta_\beta^\iota \equiv a_{\beta,\iota}(1) = \left(\frac{\delta\bar{q}_{F\beta}^\iota}{(2\pi/L)}\right)^2 = \left(\iota\delta N_{\beta,\iota}^F + \Phi_\beta(\iota q_{F\beta})\right)^2 ,$$
$$\beta = c, s1\,, \qquad \iota = \pm 1\,. \tag{102}$$

They are merely the square of the $\beta = c, s1$ and $\iota = \pm 1$ Fermi canonical momentum deviations $\delta\bar{q}_{F\beta}^\iota = (\iota\, 2\pi\, \delta N_{\beta,\iota}^F + 2\pi\, \Phi_\beta(\iota q_{F\beta}))/L$ in units of $2\pi/L$. Here $\delta N_{\beta,\iota}^F = \delta N_{\beta,\iota}^{0,F} + \iota\, \Phi_\beta^0$ so that $\delta\bar{q}_{F\beta}^\iota = (\iota\, 2\pi\, \delta N_{\beta,\iota}^{0,F} + 2\pi\, \Phi_\beta^T(\iota q_{F\beta}))/L$. Such functionals are thus controlled by the $\beta = c, s1$ and $\iota = \pm 1$ Fermi-points pseudofermion scattering phase shifts $2\pi\, \Phi_\beta(\iota q_{F\beta})$, Eq. (49). The bare deviation $\delta N_{\beta,\iota}^{0,F}$ accounts for the number of $\beta = c, s1$ pseudofermions created or annihilated at the right ($\iota = +1$) and left ($\iota = +1$) $\beta = c, s1$ Fermi points. The overall deviation $\delta N_{\beta,\iota}^F$ accounts in addition to the effects of the non-scattering phase shifts Φ_β^0 on these Fermi points.

For the present one-electron problem at finite magnetic field only the c, $s1$, and $\eta 1$ pseudofermions have an active role. For more general PSs whose excited energy eigenstates are populated by c pseudofermions and composite αn pseudofermions belonging to a larger number of $\alpha = \eta, s$ and $n = 1, ..., \infty$ branches, the four $\beta = c, s1$ and $\iota = \pm 1$ functionals, Eq. (102), can be written as,

$$2\Delta_\beta^\iota = \left(\sum_{\beta'=c,s1}\left(\iota\,\xi^0_{\beta\,\beta'}\,\frac{\delta N^F_{\beta'}}{2} + \xi^1_{\beta\,\beta'}\,\delta J^F_{\beta'}\right)\right.$$
$$\left. + \sum_{\beta''=c,\alpha n}\sum_{j'=1}^{L_{\beta''}} \Phi_{\beta,\beta''}(\iota q_{F\beta}, q_{j'})\delta N^{NF}_{\beta''}(q_{j'})\right)^2 . \tag{103}$$

In this expression $\xi^0_{\beta\,\beta'}$ and $\xi^1_{\beta\,\beta'}$ are the $\beta = c, s1$ pseudofermion phase-shift parameters, Eq. (64), $\delta N^F_{\beta'} = \sum_{\iota=\pm1}\delta N_{\beta',\iota}$, and $\delta J^F_{\beta'} = \frac{1}{2}\sum_{\iota=\pm1}(\iota)\,\delta N_{\beta',\iota}$. The deviations $\delta N^{NF}_{\beta''}(q_{j'})$ refer to $\beta'' = c, \alpha n$ band momentum values $q_{j'}$, which for the $\beta'' = c, s1$ branches are away from

the $\beta'' = c, s1$ Fermi points. (The c and $s1$ pseudofermion creation or annihilation at and in the vicinity of such points is rather accounted for by the deviations $\delta N^F_{\beta'}$ and $\delta J^F_{\beta'}$ in Eq. (103).)

A property that in the present TL plays a key role in our derivation of the σ one-electron spectral weights is that the δ-functions in the $\beta = c, s1$ pseudofermion spectral function expression, Eq. (92), impose that,

$$\frac{L}{4\pi\, v_\beta}(\omega' + \iota\, v_\beta\, k') - \Delta^\iota_\beta = m_{\beta,\iota}\,, \qquad \beta = c, s1\,, \qquad \iota = \pm 1\,. \tag{104}$$

The first term in the expression of the quantity $((L/4\pi\, v_\beta)(\omega' + \iota\, v_\beta\, k') - \Delta^\iota_\beta)$ on the left-hand side of this equation is proportional to L and for the one-electron PS excited energy eigenstates its second term is of the order of the unity. Within the TL, this thus implies that for any arbitrarily small k' and ω' values for which $0 < (\omega' + \iota\, v\, k')/(4\pi\, v) \ll 1$ the corresponding values of the $\iota = \pm 1$ integer numbers $m_{\beta,\iota} = ((L/4\pi\, v_\beta)(\omega' + \iota\, v_\beta\, k') - \Delta^\iota_\beta)$ are such that $m_{\beta,\iota} \gg 1$. Hence the following asymptotic behavior of the β, ι relative weight, Eq. (A.27) of Appendix A, is *exact* within the TL,

$$a_{\beta,\iota}(m_{\beta,\iota}) \approx \frac{1}{\Gamma(2\Delta^\iota_\beta)}\Big(m_{\beta,\iota} + \Delta^\iota_\beta\Big)^{2\Delta^\iota_\beta - 1}\,;$$
$$2\Delta^\iota_\beta \neq 0\,, \qquad \beta = c, s1\,, \qquad \iota = \pm 1\,. \tag{105}$$

It is thus used in the derivation of the spectral-function expressions given below.

A relation also useful for such a derivation involves the $\beta = c, s1$ lowest peak weight $A^{(0,0)}_\beta$, Eq. (A.25) of Appendix A, in the $\beta = c, s1$ pseudofermion spectral function $B_{Q_\beta}(k', \omega')$, Eq. (92). It reads,

$$A^{(0,0)}_\beta = \frac{F^{(0,0)}_\beta}{(L\, S_\beta)^{-1+2\Delta^{+1}_\beta + 2\Delta^{-1}_\beta}}\,, \qquad \beta = c,\ s1\,. \tag{106}$$

Here $F^{(0,0)}_\beta$ and S_β are in the TL independent of L and $2\Delta^{+1}_c$, $2\Delta^{-1}_c$, $2\Delta^{+1}_{s1}$, and $2\Delta^{-1}_{s1}$ are the four functionals, Eq. (103). (The product $S_c \times S_{s1} \approx 1$ is given by 1 both in the $u \to 0$ and $u \to \infty$ limits.)

In the general case in which the four $\beta = c, s1$ and $\iota = \pm 1$ parameters $2\Delta^\iota_\beta$ are finite, one finds that the $\beta = c, s1$ pseudofermion spectral function $B_{Q_\beta}(k', \omega')$, Eq. (92), reads in the TL,

$$B_{Q_\beta}(k', \omega') = \frac{L}{4\pi\, v_\beta}\, A^{(0,0)}_\beta \prod_{\iota=\pm 1} a_{\beta,\iota}\Big(\frac{\omega' + \iota\, v_\beta\, k'}{4\pi\, v_\beta / L}\Big)$$
$$\approx \frac{F^{(0,0)}_\beta}{4\pi\, v_\beta\, S_\beta} \prod_{\iota=\pm 1} \frac{\Theta(\omega' + \iota\, v_\beta\, k')}{\Gamma(2\Delta^\iota_\beta)}\Big(\frac{\omega' + \iota\, v_\beta\, k'}{4\pi\, v_\beta\, S_\beta}\Big)^{-1+2\Delta^\iota_\beta}\,, \qquad \beta = c, s1\,. \tag{107}$$

To reach the second expression, which in the TL is exact, Eqs. (105) and (106) were used. The $\beta = c, s1$ pseudofermion spectral functions, Eq. (92), have a different form when $2\Delta^\iota_\beta > 0$ and $2\Delta^{-\iota}_\beta = 0$, as given in Eq. (A.28) of Appendix A. When $2\Delta^\iota_\beta = 2\Delta^{-\iota}_\beta = 0$ it is δ-function like, Eq. (A.29) of that Appendix.

3.4. The small higher-order pseudofermion contributions to the σ one-electron spectral weight

The pseudofermion representation spectral functions expression, Eq. (86), includes all higher-order processes that generate little σ one-electron spectral weight and do not contribute to the

line shape near singular spectral features studied in this paper. The PDT accounts for the corresponding contributions of ground-state transitions to excited energy eigenstates of general form,

$$|f_G(i')\rangle = \hat{g}_{i'}(k)|GS_f\rangle\,, \qquad i' = 0, 1, ..., \infty\,. \tag{108}$$

Those may be populated by αn pseudofermions of branches with $n > 1$ pairs. For finite values of the spin density, the small weight contribution from such transitions higher-order pseudofermion processes appear at high excitation energy scales. Such energies are of around $n\,2\mu_\alpha$, Eq. (44), for each $n > 1$ αn pseudofermion created onto the ground state.

As for the UHB $\eta 1$ pseudofermion creation, the contribution to the σ one-electron operators matrix elements of the creation of such composite αn pseudofermions is simpler to compute than that of the c and $s1$ pseudofermions. The c and αn pseudofermion operators in the expression of any $i' \geq 0$ operator $\hat{g}_{i'}(k)$ in the spectral function expression, Eq. (86), and energy eigenstate, Eq. (108), have discrete canonical momentum values that belong to the excited energy eigenstate c and αn bands. This is as for the c, $s1$, and $\eta 1$ pseudofermion operators in the expressions of the $i' = 0$ operators $\hat{g}_\iota(k)$ and $\hat{g}(k)$ given in Eqs. (74), (76), (78), (80), (82), and (84). One then finds that,

$$\langle f_G|\hat{g}_{i'}(k)\,\hat{c}_\odot|GS\rangle = \langle GS_f|\hat{g}^\dagger_{i'}(k)\,\hat{g}_{i'}(k)\,\hat{c}_\odot|GS\rangle = \langle GS_f^{\mathrm{ex(i')}}|\hat{c}_\odot|GS\rangle\,. \tag{109}$$

Here $|GS_f^{\mathrm{ex(i')}}\rangle$ is a state with the same c and $s1$ pseudofermion occupancy as $|GS_f\rangle$. Its c and $s1$ band discrete momentum values are those of its excited energy eigenstate $|f_G(i')\rangle = \hat{g}_{i'}(k)|GS_f\rangle$.

As for the UHB $\eta 1$ pseudofermion creation, that the σ one-electron matrix elements quantum overlaps resulting from the creation of $n > 1$ αn pseudofermions by the operators $\hat{g}^\dagger_{i'}(k)\,\hat{g}_{i'}(k)$ in Eq. (109) are non-interacting like is due in part to the lack of such occupancies in the ground states $|GS_f\rangle$ and $|GS\rangle$. Symmetry also plays a role in that behavior. Their creation is thus not associated with Anderson orthogonality catastrophes. After computing such trivial quantum overlaps, one is thus left with matrix elements $\langle GS_f^{\mathrm{ex(i')}}|\hat{c}_\odot|GS\rangle$, Eq. (109), that only involve c and $s1$ pseudofermion operators. Those have the same general form as that in Eq. (89). The same applies to higher-order additional $\beta = c, s1$ pseudofermion particle–hole processes of type (A) also generated by the operators $\hat{g}^\dagger_{i'}(k)\,\hat{g}_{i'}(k)$.

However, $|\langle GS_f^{\mathrm{ex(i')}}|\hat{c}_\odot|GS\rangle|$ strongly decreases upon increasing the index $i' = 0, 1, ..., \infty$. Most of the spectral weight is indeed associated with the $i' = 0$ matrix element $\langle GS_f^{\mathrm{ex(0)}}|\hat{c}_\odot|GS\rangle = \langle GS_f^{\mathrm{ex}}|\hat{c}_\odot|GS\rangle$, Eq. (89). As a result, the corresponding higher-order pseudofermion processes lead to very small σ one-electron spectral weight contributions. Moreover, the transitions to the excited energy eigenstates, Eq. (108), generated from the ground state by such higher-order pseudofermion processes do not contribute to the σ one-electron spectral weight in the vicinity of the singular features. And this is the issue studied in this paper.

3.5. The involved state summations problem and analytical expressions obtainable near the singularities

The numerical computation of the momentum and state summations in Eqs. (86) and (87) needed to access the corresponding finite-u spectral-weight distributions over the whole (k, ω) plane is a very involved technical problem.

On the one hand, this is a procedure that enormously simplifies in the $u \rightarrow \infty$ limit. The reason is that within it the c pseudofermion phase-shift functional $2\pi\,\Phi_c^T(q_j)$ defined by Eqs. (41), (49), and (101) becomes independent of q_j, being the quantity called $Q' - Q$ in Ref. [34]. This enables, in the case of the $u \rightarrow \infty$ and $m = 0$ one-electron removal and LHB addition spectral functions, the numerical computation of all state summations. The authors of Refs. [33,34] have performed that exercise. They obtained the beautiful one-electron spectral-weight distributions plotted in Fig. 1 of Ref. [33] for the whole (k,ω) plane, $u \gg 1$, $n_e = 0.5$, and $m = 0$.

On the other hand, for finite u values the $\beta = c, s1$ pseudofermion phase-shift functionals $2\pi\,\Phi_\beta^T(q_j)$ are both momentum q_j and densities n_e and m dependent. Moreover, they have different values for each excited energy eigenstate. Hence the numerical computation of the momentum and state summations needed to access the corresponding finite-u spectral-weight distributions over the whole (k,ω) plane becomes an extremely difficult technical task.

Fortunately, though, the use of Eq. (107) and Eqs. (A.28) and (A.29) of Appendix A for the β pseudofermion spectral function $B_{Q_\beta}(k',\omega')$, Eq. (92), in the function $\breve{B}_\nu^{\odot}(\delta\omega_\nu, v_\nu)$, Eq. (99), that appears in the expression of the spectral function leading-order term $B^{\odot}(k,\omega)$, Eq. (95), enables partially performing the summations in the latter equation. This applies to the (k,ω)-plane vicinity of most σ one-electron singular spectral features.

An important such a feature is a *branch line*. In the present case of the σ one-electron spectral functions, Eq. (4), the one-parametric branch lines that at least for some momentum interval correspond to a singular feature are all contained in the two-parametric spectra given in Eqs. (75), (77), (79), (81), (83), and (85). Those correspond to excited energy eigenstates generated by the leading-order pseudofermion processes.

Such a branch line results from transitions to a well-defined subclass of these excited energy eigenstates. Specifically, a particle and hole branch line is generated by creation of one $\beta = c, s1$ pseudofermion and one $\beta = c, s1$ pseudofermion hole, respectively, of canonical momentum $\bar{q} = \bar{q}(q)$. It corresponds to a well-defined β band momentum value q, as defined by Eq. (57). The set of such transitions scans the whole corresponding β band momentum range. For a $\beta = c$ branch line the c band momentum q runs in the intervals $q \in [-\pi, -2k_F]$ and $q \in [2k_F, \pi]$ for a particle branch line. It runs in the range $q \in [-2k_F, 2k_F]$ for a hole branch line. In the case of a $\beta = s1$ branch line, the $s1$ band momentum q runs in the ranges $q \in [-k_{F\uparrow}, -k_{F\downarrow}]$ and $q \in [k_{F\downarrow}, k_{F\uparrow}]$ for a particle branch line. It runs in the interval $q \in [-k_{F\downarrow}, k_{F\downarrow}]$ for a hole branch line.

In the case of a c and $s1$ branch line, an additional $s1$ pseudofermion or pseudofermion hole and c pseudofermion or pseudofermion hole, respectively, is also created under the transitions to the excited energy eigenstates. The branch line has a one-parametric spectrum contained in one of the two-parametric spectra given in Eqs. (75), (77), (79), (81), (83), and (85). This second pseudofermion or pseudofermion hole is thus added at one of the corresponding $\iota = \pm 1$ Fermi points. As given in Eqs. (78) and (84), in the case of σ one-electron UHB addition, one $\eta 1$ pseudofermion is also created at one of the $\eta 1$ band limiting momentum values, $q = \pm(\pi - 2k_F)$.

Such processes lead to a one-parametric (k,ω)-plane $\beta = c, s1$ branch line spectrum of the general form,

$$\omega_\beta^\sigma(k) = \omega_0 + \varepsilon_\beta(q)\,\delta N_\beta(q) \geq 0\,; \qquad k = k_0 + q\,\delta N_\beta(q)\,, \qquad \beta = c, s1\,. \tag{110}$$

Here $\sigma = \uparrow, \downarrow$ refers to the one-electron spectral function under consideration, $\varepsilon_\beta(q)$ is the $\beta = c, s1$ band energy dispersion, Eq. (45), and the deviation reads $\delta N_\beta(q) = +1$ and $\delta N_\beta(q) = -1$ for a particle and hole β branch line, respectively. The energy scale ω_0 and momentum k_0 in Eq. (110) are given by,

$$\omega_0 = 2\mu\,\delta N_{\eta 1}\,, \qquad \delta N_{\eta 1} = 0, 1\,,$$
$$k_0 = 4k_F\,\delta J_c^F + 2k_{F\downarrow}\,\delta J_{s1}^F + 2(\pi - 2k_F)\,\delta J_{\eta 1}\,, \tag{111}$$

respectively. The $\beta = c, s1$ current number deviations δJ_β^F in this equation are those in Eq. (103). On the one hand, the $\eta 1$ pseudofermion number and current number deviations vanish, $\delta N_{\eta 1} = \delta J_{\eta 1} = 0$, both for σ electron removal and σ electron LHB addition. On the other hand, $\delta N_{\eta 1} = 1$, $\delta J_{\eta 1} = -\frac{1}{2}\sum_{\iota=\pm 1}(\iota)\,\delta N_{\eta 1,\iota} = \mp 1/2$, and $\delta N_{\eta 1,\iota} = 1$ for σ electron UHB addition. The UHB creation of the $\eta 1$ pseudofermion occurs at one of the two $\iota = \pm 1$ limiting $\eta 1$ band momentum values $\iota(\pi - 2k_F)$.

In the case of the (k, ω)-plane region in the vicinity of a $\beta = c, s1$ branch line, the summation $\sum_\nu$ in the function $B^{\odot}(k,\omega)$ expression, Eq. (95), runs over excited energy eigenstates with corresponding k and ω values. For the small values of the energy deviation $(\gamma\,\omega - \omega_\beta^\sigma(k))$ the two $\beta = c, s1$ lowest peak weights $A_\beta^{(0,0)}$, Eq. (A.25) of Appendix A, have nearly the same magnitude for all states. The state summations can then be partially performed. The technical details of such summations are provided in Appendix B of Ref. [39]. In the case of the present σ one-electron excitations, they lead to the following general behavior in the vicinity of a $\beta = c, s1$ branch line,

$$B_{\sigma,\gamma}(k,\omega) = C_{\sigma,\gamma,\beta}\left(\gamma\,\omega - \omega_\beta^\sigma(k)\right)^{\xi_\beta^\sigma(k)}; \qquad (\gamma\,\omega - \omega_\beta^\sigma(k)) \geq 0\,, \qquad \gamma = \pm 1\,,$$
$$\xi_\beta^\sigma(k) = -1 + \sum_{\beta'=c,s1}\sum_{\iota=\pm 1} 2\Delta_{\beta'}^\iota(q)|_{q=(k-k_0)\delta N_\beta(q)}\,. \tag{112}$$

Here $C_{\sigma,\gamma,\beta}$ is an n_e, m, and u dependent constant that has a fixed value for the k and ω ranges corresponding to small values of the energy deviation $(\gamma\,\omega - \omega_\beta^\sigma(k))$. That is the range for which this expression is valid.

Near a $\beta = c, s1$ branch line, the four functionals, Eq. (103), depend on that line excitation momentum spectrum $k = k_0 \pm q$, Eq. (110). That dependence occurs through the $\beta = c, s1$ band momentum q. Those are the four $\beta' = c, s1$ and $\iota = \pm 1$ functionals $2\Delta_{\beta'}^\iota(q)$ in the exponent $\xi_\beta^\sigma(k)$ expression, Eq. (112). They have the following specific form for the excited energy eigenstates that control the one-electron spectral weight distribution near the $\beta = c, s1$ branch line,

$$2\Delta_{\beta'}^\iota(q) = \left(\sum_{\beta''=c,s1}\left(\iota\,\xi^0_{\beta'\,\beta''}\,\frac{\delta N_{\beta''}^F}{2} + \xi^1_{\beta'\,\beta''}\,\delta J_{\beta''}^F\right) + \xi^1_{\beta'\,c}\,\delta J_{\eta 1}\right.$$
$$\left. + \Phi_{\beta'\,\beta}(\iota 2k_F, q)\,\delta N_\beta^{NF}(q)\right)^2, \qquad \text{for}\ \ \beta' = c, s1\ \ \text{and}\ \ \iota = \pm 1\,. \tag{113}$$

Here $\delta N_\beta^{NF}(q) = +1$ and $\delta N_\beta^{NF}(q) = -1$ for a particle and hole $\beta = c, s1$ branch line, respectively. The momentum q is outside the $\beta = c, s1$ Fermi points. In the case of one-electron UHB addition for which $\delta J_{\eta 1} = \mp 1/2$ in Eq. (113), the phase shift $\Phi_{\beta'',\eta 1}(\iota q_{F\beta''}, \pm(\pi - 2k_F))$ was expressed as $\Phi_{\beta'',\eta 1}(\iota q_{F\beta''}, \pm(\pi - 2k_F)) = \pm\xi^1_{\beta''\,c}/2$ by direct use of the relation, Eq. (65).

In addition to the parameter,

$$\gamma = -1 \qquad \text{for electron removal}\,,$$
$$= +1 \qquad \text{for electron addition}\,, \tag{114}$$

the σ one-electron spectra associated with the singular spectral features considered in Section 4 involve a second parameter γ_σ and the use of the symbol $\bar{\sigma}$. Those are given by,

$$\gamma_\uparrow = +1\,; \qquad \bar{\uparrow} = \downarrow\,,$$
$$\gamma_\downarrow = -1\,; \qquad \bar{\downarrow} = \uparrow\,. \tag{115}$$

The expression of the one-electron spectral functions near the branch lines, Eq. (112), is a high-energy problem beyond the reach of the techniques associated with the low-energy Tomonaga–Luttinger liquid [10–18]. In the limit of low-energy, the PDT describes though the well-known behaviors predicted by such techniques. This refers specifically to the vicinity of (k,ω)-plane points $(k_0, 0)$.

Here we consider expressions of the one-electron spectral functions in the vicinity of (k,ω)-plane points $(k_0, \gamma\omega_0)$. The Tomonaga–Luttinger liquid refers to a particular case of such expressions for which $\omega_0 = 0$. Near such points, the behavior of the $\sigma = \uparrow, \downarrow$ one-electron spectral function $B_{\sigma,\gamma}(k,\omega)$, Eq. (4), is [40],

$$B_{\sigma,\gamma}(k,\omega) \propto \Big(\gamma\,\omega - \omega_0\Big)^{\zeta^\sigma}\,, \quad (\gamma\,\omega - \omega_0) \geq 0\,,$$
$$\zeta^\sigma = -2 + \sum_{\beta'=c,s1}\sum_{\iota=\pm 1} 2\Delta^\iota_{\beta'}\,, \quad (\gamma\,\omega - \omega_0) \neq \pm v_\beta\,(k - k_0)\,, \quad \beta = c, s1\,,$$
$$B_{\sigma,\gamma}(k,\omega) \propto \Big(\gamma\,\omega - \omega_0 \mp v_\beta\,(k - k_0)\Big)^{\zeta^\sigma_\pm}\,, \quad (\gamma\,\omega - \omega_0 \mp v_\beta\,(k - k_0)) \geq 0\,,$$
$$\zeta^\sigma_\pm = -1 - 2\Delta^{\mp 1}_\beta + \sum_{\beta'=c,s1}\sum_{\iota=\pm 1} 2\Delta^\iota_{\beta'}\,, \quad (\gamma\,\omega - \omega_0) \approx \pm v_\beta\,(k - k_0)\,,$$
$$\beta = c, s1\,. \tag{116}$$

In the case of these expressions, the form of the four $\beta = c, s1$ and $\iota = \pm 1$ functionals $2\Delta^\iota_\beta$, Eq. (103), is,

$$2\Delta^\iota_\beta = \left(\sum_{\beta'=c,s1}\left(\iota\,\xi^0_{\beta\,\beta'}\,\frac{\delta N^F_{\beta'}}{2} + \xi^1_{\beta\,\beta'}\,\delta J^F_{\beta'}\right) + \xi^1_{\beta\,c}\,\delta J_{\eta 1}\right)^2\,, \quad \text{for} \quad \beta = c, s1 \quad \text{and} \quad \iota = \pm 1\,. \tag{117}$$

The σ spectral function expressions, Eq. (116), apply to the small finite-weight region near and above ($\gamma = 1$) or below ($\gamma = -1$) the (k,ω)-plane point $(k_0, \gamma\omega_0)$. It corresponds to small values of the energy deviations $(\gamma\,\omega - \omega_0)$ and $(\gamma\,\omega - \omega_0 \mp v_\beta\,(k - k_0))$.

There is a third type of (k,ω)-plane feature in the vicinity of which the PDT provides an analytical expression of the one-electron spectral functions. It is generated by processes where one c pseudofermion or c pseudofermion hole is created at a momentum value q and one $s1$ pseudofermion or one $s1$ pseudofermion hole is created at a momentum value q'. Such a feature is a line in the (k,ω) plane. Indeed, the momentum values q and q' are not independent of each other. They are such that the corresponding group velocities, Eq. (48), obey the equality $v_c(q) = v_{s1}(q')$.

Such a one-parametric feature is called a c–$s1$ border line. Its (k,ω)-plane spectrum has the following form,

$$\omega^\sigma_{c-s1}(k) = \big(\omega_0 + |\epsilon_c(q)| + |\epsilon_{s1}(q')|\big)\,\delta_{v_c(q),\,v_{s1}(q')}\,;$$
$$k = k_0 + q\,\delta N_c(q) + q'\,\delta N_{s1}(q')\,. \tag{118}$$

Whether each of the deviations $\delta N_c(q)$ and $\delta N_{s1}(q')$ reads $+1$ or -1 is unrelated and is specific to the one-electron border line under consideration.

The σ one-electron spectral functions have the following behavior in the vicinity of such a c–$s1$ border line,

$$B_{\sigma,\gamma}(k,\omega) \propto \left(\gamma\,\omega - \omega^{\sigma}_{c-s1}(k)\right)^{-1/2}, \qquad (\gamma\,\omega - \omega^{\sigma}_{c-s1}(k)) \geq 0\,. \tag{119}$$

This expression is determined by the density of the two-parametric states generated upon varying q and q' within the corresponding c and $s1$ band values, respectively. A σ one-electron border line is part of the boundary line of the two-parametric spectra, Eqs. (75), (77), (79), (81), (83), and (85), (k,ω)-plane regions.

3.6. Relation to conformal-field theory and finite-size scaling

Conformal-field theory and corresponding finite-size scaling provide important information on the exact long-distance asymptotics of correlation functions [14–18]. For electronic density $n_e < 1$ and spin density $m \in [0, n_e]$, the 1D Hubbard model finite-size corrections are of the form given in Eq. (3.6) of Ref. [15]. The matrix Z, Eq. (3.9) of that reference, in such corrections is the transposition of the dressed-charge matrix Z^1, Eq. (66). Within our representation, the entries of both these matrices are superpositions of $\beta = c, s1$ pseudofermion phase shifts at the Fermi points, Eq. (64). The form of the 1D Hubbard model finite-size corrections found in Refs. [14,15] refers to a semiproduct of two independent Virasoro algebras, both having central charge equal to one. Consistently, these corrections can be written in terms of the conformal dimensions of the corresponding primary fields, as given in Eq. (3.11) of Ref. [15].

Importantly, the PDT four functionals $2\Delta_c^{\pm 1}$ and $2\Delta_{s1}^{\pm 1}$, Eq. (103), are a generalization of the conformal dimensions of $c, \pm$ and $s, \pm$ primary fields, respectively. For low-energy excitations, for which $\delta N^{NF}_{\beta''}(q') = 0$ for all $\beta' = c, \alpha n$ branches in these four functionals expression, Eq. (103), they *are* the conformal dimensions of such fields. The corresponding PDT low-energy correlation function expressions, Eq. (116) for $\omega_0 = 0$, exactly recover those given in Eq. (5.7) of Ref. [16]. The latter expressions have been derived in that reference by Fourier transform of long-distance asymptotics of correlation functions. Such long-distance asymptotics was obtained by use of conformal-field theory and associated finite-size scaling.

The emergence within the PDT of the high-energy deviations $\delta N^{NF}_{\beta''}(q')$ for one or more $\beta' = c, \alpha n$ branches in the four functionals $2\Delta_c^{\pm 1}$ and $2\Delta_{s1}^{\pm 1}$, Eq. (103), reveals actually that such a dynamical theory is a generalization of the conformal-field theory and corresponding finite-size scaling methods that applies *both* at low- and high-energy. In contrast, the latter methods are valid *only* at low energy. Indeed, the Fourier transform of long-distance asymptotics of correlation functions only captures the low-energy behavior of such functions.

The general one-electron spectral function expressions, Eqs. (112), (116), and (119), refer to the vicinity of both low-energy and high-energy spectral features. The four functionals $2\Delta_c^{\pm 1}(q)$ and $2\Delta_{s1}^{\pm 1}(q)$, Eq. (113), in the high-energy spectral function expressions near a branch line, Eq. (112), involve phase shifts acquired by c and $s1$ pseudofermions upon scattering off c or $s1$ pseudofermions created or annihilated *outside* the corresponding Fermi points. In contrast, the four conformal dimensions $2\Delta_c^{\pm 1}$ and $2\Delta_{s1}^{\pm 1}$ of $c, \pm$ and $s, \pm$ primary fields, respectively, Eq. (117) for $\delta J_{\eta 1} = 0$, in the low-energy correlation function expressions, Eq. (116) for $\omega_0 = 0$, only involve phase shifts acquired by c and $s1$ pseudofermions upon scattering off c or $s1$ pseudofermions created or annihilated *at* the corresponding Fermi points.

Besides going beyond the conformal-field theory and finite-size scaling methods by providing high-energy correlation function expressions, the PDT recovers the low-energy correlation-function expressions obtained by these methods, Eq. (116) for $\omega_0 = 0$. (Further detailed information on the relation of the PDT to conformal-field theory and corresponding finite-size scaling is found in Ref. [40].)

3.7. Validity of the one-electron spectral functions expressions near their singularities

The general behavior, $B(k,\omega) = C_\beta\,(\omega - \omega_\beta(k))^{\xi_\beta(k)}$, in the vicinity of $\beta = c, s1$ branch lines also occurs in the case of two-particle dynamical correlation functions $B(k,\omega)$. (For those, the convention is $\gamma = 1$ and thus $\omega \geq 0$.) However, such two-particle dynamical correlation functions expressions are exact provided that a condition is met: It is required that $B(k,\omega) = 0$ for $(\omega - \omega_\beta(k)) < 0$ for the k ranges for which the expression is valid. This means that for such k ranges the $\beta = c, s1$ branch line *must* coincide with a lower threshold of the (k,ω)-plane finite spectral-weight region [42].

The (k,ω)-plane spectral weight distribution of two-particle dynamical correlation functions is in general plateau-like. Consider k ranges of a branch line for which $B(k,\omega) > 0$ for $(\omega - \omega_\beta(k)) < 0$. In this case there is a coupling of the two-particle spectral weight just below the line with that generated by the processes that contribute to the weight distribution $B(k,\omega) = C_\beta\,(\omega - \omega_\beta(k))^{\xi_\beta(k)}$ when $B(k,\omega) = 0$ for $(\omega - \omega_\beta(k)) < 0$. Such a coupling changes the type of k and ω dependence of the two-particle dynamical correlation functions for small values of the deviations $(\omega - \omega_\beta(k)) > 0$. The microscopic processes behind such a coupling are accounted for by the PDT. However, performing the corresponding state summations needed to reach a simple analytical expression for $B(k,\omega)$ at small values of the deviations $(\omega - \omega_\beta(k)) > 0$ is a complex unsolved technical problem.

In the present case of the σ one-electron spectral functions $B_{\sigma,\gamma}(k,\omega)$, Eq. (4), it holds as well that the behavior, Eq. (112), in the vicinity of a $\beta = c, s1$ branch line is exact for k ranges for which such a line coincides with a lower threshold ($\gamma = 1$) or an upper threshold ($\gamma = -1$) of the (k,ω)-plane finite spectral-weight regions. Such regions are those of the corresponding two-parametric spectra, Eqs. (75), (77), (79), (81), (83), and (85). This requires again that $B_{\sigma,\gamma}(k,\omega) = 0$ for $\gamma\,\omega < \omega^\sigma_\beta(k)$.

The physically more important $\beta = c, s1$ branch line k ranges are those for which the exponent $\xi^\sigma_\beta(k)$, Eq. (112), is negative. For these ranges the line corresponds to a singular feature. On the one hand, if $B_{\sigma,\gamma}(k,\omega) = 0$ for small $(\gamma\,\omega - \omega^\sigma_\beta(k)) < 0$, the expression, Eq. (112), is exact in the vicinity of the $\beta = c, s1$ branch line for these k ranges. On the other hand, if $B_{\sigma,\gamma}(k,\omega) > 0$ for small $(\gamma\,\omega - \omega^\sigma_\beta(k)) < 0$ the spectral function expression in Eq. (112) is a good approximation in the vicinity of the $\beta = c, s1$ branch line for the k ranges under consideration.

This is in contrast to two-particle dynamical correlation functions. For k ranges of a one-electron $\beta = c, s1$ branch line for which $\xi^\sigma_\beta(k) < 0$ and $B_{\sigma,\gamma}(k,\omega) > 0$ for small $(\gamma\,\omega - \omega^\sigma_\beta(k)) < 0$, the difference stems from the relative amounts of spectral weight above and below the branch line. It turns out that in the case of the one-electron spectral functions the amount of weight in the vicinity of the branch line at $\gamma\,\omega > \omega^\sigma_\beta(k)$ is *much larger* than that near that line at $\gamma\,\omega < \omega^\sigma_\beta(k)$. Hence the coupling of the small latter weight to that at $\gamma\,\omega > \omega^\sigma_\beta(k)$ changes very little the one-electron spectral function expression near the branch line given in Eq. (112).

The processes that generate the small weight near a $\beta = c, s1$ branch line at $\gamma\,\omega < \omega^\sigma_\beta(k)$ are generated as well by a pseudofermion leading-order operator term. Depending on the σ one-electron spectral function under consideration, it is one of the operators given in Eqs. (74), (76),

(78), (80), (82), and (84). For the k ranges for which $B_{\sigma,\gamma}(k,\omega) > 0$ at $\gamma\,\omega < \omega^{\sigma}_{\beta}(k)$, the spectral function $B_{\sigma,\gamma}(k,\omega)$ remains having the power-law like behavior, Eq. (112), near the branch line for $\gamma\,\omega > \omega^{\sigma}_{\beta}(k)$. This holds provided that $\xi^{\sigma}_{\beta}(k) < 0$. The power-law like behavior survives for $\gamma\,\omega > \omega^{\sigma}_{\beta}(k)$ even if $0 < \xi^{\sigma}_{\beta}(k) < 1$.

Specifically, the line spectrum $\omega^{\sigma}_{\beta}(k)$, Eq. (110), remains insensitive to the coupling, which only slightly affects the value of the exponent $\xi^{\sigma}_{\beta}(k)$. Such an effect is small and very small when $0 < \xi^{\sigma}_{\beta}(k) < 1$ and $\xi^{\sigma}_{\beta}(k) < 0$, respectively, in Eq. (112). The theory includes actually a small k-dependent parameter,

$$\gamma_{\sigma,\gamma}(k) = \left(\frac{\int_{\omega^{\sigma}_{\beta}(k)-\Omega}^{\omega^{\sigma}_{\beta}(k)} B_{\sigma,\gamma}(k,\omega)\,d\omega}{\int_{\omega^{\sigma}_{\beta}(k)}^{\omega^{\sigma}_{\beta}(k)+\Omega} B_{\sigma,\gamma}(k,\omega)\,d\omega} \right)^{\gamma} , \qquad \gamma = \pm 1 . \tag{120}$$

Here Ω is the same energy scale that defines the energy range, $\delta\omega_{\upsilon} \in [0,\Omega]$, of the processes (C), Eq. (97). One can then expand the exponent expression in the small parameter $\gamma_{\sigma,\gamma}(k)$, Eq. (120). One finds that the exponent zeroth order leading term is $\xi^{\sigma}_{\beta}(k)$, as given in Eq. (112).

When $B_{\sigma,\gamma}(k,\omega) > 0$ for small $(\gamma\,\omega - \omega^{\sigma}_{\beta}(k)) < 0$, the k-dependent parameter $\gamma_{\sigma,\gamma}(k)$, Eq. (120), is extremely small and small for the k intervals for which $\xi^{\sigma}_{\beta}(k) < 0$ and $0 < \xi^{\sigma}_{\beta}(k) < 1$ in Eq. (112), respectively. The corresponding exponent corrections are also extremely small and small, respectively. Since they do not change the physics, for simplicity in the studies of Section 4 we use the leading-order exponent expression $\xi^{\sigma}_{\beta}(k)$, Eq. (112), for the $\beta = c, s1$ branch line k ranges for which $\xi^{\sigma}_{\beta}(k) < 1$. The otherwise very small or small exponent corrections exactly vanish for the $\beta = c, s1$ branch line k ranges for which $B_{\sigma,\gamma}(k,\omega) = 0$ for $\gamma\,\omega < \omega^{\sigma}_{\beta}(k)$.

Another condition that must be met for the σ one-electron spectral function expression near a $\beta = c, s1$ branch line, Eq. (112), to be valid is that $\xi^{\sigma}_{\beta}(k) > -1$. That for a given $\beta = c, s1$ branch line k range that exponent reads $\xi^{\sigma}_{\beta}(k) = -1$ means that the exact expression of the spectral function is not that given in Eq. (112). For these k ranges the four functionals $2\Delta^{\iota}_{\beta}$, Eq. (117) for $\beta = c, s1$ and $\iota = \pm 1$, all exactly vanish. This corresponds to the $\beta = c, s1$ pseudofermion spectral function form, Eq. (A.29) of Appendix A. One then finds that the corresponding σ one-electron spectral function behavior is also δ-function-like and given by,

$$B_{\sigma,\gamma}(k,\omega) = \delta\Big(\gamma\,\omega - \omega^{\sigma}_{\beta}(k)\Big) . \tag{121}$$

As expected, it is confirmed in the ensuing section that only as $u \rightarrow 0$ some $\beta = c, s1$ branch line exponents read $\xi^{\sigma}_{\beta}(k) = -1$. For the corresponding k momentum ranges, one recovers parts of the exact $u = 0$ σ one-electron spectrum. One indeed finds that the corresponding $u > 0$ spectrum $\omega^{\sigma}_{\beta}(k)$ on the right-hand side of Eq. (121) becomes in these cases the corresponding non-interacting electronic spectrum as $u \rightarrow 0$. This is found by the use of the $u \rightarrow 0$ limiting behaviors of the $\beta = c, s1$ energy dispersions $\varepsilon_{\beta}(q)$ appearing in the spectrum $\omega^{\sigma}_{\beta}(k)$, Eq. (110). Such limiting behaviors are reported in Eqs. (B.1) and (B.2) of Appendix B.

Furthermore, the branch-line exponent expression, Eq. (112), is not valid in its limiting k points when they coincide with boundary points (k_0,ω_0). In the (k,ω)-plane vicinity of such points, the line shape has rather the form given in Eqs. (116) and (117). The PDT naturally accesses such an alternative behavior. For σ electron removal and LHB addition it corresponds to the known low-energy behavior of the spectral function in the vicinity of (k,ω)-plane points $(k_0, 0)$. For the densities ranges $n_e \in [0, 1[$ and $m \in [0, n_e]$ considered here, the latter low-energy behavior is known. It coincides with that reported in Eq. (5.7) of Ref. [16]. Hence we restrict our study of Section 4 to the (k,ω)-plane vicinity of the high-energy one-electron spectral functions

singular features. The previous studies of high-energy one-electron spectral functions expressions of the 1D Hubbard model by means of the PDT [46–49] and most of those relying on other methods [44,45,50,51] have been limited to zero spin density. In contrast, the analysis of Section 4 is mainly focused on finite magnetic fields $h \in [0, h_c]$ and corresponding spin density interval $m \in [0, n_e]$.

The one-electron spectral functions behave near the border lines as given in Eq. (119). In the related cases of charge–charge and spin–spin two-particle dynamical correlation functions, the border line exponent $-1/2$ that results from the density of the two-parametric states is changed to $1/2$. This effect stems from the two-particle matrix elements between the ground state and the excited energy eigenstates. This always occurs when the two values q and q' and corresponding group velocities $v_\beta(q)$ and $v_\beta(q')$, such that $v_\beta(q) = v_\beta(q')$, belong to the same β band.

In the present case of the one-electron spectral functions, the border lines are generated by pairs of values q and q' belonging to the c and $s1$ bands, respectively, such that $v_c(q) = v_{s1}(q')$. Hence the two involved group velocities refer to different $\beta = c$ and $\beta = s1$ bands, respectively. In this case, the one-electron matrix elements between the ground state and the excited energy eigenstates do not change the exponent $-1/2$. That exponent results from the density of the two-parametric states whose spectra are given in Eqs. (75), (77), (79), (81), (83), and (85). The border lines of the σ one-electron removal and LHB addition spectral functions are plotted in Figs. 1–5. For simplicity, the specific form of their (k, ω)-plane spectrum is not given in this paper. In all cases it is of the general form, Eq. (118). Moreover, the corresponding singularity is always controlled by an exponent $-1/2$.

3.8. General effects of symmetry on the one-electron spectral functions

The symmetries of the 1D Hubbard model imply that from results referring to densities $n_e \in [0, 1[$ and $m \in [-n_e, n_e]$ one can fully extract corresponding results valid for $n_e \in]1, 2]$ and $m \in [-(2-n_e), (2-n_e)]$, respectively. This is why for simplicity in this paper we consider electronic densities $n_e \in [0, 1[$. Often we comment as well behaviors associated with the Mott–Hubbard insulator phase at $n_e = 1$.

Moreover, that for electronic densities $n_e \in [0, 1[$ our results refer to spin densities $m \in [0, n_e]$ relies on the following exact relation involving the one-electron spectral functions, Eq. (4),

$$B_{\sigma,\gamma}(k, \omega)|_{(N_\uparrow - N_\downarrow)/L = m} = B_{\bar{\sigma},\gamma}(k, \omega)|_{(N_\uparrow - N_\downarrow)/L = -m}\,, \qquad m \in [0, n_e]\,. \tag{122}$$

As given in Eq. (115), here σ and $\bar{\sigma}$ denote opposite spin projections and the electronic density $n_e = (N_\uparrow + N_\downarrow)/L$ is the same for the one-electron spectral functions on both sides of this equation. This trivial relation follows again from known symmetries of the model. Here we provide it explicitly because of its usefulness for the understanding of the relation of the one-electron spectral functions behaviors in the $m \to 0$ limit to those at $m = 0$ considered in Section 4.

Symmetry has also effects on the relation between the σ one-electron removal spectral function and $\bar{\sigma}$ one-electron UHB addition spectral function, respectively. This applies at $n_e = 1$ for $m \in [0, 1]$. Nonetheless, as reported in the following, there are related weaker effects for densities $n_e \in [0, 1[$ and $m \in [0, n_e]$.

On the one hand, at $n_e = 1$ there is no one-electron LHB. That electronic density refers to the Mott–Hubbard insulator phase at which there is a gap $2\mu_u$, Eq. (54), between the top of the $\sigma = \uparrow, \downarrow$ one-electron removal bands and the corresponding addition UHBs.

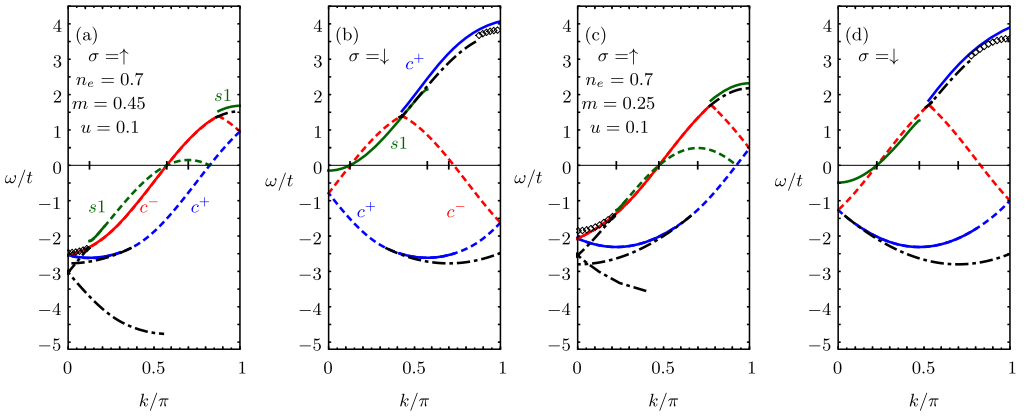

Fig. 1. The singular branch lines k ranges (solid lines) and other branch lines k ranges (dashed lines) for which the corresponding exponent $\xi^{\sigma}_{\beta}(k)$, Eq. (112), is negative and positive, respectively, and the singular boundary lines (dashed–dotted lines) of the weight distribution associated with the $\uparrow$ and $\downarrow$ one-electron spectral function are plotted in the (k,ω) plane. The curves refer to $u = 0.1$, electronic density $n_e = 0.7$, and (a)–(b) spin densities $m = 0.45$ and (c)–(d) $m = 0.25$. The branch line spectra plotted here are defined in Section 4. The c^+, c^-, and $s1$ branch-line labels appearing in panels (a) for $\sigma =\uparrow$ and (b) for $\sigma =\downarrow$ apply to the branch lines with similar topology in panels (c) and (d), respectively. (Online, the c^+, c^-, and $s1$ branch lines appear in blue, red, and green, respectively.) The lines represented by sets of diamond symbols contribute to the $u \rightarrow 0$ one-electron spectrum yet are not branch lines. In the case of σ one-electron UHB addition, only the branch lines that contribute to the $u \rightarrow 0$ spectral weight are represented.

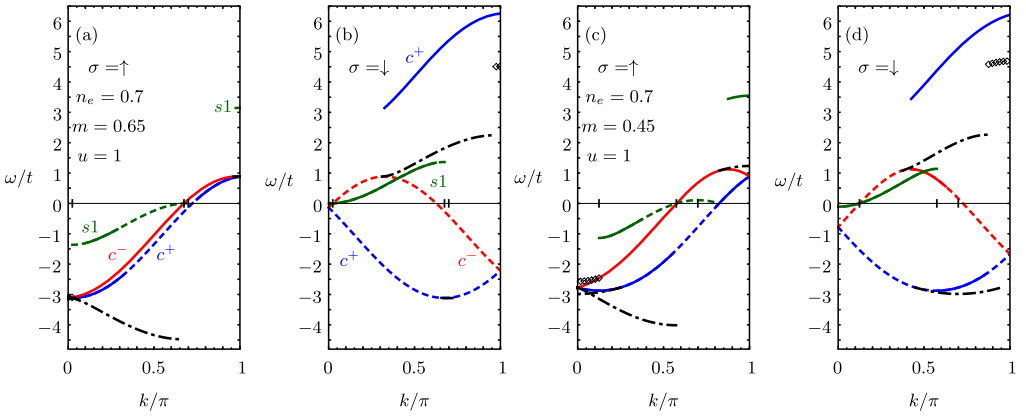

Fig. 2. The same singular branch lines k ranges (solid lines) and other branch lines k ranges (dashed lines) as in Fig. 1 for $u = 1$, electronic density $n_e = 0.7$, and spin densities (a)–(b) $m = 0.65$ and (c)–(d) $m = 0.45$. (Online, the c^+, c^-, and $s1$ branch lines are blue, red, and green, respectively.)

On the other hand, for the metallic phase electronic density range $n_e \in [0, 1[$ considered in the studies of this paper, the spectral weight associated with the σ one-electron addition LHB has not an exact top. However, such a weight becomes very small above some $u > 0$, $n_e \in [0, 1[$, and $m \in [0, n_e]$ dependent finite energy scale. Indeed, for intermediate and large u values there emerges a pseudogap between that region of the σ one-electron addition LHB and the well-defined bottom of the σ one-electron UHB. Our study focuses on singular spectral features. Such a pseudogap is clearly visible in Figs. 2–5 for intermediate and large u values. As discussed

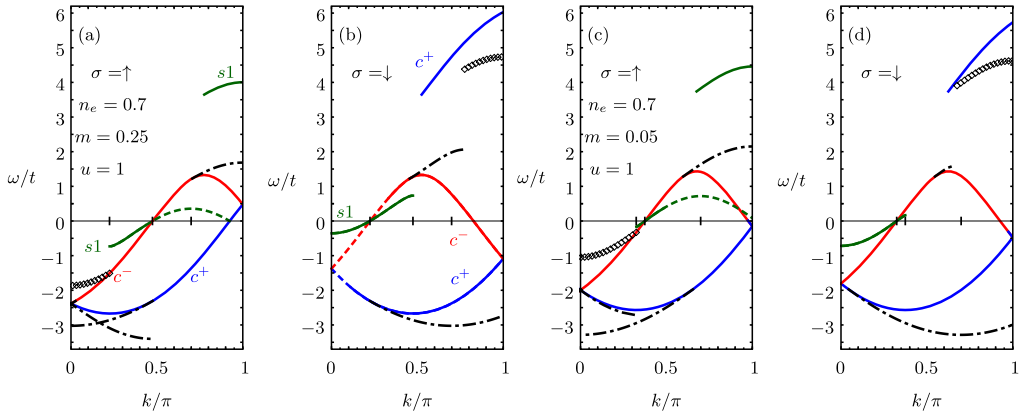

Fig. 3. The singular branch lines k ranges (solid lines) and other branch lines k ranges (dashed lines) for which the corresponding exponent $\xi^{\sigma}_{\beta}(k)$, Eq. (112), is negative and positive, respectively, and the singular boundary lines (dashed–dotted lines) of the weight distribution associated with the $\uparrow$ and $\downarrow$ one-electron spectral function are plotted in the (k,ω) plane. The curves refer to $u = 1$, electronic density $n_e = 0.7$, and spin densities (a)–(b) $m = 0.25$ and (c)–(d) $m = 0.05$. (Online, the c^+, c^-, and $s1$ branch lines are blue, red, and green, respectively.)

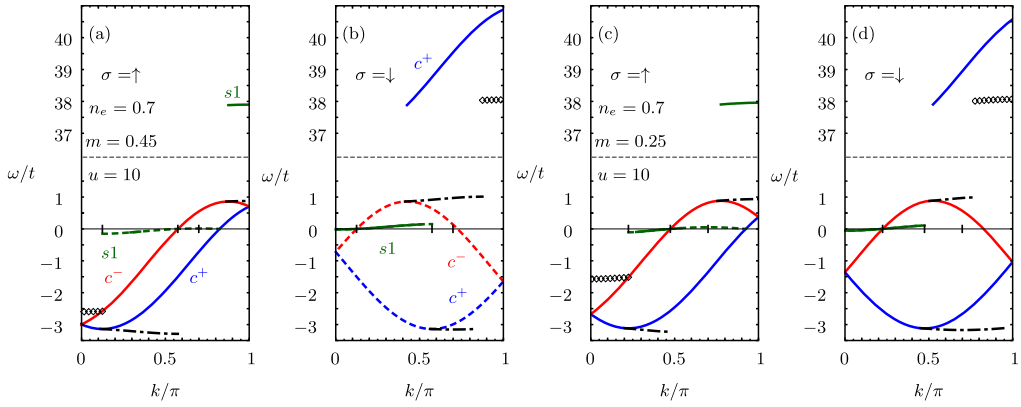

Fig. 4. The same singular branch lines k ranges (solid lines) and other branch lines k ranges (dashed lines) as in Fig. 3 for $u = 10$, electronic density $n_e = 0.7$, and spin densities (a)–(b) $m = 0.45$ and (c)–(d) $m = 0.25$. Note the different ω intervals separated by a horizontal dashed line used for the removal and LHB addition spectral features and the UHB addition branch line, respectively. (Online, the c^+, c^-, and $s1$ branch lines are blue, red, and green, respectively.)

below, the (k,ω)-plane solid lines and dashed–dotted lines refer in these figures to negative-exponent singular branch lines k ranges and singular border lines, respectively.

The following property follows from symmetry: When expressed as function of the $\beta = c, s1$ band momentum q, the $\sigma =\uparrow,\downarrow$ one-electron UHB addition $\beta = c, s1$ branch lines spectrum and exponent, Eq. (112), are exactly the same as for the $\beta = c, s1$ branch lines of the $\bar{\sigma} =\downarrow,\uparrow$ one-electron removal spectral function. That relation is also preserved in terms of the momentum k and energy ω, provided they are replaced by $\pi - k$ and $2\mu - \omega$, respectively.

The consequences of the model symmetries behind the above relation become fully explicit at $n_e = 1$. Then the following exact relation holds,

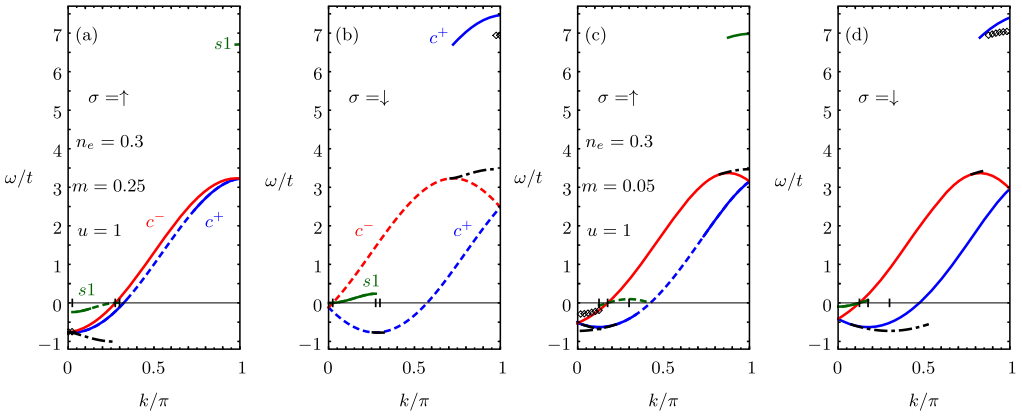

Fig. 5. The singular branch lines k ranges (solid lines) and other branch lines k ranges (dashed lines) for which the corresponding exponent $\xi^{\sigma}_{\beta}(k)$, Eq. (112), is negative and positive, respectively, and the singular boundary lines (dashed–dotted lines) of the weight distribution associated with the $\uparrow$ and $\downarrow$ one-electron spectral function are plotted in the (k,ω) plane. The curves refer to $u = 1$, electronic density $n_e = 0.3$, and spin densities (a)–(b) $m = 0.25$ and (c)–(d) $m = 0.05$. (Online, the c^+, c^-, and $s1$ branch lines are blue, red, and green, respectively.)

$$B^{\rm UHB}_{\sigma,+1}(k,\omega) = B_{\bar{\sigma},-1}(\pi - k, 2\mu - \omega)\,, \qquad n_e = 1\,, \qquad \mu \in [-\mu_u, \mu_u]\,. \tag{123}$$

This relation simplifies to $B^{\rm UHB}_{\sigma,+1}(k,\omega) = B_{\bar{\sigma},-1}(\pi - k, -\omega)$ when the chemical potential reads $\mu = 0$ and thus lays at the middle of the Mott–Hubbard gap.

On the one hand, at $n_e = 1$ the rotated-electron doubly occupied site of the excited energy eigenstates associated with the σ one-electron UHB addition spectral function corresponds to an η-spin doublet configuration of a single unpaired rotated spin of projection $-1/2$. On the other hand, for electronic densities $n_e \in [0, 1[$ such states are rather populated by one $\eta 1$ pseudofermion that corresponds to an η-spin singlet configuration of two paired rotated η-spins of opposite projection. For $n_e \rightarrow 1$ there is a doped Mott–Hubbard insulator phase for which the σ one-electron UHB addition spectral function has contributions from both such η-spin doublet and singlet configurations [68].

As reported above, for electronic densities in the range $n_e \in [0, 1[$ and under the transformations $k \rightarrow \pi - k$ and $\omega \rightarrow 2\mu - \omega$ the σ one-electron UHB addition $s1$ and $c^{\pm}$ branch lines (k,ω)-plane spectrum and exponent momentum dependence are exactly the same as for the $\bar{\sigma}$ one-electron removal $s1$ and $c^{\pm}$ branch lines, respectively. This is though a weaker consequence of the symmetry behind the $n_e = 1$ relation, Eq. (123). It follows from the $\eta 1$ pseudofermion of canonical momentum values $\bar{q} = q = \pm(\pi - 2k_F)$, Eq. (39), being invariant under the pseudoparticle–pseudofermion unitary transformation. As discussed in previous sections, such an $\eta 1$ pseudofermion acquires no phase shifts under ground-state transitions.

The $\uparrow$ and $\downarrow$ one-electron UHB addition singular features studied in the ensuing section result from microscopic processes generated by the leading-order operators given in Eqs. (78) and (84), respectively. Those create a single $\eta 1$ pseudofermion at one of the canonical momentum values $\bar{q} = q = \pm(\pi - 2k_F)$. The corresponding $\eta 1$ pseudofermion energy, Eq. (45) for $\beta = \eta 1$, reads $\varepsilon_{\eta 1}(\pm(\pi - 2k_F)) = 2\mu_{\eta} = 2\mu$. It equals that of two unpaired rotated η-spins of opposite projection, Eq. (50) for $\alpha = \eta$. The invariance under the pseudoparticle–pseudofermion unitary transformation is behind this property. It implies that the anti-binding energy $\varepsilon^0_{\eta 1}(q) \geq 0$

in Eq. (51) for $\alpha n = \eta 1$ of the η-spin singlet configuration of the two rotated η-spins paired within the composite $\eta 1$ pseudofermion exactly vanishes, $\varepsilon^0_{\eta 1}(\pm(\pi - 2k_F)) = 0$.

Furthermore, for the electronic densities $n_e < 1$ considered in our study, the energy of such an $\eta 1$ pseudofermion, $\varepsilon_{\eta 1}(\pm(\pi - 2k_F)) = 2\mu_\eta = 2\mu$, equals that given in Eq. (43) for $\alpha = \eta$ of an η-spin doublet configuration corresponding to a single rotated η-spin of projection $-1/2$. This is the same η-spin configuration as for the $n_e = 1$ unpaired rotated η-spin of projection $-1/2$ associated with the rotated-electron doubly occupied site of the σ one-electron UHB addition spectral function $B^{\rm UHB}_{\sigma,+1}(k,\omega)$, Eq. (123).

However, for $n_e < 1$ the relation $B^{\rm UHB}_{\sigma,+1}(k,\omega) = B_{\bar\sigma,-1}(\pi - k, 2\mu - \omega)$ is not exact. This follows from microscopic processes involving the creation of one $\eta 1$ pseudofermion of canonical momentum $\bar q$ other than $\pm(\pi - 2k_F)$ belonging to the $\eta 1$ band interval $\bar q \in [-(\pi - 2k_F), (\pi - 2k_F)]$. Indeed, such processes also contribute to the σ one-electron UHB addition spectral weight. Although the amount of weight they generate is small, it leads to contributions that render the relation $B^{\rm UHB}_{\sigma,+1}(k,\omega) = B_{\bar\sigma,-1}(\pi - k, 2\mu - \omega)$ not exact for $n_e < 1$. In a weaker way than at $n_e = 1$, such a relation nevertheless survives for $n_e \in [0, 1[$. This refers to the σ one-electron UHB addition singular $\beta = c, s1$ branch lines (k,ω)-plane spectrum $\omega^\sigma_\beta(k)$ and exponent $\xi^\sigma_\beta(k)$, Eq. (112). Their specific form and values for the one-electron spectral features under consideration are given below in Section 4. Such spectral features are generated by ground-state transitions to excited states populated by one $\eta 1$ pseudofermion with one of the canonical momentum values $\pm(\pi - 2k_F)$.

4. The singular σ one-electron spectral features

In this section the line shape behavior of the σ one-electron spectral functions, Eq. (4), in the vicinity of the branch lines shown in Figs. 1–5 is studied. For the k ranges for which the exponents controlling the line shape near these lines are negative, there are singularity cusps in the corresponding σ one-electron spectral functions.

In these figures the $\uparrow$ and $\downarrow$ one-electron removal and LHB addition β branch lines whose exponent $\xi^\sigma_\beta(k)$, Eq. (112), is negative for at least some k interval and u, n_e, and m ranges and the border lines considered in the following are plotted in the (k,ω) plane. The curves refer to several values of u, electronic densities $n_e = 0.3$ and $n_e = 0.7$, and sets of spin density values $m < n_e$. For $\uparrow$ and $\downarrow$ one-electron UHB addition, only the main branch lines that in the $u \to 0$ limit contribute to the $u = 0$ σ one-electron addition spectrum are plotted. (Online, the c^+, c^-, and $s1$ branch lines defined below and plotted in these figures are blue, red, and green, respectively.)

The $\beta = c, s1$ branch lines (k,ω)-plane spectra $\omega^\sigma_\beta(k)$ and exponents $\xi^\sigma_\beta(k)$, Eq. (112), of the (i) $\uparrow$ and $\downarrow$ one-electron UHB $\gamma = +1$ addition spectral functions and (ii) $\downarrow$ and $\uparrow$ one-electron $\gamma = -1$ removal spectral functions are, under the excitation momentum and energy transformations $k \to \pi - k$ and $\omega \to 2\mu - \omega$, respectively, exactly the same. The behavior of the latter (ii) $\downarrow$ and $\uparrow$ one-electron removal spectral functions near their $\beta = c, s1$ branch lines is studied in this section in some detail. For simplicity, following the above exact equalities, the study of the related former (i) $\uparrow$ and $\downarrow$ one-electron UHB addition branch lines is limited to those that in the $u \to 0$ limit contribute to the $u = 0$ σ one-electron addition δ-function-like spectrum.

The σ one-electron β branch lines are in Figs. 1–5 represented by solid lines and dashed lines for the k ranges for which the corresponding exponent $\xi^\sigma_\beta(k)$, Eq. (112), is negative and positive, respectively. The σ one-electron removal and LHB addition border lines are represented

by dashed–dotted lines. Most of the $u = 0$ δ-function like σ one-electron spectrum k ranges are recovered from specific branch lines in the $u \rightarrow 0$ limit. There are two exceptions related by the above excitation momentum and energy transformations $k \rightarrow \pi - k$ and $\omega \rightarrow 2\mu - \omega$, respectively. One refers to the $u = 0$ $\uparrow$ one-electron removal spectrum for the momentum range $k \in [-k_{F\downarrow}, k_{F\downarrow}]$. The other is the corresponding $u = 0$ $\downarrow$ one-electron UHB addition spectrum for the two k intervals $k \in [-\pi, -(\pi - k_{F\downarrow})]$ and $k \in [\pi - k_{F\downarrow}, \pi]$ brought to the first Brillouin zone. The corresponding $u = 0$ δ-function like one-electron spectra are in these k ranges recovered in the $u \rightarrow 0$ limit from well-defined $u > 0$ spectral features that are not branch lines. Those are represented in Figs. 1–5 by sets of diamond symbols.

The σ one-electron removal and LHB addition $c^{\pm}$ and $s1$ branch lines are the topics of Sections 4.1 and 4.2, respectively. Section 4.3 addresses the issue of the σ one-electron UHB addition branch lines. Finally, the $\uparrow$ one-electron removal and $\downarrow$ one-electron UHB addition $s1'$ spectral features that are not non-branch lines and for $m \neq 0$ contribute to the $u \rightarrow 0$ one-electron spectrum is the subject of Section 4.4.

4.1. The σ one-electron removal and LHB addition $c^{\pm}$ branch lines

The σ electron removal and LHB addition $c^{\pm}$ branch lines are generated by processes that correspond to particular cases of those generated by the leading-order operators, Eqs. (74), (76), (80), and (82). Their general processes are behind the $\uparrow$ one-electron removal spectrum, Eq. (75), $\uparrow$ one-electron LHB addition spectrum, Eq. (77), $\downarrow$ one-electron removal spectrum, Eq. (81), and $\downarrow$ one-electron LHB addition spectrum, Eq. (83). Hence these lines one-parametric spectra plotted in Figs. 1–5 are contained within such two-parametric spectra. Those occupy well defined regions in the (k, ω) plane. (Online, the c^{+} and c^{-} branch lines are blue and red, respectively, in these figures.)

The one-parametric spectra $\omega^{\sigma}_{c^{\pm}}(k)$ and the exponents $\xi^{\sigma}_{c^{\pm}}(k)$ associated with these branch lines are related by the following symmetry,

$$\omega^{\sigma}_{c^{+}}(k) = \omega^{\sigma}_{c^{-}}(-k)\,; \qquad \xi^{\sigma}_{c^{+}}(k) = \xi^{\sigma}_{c^{-}}(-k)\,, \qquad \sigma = \uparrow, \downarrow\,. \tag{124}$$

Within a reduced first-Brillouin zone scheme, considering both the c^{+} and c^{-} branch lines for $k \in [0, \pi]$ or only the c^{+} branch line for $k \in [-\pi, \pi]$ contains exactly the same information. Here we chose the latter option.

The σ one-electron removal and LHB addition c^{+} branch line refers to excited energy eigenstates with the following number deviations relative to those of the initial ground state,

$$\delta N^{F}_{c} = 0\,; \qquad \delta J^{F}_{c} = \delta_{\sigma,\downarrow}/2\,; \qquad \delta N^{NF}_{c} = \gamma\,; \qquad \delta N^{F}_{s1} = \delta_{\sigma,\downarrow}\,\gamma\,; \qquad \delta J^{F}_{s1} = \gamma_{\sigma}/2\,. \tag{125}$$

The spectrum of general form, Eq. (110), that defines the (k, ω)-plane shape of the σ one-electron removal and LHB addition c^{+} branch line reads,

$$\begin{aligned} &\omega^{\sigma}_{c^{+}}(k) = \gamma\,\varepsilon_{c}(q)\,, \qquad \gamma = \pm 1\,, \\ &\quad q \in [-2k_{F}, 2k_{F}] \quad \text{for } \sigma \text{ electron removal}\,, \\ &\quad q \in [-\pi, -2k_{F}] \text{ and } q \in [2k_{F}, \pi] \quad \text{for } \sigma \text{ electron LHB addition}\,, \end{aligned} \tag{126}$$

where $\varepsilon_{c}(q)$ is the c band energy dispersion, Eq. (45) for $\beta = c$. The relation of the c band momentum q to the excitation momentum k is within an extended-zone scheme given by,

$$
\begin{aligned}
& k = \gamma\, q + k_{F\bar{\sigma}}\,, \\
& k \in [-k_{F\sigma}\,, (2k_F + k_{F\bar{\sigma}})] \quad \text{for } \gamma = -1 \\
& k \in [-(\pi - k_{F\bar{\sigma}}), -k_{F\sigma}] \text{ and } k \in [(2k_F + k_{F\bar{\sigma}}), (\pi + k_{F\bar{\sigma}})] \quad \text{for } \gamma = +1\,.
\end{aligned} \tag{127}
$$

As mentioned above, we consider a reduced first Brillouin-zone scheme for $k \in [-\pi, \pi]$ within which the c^+ branch line separates into several subbranches. On the one hand, one finds that these subbranches refer to the following momentum k intervals,

$$
\begin{aligned}
& k = \gamma\, q + k_{F\bar{\sigma}} \ \text{ subbranch}\,, \\
& k \in [-k_{F\sigma}\,, (2k_F + k_{F\bar{\sigma}})] \quad \text{for } \gamma = -1 \\
& k \in [-(\pi - k_{F\bar{\sigma}}), -k_{F\sigma}] \text{ and } k \in [(2k_F + k_{F\bar{\sigma}}), \pi] \quad \text{for } \gamma = +1\,, \\
& k = q + k_{F\bar{\sigma}} - 2\pi \ \text{ subbranch}\,, \\
& k \in [-\pi, -(\pi - k_{F\bar{\sigma}})] \quad \text{for } \gamma = +1\,,
\end{aligned} \tag{128}
$$

that are valid for the densities ranges,

$$
\begin{aligned}
& \uparrow \text{ electron: } (i)\ n_e \in [0, 2/3] \text{ and } m \in [0, n_e] \\
& \qquad\qquad \text{and } (ii)\ n_e \in [2/3, 1] \text{ and } m \in [(3n_e - 2), n_e]\,, \\
& \downarrow \text{ electron: } (i)\ n_e \in [0, 1/2] \text{ and } m \in [0, n_e] \\
& \qquad\qquad \text{and } (ii)\ n_e \in [1/2, 2/3] \text{ and } m \in [0, (2 - 3n_e)]\,.
\end{aligned}
$$

On the other hand, the momentum k intervals,

$$
\begin{aligned}
& k = \gamma\, q + k_{F\bar{\sigma}} \ \text{ subbranch}\,, \\
& k \in [-k_{F\sigma}\,, \pi] \quad \text{for } \gamma = -1 \\
& k \in [-(\pi - k_{F\bar{\sigma}}), -k_{F\sigma}] \quad \text{for } \gamma = +1\,, \\
& k = q + k_{F\bar{\sigma}} - 2\pi \ \text{ subbranch}\,, \\
& k \in [-\pi, -(2\pi - 2k_F - k_{F\bar{\sigma}})] \quad \text{for } \gamma = -1 \\
& k \in [-(2\pi - 2k_F - k_{F\bar{\sigma}}), -(\pi - k_{F\bar{\sigma}})] \quad \text{for } \gamma = +1\,,
\end{aligned} \tag{129}
$$

are valid for the densities ranges,

$$
\begin{aligned}
& \uparrow \text{ electron: } n_e \in [2/3, 1] \text{ and } m \in [0, (3n_e - 2)]\,, \\
& \downarrow \text{ electron: } (i)\ n_e \in [1/2, 2/3] \text{ and } m \in [(2 - 3n_e), n_e] \\
& \qquad\qquad \text{and } (ii)\ n_e \in [2/3, 1] \text{ and } m \in [0, n_e]\,.
\end{aligned}
$$

The corresponding k intervals of the c^- branch line subbranches are obtained from those provided here upon exchanging k by $-k$.

The one-parametric spectrum $\omega^{\sigma}_{c^+}(k)$ of each c^+ branch line subbranch is given by Eq. (126). The relation between the excitation momentum k and the c band momentum q is provided in the corresponding k intervals, Eqs. (128) and (129). Combining the analysis of such momentum k intervals with the relation $\omega^{\sigma}_{c^+}(k) = \omega^{\sigma}_{c^-}(-k)$, Eq. (124), reveals that the σ one-electron LHB addition $c^{\pm}$ branch lines are the natural continuation of the σ one-electron removal $c^{\pm}$ branch lines.

We use the values of the functional, Eq. (113), specific to the excited energy eigenstates that determine spectral weight distribution near the $c^{\pm}$ branch lines, to access the momentum dependence of the exponents of general form, Eq. (112), that control such a line shape. One finds that they read,

$$\xi^{\uparrow}_{c^+}(k) = \xi^{\uparrow}_{c^-}(-k) = -1 + \sum_{\iota=\pm 1}\left(\frac{\xi^1_{c\,s1}}{2} + \gamma\,\Phi_{c,c}(\iota 2k_F, q)\right)^2 + \sum_{\iota=\pm 1}\left(\frac{\xi^1_{s1\,s1}}{2} + \gamma\,\Phi_{s1,c}(\iota k_{F\downarrow}, q)\right)^2 , \quad (130)$$

for the $\sigma = \uparrow$ one-electron $c^{\pm}$ branch lines and,

$$\xi^{\downarrow}_{c^+}(k) = \xi^{\downarrow}_{c^-}(-k) = -1 + \sum_{\iota=\pm 1}\left(\frac{\iota\,\gamma\,\xi^0_{c\,s1}}{2} + \frac{(\xi^1_{c\,c} - \xi^1_{c\,s1})}{2} + \gamma\,\Phi_{c,c}(\iota 2k_F, q)\right)^2 + \sum_{\iota=\pm 1}\left(\frac{\iota\,\gamma\,\xi^0_{s1\,s1}}{2} + \frac{(\xi^1_{s1\,c} - \xi^1_{s1\,s1})}{2} + \gamma\,\Phi_{s1,c}(\iota k_{F\downarrow}, q)\right)^2 , \quad (131)$$

for the $\sigma = \downarrow$ one-electron $c^{\pm}$ branch lines. These $\uparrow$ and $\downarrow$ one-electron exponents are plotted in Figs. 6 and 7, respectively, as a function of the momentum $k/\pi \in]-1, 1[$. The curves correspond to several u values, electronic densities $n_e = 0.3$ and $n_e = 0.7$, and a set of spin density values $m < n_e$.

The specific form of the general expression, Eq. (112), of the σ one-electron spectral function $B_{\sigma,\gamma}(k,\omega)$, Eq. (4), in the vicinity of the present $c^{\pm}$ branch lines is,

$$B_{\sigma,\gamma}(k,\omega) = C_{\sigma,\gamma,c^{\pm}}\left(\gamma\omega - \omega^{\sigma}_{c^{\pm}}(k)\right)^{\xi^{\sigma}_{c^{\pm}}(k)}; \qquad (\gamma\,\omega - \omega^{\sigma}_{c^{\pm}}(k)) \geq 0\,, \qquad \gamma = \pm 1\,, \quad (132)$$

where $C_{\sigma,\gamma,c^{\pm}}$ are constants that have a fixed value for the k and ω ranges corresponding to small values of the energy deviation $(\gamma\omega - \omega^{\sigma}_{c^{\pm}}(k))$. The spectra $\omega^{\sigma}_{c^+}(k) = \omega^{\sigma}_{c^-}(-k)$ in that energy deviation of the several subbranches are given in Eqs. (126), (128), and (129), and the exponents $\xi^{\sigma}_{c^+}(k) = \xi^{\sigma}_{c^-}(-k)$ are defined in Eqs. (130) and (131) for $\sigma = \uparrow$ and $\sigma = \downarrow$, respectively.

The following exponents behaviors reached in the $u \to 0$ limit are derived from the use in Eqs. (130) and (131) of the values corresponding to that limit of the phase-shift parameters $\xi^{j}_{\beta\,\beta'}$ and $\beta = c, s1$ pseudofermion phase shifts in units of 2π, $\Phi_{\beta,\beta'}(\iota q_{F\beta}, q)$, given in Eqs. (B.15) and (B.10) of Appendix B, respectively. The found behaviors in the $u \to 0$ limit of the c^+ branch line subbranches exponents for $\sigma = \uparrow$ one-electron removal ($\gamma = -1$) are,

$$\lim_{u\to 0}\xi^{\uparrow}_{c^+}(k) = -1\,, \qquad k \in [-k_{F\uparrow}, -k_{F\downarrow}] \text{ for } \gamma = -1 \quad \text{for } n_e \in [0,1] \text{ and } m \in [0, n_e]\,, \quad (133)$$

$$\lim_{u\to 0}\xi^{\uparrow}_{c^+}(k) = 0\,, \quad k \in [-k_{F\downarrow}, 3k_{F\downarrow}] \text{ for } \gamma = -1 \quad \text{for } n_e \in [0, 2/3] \text{ and } m \in [0, n_e] \quad \text{for } n_e \in [2/3, 1] \text{ and } m \in [(n_e - 2/3), n_e]$$

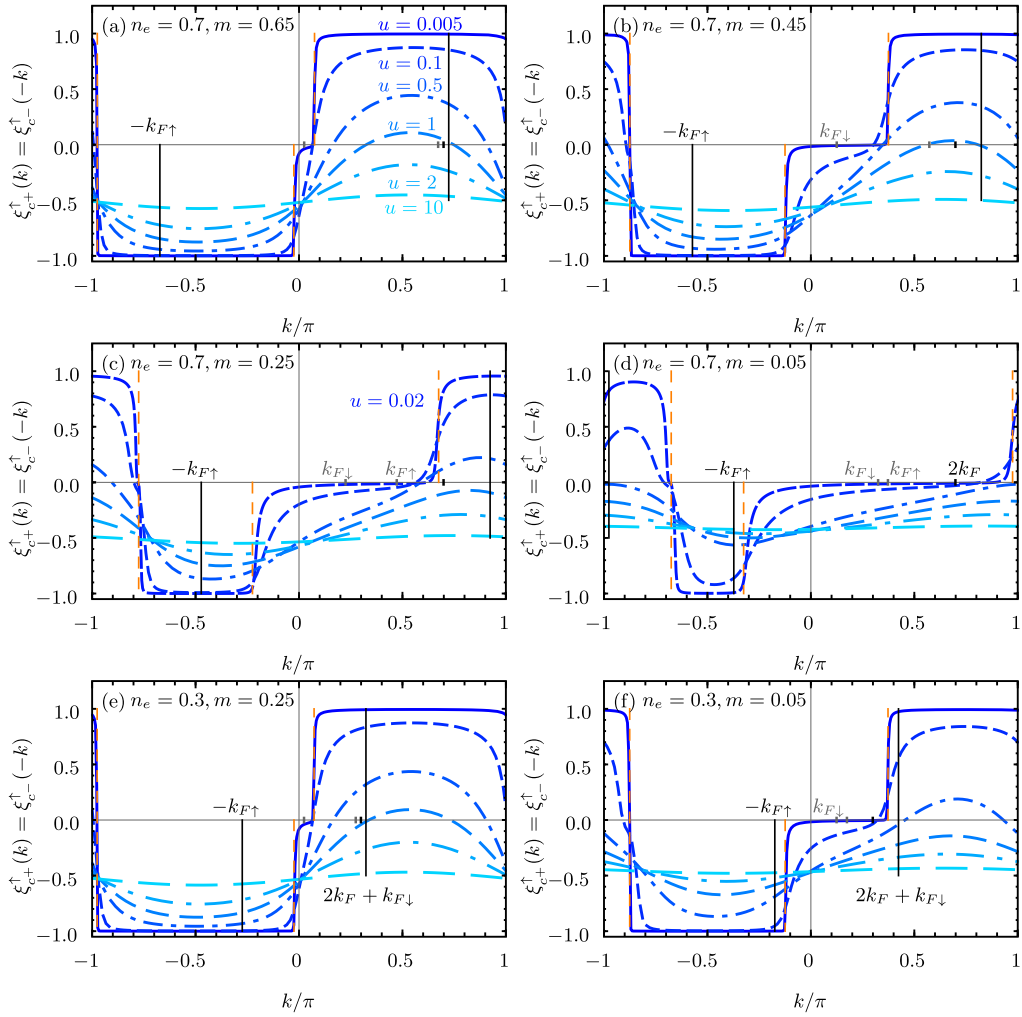

Fig. 6. The exponent $\xi^{\uparrow}_{c^+}(k) = \xi^{\uparrow}_{c^-}(-k)$, Eq. (130), that controls the singularities in the vicinity of the c^+ branch line whose (k,ω)-plane one-parametric spectrum is defined by Eqs. (126), (128), and (129) is plotted for the $\sigma = \uparrow$ one-electron removal and LHB addition spectral function, Eq. (132), as a function of the momentum $k/\pi \in]-1, 1[$. The curves refer to several u values, electronic density $n_e = 0.7$, and spin densities (a) $m = 0.65$, (b) $m = 0.45$, (c) $m = 0.25$, and (d) $m = 0.05$, and for electronic density $n_e = 0.3$ and spin densities (e) $m = 0.25$ and (f) $m = 0.05$. The type of exponent line associated with each u value is for all figures the same. Full and dashed vertical lines denote specific momentum values between different subbranches and momenta where the $u \rightarrow 0$ limiting value of the exponent changes, respectively.

$$k \in [-k_{F\downarrow}, \pi] \text{ and } k \in [-\pi, -(2\pi - 3k_{F\downarrow})] \text{ for } \gamma = -1$$
$$\text{for } n_e \in [2/3, 1] \text{ and } m \in [0, (n_e - 2/3)]\,, \tag{134}$$

$$\lim_{u\rightarrow 0} \xi^{\uparrow}_{c^+}(k) = 1\,,$$
$$k \in [3k_{F\downarrow}, (2k_F + k_{F\downarrow})] \text{ for } \gamma = -1$$

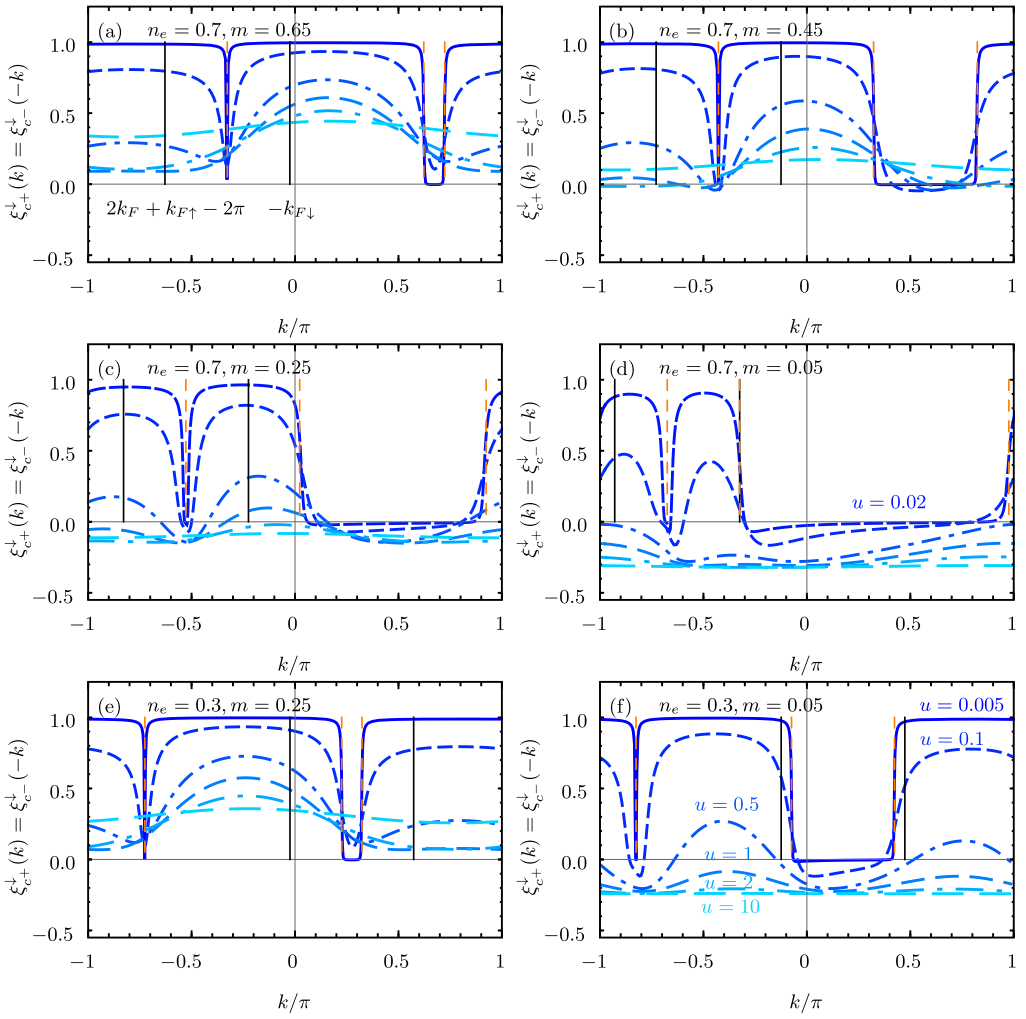

Fig. 7. The exponent $\xi^{\downarrow}_{c^+}(k) = \xi^{\downarrow}_{c^-}(-k)$, Eq. (131), that controls the singularities in the vicinity of the c^+ branch line whose (k,ω)-plane shape is defined by Eqs. (126), (128), and (129) is plotted for the $\sigma = \downarrow$ one-electron removal and LHB addition spectral function, Eq. (132), as a function of the momentum $k/\pi \in]-1, 1[$. The curves refer to the same values of u, electronic density n_e, and spin density m as in Fig. 6.

$$
\begin{aligned}
&\text{for } n_e \in [0, 2/3] \text{ and } m \in [0, n_e] \\
&\text{for } n_e \in [2/3, 1] \text{ and } m \in [(3n_e - 2), n_e] \\
&k \in [3k_{F\downarrow}, \pi] \text{ and } k \in [-\pi, -(2\pi - 2k_F - k_{F\downarrow})] \text{ for } \gamma = -1 \\
&\text{for } n_e \in [2/3, 1] \text{ and } m \in [(n_e - 2/3), (3n_e - 2)] \\
&k \in [-(2\pi - 3k_{F\downarrow}), -(2\pi - 2k_F - k_{F\downarrow})] \\
&\text{for } n_e \in [2/3, 1] \text{ and } m \in [0, (n_e - 2/3)] \,. \qquad (135)
\end{aligned}
$$

For LHB addition ($\gamma = +1$), one finds,

$$\lim_{u\to 0} \xi^{\uparrow}_{c^+}(k) = -1\,, \qquad k \in [-(\pi - k_{F\downarrow}), -k_{F\uparrow}] \text{ for } \gamma = +1$$
$$\text{for } n_e \in [0,1] \text{ and } m \in [0, n_e]\,,$$
$$\lim_{u\to 0} \xi^{\uparrow}_{c^+}(k) = 1 \text{ for } \gamma = +1$$
$$\text{for the other } k \text{ ranges in Eqs. (128) and (129) with } \sigma = \uparrow \text{ and } \bar{\sigma} = \downarrow\,. \tag{136}$$

Similar values for the exponent $\xi^{\downarrow}_{c^-}(k)$ are obtained upon exchanging k by $-k$. Important c^- branch line subbranches are those for which $\lim_{u\to 0} \xi^{\uparrow}_{c^-}(k) = -1$. They refer to the k ranges,

$$\lim_{u\to 0} \xi^{\uparrow}_{c^-}(k) = -1\,,$$
$$k \in [k_{F\downarrow}, k_{F\uparrow}] \text{ for } \gamma = -1 \text{ and } k \in [k_{F\uparrow}, (\pi - k_{F\downarrow})] \text{ for } \gamma = +1\,, \tag{137}$$

that are valid for $n_e \in [0, 1[$ and $m \in [0, n_e]$.

For the k ranges for which $\lim_{u\to 0} \xi^{\uparrow}_{c^\pm}(k) = -1$, the line shape has not the form given in Eq. (132). It rather is δ-function like, Eq. (121). In the present case, this gives,

$$\begin{aligned}
\lim_{u\to 0} B_{\uparrow,-1}(k,\omega) &= \delta\Big(\omega + \omega^{\uparrow}_{c^+}(k)\Big) \\
&= \delta\Big(\omega - 2t\,(\cos k - \cos k_{F\uparrow})\Big)\,, \qquad k \in [-k_{F\uparrow}, -k_{F\downarrow}]\,, \\
\lim_{u\to 0} B_{\uparrow,+1}(k,\omega) &= \delta\Big(\omega - \omega^{\uparrow}_{c^+}(k)\Big) \\
&= \delta\Big(\omega + 2t\,(\cos k - \cos k_{F\uparrow})\Big)\,, \qquad k \in [-(\pi - k_{F\downarrow}), -k_{F\uparrow}]\,, \\
\lim_{u\to 0} B_{\uparrow,-1}(k,\omega) &= \delta\Big(\omega + \omega^{\uparrow}_{c^-}(k)\Big) \\
&= \delta\Big(\omega - 2t\,(\cos k - \cos k_{F\uparrow})\Big)\,, \qquad k \in [k_{F\downarrow}, k_{F\uparrow}]\,, \\
\lim_{u\to 0} B_{\uparrow,+1}(k,\omega) &= \delta\Big(\omega - \omega^{\uparrow}_{c^-}(k)\Big) \\
&= \delta\Big(\omega + 2t\,(\cos k - \cos k_{F\uparrow})\Big)\,, \qquad k \in [k_{F\uparrow}, (\pi - k_{F\downarrow})]\,.
\end{aligned} \tag{138}$$

The behaviors reported here thus recover parts of the exact $u = 0$ σ one-electron spectrum. That the spectra $\omega^{\sigma}_{c^\pm}(k)$ become in the $u \to 0$ limit the corresponding non-interacting electronic spectra is confirmed by accounting for the limiting behavior of the c energy dispersion $\varepsilon_c(q)$ appearing in these $u > 0$ general spectra expression, Eq. (126). Such a limiting behavior is reported in Eq. (B.1) of Appendix B.

For the k ranges for which the exponents are for $u \to 0$ given by 0 and/or 1, the $\uparrow$ one-electron spectral weight at and near the corresponding branch lines vanishes in the $u \to 0$ limit.

One finds that in the $u \to 0$ limit the $\sigma = \downarrow$ one-electron removal exponent, Eq. (131), has the following behaviors,

$$\lim_{u\to 0} \xi^{\downarrow}_{c^+}(k) = 1\,,$$
$$k \in [-k_{F\downarrow}, (k_{F\uparrow} - 2k_{F\downarrow})] \text{ for } \gamma = -1$$
$$\text{for } n_e \in [0,1] \text{ and } m \in [0, n_e]$$

$$
\begin{aligned}
&k \in [(2k_F + k_{F\downarrow}), (2k_F + k_{F\uparrow})] \text{ for } \gamma = -1 \\
&\quad \text{for } n_e \in [0, 1/2] \text{ and } m \in [0, n_e] \\
&\quad \text{for } n_e \in [1/2, 2/3] \text{ and } m \in [0, (2 - 3n_e)] \\
&k \in [(2k_F + k_{F\downarrow}), \pi] \text{ and } k \in [-\pi, -(2\pi - 2k_F - k_{F\uparrow})] \text{ for } \gamma = -1 \\
&\quad \text{for } n_e \in [1/2, 2/3] \text{ and } m \in [(2 - 3n_e), n_e] \\
&\quad \text{for } n_e \in [2/3, 1] \text{ and } m \in [(3n_e - 2), n_e] \\
&k \in [-(2\pi - 2k_F - k_{F\downarrow}), -(2\pi - 2k_F - k_{F\uparrow})] \text{ for } \gamma = -1 \\
&\quad \text{for } n_e \in [2/3, 1] \text{ and } m \in [0, (3n_e - 2)]
\end{aligned}
\tag{139}
$$

and

$$
\begin{aligned}
&\lim_{u\to 0} \xi^{\downarrow}_{c^+}(k) = 0\,, \\
&\quad k \in [(k_{F\uparrow} - 2k_{F\downarrow}), (2k_F + k_{F\downarrow})] \text{ for } \gamma = -1 \\
&\quad\quad \text{for } n_e \in [0, 2/3] \text{ and } m \in [0, n_e] \\
&\quad\quad \text{for } n_e \in [2/3, 1] \text{ and } m \in [(3n_e - 2), n_e] \\
&\quad k \in [(k_{F\uparrow} - 2k_{F\downarrow}), \pi] \text{ and } k \in [-\pi, -(2\pi - 2k_F - k_{F\downarrow})] \text{ for } \gamma = -1 \\
&\quad\quad \text{for } n_e \in [2/3, 1] \text{ and } m \in [0, (3n_e - 2)]\,.
\end{aligned}
\tag{140}
$$

The $\sigma = \downarrow$ one-electron LHB exponent is found to behave as,

$$
\begin{aligned}
&\lim_{u\to 0} \xi^{\downarrow}_{c^+}(k) = 1 \text{ for } \gamma = +1 \text{ and the } k \text{ ranges in Eqs. (128) and (129)} \\
&\quad \text{with } \sigma = \downarrow \text{ and } \bar{\sigma} = \uparrow\,.
\end{aligned}
\tag{141}
$$

Hence the $\downarrow$ one-electron spectral weight at and near these branch lines vanishes in the $u \to 0$ limit both for electron removal and LHB addition. Similar values for the exponent $\xi^{\downarrow}_{c^-}(k)$ are obtained upon exchanging k by $-k$.

Analytical expressions for the above exponents can be derived for $u \gg 1$. These expressions are continuous functions of the spin density m whose limiting behaviors for $m \to 0$ and $m \to n_e$ we provide in the following. For $u \gg 1$ and spin density $m \to 0$ such expressions are derived from the use in Eqs. (130) and (131) of the parameters $\xi^{j}_{\beta\,\beta'}$ expressions obtained by combining Eqs. (B.17) and (B.18) of Appendix B for $u \gg 1$ with those of the $\beta = c, s1$ pseudofermion phase shifts provided in Eq. (B.12) of that Appendix. One then finds the following c^+ branch line exponent expression,

$$
\xi^{\sigma}_{c^\pm}(k) = -\frac{3}{8} + \frac{\ln 2}{4\pi\, u}\left(\sin(\pi n_e) \pm 2\sin\left(k \mp \frac{\pi}{2}n_e\right)\right)\,, \qquad \sigma = \uparrow, \downarrow\,. \tag{142}
$$

It applies to all its above subbranches k intervals. For the twin c^- branch line, it refers to subbranches k intervals generated from those of the c^+ branch line upon exchanging k by $-k$. Following the exact relation, Eq. (122), similar results are reached if one considers the $m \to 0$ limit of corresponding one-electron spectral functions expressions valid for spin densities $m \in [-n_e, 0]$. Hence, the same behaviors apply to the $c^\pm$ branch lines of the $m = 0$ one-electron spectral functions under consideration.

For $u \gg 1$ and spin density $m \to n_e$ one uses in Eqs. (130) and (131) the parameters $\xi^{j}_{\beta\,\beta'}$ expressions obtained by combining Eqs. (B.19) and (B.20) of Appendix B with those of the $\beta =$

$c, s1$ pseudofermion phase shifts provided in Eq. (B.14) of that Appendix. One then finds that the $c^{\pm}$ branch line exponents have different expressions for the $\uparrow$ one-electron and $\downarrow$ one-electron spectral functions that read,

$$\xi^{\uparrow}_{c^{\pm}}(k) = -\frac{1}{2} \pm \frac{2}{\pi u}\sin k\,,$$
$$\xi^{\downarrow}_{c^{\pm}}(k) = \frac{1}{2} - \frac{2}{\pi u}\left(\sin(\pi n_e) \pm \sin(k \mp \pi n_e)\right)\,, \qquad (143)$$

respectively.

On the one hand and as shown in Fig. 6, the main effect on the k dependence of the $\uparrow$ one-electron removal and LHB addition exponent $\xi^{\uparrow}_{c^+}(k) = \xi^{\uparrow}_{c^-}(-k)$, Eq. (130), of increasing the on-site repulsion u from $u \ll 1$ to $u \gg 1$ is to continuously changing its $u \rightarrow 0$ values -1, 0, and 1 for the k ranges given in Eqs. (133)–(136) to a k independent negative value for $k \in [-\pi, \pi]$ as $u \rightarrow \infty$. The latter smoothly changes from $-3/8$ for $m \rightarrow 0$ to $-1/2$ for $m \rightarrow n_e$. The general trend of such an exponent u dependence is the following: For the momentum k ranges for which it reads 0 and 1 in the $u \rightarrow 0$ limit, it decreases upon increasing u; For the k intervals for which it is given by -1 in that limit, it rather increases for increasing u values.

On the other hand, the exponent $\xi^{\downarrow}_{c^+}(k) = \xi^{\downarrow}_{c^-}(k)$, Eq. (131), plotted in Fig. 7 becomes negative only for large u and small spin density values. For $u \rightarrow 0$ it reads 0 and 1 for the k intervals provided in Eqs. (139)–(141). As $u \rightarrow \infty$ it continuously evolves to a k independent value for $k \in [-\pi, \pi]$. Such a value smoothly changes from $-3/8$ for $m \rightarrow 0$ to $1/2$ for $m \rightarrow n_e$. The general trend of that exponent u dependence is different upon changing the densities. As shown in Fig. 7, for some densities it always decreases upon increasing u. For other densities it first decreases upon increasing u until reaching some minimum at a finite u value above which it increases upon further increasing u.

4.2. The σ one-electron removal and LHB addition $s1$ branch line

The σ electron removal and LHB addition $s1$ branch line is generated by processes that correspond again to a particular case of those generated by the leading-order operators, Eqs. (74), (76), (80), and (82). For the $\uparrow$ and $\downarrow$ one-electron spectral functions its one-parametric spectrum plotted in Figs. 1–5 is thus contained within the (k, ω)-plane region occupied by the two-parametric spectra corresponding to such more general processes. (Online, the $s1$ branch lines are green in these figures.)

The one-parametric spectrum of this branch line is an even function of k, $\omega^{\sigma}_{s1}(k) = \omega^{\sigma}_{s1}(-k)$. The corresponding exponent given below is also an even function of k, $\xi^{\sigma}_{s1}(k) = \xi^{\sigma}_{s1}(-k)$. Hence for simplicity we restrict our following analysis to $k \geq 0$. For such a momentum range the σ electron removal and LHB addition parts of the $s1$ branch line refer to excited energy eigenstates with the following number deviations relative to those of the initial ground state,

$$\delta N^F_c = \gamma\,; \quad \delta J^F_c = \delta_{\sigma,\uparrow}/2\,; \quad \delta N^F_{s1} = \delta_{\sigma,\uparrow}\,\gamma\,; \quad \delta J^F_{s1} = 0\,;$$
$$\delta N^{NF}_{s1} = -\gamma_\sigma\,\gamma\,. \qquad (144)$$

The spectrum $\omega^{\sigma}_{s1}(k)$ of general form, Eq. (110), is for the present branch line given by,

$$\omega^{\sigma}_{s1}(k) = -\gamma_\sigma\,\gamma\,\varepsilon_{s1}(q)\,,$$
$$q \in [-k_{F\uparrow}, -k_{F\downarrow}] \quad \text{for } \uparrow \text{ electron removal}\,,$$

$$
\begin{aligned}
&q \in [-k_{F\downarrow}, k_{F\downarrow}] \quad \text{for } \uparrow \text{ electron LHB addition}\,,\\
&q \in [-k_{F\downarrow}, 0] \quad \text{for } \downarrow \text{ electron removal}\,,\\
&q \in [k_{F\downarrow}, k_{F\uparrow},] \quad \text{for } \downarrow \text{ electron LHB addition}\,,
\end{aligned}
\tag{145}
$$

where $\varepsilon_{s1}(q)$ is the $s1$ band energy dispersion, Eq. (45) for $\beta = s1$.

The relation of the $s1$ band momentum q to the excitation momentum k is,

$$
k = \delta_{\sigma,\uparrow}\, 2k_F - \gamma_\sigma\, \gamma\, q \geq 0\,. \tag{146}
$$

This gives,

$$
\begin{aligned}
&k \in [k_{F\downarrow}, k_{F\uparrow}] \quad \text{for } \uparrow \text{ electron removal}\,,\\
&k \in [k_{F\uparrow}, (2k_F + k_{F\downarrow})] \quad \text{for } \uparrow \text{ electron LHB addition}\,,
\end{aligned}
\tag{147}
$$

and

$$
\begin{aligned}
&k \in [0, k_{F\downarrow}] \quad \text{for } \downarrow \text{ electron removal}\,,\\
&k \in [k_{F\downarrow}, k_{F\uparrow}] \quad \text{for } \downarrow \text{ electron LHB addition}\,,
\end{aligned}
\tag{148}
$$

respectively.

Except for $\uparrow$ one-electron LHB addition, the above $s1$ branch-line k ranges are within the first Brillouin-zone. In that specific case, it refers for some densities to an extended-zone scheme. Here we consider a reduced first Brillouin-zone scheme for $k \in [0, \pi]$. Within it the $s1$ branch line separates for $\uparrow$ one-electron LHB addition into two subbranches. Actually, one of such subbranches stems for $k > 0$ from k momentum values that within an extended-zone scheme arise from second Brillouin-zone $k < 0$ momentum values. (For such processes, one has in Eq. (144) that $\delta J_c^F = -1/2$ rather than $\delta J_c^F = 1/2$.) This gives,

$$
\begin{aligned}
&k = 2k_F - q \ \ \text{subbranch}\,,\\
&k \in [k_{F\uparrow}, (2k_F + k_{F\downarrow})] \quad \text{for } \gamma = 1\,,\\
&\quad \uparrow \text{ electron addition } (i)\ n_e \in [0, 2/3] \text{ and } m \in [0, n_e]\\
&\quad \text{and } (ii)\ n_e \in [2/3, 1] \text{ and } m \in [(3n_e - 2), n_e]\,,\\
&k = 2k_F - q \ \ \text{subbranch}\,,\\
&k \in [k_{F\uparrow}, \pi] \quad \text{for } \gamma = 1\,,\\
&k = -2k_F - q + 2\pi \ \ \text{subbranch}\,,\\
&k \in [(2\pi - 2k_F - k_{F\downarrow}), \pi] \quad \text{for } \gamma = 1\,,\\
&\quad \uparrow \text{ electron addition } n_e \in [2/3, 1] \text{ and } m \in [0, (3n_e - 2)]\,.
\end{aligned}
\tag{149}
$$

Analysis of the momentum k intervals in Eqs. (148) and (149) reveals that the σ one-electron LHB addition $s1$ branch line is the natural continuation of the σ one-electron removal $s1$ branch line. The momentum dependent exponent of general form, Eq. (112), that controls the line shape near the $\sigma = \uparrow$ one-electron removal and LHB addition $s1$ branch line is given by,

$$
\begin{aligned}
\xi_{s1}^{\uparrow}(k) = -1 &+ \sum_{\iota=\pm 1} \left(\frac{\iota\, \gamma (\xi^0_{c\,c} + \xi^0_{c\,s1})}{2} + \frac{\xi^1_{c\,c}}{2} - \gamma\, \Phi_{c,s1}(\iota 2k_F, q) \right)^2\\
&+ \sum_{\iota=\pm 1} \left(\frac{\iota\, \gamma (\xi^0_{s1\,c} + \xi^0_{s1\,s1})}{2} + \frac{\xi^1_{s1\,c}}{2} - \gamma\, \Phi_{s1,s1}(\iota k_{F\downarrow}, q) \right)^2 .
\end{aligned}
\tag{150}
$$

The exponent that controls it in the vicinity of the $\sigma =\downarrow$ one-electron removal and LHB addition $s1$ branch line reads,

$$\xi^{\downarrow}_{s1}(k) = -1 + \sum_{\iota=\pm 1}\left(\frac{\iota\,\xi^{0}_{c\,c}}{2} + \Phi_{c,s1}(\iota 2k_F, q)\right)^2 + \sum_{\iota=\pm 1}\left(\frac{\iota\,\xi^{0}_{s1\,c}}{2} + \Phi_{s1,s1}(\iota k_{F\downarrow}, q)\right)^2 . \quad (151)$$

This latter exponent has the same formal expression for $\gamma = -1$ and $\gamma = +1$, respectively. The corresponding q ranges are though different, as given in Eq. (145). These $\uparrow$ and $\downarrow$ one-electron exponents are plotted in Figs. 8 and 9, respectively, as a function of the momentum $k/\pi \in]0, 1[$. The curves correspond to several u values, electronic densities $n_e = 0.3$ and $n_e = 0.7$, and a set of spin density values $m < n_e$.

The general expression, Eq. (112), of the σ one-electron spectral function $B_{\sigma,\gamma}(k,\omega)$, Eq. (4), near the $s1$ branch lines is in the present case given by,

$$B_{\sigma,\gamma}(k,\omega) = C_{\sigma,\gamma,s1}\left(\gamma\omega - \omega^{\sigma}_{s1}(k)\right)^{\xi^{\sigma}_{s1}(k)}; \qquad (\gamma\,\omega - \omega^{\sigma}_{s1}(k)) \geq 0\,, \qquad \gamma = \pm 1\,, \quad (152)$$

where $C_{\sigma,\gamma,s1}$ is a constant that has a fixed value for the k and ω ranges corresponding to small values of the energy deviation $(\gamma\omega - \omega^{\sigma}_{s1}(k))$. The spectrum $\omega^{\sigma}_{s1}(k)$ in such an energy deviation is that in Eq. (145). The exponent $\xi^{\sigma}_{s1}(k)$ is given in Eqs. (150) and (151).

The behaviors reached in the $u \rightarrow 0$ limit by the exponents, Eqs. (150) and (151), can be found by use in these equations of the parameters $\xi^{j}_{\beta\,\beta'}$ values given in Eq. (B.15) of Appendix B and of the $\beta = c, s1$ pseudofermion phase shifts $\Phi_{\beta,\beta'}(\iota q_{F\beta}, q)$ expressions provided in Eq. (B.10) of that Appendix. One then finds that the $\sigma =\uparrow$ one-electron removal exponent and the $\sigma =\downarrow$ one-electron LHB addition exponent have the following related behaviors,

$$\begin{aligned}
&\lim_{u\rightarrow 0}\xi^{\sigma}_{s1}(k) = \gamma_{\sigma}\,, \qquad k \in [k_{F\downarrow}, k_{F\uparrow}] \\
&\qquad\qquad \text{for } m \in [0, n_e] \text{ and } n_e \in [0, 1/2] \text{ and for } m \in [0, 1-n_e] \text{ and } n_e \in [1/2, 1] \\
&\lim_{u\rightarrow 0}\xi^{\sigma}_{s1}(k) = \gamma_{\sigma}\,, \qquad k \in [k_{F\downarrow}, \pi - k_{F\uparrow}] \\
&\qquad\qquad = 0\,, \qquad k \in [\pi - k_{F\uparrow}, k_{F\uparrow}] \\
&\qquad\qquad \text{for } m \in [1-n_e, n_e] \text{ and } n_e \in [1/2, 1]\,.
\end{aligned} \quad (153)$$

Furthermore, one finds that the $\sigma =\uparrow$ electron LHB addition and $\sigma =\downarrow$ electron removal exponents have also related behaviors given by,

$$\lim_{u\rightarrow 0}\xi^{\sigma}_{s1}(k) = \gamma_{\sigma} \quad \text{(for the whole branch lines } k \text{ range)}\,. \quad (154)$$

Hence the $\sigma =\uparrow$ one-electron spectral weight at and near these $s1$ branch lines vanishes in the $u \rightarrow 0$ limit both for electron removal and LHB addition.

As given generally in Eq. (121), for the n_e, m, and k ranges for which $\lim_{u\rightarrow 0}\xi^{\downarrow}_{s1}(k) = -1$ the line shape near the branch line is not of the power-law form, Eq. (152). In that limit it rather corresponds to the following δ-function-like $\sigma =\downarrow$ one-electron spectral weight distribution along it,

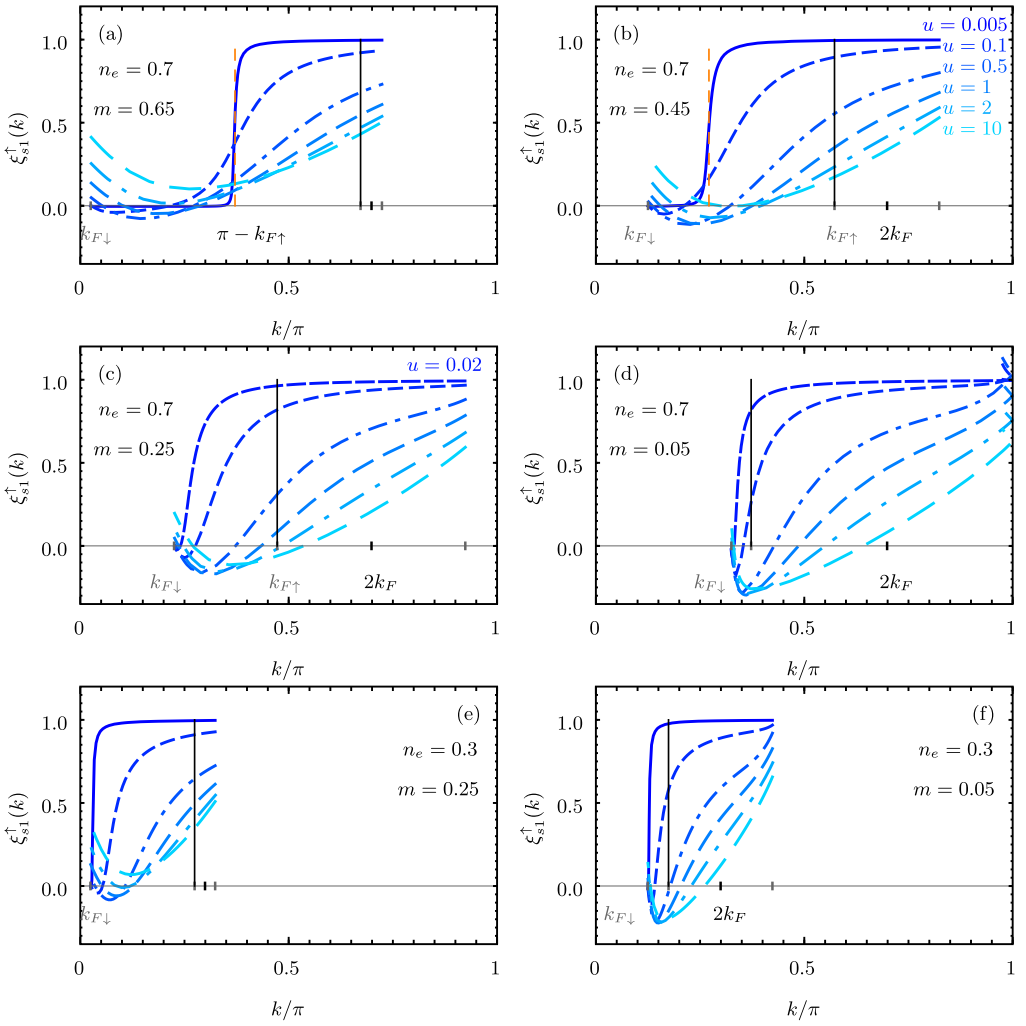

Fig. 8. The exponent $\xi^{\uparrow}_{s1}(k)$, Eq. (150), that controls the singularities in the vicinity of the $s1$ branch line whose (k,ω)-plane shape is defined by Eqs. (145), (147), and (149) is plotted for the $\sigma = \uparrow$ one-electron removal and LHB addition spectral function, Eq. (152), as a function of the momentum $k/\pi \in]0,1[$. The curves correspond to the same values of u, electronic density n_e, and spin density m as in Fig. 6. (For $k/\pi \in]-1,0[$ the exponent $\xi^{\uparrow}_{s1}(k)$ is given by $\xi^{\uparrow}_{s1}(k) = \xi^{\uparrow}_{s1}(-k)$ with $-k/\pi \in]0,1[$ as plotted here.)

$$\lim_{u\to 0} B_{\downarrow,-1}(k,\omega) = \delta\Big(\omega + \omega^{\downarrow}_{s1}(k)\Big) = \delta\Big(\omega - 2t\,(\cos k - \cos k_{F\downarrow})\Big)\,, \quad k \in [-k_{F\downarrow}, k_{F\downarrow}]\,,$$

$$\lim_{u\to 0} B_{\downarrow,+1}(k,\omega) = \delta\Big(\omega - \omega^{\downarrow}_{s1}(k)\Big) = \delta\Big(\omega + 2t\,(\cos k - \cos k_{F\downarrow})\Big)\,,$$

$$k \in [k_{F\downarrow}, k_{F\uparrow}] \ \text{ for } m \in [0, n_e] \text{ and } n_e \in [0,\, 1/2] \text{ and for } m \in [0,\, 1-n_e]$$

$$\text{and } n_e \in [1/2,\, 1]$$

$$k \in [k_{F\downarrow}, \pi - k_{F\uparrow}] \ \text{ for } m \in [1-n_e, n_e] \text{ and } n_e \in [1/2,\, 1]\,. \tag{155}$$

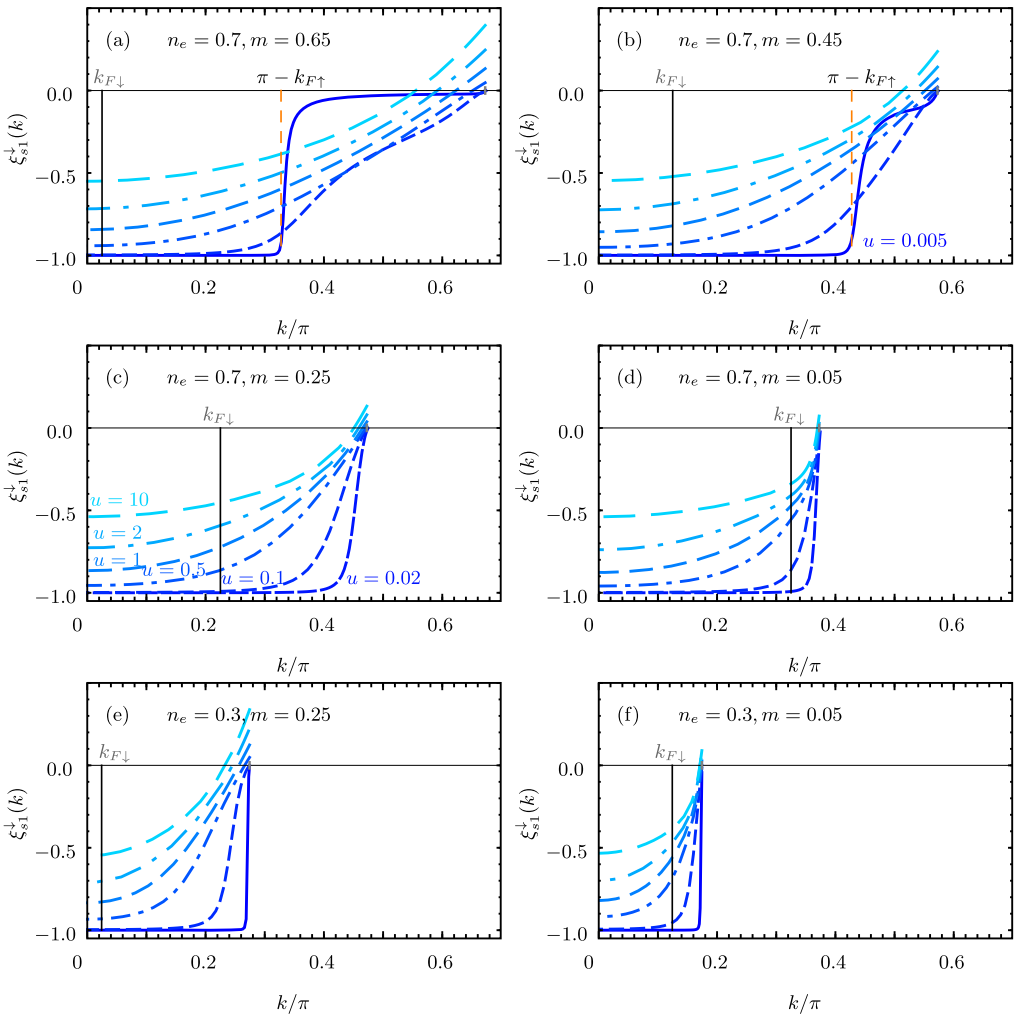

Fig. 9. The exponent $\xi^{\downarrow}_{s1}(k)$, Eq. (151), that controls the singularities in the vicinity of the $s1$ branch line whose (k,ω)-plane one-parametric spectrum is defined by Eqs. (145) and (148) is plotted for the $\sigma = \downarrow$ one-electron removal and LHB addition spectral function, Eq. (152), as a function of the momentum $k/\pi \in]0,1[$. The curves refer to the same values of u, electronic density n_e, and spin density m as in Fig. 6. (For $k/\pi \in]-1,0[$ the exponent $\xi^{\downarrow}_{s1}(k)$ is again given by $\xi^{\downarrow}_{s1}(k) = \xi^{\downarrow}_{s1}(-k)$ with $-k/\pi \in]0,1[$ as plotted here.)

The $u \rightarrow 0$ limiting behavior reported in Eq. (B.2) of Appendix B for the $s1$ energy dispersion $\varepsilon_{s1}(q)$ appearing in the spectrum $\omega^{\downarrow}_{s1}(k)$, Eq. (145), confirms that the latter spectrum becomes in the $u \rightarrow 0$ limit the corresponding $u = 0$ non-interacting electronic spectrum, as given in Eq. (155).

For the k range for which $\lim_{u\rightarrow 0}\xi^{\downarrow}_{s1}(k) = 0$, the $\downarrow$ one-electron addition spectral weight at and near the present $s1$ branch line vanishes in the $u \rightarrow 0$ limit.

For $u \gg 1$ the $s1$ branch line exponent expression is a continuous function of the spin density m. We have derived the corresponding exponent analytical expressions valid for $u \gg 1$ in

the $m \to 0$ and $m \to n_e$ limits. The $s1$ branch line momentum width vanishes in the $m \to 0$ limit both for $\downarrow$ one-electron LHB addition and $\uparrow$ one-electron removal.

The understanding of the relation of the behavior of these one-electron spectral functions in the $m \to 0$ limit to that at $m = 0$ involves the exact relation, Eq. (122). Consider the $m \to 0$ limit of corresponding one-electron spectral functions expressions valid for spin densities $m \in [-n_e, 0]$. According to that relation, the behaviors found here for the $s1$ branch line for $\uparrow$ one-electron LHB addition and $\downarrow$ one-electron removal are reached in that alternative limit for $\downarrow$ one-electron LHB addition and $\uparrow$ one-electron removal, respectively. This implies that the behavior found in the following for the $s1$ branch line for $\uparrow$ one-electron LHB addition and $\downarrow$ one-electron removal in the $m \to 0$ limit is that of the $s1$ branch line for one-electron LHB addition and removal, respectively, at $m = 0$.

We use in Eqs. (150) and (151) the values of the parameters $\xi^{j}_{\beta\,\beta'}$ obtained by combining Eqs. (B.17) and (B.18) of Appendix B for $u \gg 1$ with the expressions of the $\beta = c, s1$ pseudofermion phase shifts provided in Eq. (B.12) of that Appendix. Those refer to $u \gg 1$ and spin density $m \to 0$. We then find that the exponent in the spectral function expression, Eq. (152), that controls the line shape near the $\downarrow$ one-electron removal and $\uparrow$ one-electron LHB addition $s1$ branch line reads in these limits,

$$\begin{aligned}
\xi^{\sigma}_{s1}(k) = &-\frac{1}{2}\left(1-\left(\frac{k}{\pi n_e}\right)^2\right)\left(1+\frac{2\ln 2}{\pi\, u}\sin(\pi n_e)\right)-\frac{1}{2u}\cos\left(\frac{k}{n_e}\right)\sin(\pi n_e)\,, \\
&\sigma = \uparrow \text{ electron addition for } k \in [k_F, 3k_F] \text{ and } n_e \in [0, 2/3] \\
&\sigma = \uparrow \text{ electron addition for } k \in [k_F, \pi] \text{ and } n_e \in [2/3, 1] \\
&\sigma = \downarrow \text{ electron removal for } k \in [0, k_F] \text{ and } n_e \in [0, 1] \\
\xi^{\uparrow}_{s1}(k) = &-\frac{1}{2}\left(1-\left(\frac{(k-2\pi)}{\pi n_e}\right)^2\right)\left(1+\frac{2\ln 2}{\pi\, u}\sin(\pi n_e)\right)-\frac{1}{2u}\cos\left(\frac{k-2\pi}{n_e}\right)\sin(\pi n_e)\,, \\
&\uparrow \text{ electron addition for } k \in [(2\pi - 3k_F), \pi] \text{ and } n_e \in [2/3, 1]\,. \qquad (156)
\end{aligned}$$

This implies that,

$$\begin{aligned}
&\lim_{k\to 0}\xi^{\downarrow}_{s1}(k) = -\frac{1}{2}-\frac{1}{2u}\left(1+\frac{2\ln 2}{\pi}\right)\sin(\pi n_e)\,, \\
&\lim_{k\to k_F}\xi^{\sigma}_{s1}(k) = -\frac{3}{8}-\frac{3\ln 2}{4\pi\, u}\sin(\pi n_e)\,; \qquad \lim_{k\to 2k_F}\xi^{\sigma}_{s1}(k) = \frac{1}{2u}\sin(\pi n_e)\,, \\
&\lim_{k\to 3k_F}\xi^{\sigma}_{s1}(3k_F) = \lim_{k\to 2\pi-3k_F}\xi^{\uparrow}_{s1}(k) = \frac{5}{8}+\frac{5\ln 2}{4\pi\, u}\sin(\pi n_e)\,. \qquad (157)
\end{aligned}$$

There are two alternative procedures to reach the second exponent expression given in Eq. (156):

(i) One can use a new general exponent expression obtained upon replacing $\delta J^F_c = 1/2$ by $\delta J^F_c = -1/2$. It changes the terms $\xi^1_{c\,c}/2$ and $\xi^1_{s1\,c}/2$ in Eq. (150) to $-\xi^1_{c\,c}/2$ and $-\xi^1_{s1\,c}/2$, respectively.

(ii) One can alternatively use the present exponent expression, Eq. (150), upon bringing a $k > 0$ second Brillouin zone contribution to $k \in [-\pi, -(2\pi - 3k_F)]$. Relying on the $\xi^{\uparrow}_{s1}(k) = \xi^{\uparrow}_{s1}(-k)$ symmetry, we can then reach the expression valid for $k \in [(2\pi - 3k_F), \pi]$.

For $u \gg 1$ and $m \to 0$ the $\uparrow$ one-electron LHB addition exponent $\xi^{\uparrow}_{s1}(k)$ continuously changes from $\xi^{\uparrow}_{s1}(k) = -3/8$ for $k \to k_F$ to $\xi^{\uparrow}_{s1}(k) = 0$ for $k \to 2k_F$. For its other k ranges it is positive.

In these limits the $\downarrow$ one-electron removal exponent $\xi^{\downarrow}_{s1}(k)$ continuously changes from $\xi^{\downarrow}_{s1}(k) = -1/2$ for $k \rightarrow 0$ to $\xi^{\sigma}_{s1}(k) = -3/8$ for $k \rightarrow k_F$. The corresponding $m = 0$ one-electron LHB addition and one-electron removal exponents $\xi_{s1}(k)$, respectively, have similar behaviors.

In the $m \rightarrow n_e$ limit the $s1$ branch line momentum width vanishes both for $\uparrow$ one-electron LHB addition and $\downarrow$ one-electron removal. We use in the exponent expressions, Eqs. (150) and (151), the values for $u \gg 1$ and spin density $m \rightarrow n_e$ of the parameters $\xi^{j}_{\beta,\beta'}$ obtained by combining Eqs. (B.19) and (B.20) of Appendix B for $u \gg 1$ with the expressions of the $\beta = c, s1$ pseudofermion phase shifts provided in Eq. (B.14) of that Appendix. We then find the following exponent expressions for the $\uparrow$ one-electron removal and $\downarrow$ one-electron LHB addition $s1$ branch line,

$$\begin{aligned}
\xi^{\uparrow}_{s1}(k) &= \frac{1}{2}\left(\frac{k}{\pi n_e}\right)^2 + \frac{2}{\pi^2}\left[\arctan\left(\frac{1}{2}\cot\left(\frac{k}{2n_e}\right)\right)\right]^2 \\
&\quad - \frac{2}{\pi u}\left[\cos^2\left(\frac{k}{2n_e}\right) - \frac{k}{\pi n_e}\frac{2}{\pi}\arctan\left(\frac{1}{2}\cot\left(\frac{k}{2n_e}\right)\right)\right]\sin(\pi n_e)\,, \\
&\quad \uparrow \text{electron removal for } k \in [0, 2k_F]\,, \\
\xi^{\downarrow}_{s1}(k) &= -\frac{1}{2}\left(1 - \left(\frac{k}{\pi n_e}\right)^2\right) + \frac{2}{\pi^2}\left[\arctan\left(\frac{1}{2}\tan\left(\frac{k}{2n_e}\right)\right)\right]^2 \\
&\quad - \frac{2}{\pi u}\left[\cos^2\left(\frac{k}{2n_e}\right) + \frac{k}{\pi n_e}\frac{2}{\pi}\arctan\left(\frac{1}{2}\tan\left(\frac{k}{2n_e}\right)\right)\right]\sin(\pi n_e)\,, \\
&\quad \downarrow \text{electron addition for } k \in [0, 2k_F]\,.
\end{aligned} \tag{158}$$

This then implies that,

$$\begin{aligned}
\lim_{k\rightarrow 0}\xi^{\uparrow}_{s1}(k) &= \frac{1}{2} - \frac{2}{\pi u}\sin(\pi n_e)\,, \\
\lim_{k\rightarrow k_F}\xi^{\uparrow}_{s1}(k) &= \frac{1}{8} + 2\left(\frac{1}{\pi}\arctan\left(\frac{1}{2}\right)\right)^2 - \frac{1}{\pi u}\left(1 - \frac{2}{\pi}\arctan\left(\frac{1}{2}\right)\right)\sin(\pi n_e) \\
&\approx 0.16856 - \frac{0.22436}{u}\sin(\pi n_e)\,, \\
\lim_{k\rightarrow 2k_F}\xi^{\uparrow}_{s1}(k) &= \frac{1}{2}\,, \\
\lim_{k\rightarrow 0}\xi^{\downarrow}_{s1}(k) &= -\frac{1}{2} - \frac{2}{\pi u}\sin(\pi n_e)\,, \\
\lim_{k\rightarrow k_F}\xi^{\downarrow}_{s1}(k) &= -\frac{3}{8} + 2\left(\frac{1}{\pi}\arctan\left(\frac{1}{2}\right)\right)^2 - \frac{1}{\pi u}\left(1 + \frac{2}{\pi}\arctan\left(\frac{1}{2}\right)\right)\sin(\pi n_e) \\
&\approx -0.33144 - \frac{0.41226}{u}\sin(\pi n_e), \\
\lim_{k\rightarrow 2k_F}\xi^{\downarrow}_{s1}(k) &= \frac{1}{2} - \frac{2}{\pi u}\sin(\pi n_e)\,.
\end{aligned} \tag{159}$$

Analysis of these expressions and values reveals that in the $u \gg 1$ limit and $m \rightarrow n_e$ the $\uparrow$ one-electron removal exponent $\xi^{\uparrow}_{s1}(k)$ smoothly decreases from $\xi^{\uparrow}_{s1}(k) = 1/2$ for $k \rightarrow 0$ until it reaches a minimum value at $k = k_F$. For $k > k_F$ it continuously increases to $\xi^{\uparrow}_{s1}(k) = 1/2$ as

$k \rightarrow 2k_F$. In the same limits, the $\downarrow$ one-electron LHB addition exponent $\xi^{\downarrow}_{s1}(k)$ smoothly varies from $\xi^{\downarrow}_{s1}(k) = -1/2$ for $k \rightarrow 0$ to $\xi^{\downarrow}_{s1}(k) = 1/2$ for $k \rightarrow 2k_F$.

Moreover, analysis of Fig. 8 shows that the exponent $\xi^{\uparrow}_{s1}(k)$ only becomes negative for a part of the $s1$ branch line k interval. It starts at $k = k_{F\downarrow}$ and ends at a k momentum that for smaller and larger spin density values refers to one-electron LHB addition and removal, respectively. The u values for which it is negative are dependent of the densities. For the densities ranges $n_e \in [0, 1/2]$ and $m \in [0, 1 - n_e]$ and also for $n_e \in [1/2, 1]$ and $m \in [0, 1 - n_e]$ the exponent $\xi^{\uparrow}_{s1}(k)$ decreases upon increasing u from 1 for $u \rightarrow 0$ to its $u \gg 1$ values. In addition, according to Fig. 8 its u dependence is more involved for the densities intervals $n_e \in [1/2, 1]$ and $m \in [1 - n_e, n_e]$ for which it is given by 0 and 1 in the $u \rightarrow 0$ limit for different k ranges, respectively. For the k ranges for which it reads 1 for $u \rightarrow 0$ it remains being an increasing function of u for the whole u interval. For the k intervals for which it is given by 0 in the $u \rightarrow 0$ limit, upon increasing u it first decreases, goes through a minimum value, and then becomes an increasing function of u, until reaching its $u \rightarrow \infty$ k dependent values.

For $u > 0$ the exponent $\xi^{\downarrow}_{s1}(k)$, whose k dependence is plotted in Fig. 9, is in general negative. The exception refers to a small k region. It corresponds to the larger k values of its range. Both for the densities ranges $n_e \in [0, 1/2]$ and $m \in [0, 1 - n_e]$ and for $n_e \in [1/2, 1]$ and $m \in [0, 1 - n_e]$ the exponent $\xi^{\downarrow}_{s1}(k)$ increases upon increasing u from -1 for $u \rightarrow 0$ to its $u \gg 1$ k-dependent values. As also shown in that figure, its u dependence is more complex for the densities intervals $n_e \in [1/2, 1]$ and $m \in [1 - n_e, n_e]$ for which it is given by -1 and 0 in the $u \rightarrow 0$ limit for different k ranges, respectively. For the k ranges for which it reads -1 for $u \rightarrow 0$, it remains being an increasing function of u for the whole u interval. However, for the k domains for which it is given by 0 in the $u \rightarrow 0$ limit, upon increasing u it first decreases, goes through a minimum value, and then becomes an increasing function of u, until reaching its $u \rightarrow \infty$ k dependent values.

4.3. The σ one-electron UHB addition branch lines

The σ one-electron UHB addition branch lines are generated by processes that correspond to particular cases of those generated by the leading-order operators, Eqs. (78) and (84). Such general processes are behind the $\uparrow$ one-electron UHB addition spectrum, Eq. (79), and $\downarrow$ one-electron UHB addition spectrum, Eq. (85). Hence they are contained within such two-parametric spectra that occupy well defined regions in the (k, ω) plane.

As discussed in Section 3.8, following the direct relation of the σ one-electron UHB addition branch lines spectra and exponents to those of the $\bar{\sigma}$ one-electron removal branch lines, for simplicity here we limit our study to the σ one-electron UHB addition branch lines that in the $u \rightarrow 0$ limit contribute to the $u = 0$ σ one-electron addition spectrum. In the case of the $\uparrow$ and $\downarrow$ one-electron UHB addition spectral functions, those are the $s1$ branch line and one of the subbranches of the $c^{\pm}$ branch lines, respectively.

As for the $\downarrow$ one-electron removal $s1$ branch line, the spectrum that defines the (k, ω)-plane spectrum of the $\uparrow$ one-electron UHB addition $s1$ branch line and the corresponding exponent given below are even functions of k, $\omega^{\sigma}_{s1}(k) = \omega^{\sigma}_{s1}(-k)$ and $\xi^{\sigma}_{s1}(k) = \xi^{\sigma}_{s1}(-k)$, respectively. For simplicity, we thus restrict our following analysis to a reduced first Brillouin-zone scheme for positive momentum values, $k \in [0, \pi]$.

This $s1$ branch line refers to excited energy eigenstates with the following number deviations relative to those of the initial ground state,

$$\delta N_c^F = -1\,; \quad \delta J_c^F = 1/2\,; \quad \delta N_{s1}^F = \delta J_{s1}^F = 0\,; \quad \delta N_{s1}^{NF} = -1\,;$$
$$\delta N_{\eta 1} = 1\,; \quad \delta J_{\eta 1} = -1/2\,. \tag{160}$$

Its (k,ω)-plane one-parametric spectrum reads,

$$\omega_{s1}^{\uparrow}(k) = 2\mu - \varepsilon_{s1}(q)\,; \quad q \in [-k_{F\downarrow}, k_{F\downarrow}]\,. \tag{161}$$

Here $\varepsilon_{s1}(q)$ is the $s1$ band energy dispersion, Eq. (45) for $\beta = s1$. Moreover, 2μ stands for the energy scale defined in Eq. (52). Within an extended zone scheme, the general relation of the $k > 0$ excitation momentum to the $s1$ band momentum q in Eq. (161) is,

$$k = \pi - q \in [(\pi - k_{F\downarrow}), (\pi + k_{F\downarrow})]\,. \tag{162}$$

On the one hand, bringing this spectrum to the first Brillouin zone leads to two subbranches that refer to excitation momentum ranges $k \in [(\pi - k_{F\downarrow}), \pi]$ and $k = \in [-\pi, -(\pi - k_{F\downarrow})]$, respectively. On the other hand, a contribution from $k < 0$ extended zone scheme second Brillouin zone interval also leads to the $k \in [(\pi - k_{F\downarrow}), \pi]$ range. We checked that the two corresponding spectral-function contributions to the momentum range $k \in [(\pi - k_{F\downarrow}), \pi]$ lead to the same power-law type of spectral-weight distributions in the vicinity of the $s1$ branch line. The corresponding reduced first-Brillouin-zone scheme used here for $k \in [0, \pi]$ excitation momentum relates to the $s1$ band momentum as,

$$k = \pi - q = [(\pi - k_{F\downarrow}), \pi]\,, \tag{163}$$

for $q \in [0, k_{F\downarrow}]$. (Online, the $\uparrow$ one-electron UHB addition $s1$ branch line is green in Figs. 1–5; This branch line lays above the UHB pseudogap in Figs. 2–5, which refer to intermediate and large u values.)

The momentum dependent exponent of general form, Eq. (112), that controls the line shape near the branch line is given by,

$$\xi_{s1}^{\uparrow}(k) = -1 + \sum_{\iota=\pm 1}\left(-\frac{\iota\,\xi_{c\,c}^0}{2} - \Phi_{c,s1}(\iota 2k_F, q)\right)^2 + \sum_{\iota=\pm 1}\left(-\frac{\iota\,\xi_{s1\,c}^0}{2} - \Phi_{s1,s1}(\iota k_{F\downarrow}, q)\right)^2 . \tag{164}$$

This exponent is plotted in Fig. 10 as a function of the momentum $k/\pi \in]0, 1[$. The curves refer to several u values, electronic densities $n_e = 0.3$ and $n_e = 0.7$, and a set of spin density values $m < n_e$.

Near the present $s1$ branch line, the $\sigma = \uparrow$ one-electron addition spectral function $B_{\uparrow,+1}(k,\omega)$, Eq. (4), corresponds to the UHB. It has the following power-law behavior,

$$B_{\uparrow,+1}^{\rm UHB}(k,\omega) = C_{\uparrow,s1}^{\rm UHB}\left(\omega - \omega_{s1}^{\uparrow}(k)\right)^{\xi_{s1}^{\uparrow}(k)}\,; \quad (\omega - \omega_{s1}^{\uparrow}(k)) \geq 0\,. \tag{165}$$

Here $C_{\uparrow,s1}^{\rm UHB}$ is a constant that has a fixed value for the k and ω ranges corresponding to small values of the energy deviation $(\omega - \omega_{s1}^{\uparrow}(k))$. The spectrum $\omega_{s1}^{\uparrow}(k)$ in such an energy deviation is that in Eq. (161). The exponent $\xi_{s1}^{\uparrow}(k)$ is given in Eq. (164).

The direct relation of such an exponent to that of the $\downarrow$ one-electron removal $s1$ branch line enables deriving its behaviors for both $u \to 0$ and $u \gg 1$ from those of that other exponent. In the $u \to 0$ limit one finds the following value,

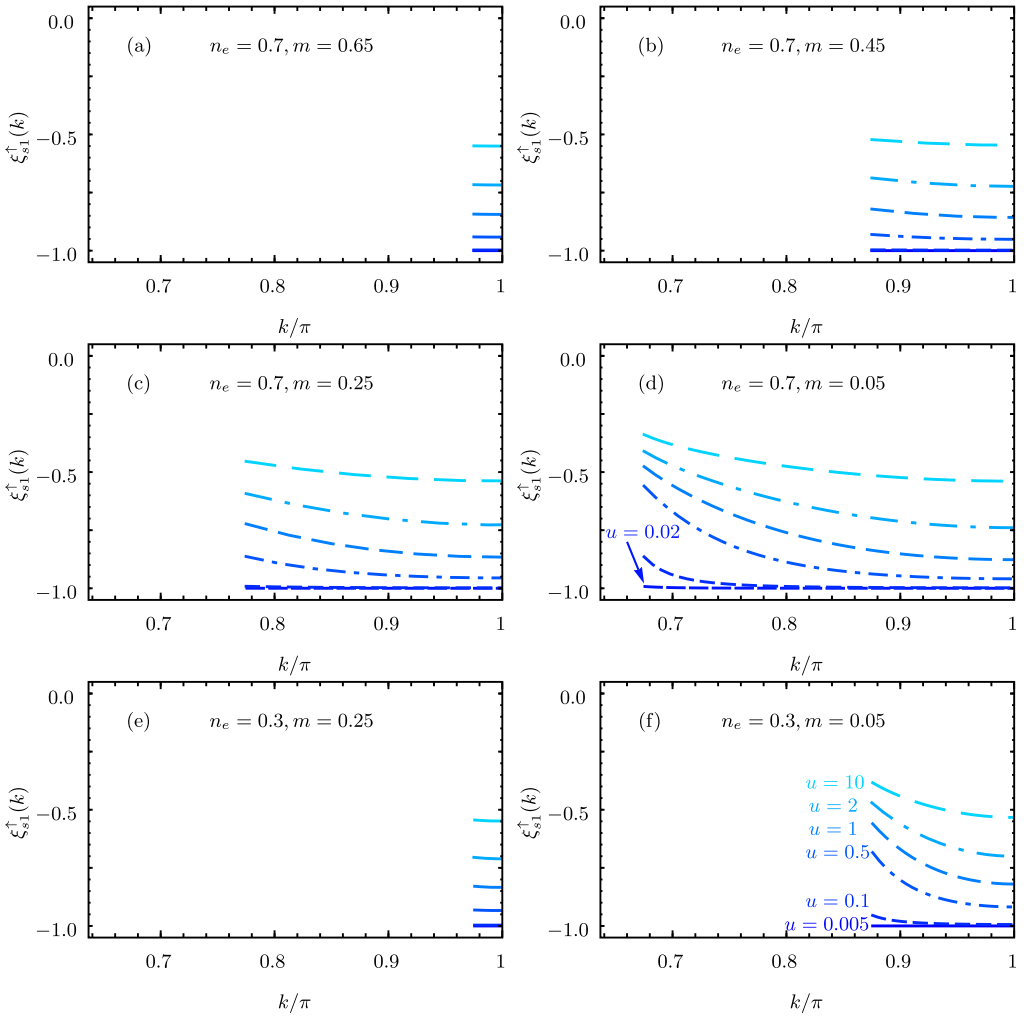

Fig. 10. The exponent $\xi^{\uparrow}_{s1}(k)$, Eq. (164), that controls the singularities in the vicinity of the $s1$ branch line whose (k,ω)-plane one-parametric spectrum is defined by Eq. (161) is plotted for the $\sigma = \uparrow$ one-electron UHB addition spectral function, Eq. (165), as a function of the momentum $k/\pi \in]k_0/\pi, 1[$. Here $]k_0/\pi, 1[$ with $0 < k_0 < \pi$ is a k interval that contains the branch line. The curves correspond to the same values of u, electronic density n_e, and spin density m as in Fig. 6. (For $k/\pi \in]-1, -k_0/\pi[$ the exponent $\xi^{\uparrow}_{s1}(k)$ is given by $\xi^{\uparrow}_{s1}(k) = \xi^{\uparrow}_{s1}(-k)$ with $-k/\pi \in]k_0/\pi, 1[$ as plotted here.)

$$\lim_{u\to 0} \xi^{\uparrow}_{s1}(k) = -1 \quad \text{(for the whole above branch line } k \text{ range)}. \tag{166}$$

Hence, consistently with Eq. (121), for $u \to 0$ this branch line acquires the following δ-function-like one-electron spectral weight distribution along it,

$$\lim_{u\to 0} B^{\rm UHB}_{\uparrow,+1}(k,\omega) = \delta\Big(\omega - \omega^{\uparrow}_{s1}(k)\Big) = \delta\Big(\omega + 2t(\cos k - \cos k_{F\uparrow})\Big), \quad |k| \in [(\pi - k_{F\downarrow}), \pi]. \tag{167}$$

The $u \rightarrow 0$ limiting behavior reported in Eq. (B.2) of Appendix B for the $s1$ energy dispersion $\varepsilon_{s1}(q)$ appearing in the spectrum $\omega^{\uparrow}_{s1}(k)$, Eq. (161), confirms that the latter spectrum becomes in the $u \rightarrow 0$ limit the corresponding $u = 0$ non-interacting electronic spectrum, as given in Eq. (167).

The expression found for $u \gg 1$ and $m \rightarrow 0$ for the exponent, Eq. (164), is given by,

$$\xi^{\uparrow}_{s1}(k) = -\frac{1}{2}\left(1 - \left(\frac{\pi - k}{\pi n_e}\right)^2\right)\left(1 + \frac{2\ln 2}{\pi\, u}\sin(\pi n_e)\right) - \frac{1}{2u}\cos\left(\frac{\pi - k}{n_e}\right)\sin(\pi n_e)\,. \tag{168}$$

This implies that,

$$\lim_{k\rightarrow \pi - k_F} \xi^{\uparrow}_{s1}(k) = -\frac{3}{8} - \frac{3\ln 2}{4\pi\, u}\sin(\pi n_e)\,,$$
$$\lim_{k\rightarrow \pi} \xi^{\uparrow}_{s1}(k) = -\frac{1}{2} - \frac{1}{2u}\left(1 + \frac{2\ln 2}{\pi}\right)\sin(\pi n_e)\,. \tag{169}$$

It follows from the use of the exact relation, Eq. (122), that similar behaviors apply to the $s1$ branch line of the $m = 0$ one-electron UHB addition spectral function. In the $m \rightarrow n_e$ limit the present $s1$ branch line momentum width vanishes. Hence it does not exist in that limit.

Analysis of Fig. 10 reveals that for $m < n_e$ the $s1$ branch-line exponent, Eq. (164), is a decreasing function of the momentum k. Moreover, it increases upon increasing u and remains negative for all momentum k and $m < n_e$ densities ranges.

Next, we consider the $\downarrow$ one-electron UHB addition spectral function. The spectra $\omega^{\sigma}_{c^{\pm}}(k)$ that define the (k,ω)-plane shape of the c^{+} branch line and its twin c^{-} branch line and the corresponding exponents $\xi^{\sigma}_{c^{\pm}}(k)$, are related as given in Eq. (124) for $\uparrow$ electron removal. Considering the c^{+} branch line in a reduced first Brillouin-zone scheme for which $k \in [-\pi, \pi]$, contains exactly the same information as considering both the c^{+} and c^{-} branch lines for the positive excitation momentum range $k \in [0, \pi]$.

In the following we consider only the k range associated with the subbranches for which the exponent $\xi^{\downarrow}_{c^{+}}(k) = \xi^{\downarrow}_{c^{-}}(-k)$ contributes to the $\downarrow$ one-electron spectral weight as $u \rightarrow 0$. It turns out that for the exponent $\xi^{\downarrow}_{c^{+}}(k)$ such a subbranch is contained in the positive excitation momentum range $k \in [0, \pi]$.

The one σ one-electron UHB addition c^{+} branch line is associated with excited energy eigenstates with the following number deviations relative to those of the initial ground state,

$$\delta N^{F}_{c} = 0\,; \quad \delta J^{F}_{c} = \mp 1/2\,; \quad \delta N^{NF}_{c} = -1\,; \quad \delta N^{F}_{s1} = 0\,; \quad \delta J^{F}_{s1} = 1/2\,;$$
$$\delta N_{\eta 1} = 1\,; \quad \delta J_{\eta 1} = \pm 1/2\,. \tag{170}$$

The one-parametric spectrum of general form, Eq. (110), that defines the (k,ω)-plane shape of this line reads,

$$\omega^{\downarrow}_{c^{+}}(k) = 2\mu - \varepsilon_{c}(q)\,; \quad q \in [-2k_F, 2k_F]\,. \tag{171}$$

Here $\varepsilon_{c}(q)$ is the c band energy dispersion, Eq. (45) for $\beta = c$. The corresponding c band momentum q is within an extended zone scheme related to the excitation momentum k as,

$$k = \pi + k_{F\downarrow} - q \in [(\pi - k_{F\uparrow}), (\pi + 2k_F + k_{F\downarrow})]\,. \tag{172}$$

Bringing this spectrum to the $k \in [-\pi, \pi]$ reduced first Brillouin-zone, leads to two (k, ω)-plane c^+ branch line subbranches. Their k intervals are given by $k = -\pi + k_{F\downarrow} - q \in [-\pi, -(\pi - 2k_F - k_{F\downarrow})]$ and $k = \pi + k_{F\downarrow} - q \in [(\pi - k_{F\uparrow}), \pi]$, respectively. As mentioned above, in the following we only consider the second of such momentum ranges,

$$k = \pi + k_{F\downarrow} - q \in [(\pi - k_{F\uparrow}), \pi]\,. \tag{173}$$

Indeed, it is that for which the exponent $\xi^{\downarrow}_{c^+}(k) = \xi^{\downarrow}_{c^-}(-k)$ reads -1 in the $u \rightarrow 0$ limit. Hence for that k range the corresponding branch line contributes to the δ-function-like $\downarrow$ one-electron spectrum in that limit. (Online, the $\downarrow$ one-electron UHB addition c^+ branch line is blue in Figs. 1–5; This branch line lays above the UHB pseudogap in Figs. 2–5, which refer to intermediate and large u values.)

The momentum dependent exponent of general form, Eq. (112), that controls the line shape near the branch line is in the present case given by,

$$\xi^{\downarrow}_{c^+}(k) = \xi^{\downarrow}_{c^-}(-k) = -1 + \sum_{\iota=\pm 1}\left(\frac{\xi^{1}_{c\,s1}}{2} - \Phi_{c,c}(\iota 2k_F, q)\right)^2 + \sum_{\iota=\pm 1}\left(\frac{\xi^{1}_{s1\,s1}}{2} - \Phi_{s1,c}(\iota k_{F\downarrow}, q)\right)^2 . \tag{174}$$

It is plotted in Fig. 11 as a function of the momentum $k/\pi \in]0, 1[$. The curves correspond to several u values, electronic densities $n_e = 0.3$ and $n_e = 0.7$, and a set of spin density values $m < n_e$.

In the vicinity of the present $c^{\pm}$ branch lines, the $\sigma = \downarrow$ one-electron addition spectral function $B_{\downarrow,+1}(k, \omega)$, Eq. (4), refers to the UHB. It has the following power-law behavior,

$$B^{\rm UHB}_{\downarrow,+1}(k, \omega) = C^{\rm UHB}_{\downarrow,c^{\pm}}\left(\omega - \omega^{\downarrow}_{c^{\pm}}(k)\right)^{\xi^{\downarrow}_{c^{\pm}}(k)}\,; \qquad (\omega - \omega^{\downarrow}_{c^{\pm}}(k)) \geq 0\,. \tag{175}$$

Here $C^{\rm UHB}_{\downarrow,c^{\pm}}$ is a constant that has a fixed value for the k and ω ranges corresponding to small values of the energy deviation $(\omega - \omega^{\downarrow}_{c^{\pm}}(k))$. The spectrum $\omega^{\downarrow}_{c^+}(k)$ in such an energy deviation is that in Eqs. (171) and (173). The exponent $\xi^{\downarrow}_{c^+}(k)$ is given in Eq. (174). Furthermore, $\omega^{\downarrow}_{c^-}(k) = \omega^{\downarrow}_{c^+}(-k)$ and $\xi^{\downarrow}_{c^-}(k) = \xi^{\downarrow}_{c^+}(-k)$.

The direct relation of the exponent, Eq. (174), to that of the corresponding $\uparrow$ one-electron removal $c^{\pm}$ branch lines subbranches enables deriving its behaviors for both $u \rightarrow 0$ and $u \gg 1$ from those of these other exponents. In the $u \rightarrow 0$ limit one finds the following values in the k range, Eq. (173),

$$\begin{aligned}
\lim_{u\rightarrow 0}\xi^{\downarrow}_{c^+}(k) &= 0\,, \qquad k \in [(\pi - k_{F\downarrow}), \pi]\,,\\
&= -1\,, \qquad k \in [(\pi - k_{F\uparrow}), (\pi - k_{F\downarrow})]\,,\\
\lim_{u\rightarrow 0}\xi^{\downarrow}_{c^-}(k) &= -1\,, \qquad k \in [-(\pi - k_{F\downarrow}), -(\pi - k_{F\uparrow})]\,,\\
&= 0\,, \qquad k \in [-\pi, -(\pi - k_{F\downarrow})]\,.
\end{aligned} \tag{176}$$

For the k ranges for which such exponents read -1 the line shape becomes δ-function-like for $u \rightarrow 0$, as given in Eq. (121). In the present cases we find,

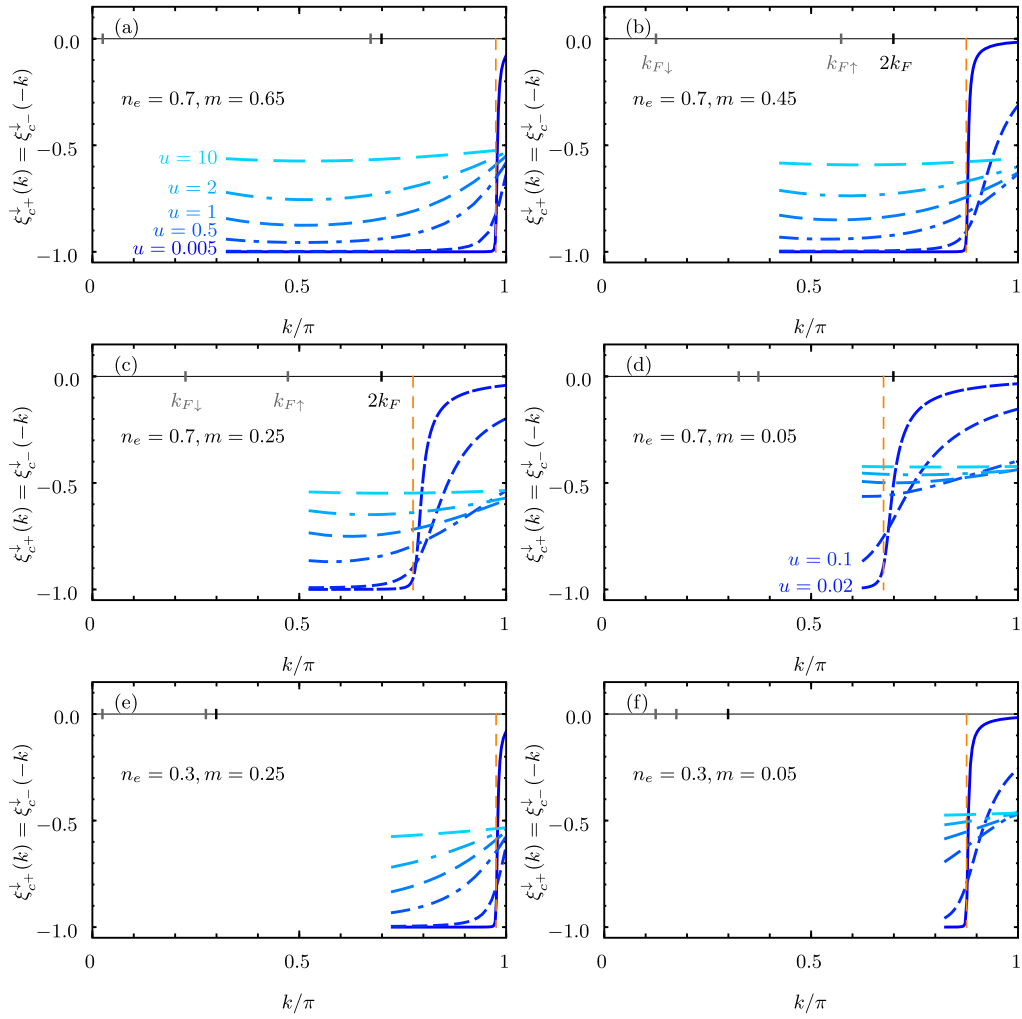

Fig. 11. The exponent $\xi^{\downarrow}_{c^+}(k) = \xi^{\downarrow}_{c^-}(-k)$, Eq. (174), that controls the singularities in the vicinity of the c^+ branch line whose (k,ω)-plane one-parametric spectrum is defined by Eq. (171) is plotted for the $\sigma = \downarrow$ one-electron UHB addition spectral function, Eq. (175), as a function of the momentum $k/\pi \in]0,1[$. The curves refer to the same values of u, electronic density n_e, and spin density m as in Fig. 6.

$$\lim_{u\to 0} B^{\rm UHB}_{\downarrow,+1}(k,\omega) = \delta\Big(\omega - \omega^{\downarrow}_{c^-}(k)\Big) = \delta\Big(\omega + 2t(\cos k - \cos k_{F\downarrow})\Big)\,,$$
$$k \in [-(\pi - k_{F\downarrow}), -(\pi - k_{F\uparrow})]\,,$$
$$= \delta\Big(\omega - \omega^{\downarrow}_{c^+}(k)\Big) = \delta\Big(\omega + 2t(\cos k - \cos k_{F\downarrow})\Big)\,,$$
$$k \in [(\pi - k_{F\uparrow}), (\pi - k_{F\downarrow})]\,. \qquad (177)$$

That the spectrum $\omega^{\downarrow}_{c^+}(k) = \omega^{\downarrow}_{c^-}(-k)$, Eq. (171), becomes in the $u \to 0$ limit the corresponding $u = 0$ non-interacting electronic spectrum is confirmed by the $u \to 0$ limiting behavior reported in Eq. (B.1) of Appendix B for the c band energy dispersion $\varepsilon_c(q)$ appearing in the $u > 0$ spectrum general expression, Eq. (171). For the k ranges for which the exponent is given by 0 for

$u \to 0$, the one-electron spectral weight at and near the corresponding branch lines vanishes in the $u \to 0$ limit.

For $u \gg 1$ and $m \to 0$ one finds the following expressions,

$$\xi^{\downarrow}_{c^{\pm}}(k) = -\frac{3}{8} + \frac{\ln 2}{4\pi\, u}\left(\sin(\pi n_e) \mp 2\sin\left(k \mp \frac{\pi}{2}n_e\right)\right) . \tag{178}$$

These expressions apply as well to the $c^{\pm}$ branch lines of the $m = 0$ one-electron UHB addition spectral function.

In the $m \to n_e$ limit the exponents expressions are found to read,

$$\xi^{\downarrow}_{c^{\pm}}(k) = -\frac{1}{2} \mp \frac{2}{\pi\, u}\sin k\,. \tag{179}$$

Analysis of Fig. 11 confirms the main effect on the k dependence of the $\downarrow$ one-electron UHB addition exponent $\xi^{\downarrow}_{c^+}(k) = \xi^{\downarrow}_{c^-}(-k)$, Eq. (174), of increasing the on-site repulsion u from $u \ll 1$ to $u \gg 1$. This continuously changes its $u \to 0$ values -1 and 0 for the k ranges given in Eq. (176) to a k independent negative value for $k \in [0, \pi]$ as $u \to \infty$. The latter value smoothly changes from $-3/8$ for $m \to 0$ to $-1/2$ for $m \to n_e$.

4.4. The ↑ one-electron removal and ↓ one-electron UHB addition spectral functions near other $s1'$ spectral features for $0 < m < n_e$

The importance of the branch lines is confirmed by in the $u \to 0$ limit they recovering most of the $u = 0$ δ-function-like σ one-electron spectrum k ranges. This is confirmed by combining Eqs. (138), (155), (167), (177). Interestingly, part of that spectral weight stems from the $u > 0$ UHB.

The k subrange of the $u = 0$ σ one-electron spectrum that does not stem from branch lines refers for $0 < m < n_e$ to the momentum interval $k \in [-k_{F\downarrow}, k_{F\downarrow}]$ for $\uparrow$ one-electron removal. For $\downarrow$ one-electron UHB addition it is related to that of $\uparrow$ one-electron removal by the excitation momentum and energy transformations $k \to \pi - k$ and $\omega \to 2\mu - \omega$, respectively. When brought to the first Brillouin zone, it thus corresponds to the two k ranges $k \in [-\pi, -(\pi - k_{F\downarrow})]$ and $k \in [\pi - k_{F\downarrow}, \pi]$. The corresponding $u = 0$ spectral weight stems from well-defined $u > 0$ spectral features in the vicinity of which the PDT spectral functions expressions involve state summations difficult to compute.

On the one hand, in the $m \to 0$ limit the width of the above momentum intervals vanish. Consistently, at $m = 0$ the whole $u = 0$ one-electron spectral weight is generated in the $u \to 0$ limit from that of $u > 0$ branch lines.

On the other hand, for spin densities $m \in]0, n_e]$ the $u = 0$ $\uparrow$ one-electron removal spectral weight missing for $k \in [-k_{F\downarrow}, k_{F\downarrow}]$ stems from a $u > 0$ $s1'$ feature that is generated by transitions to excited energy eigenstates with the following number deviations relative to those of the initial ground state,

$$\begin{aligned} &\delta N^F_c = \delta J^F_c = 0\,; \quad \delta N^{NF}_c = -1\,; \quad \delta N^F_{s1} = 1\,; \\ &\delta J^F_{s1} = \pm 1\,; \quad \delta N^{NF}_{s1} = -1\,. \end{aligned} \tag{180}$$

The one-parametric spectrum of this line is given by,

$$\begin{aligned} \omega^{\uparrow}_{s1'}(k) &= -\varepsilon_{s1}(-k) - \varepsilon_c(\pm 2k_{F\downarrow}) = -\varepsilon_{s1}(q) - \varepsilon_c(\pm 2k_{F\downarrow})\,, \quad q \in [-k_{F\downarrow}, k_{F\downarrow}]\,, \\ k &= -q \in [-k_{F\downarrow}, k_{F\downarrow}]\,. \end{aligned} \tag{181}$$

The c and $s1$ band energy dispersions appearing here are defined in Eq. (45) for $\beta = c, s1$.

While the line shape analytical expression near the present $s1'$ line remains an unsolved problem for $u > 0$, in the $u \rightarrow 0$ limit it becomes δ-function-like,

$$\lim_{u\rightarrow 0} B_{\uparrow,-1}(k,\omega) = \delta\Big(\omega + \omega^{\uparrow}_{s1'}(k)\Big) = \delta\Big(\omega - 2t\,(\cos k - \cos k_{F\uparrow})\Big)\,,$$
$$k \in [-k_{F\downarrow}, k_{F\downarrow}]\,. \quad (182)$$

Moreover, for spin densities $m \in]0, n_e]$ the $u = 0$ $\downarrow$ one-electron addition spectral weight missing for $|k| \in [\pi - k_{F\downarrow}, \pi]$ stems from a $u > 0$ UHB $s1'$ feature that is generated by transitions to excited energy eigenstates with the following number deviations relative to those of the initial ground state,

$$\delta N^F_c = -1\,; \quad \delta J^F_c = 0\,; \quad \delta N^F_{s1} = 0\,; \quad \delta J^F_{s1} = 1/2\,;$$
$$\delta N_{\eta 1} = 1\,; \quad \delta J_{\eta 1} = -1/2\,. \quad (183)$$

There is another such an $s1'$ line for $k < 0$.

The one-parametric spectrum that defines the (k,ω)-plane form of this line reads,

$$\omega^{\downarrow}_{s1'}(k) = 2\mu - \varepsilon_{s1}(\pi - k) + \varepsilon_{s1}(k_{F\uparrow}) = 2\mu - \varepsilon_{s1}(q) + \varepsilon_{s1}(k_{F\uparrow})\,, \quad q \in [0, k_{F\downarrow}]\,.$$
$$k = \pi - q \in [\pi - k_{F\downarrow}, \pi]\,. \quad (184)$$

The line shape analytical expression near this $s1'$ feature remains again an open problem for $u > 0$ except in the $u \rightarrow 0$ limit in which it is δ-function-like,

$$\lim_{u\rightarrow 0} B^{\rm UHB}_{\downarrow,+1}(k,\omega) = \delta\Big(\omega - \omega^{\downarrow}_{s1'}(k)\Big) = \delta\Big(\omega + 2t\,(\cos k - \cos k_{F\downarrow})\Big)\,,$$
$$|k| \in [\pi - k_{F\downarrow}, \pi]\,. \quad (185)$$

The present $\uparrow$ one-electron removal and $\downarrow$ one-electron UHB addition $s1'$ lines are represented in Figs. 1–5 by sets of diamond symbols.

5. Concluding remarks

In this paper we have studied the momentum and energy dependence of the σ one-electron spectral functions, Eq. (4), of the 1D Hubbard model at finite magnetic field. Our analysis of the problem focused on the vicinity of two types of singular features: The branch lines and border lines whose (k,ω)-plane spectra general form is given in Eqs. (110) and (118), respectively. The branch lines are represented in Figs. 1–5 by solid lines and dashed lines for the k ranges for which the corresponding exponent $\xi^{\sigma}_{\beta}(k)$, Eq. (112), is negative and positive, respectively. The one-electron removal and LWS addition border lines are in these figures represented by dashed–dotted lines.

To access the expressions of the one-electron spectral functions near these singular features, we have used the PDT introduced in Refs. [39,40]. Its applications to the study of the 1D Hubbard model one-electron spectral functions had been limited to zero magnetic field [46–49]. The momentum dependence of the exponents that in the TL control the line shapes in the vicinity of the σ one-electron spectral functions branch lines in a magnetic field was derived here for the whole $u > 0$ range and all densities. For the k ranges for which such exponents $\xi^{\sigma}_{\beta}(k)$ (which are plotted in Figs. 6–11) are negative, there are singularity cusps in the corresponding σ one-electron spectral functions, Eq. (4). The same occurs in the (k,ω)-plane vicinity of the border lines.

The $u > 0$ branch lines singularity cusps play an important role in the model physics. For instance, in the $u \rightarrow 0$ limit they recover the $u = 0$ δ-function-like σ one-electron spectrum for

most of its momentum k range. This can be confirmed from a combined analysis of Eqs. (138), (155), (167), and (177). At vanishing spin density, $m = 0$, the whole $u = 0$ one-electron spectral weight stems in the $u \rightarrow 0$ limit from that of $u > 0$ branch lines.

The momentum subrange for which the $u = 0$ δ-function-like σ one-electron spectrum does not stem from branch lines for $m \neq 0$ is $k \in [0, k_{F\downarrow}]$ for $\uparrow$ one-electron removal and $k \in [\pi - k_{F\downarrow}, \pi]$ for $\downarrow$ one-electron addition. The PDT also accounts for the processes that give rise in the $u \rightarrow 0$ limit to the $u = 0$ one-electron spectrum for such a k intervals. However, the expression of the corresponding one-electron spectral functions near the line spectral features under consideration remains for $u > 0$ an involved unsolved technical problem. (These $u > 0$ line features are represented in Figs. 1–5 by sets of diamond symbols.)

The low-energy behavior of the correlation functions of the 1D Hubbard model at finite magnetic field has been the subject of several previous studies [14–16,32]. To our knowledge, no previous investigations accessed for finite magnetic fields the repulsion u, electronic density n_e, spin density m, and momentum dependence of the exponents that in the TL control at high-energy the σ one-electron spectral functions expressions in the vicinity of their branch lines singularity cusps.

Our study clarifies beyond the results of Refs. [39,40] how the σ one-electron creation and annihilation operators matrix elements between the ground state and excited energy eigenstates are accounted for by the PDT. Specifically, we have shown that the corresponding microscopic processes involve the rotated electrons as a needed link of the non-perturbative relation between the electrons and the pseudofermions. Moreover, in this paper the σ one-electron addition LHB and UHB were defined in terms of the occupancy configurations of such rotated electrons for the whole $u > 0$ range and all electronic densities and spin densities.

Concerning the relation of our theoretical results to actual condensed-matter systems, angle-resolved photoemission spectroscopy at finite magnetic field is not possible, since the field would severely deflect the photoelectrons. However, it is possible to measure the local spectral function on quasi-1D metals by (scanning) tunneling spectroscopy at finite magnetic field. Such experiments would provide some partial information on the spectral features theoretically studied in this paper by means of the 1D Hubbard model at finite magnetic field.

Such a model has been implemented with ultra-cold atoms on optical lattices [69,70]. The related antiferromagnetic Heisenberg spin chain has been prepared to characterize its spin configurations [71]. An interesting program would be the observation of the one-atom spectral weight distributions over the (k, ω) plane associated with the spectral functions studied in this paper in systems of spin $1/2$ ultra-cold fermionic atoms on optical lattices.

Acknowledgements

We thank Ralph Claessen, Henrik Johannesson, Alexander Moreno, and Pedro D. Sacramento for illuminating discussions and the support by the Portuguese FCT through the Grant UID/FIS/04650/2013. J.M.P.C. acknowledges the hospitality of the Department of Physics at the University of Gothenburg, where the final part of this work was conducted.

Appendix A. The Bethe-ansatz equations within the β pseudoparticle representation and related quantities needed for the studies of this paper

Here the pseudoparticle momentum distribution functional notation used in this paper for the 1D Hubbard model BA equations in the TL [7] is revisited. Moreover, the energy eigenvalues

are expressed in terms of the rapidities that are the solutions of such equations. We also provide useful information on the specific solutions of these equations for the excited energy eigenstates belonging to a PS, as defined in Section 2.4.

The integral equations that define the rapidity dressed phase shifts $2\pi\,\bar{\Phi}_{\beta,\beta'}(r,r')$ in the expression, Eq. (47), of the related β pseudofermion phase shifts $2\pi\,\Phi_{\beta,\beta'}(q_j,q_{j'})$ are also provided. The f functions in the second-order terms of the energy functional, Eq. (42), are expressed in terms of such β pseudofermion phase shifts.

Furthermore, the $\beta = c, s1$ lowest peak weights $A_{\beta}^{(0,0)}$ and corresponding relative weights $a_\beta = a_\beta(m_{\beta,+1}, m_{\beta,-1})$ in the β pseudofermion spectral functions, Eq. (92), are written in terms of the β pseudofermion phase-shift functional $\Phi_\beta^T(q_j)$, Eq. (101). Finally, two different forms that the related $\beta = c, s1$ pseudofermion spectral function $B_{Q_\beta}(k',\omega')$ acquires in the TL are given.

Within the pseudoparticle momentum distribution functional notation used in this paper, the BA equations considered in Ref. [7] read,

$$q_j = k^c(q_j) + \frac{2}{L}\sum_{n=1}^{\infty}\sum_{j'=1}^{L_{sn}} N_{sn}(q_{j'})\arctan\left(\frac{\sin k^c(q_j) - \Lambda^{sn}(q_{j'})}{nu}\right)$$

$$+\,\frac{2}{L}\sum_{n=1}^{\infty}\sum_{j'=1}^{L_{\eta n}} N_{\eta n}(q_{j'})\arctan\left(\frac{\sin k^c(q_j) - \Lambda^{\eta n}(q_{j'})}{nu}\right), \qquad j = 1,...,L\,, \tag{A.1}$$

and

$$q_j = \delta_{\alpha,\eta}\sum_{\iota=\pm 1}\arcsin(\Lambda^{\alpha n}(q_j) - i\,\iota\,u)$$

$$+\,\frac{2\,(-1)^{\delta_{\alpha,\eta}}}{L}\sum_{j'=1}^{L} N_c(q_{j'})\arctan\left(\frac{\Lambda^{\alpha n}(q_j) - \sin k^c(q_{j'})}{nu}\right)$$

$$-\,\frac{1}{L}\sum_{n'=1}^{\infty}\sum_{j'=1}^{L_{\alpha n'}} N_{\alpha n'}(q_{j'})\Theta_{n\,n'}\left(\frac{\Lambda^{\alpha n}(q_j) - \Lambda^{\alpha n'}(q_{j'})}{u}\right),$$

$$j = 1,...,L_{\alpha n}\,, \quad \alpha = \eta, s\,, \quad n = 1,...,\infty\,. \tag{A.2}$$

The sets of $j = 1,...,L$ and $j = 1,...,L_{\alpha n}$ quantum numbers q_j in Eqs. (A.1) and (A.2), respectively, which are defined in Eqs. (18) and (19), play the role of microscopic momentum values of different BA excitation branches. The corresponding β-band momentum distribution functions $N_\beta(q_j)$ read $N_\beta(q_j) = 1$ and $N_\beta(q_j) = 0$ for occupied and unoccupied discrete momentum values, respectively. Moreover, the rapidity function $\Lambda^{\alpha n}(q_j)$ is the real part of the complex rapidity, Eq. (16), and $\Theta_{n\,n'}(x)$ is the function,

$$\Theta_{n\,n'}(x) = \delta_{n,n'}\Big\{2\arctan\Big(\frac{x}{2n}\Big)+\sum_{l=1}^{n-1}4\arctan\Big(\frac{x}{2l}\Big)\Big\}$$
$$+\,(1-\delta_{n,n'})\Big\{2\arctan\Big(\frac{x}{|n-n'|}\Big)+2\arctan\Big(\frac{x}{n+n'}\Big)$$
$$+\sum_{l=1}^{\frac{n+n'-|n-n'|}{2}-1}4\arctan\Big(\frac{x}{|n-n'|+2l}\Big)\Big\}\,, \tag{A.3}$$

where $n, n' = 1, ..., \infty$. The indices $\alpha = \eta, s$ and numbers $n = 1, ..., \infty$ refer to different BA excitation branches that are associated with the composite αn pseudoparticles as defined in this paper.

The corresponding energy eigenvalues have for densities ranges $n_e \in [0, 1[$ and $m \in [0, n_e]$ the following form,

$$E = \sum_{j=1}^{L}\big(N_c(q_j)\,E_c(q_j) + U/4 - \mu_\eta\big) + \sum_{\alpha=\eta,s}\sum_{n=1}^{\infty}\sum_{j=1}^{L_{\alpha n}} N_{\alpha n}(q_j)\,E_{\alpha n}(q_j)$$
$$+\sum_{\alpha=\eta,s} 2\mu_\alpha\,(S_\alpha + S_\alpha^z)\,. \tag{A.4}$$

Here the $\alpha = \eta, s$ energy scales $2\mu_\alpha$ are given in Eq. (44) and the spectra $E_c(q_j)$ and $E_{\alpha n}(q_j)$ read,

$$E_c(q_j) = -2t\cos k^c(q_j) - U/2 + \mu_\eta - \mu_s\,,$$
$$E_{\alpha n}(q_j) = n\,2\mu_\alpha + \delta_{\alpha,\eta}\left(4t\,\mathrm{Re}\Big\{\sqrt{1-(\Lambda^{\eta n}(q_j) - i\,nu)^2}\Big\} - n\,U\right),$$
$$\alpha = \eta, s\,, \qquad n = 1, ..., \infty\,, \tag{A.5}$$

respectively. (The corresponding momentum eigenvalues of general $u > 0$ energy and momentum eigenstates are provided in Eq. (21).)

Useful solutions for our studies of the BA equations, Eqs. (A.1) and (A.2), are those for a ground state and its excited energy eigenstates that span a PS, as defined in Section 2.4. We denote the c and $s1$ band PS ground-state rapidity functions by $\Lambda_0^c(q_j) = \sin k_0^c(q_j)$ and $\Lambda_0^{s1}(q_j)$, respectively. They are the solutions of the BA equations, Eq. (A.1) and Eq. (A.2) for $\alpha n = s1$, respectively, with the $\beta = c, \alpha n$ band momentum distribution functions as given in Eq. (26). Hence they read,

$$q_j = k_0^c(q_j) + \frac{2}{L}\sum_{q'=-k_{F\downarrow}}^{k_{F\downarrow}}\arctan\left(\frac{\sin k_0^c(q_j) - \Lambda_0^{s1}(q')}{u}\right), \qquad j = 1, ..., L\,,$$
$$q_j = \frac{2}{L}\sum_{q'=-2k_F}^{2k_F}\arctan\left(\frac{\Lambda_0^{s1}(q_j) - \sin k_0^c(q')}{u}\right)$$
$$-\frac{2}{L}\sum_{q'=-k_{F\downarrow}}^{k_{F\downarrow}}\arctan\left(\frac{\Lambda_0^{s1}(q_j) - \Lambda_0^{s1}(q')}{2u}\right), \qquad j = 1, ..., N_\uparrow\,. \tag{A.6}$$

In the TL the ground state momentum rapidity function $k_0^c(q)$ and rapidity function $\Lambda_0^{s1}(q)$ have well-defined inverse functions $q^c = q^c(k)$. Here $k \in [-\pi, \pi]$ and $q^{s1} = q^{s1}(\Lambda)$ where $\Lambda \in [-\infty, \infty]$, respectively. One can then derive coupled integral equations from the coupled algebraic equations, Eq. (A.6). Their solutions are the distributions $2\pi\rho(k) = \partial q^c(k)/\partial k$ and $2\pi\sigma(\Lambda) = \partial q^{s1}(\Lambda)/\partial\Lambda$. One can access from such solutions the TL ground-state momentum rapidity function $k_0^c(q)$ and rapidity function $\Lambda_0^{s1}(q)$, respectively.

The c and $s1$ band rapidity functions $\Lambda^c(q_j) = \sin k^c(q_j)$ and $\Lambda^{s1}(q_j)$ of a PS excited energy eigenstates can be expressed in terms of those of the corresponding initial ground state. From straightforward yet lengthly manipulations of the BA equations, Eqs. (A.1) and (A.2), which involve expansions up to arbitrary order in the deviations $\delta N_\beta(q_j)$, Eq. (40), one finds that,

$$\begin{aligned}
&\Lambda^c(q_j) = \Lambda_0^c\Big(\bar{q}(q_j)\Big) = \sin k_0^c\Big(\bar{q}(q_j)\Big)\,, \qquad j = 1, ..., L_c\,, \\
&\Lambda^{s1}(q_j) = \Lambda_0^{s1}\Big(\bar{q}(q_j)\Big)\,, \qquad j = 1, ..., L_{s1}\,.
\end{aligned} \tag{A.7}$$

Here the $j = 1, ..., L_\beta$ quantum numbers $\bar{q}_j = \bar{q}(q_j)$ are the discrete $\beta = c, s1$ band canonical momentum values given in Eq. (57).

The integral equations that define the rapidity dressed phase shifts $2\pi\,\bar{\Phi}_{\beta,\beta'}(r, r')$ in Eq. (47) are for densities in the ranges $n_e \in [0, 1]$ and $m \in [0, n_e]$ derived by solving the BA equations up to first order in the deviations $\delta N_\beta(q_j)$. In the following we write the rapidity dressed phase shifts in units of 2π. A first set of rapidity dressed phase shifts obey integral equations by their own. They read,

$$\bar{\Phi}_{s1,c}\left(r, r'\right) = -\frac{1}{\pi}\arctan(r - r') + \int_{-r_s^0}^{r_s^0} dr''\, G(r, r'')\,\bar{\Phi}_{s1,c}\left(r'', r'\right)\,, \tag{A.8}$$

$$\bar{\Phi}_{s1,\eta n}\left(r, r'\right) = -\frac{1}{\pi^2}\int_{-r_c^0}^{r_c^0} dr''\frac{\arctan\left(\frac{r''-r'}{n}\right)}{1 + (r - r'')^2} + \int_{-r_s^0}^{r_s^0} dr''\, G(r, r'')\,\bar{\Phi}_{s1,\eta n}\left(r'', r'\right)\,, \tag{A.9}$$

and

$$\begin{aligned}
\bar{\Phi}_{s1,sn}\left(r, r'\right) = {} & \delta_{1,n}\frac{1}{\pi}\arctan\left(\frac{r - r'}{2}\right) + (1 - \delta_{1,n})\frac{1}{\pi}\left\{\arctan\left(\frac{r - r'}{n - 1}\right) + \arctan\left(\frac{r - r'}{n + 1}\right)\right\} \\
& - \frac{1}{\pi^2}\int_{-r_c^0}^{r_c^0} dr''\frac{\arctan\left(\frac{r''-r'}{n}\right)}{1 + (r - r'')^2} + \int_{-r_s^0}^{r_s^0} dr''\, G(r, r'')\,\bar{\Phi}_{s1,s1}\left(r'', r'\right)\,.
\end{aligned} \tag{A.10}$$

The parameters r_c^0 and r_s^0 appearing in these equations are defined in Eq. (46) and the kernel $G(r, r')$ is given by,

$$G(r, r') = -\frac{1}{2\pi}\left[\frac{1}{1 + ((r - r')/2)^2}\right]\left[1 - \frac{1}{2}\left(t(r) + t(r') + \frac{l(r) - l(r')}{r - r'}\right)\right]. \tag{A.11}$$

Here

$$t(r) = \frac{1}{\pi}\left[\arctan(r + r_c^0) - \arctan(r - r_c^0)\right], \tag{A.12}$$

and

$$l(r) = \frac{1}{\pi}\left[\ln(1+(r+r_c^0)^2) - \ln(1+(r-r_c^0)^2)\right]. \tag{A.13}$$

A second set of rapidity dressed phase shifts are expressed in terms of those in Eqs. (A.8)–(A.10) as follows,

$$\bar{\Phi}_{c,c}\left(r,r'\right) = \frac{1}{\pi}\int_{-r_s^0}^{r_s^0} dr''\,\frac{\bar{\Phi}_{s1,c}\left(r'',r'\right)}{1+(r-r'')^2}\,, \tag{A.14}$$

$$\bar{\Phi}_{c,\eta n}\left(r,r'\right) = -\frac{1}{\pi}\arctan\Big(\frac{r-r'}{n}\Big) + \frac{1}{\pi}\int_{-r_s^0}^{r_s^0} dr''\,\frac{\bar{\Phi}_{s1,\eta n}\left(r'',r'\right)}{1+(r-r'')^2}\,, \tag{A.15}$$

and

$$\bar{\Phi}_{c,sn}\left(r,r'\right) = -\frac{1}{\pi}\arctan\Big(\frac{r-r'}{n}\Big) + \frac{1}{\pi}\int_{-r_s^0}^{r_s^0} dr''\,\frac{\bar{\Phi}_{s1,sn}\left(r'',r'\right)}{1+(r-r'')^2}\,. \tag{A.16}$$

Finally, the remaining rapidity dressed phase shifts can be expressed either in terms of those in Eqs. (A.14)–(A.16) only,

$$\bar{\Phi}_{\eta n,c}\left(r,r'\right) = \frac{1}{\pi}\arctan\Big(\frac{r-r'}{n}\Big) - \frac{1}{\pi}\int_{-r_c^0}^{+r_c^0} dr''\,\frac{\bar{\Phi}_{c,c}\left(r'',r'\right)}{n[1+(\frac{r-r''}{n})^2]}\,, \tag{A.17}$$

$$\bar{\Phi}_{\eta n,\eta n'}\left(r,r'\right) = \frac{\Theta_{n,n'}(r-r')}{2\pi} - \frac{1}{\pi}\int_{-r_c^0}^{+r_c^0} dr''\,\frac{\bar{\Phi}_{c,\eta n'}\left(r'',r'\right)}{n[1+(\frac{r-r''}{n})^2]}\,, \tag{A.18}$$

$$\bar{\Phi}_{\eta n,sn'}\left(r,r'\right) = -\frac{1}{\pi}\int_{-r_c^0}^{+r_c^0} dr''\,\frac{\bar{\Phi}_{c,sn'}\left(r'',r'\right)}{n[1+(\frac{r-r''}{n})^2]}\,, \tag{A.19}$$

or in terms of both those in Eqs. (A.8)–(A.10) and in Eqs. (A.14)–(A.16),

$$\begin{aligned}\bar{\Phi}_{sn,c}\left(r,r'\right) = &-\frac{1}{\pi}\arctan\Big(\frac{r-r'}{n}\Big) + \frac{1}{\pi}\int_{-r_c^0}^{r_c^0} dr''\,\frac{\bar{\Phi}_{c,c}\left(r'',r'\right)}{n[1+(\frac{r-r''}{n})^2]} \\ &- \int_{-r_s^0}^{r_s^0} dr''\bar{\Phi}_{s1,c}\left(r'',r'\right)\frac{\Theta_{n,1}^{[1]}(r-r'')}{2\pi}\,; \qquad n>1\,,\end{aligned} \tag{A.20}$$

$$\bar{\Phi}_{sn,\eta n'}\left(r,r'\right) = \frac{1}{\pi}\int_{-r_c^0}^{r_c^0} dr'' \frac{\bar{\Phi}_{c,\eta n'}\left(r'',r'\right)}{n[1+(\frac{r-r''}{n})^2]} - \int_{-r_s^0}^{r_s^0} dr'' \bar{\Phi}_{s1,\eta n'}\left(r'',r'\right)\frac{\Theta_{n,1}^{[1]}(r-r'')}{2\pi}\,; \qquad n>1\,, \tag{A.21}$$

$$\bar{\Phi}_{sn,sn'}\left(r,r'\right) = \frac{\Theta_{n,n'}(r-r')}{2\pi} + \frac{1}{\pi}\int_{-r_c^0}^{r_c^0} dr'' \frac{\bar{\Phi}_{c,sn'}\left(r'',r'\right)}{n[1+(\frac{r-r''}{n})^2]} - \int_{-r_s^0}^{r_s^0} dr'' \bar{\Phi}_{s1,sn'}\left(r'',r'\right)\frac{\Theta_{n,1}^{[1]}(r-r'')}{2\pi}\,. \tag{A.22}$$

In the above equations, $\Theta_{n\,n'}(x)$ is the function given in Eq. (A.3) and $\Theta_{n\,n'}^{[1]}(x)$ is its derivative,

$$\Theta_{n,n'}^{[1]}(x) = \frac{\partial\Theta_{n,n'}(x)}{\partial x} = \delta_{n,n'}\Big\{\frac{1}{n[1+(\frac{x}{2n})^2]} + \sum_{l=1}^{n-1}\frac{2}{l[1+(\frac{x}{2l})^2]}\Big\} + (1-\delta_{n,n'})\Big\{\frac{2}{|n-n'|[1+(\frac{x}{|n-n'|})^2]} + \frac{2}{(n+n')[1+(\frac{x}{n+n'})^2]} + \sum_{l=1}^{\frac{n+n'-|n-n'|}{2}-1}\frac{4}{(|n-n'|+2l)[1+(\frac{x}{|n-n'|+2l})^2]}\Big\}\,. \tag{A.23}$$

The f functions in the second-order terms of the energy functional, Eq. (42), can be expressed in terms of the related β pseudofermion phase shifts $2\pi\,\Phi_{\beta,\beta'}(q_j,q_{j'})$, Eq. (47), as follows [57],

$$f_{\beta\,\beta'}(q_j,q_{j'}) = v_\beta(q_j)\,2\pi\,\Phi_{\beta,\beta'}(q_j,q_{j'}) + v_{\beta'}(q_{j'})\,2\pi\,\Phi_{\beta',\beta}(q_{j'},q_j) + \frac{1}{2\pi}\sum_{\beta''=c,s1}\sum_{\iota=\pm1} v_{\beta''}\,2\pi\,\Phi_{\beta'',\beta}(\iota q_{F\beta''},q_j)\,2\pi\,\Phi_{\beta'',\beta'}(\iota q_{F\beta''},q_{j'})\,. \tag{A.24}$$

The group velocities appearing here are defined in Eq. (48).

Other important quantities controlled by β pseudofermion phase shifts are the $\beta=c,s1$ lowest peak weights $A_\beta^{(0,0)}$ and relative weights $a_\beta = a_\beta(m_{\beta,+1},m_{\beta,-1})$ in the β pseudofermion spectral functions, Eq. (92). These weights are derived by the use of the pseudofermion anticommutators, Eq. (101), in Eq. (94). After some suitable algebra one finds,

$$A_\beta^{(0,0)} = \Big(\frac{1}{L}\Big)^{2N_\beta^\odot}\prod_{j=1}^{L_\beta}\sin^2\Big(\frac{\pi}{2}\Big(1-(1-2\Phi_\beta^T(q_j))N_\beta^\odot(q_j)\Big)\Big)\prod_{j=1}^{L_\beta-1}\Big(\sin\Big(\frac{\pi j}{L}\Big)\Big)^{2(L_\beta-j)} \times\prod_{i=1}^{L_\beta}\prod_{j=1}^{L_\beta}\theta(j-i)\,\sin^2\Big(\frac{\pi}{2}\Big(1-\Big(1-\frac{(2(j-i)+2\Phi_\beta^T(q_j)-2\Phi_\beta^T(q_i))}{L}\Big)\times N_\beta^\odot(q_j)N_\beta^\odot(q_i)\Big)\Big)$$

$$\times \prod_{i=1}^{L_\beta}\prod_{j=1}^{L_\beta} \frac{1}{\sin^2\left(\frac{\pi}{2}\left(1-\left(1-\frac{2(j-i)+2\Phi^T_\beta(q_j)}{L}\right)N^{\odot}_\beta(q_i)N^{\odot}_\beta(q_j)\right)\right)}\,, \qquad \beta = c, s1\,, \tag{A.25}$$

and

$$a_\beta(m_{\beta,+1}, m_{\beta,-1}) = \Big(\prod_{\iota=\pm 1} a_{\beta,\iota}(m_{\beta,\iota})\Big)\Big(1+\mathcal{O}\Big(\ln L/L\Big)\Big)\,, \qquad \beta = c, s1\,, \tag{A.26}$$

respectively, where,

$$a_{\beta,\iota}(m_{\beta,\iota}) = \prod_{j=1}^{m_{\beta,\iota}} \frac{(2\Delta^\iota_\beta + j - 1)}{j} = \frac{\Gamma(m_{\beta,\iota}+2\Delta^\iota_\beta)}{\Gamma(m_{\beta,\iota}+1)\,\Gamma(2\Delta^\iota_\beta)}\,, \qquad \beta = c, s1\,, \qquad \iota = \pm 1\,. \tag{A.27}$$

In these expressions, $N^{\odot}_\beta = \sum_{j=1}^{L_\beta} N^{\odot}_\beta(q_j)$ and $N^{\odot}_\beta(q_j)$ are the number of $\beta = c, s1$ pseudofermions and the β band momentum distribution function, respectively, of the excited energy eigenstate generated by the PDT processes (A) and (B) defined in Section 3.2. Furthermore, L_β denotes the number of $\beta = c, s1$ band discrete momentum values $L_c = L$ and L_{s1}. The latter is given in Eq. (17) for $\alpha n = s1$. The quantity $\Phi^T_\beta(q_j)$ is in the above equations the $\beta = c, s1$ pseudofermion phase-shift functional, Eq. (101), $\Gamma(x)$ is the usual gamma function, and the functionals $2\Delta^\iota_\beta$ are defined in Eqs. (102) and (103).

On the one hand, when the latter functionals are such that $2\Delta^\iota_\beta > 0$ and $2\Delta^{-\iota}_\beta = 0$, the $\beta = c, s1$ pseudofermion spectral function $B_{Q_\beta}(k', \omega')$, Eq. (92), has in the TL the following form,

$$\begin{aligned} B_{Q_\beta}(k', \omega') &= \frac{A^{(0,0)}_\beta}{v_\beta}\, a_{\beta,\iota}\left(\frac{L}{2\pi\, v_\beta}\,\omega' - \Delta^\iota_\beta\right)\delta\Big(k' - \frac{\iota\,\omega'}{v_\beta}\Big) \\ &\approx \frac{F^{(0,0)}_\beta}{v_\beta\,\Gamma(2\Delta^\iota_\beta)}\,\Theta(\iota\,\omega')\left(\frac{\omega'}{2\pi\, S_\beta\, v_\beta}\right)^{-1+2\Delta^\iota_\beta}\delta\Big(k' - \frac{\iota\,\omega'}{v_\beta}\Big)\,, \qquad \beta = c, s1\,. \end{aligned} \tag{A.28}$$

The second expression provided here is obtained from the use of Eqs. (105) and (106).

On the other hand, when $2\Delta^\iota_\beta = 2\Delta^{-\iota}_\beta = 0$ one finds that in the TL such a function reads,

$$B_{Q_\beta}(k', \omega') = \frac{2\pi}{L}\, A^{(0,0)}_\beta\, \delta(k')\,\delta(\omega') \approx 2\pi\, F^{(0,0)}_\beta\, S_\beta\, \delta(k')\,\delta(\omega')\,, \qquad \beta = c, s1\,. \tag{A.29}$$

Appendix B. Limiting behaviors of the $\beta = c, s1$ band energy dispersions, group velocities, and pseudofermion phase shifts

The one-parametric spectra of the σ one-electron spectral functions branch lines and border lines given in Eqs. (110) and (118), respectively, are expressed in terms of the c and $s1$ band energy dispersions, Eq. (45) for $\beta = c, s1$. The corresponding σ one-electron spectral weight distribution in the vicinity of the branch lines is controlled by the exponent $\xi^\sigma_\beta(k)$, Eq. (112). Its expression is linear in the functionals, Eq. (113), that involve the β pseudofermion phase shifts $2\pi\,\Phi_{\beta,\beta'}(q_j, q_{j'})$.

Here we provide limiting behaviors of such c and $s1$ band energy dispersions, corresponding c and $s1$ band group velocities, Eq. (48) for $\beta = c, s1$, and β pseudofermion phase shifts

$2\pi\,\Phi_{\beta,\beta'}(q_j,q_{j'})$, Eq. (47). Except if otherwise stated, the expressions given in the following refer to electronic densities and spin densities in the ranges $n_e\in[0,1[$ and $m\in]0,n_e]$, respectively.

The c and $s1$ energy dispersions, Eq. (45) for $\beta=c,s1$, have in the $u\rightarrow 0$ limit the following behaviors,

$$\begin{aligned}\varepsilon_c(q) &= -2t\left(2\cos\left(\frac{q}{2}\right)-\cos k_{F\uparrow}-\cos k_{F\downarrow}\right)\,, \qquad |q|\leq 2k_{F\downarrow}\,,\\ &= -2t\left(\cos(|q|-k_{F\downarrow})-\cos k_{F\uparrow}\right)\,, \qquad 2k_{F\downarrow}\leq|q|<\pi\,,\end{aligned} \tag{B.1}$$

and

$$\varepsilon_{s1}(q) = -2t\left(\cos q-\cos k_{F\downarrow}\right)\,, \qquad q\in[-k_{F\uparrow},k_{F\uparrow}]\,, \tag{B.2}$$

respectively.

For $u\gg 1$ and $m\rightarrow 0$, the behavior of these energy dispersions is,

$$\begin{aligned}\varepsilon_c(q) &= -2t\left(\cos q-\cos 2k_F+\frac{n\ln 2}{u}(\sin^2 q-\sin^2 2k_F)\right)\,, \qquad q\in[-\pi,\pi]\,,\\ \varepsilon_{s1}(q) &= -\frac{\pi n_e\,t}{2u}\left(1-\frac{\sin 2\pi n_e}{2\pi n_e}\right)\cos\left(\frac{q}{n_e}\right)\,, \qquad q\in[-k_F,k_F]\,.\end{aligned} \tag{B.3}$$

For $u\gg 1$ and $m\rightarrow n_e$ they read,

$$\begin{aligned}\varepsilon_c(q) &= -2t\,(\cos q-\cos 2k_F)\,, \qquad q\in[-\pi,\pi]\,,\\ \varepsilon_{s1}(q) &= -\frac{n_e\,t}{u}\left(1-\frac{\sin 2\pi n_e}{2\pi n_e}\right)\left(\cos\left(\frac{q}{n_e}\right)-1\right)\,, \qquad q\in[-2k_F,2k_F]\,.\end{aligned} \tag{B.4}$$

In the $u\rightarrow 0$ limit the corresponding c and $s1$ group velocities, Eq. (48) for $\beta=c,s1$, have the following behaviors,

$$\begin{aligned}v_c(q) &= 2t\sin\left(\frac{q}{2}\right)\,, \qquad |q|\leq 2k_{F\downarrow}\,,\\ &= \mathrm{sgn}\{q\}\,2t\sin(|q|-k_{F\downarrow})\,, \qquad 2k_{F\downarrow}\leq|q|<\pi\,,\end{aligned} \tag{B.5}$$

and

$$v_{s1}(q) = 2t\sin q\,, \qquad q\in[-k_{F\uparrow},k_{F\uparrow}]\,, \tag{B.6}$$

respectively. Moreover, for $u\gg 1$ and $m\rightarrow 0$ the group velocities behavior is,

$$\begin{aligned}v_c(q) &= 2t\left(\sin q-\frac{n_e\ln 2}{u}\sin 2q\right)\,, \qquad q\in[-\pi,\pi]\,,\\ v_{s1}(q) &= \frac{\pi\,t}{2u}\left(1-\frac{\sin 2\pi n_e}{2\pi n_e}\right)\sin\left(\frac{q}{n_e}\right)\,, \qquad q\in[-k_F,k_F]\,.\end{aligned} \tag{B.7}$$

For $u\gg 1$ and $m\rightarrow n_e$ they are given by,

$$\begin{aligned}v_c(q) &= 2t\sin q\,, \qquad q\in[-\pi,\pi]\,,\\ v_{s1}(q) &= \frac{t}{u}\left(1-\frac{\sin 2\pi n_e}{2\pi n_e}\right)\sin\left(\frac{q}{n_e}\right)\,, \qquad q\in[-2k_F,2k_F]\,.\end{aligned} \tag{B.8}$$

In the $u\rightarrow 0$ limit the phase shifts $2\pi\,\Phi_{\beta,\beta'}(q_j,q_{j'})$, Eq. (47), acquired by $\beta=c,s1$ pseudofermions due to the creation or annihilation under transitions to excited energy eigenstates of other $\beta'=c,s1$ pseudofermions have the following limiting behaviors,

$$
\begin{aligned}
\Phi_{s1,s1}(q,q') &= 0\,, \\
\Phi_{s1,c}(q,q') &= -\frac{1}{2}\mathrm{sgn}\left\{\sin q - \sin\left(\frac{q'}{2}\right)\right\}\,, \qquad |q'| \leq 2k_{F\downarrow} \\
&= -\frac{1}{2}\mathrm{sgn}\left\{\sin q - \mathrm{sgn}\{q'\}\sin(|q'| - k_{F\downarrow})\right\}\,, \qquad 2k_{F\downarrow} \leq |q'| < \pi\,, \\
\Phi_{c,c}(q,q') &= -\frac{1}{2}\mathrm{sgn}\{q-q'\}\,, \qquad |q|, |q'| \leq 2k_{F\downarrow} \\
&= \frac{1}{2}\mathrm{sgn}\{q'\}\,, \qquad |q| \leq 2k_{F\downarrow}\,, \qquad 2k_{F\downarrow} \leq |q'| < \pi \\
&= 0\,, \qquad 2k_{F\downarrow} < |q| < \pi\,, \\
\Phi_{c,s1}(q,q') &= -\frac{1}{2}\mathrm{sgn}\left\{\sin\left(\frac{q}{2}\right) - \sin q'\right\}\,, \qquad |q| \leq 2k_{F\downarrow} \\
&= -\frac{1}{2}\mathrm{sgn}\left\{\mathrm{sgn}\{q\}\sin(|q'| - k_{F\downarrow}) - \sin q'\right\}\,, \qquad 2k_{F\downarrow} \leq |q| < \pi\,. \qquad \text{(B.9)}
\end{aligned}
$$

Particular cases of these $\beta = c, s1$ pseudofermion phase shifts are those involved in the functionals, Eq. (113). In the $u \to 0$ limit they are given by,

$$
\begin{aligned}
\Phi_{s1,s1}\left(\iota k_{F\downarrow}, q\right) &= \Phi_{c,c}\left(\iota 2k_F, q\right) = 0\,, \\
\Phi_{s1,c}\left(\iota k_{F\downarrow}, q\right) &= -\frac{\iota}{2}\,, \qquad |q| < 2k_{F\downarrow}\,, \qquad q = -\iota 2k_{F\downarrow}\,, \qquad \iota = \pm 1 \\
&= 0\,, \qquad q = \iota 2k_{F\downarrow}\,, \qquad \iota = \pm 1 \\
&= -\frac{1}{2}\mathrm{sgn}\left\{\iota \sin k_{F\downarrow} - \mathrm{sgn}\{q\}\sin(|q| - k_{F\downarrow})\right\}\,, \\
&\quad 2k_{F\downarrow} \leq |q| < \pi\,, \qquad \iota = \pm 1\,, \\
\Phi_{c,s1}\left(\iota 2k_F, q\right) &= -\frac{\iota}{2}\,, \qquad |q| < k_{F\uparrow}\,, \qquad \iota = \pm 1 \\
&= \frac{1}{2}\mathrm{sgn}\{q\}\,, \qquad |q| = k_{F\uparrow}\,. \qquad \text{(B.10)}
\end{aligned}
$$

For $u \gg 1$ and spin density $m \to 0$, the above $\beta = c, s1$ pseudofermion phase shifts behave as,

$$
\begin{aligned}
\Phi_{s1,s1}(q,q') &= \frac{1}{\pi}\int_0^\infty d\omega \frac{\sin\left(\omega\,\frac{2}{\pi}\left[\mathrm{arcsinh}\left(\tan\left(\frac{q}{n_e}\right)\right) - \mathrm{arcsinh}\left(\tan\left(\frac{q'}{n_e}\right)\right)\right]\right)}{\omega\left(1+e^{2\omega}\right)} \\
&\quad + \frac{q'}{4u}\frac{\sin(\pi n_e)}{\pi n_e}\cos\left(\frac{q}{n_e}\right)\,, \qquad |q| \neq k_F \\
&= \frac{\iota}{2\sqrt{2}}\,, \qquad q = \iota k_F\,, \qquad q' \neq \iota k_F\,, \qquad \iota = \pm 1 \\
&= \frac{\iota}{2\sqrt{2}}(3 - 2\sqrt{2})\,, \qquad q = q' = \iota k_F\,, \qquad \iota = \pm 1\,, \\
\Phi_{s1,c}(q,q') &= -\frac{q}{2\pi n_e} + \frac{1}{4u}\cos\left(\frac{q}{n_e}\right)\sin q'\,, \qquad |q| \neq k_F \\
&= -\frac{\iota}{2\sqrt{2}}\,, \qquad q = \iota k_F\,, \qquad \iota = \pm 1\,,
\end{aligned}
$$

$$\Phi_{c,c}(q,q') = -\frac{\ln 2}{2\pi u}(\sin q - \sin q')\,,$$
$$\Phi_{c,s1}(q,q') = \frac{q'}{2\pi n_e} - \frac{1}{4u}\sin q\,\cos\left(\frac{q'}{n_e}\right) + q'\,\frac{\ln 2}{2\pi u}\,\frac{\sin(\pi n_e)}{\pi n_e}\,. \tag{B.11}$$

Those involved in the functionals, Eq. (113), are in that limit and for the same densities then given by,

$$\begin{aligned}
\Phi_{s1,s1}(\iota k_F, q) &= \frac{\iota}{2\sqrt{2}}\,, \qquad q \neq \iota k_F\,, \qquad \iota = \pm 1 \\
&= \frac{\iota}{2\sqrt{2}}(3-2\sqrt{2})\,, \qquad q = \iota k_F\,, \qquad \iota = \pm 1\,, \\
\Phi_{s1,c}(\iota k_F, q) &= -\frac{\iota}{2\sqrt{2}}\,, \qquad \iota = \pm 1\,, \\
\Phi_{c,c}(\iota 2k_F, q) &= -\frac{\ln 2}{2\pi u}(\iota\sin(\pi n_e) - \sin q)\,, \\
\Phi_{c,s1}(\iota 2k_F, q) &= \frac{q}{2\pi n_e} - \frac{\iota}{4u}\sin 2k_F\,\cos\left(\frac{q}{n_e}\right) + q\,\frac{\ln 2}{2\pi u}\,\frac{\sin(\pi n_e)}{\pi n_e}\,.
\end{aligned} \tag{B.12}$$

For $u \gg 1$ and $m \to n_e$ the $\beta = c, s1$ pseudofermion phase shifts under consideration behave as,

$$\begin{aligned}
\Phi_{s1,s1}(q,q') &= \frac{1}{\pi}\arctan\left(\frac{\tan\left(\frac{q}{2n_e}\right) - \tan\left(\frac{q'}{2n_e}\right)}{2}\right) + \frac{q'}{\pi u}\,\frac{\sin(\pi n_e)}{\pi n_e}\cos^2\left(\frac{q}{2n_e}\right), \\
\Phi_{s1,c}(q,q') &= -\frac{q}{2\pi n_e} + \frac{1}{\pi u}\cos^2\left(\frac{q}{2n_e}\right)\sin q'\,, \\
\Phi_{c,c}(q,q') &= 0\,, \\
\Phi_{c,s1}(q,q') &= \frac{q'}{2\pi n_e} - \frac{1}{\pi u}\sin q\,\cos^2\left(\frac{q'}{2n_e}\right).
\end{aligned} \tag{B.13}$$

As a result, in that limit in which $k_{F\downarrow} = 0$ the $\beta = c, s1$ pseudofermion phase shifts involved in the functionals, Eq. (113), read,

$$\begin{aligned}
\Phi_{s1,s1}(0,q) &= -\frac{1}{\pi}\arctan\left(\frac{1}{2}\tan\left(\frac{q}{2n_e}\right)\right) + \frac{q}{\pi u}\,\frac{\sin(\pi n_e)}{\pi n_e}\,, \\
\Phi_{s1,c}(0,q) &= \frac{\sin q}{\pi u}\,; \qquad \Phi_{c,c}(\iota 2k_F, q) = 0\,, \\
\Phi_{c,s1}(\iota 2k_F, q) &= \frac{q}{2\pi n_e} - \frac{\iota}{\pi u}\sin(\pi n_e)\,\cos^2\left(\frac{q}{2n_e}\right), \qquad \iota = \pm 1\,.
\end{aligned} \tag{B.14}$$

The limiting behaviors of the related $\beta = c, s1$ pseudofermion phase-shift parameters, Eq. (64), which are the entries of the matrices, Eq. (66), are given in the following. In the $u \to 0$ limit such matrices read,

$$\begin{aligned}
\lim_{u\to 0} Z^1 &= \lim_{u\to 0}\begin{bmatrix} \xi^1_{c\,c} & \xi^1_{c\,s1} \\ \xi^1_{s1\,c} & \xi^1_{s1\,s1} \end{bmatrix} = \begin{bmatrix} 1 & 0 \\ 1 & 1 \end{bmatrix}; \\
\lim_{u\to 0} Z^0 &= \lim_{u\to 0}\begin{bmatrix} \xi^0_{c\,c} & \xi^0_{c\,s1} \\ \xi^0_{s1\,c} & \xi^0_{s1\,s1} \end{bmatrix} = \begin{bmatrix} 1 & -1 \\ 0 & 1 \end{bmatrix}.
\end{aligned} \tag{B.15}$$

These values apply to the limit $\lim_{u\rightarrow 0}\lim_{m\rightarrow 0}$. However, if one takes the limit $\lim_{m\rightarrow 0}$ before $\lim_{u\rightarrow 0}$, one finds instead,

$$\lim_{u\rightarrow 0}\lim_{m\rightarrow 0} Z^1 = \begin{bmatrix} \sqrt{2} & 1/\sqrt{2} \\ 0 & 1/\sqrt{2} \end{bmatrix}; \qquad \lim_{u\rightarrow 0}\lim_{m\rightarrow 0} Z^0 = \begin{bmatrix} 1/\sqrt{2} & 0 \\ -1/\sqrt{2} & \sqrt{2} \end{bmatrix}. \tag{B.16}$$

Interestingly, this singular behavior does nor show up in the physical quantities whose expressions involve the $\beta = c, s1$ pseudofermion phase-shift parameters, Eq. (64), which are the entries of the matrices under consideration.

For $m \rightarrow 0$ and all u values the matrices in Eq. (66) are given by,

$$\lim_{m\rightarrow 0} Z^1 = \begin{bmatrix} \xi_0 & \xi_0/2 \\ 0 & 1/\sqrt{2} \end{bmatrix}; \qquad \lim_{m\rightarrow 0} Z^0 = \begin{bmatrix} 1/\xi_0 & 0 \\ -1/\sqrt{2} & \sqrt{2} \end{bmatrix}. \tag{B.17}$$

Here the $m \rightarrow 0$ parameter ξ_0 has the following limiting behaviors,

$$\begin{aligned} \xi_0 &= \sqrt{2}\,, \qquad u \rightarrow 0\,, \\ &= 1 + \frac{\ln 2}{\pi u}\sin(\pi n_e)\,, \qquad u \gg 1\,. \end{aligned} \tag{B.18}$$

In the $m \rightarrow n_e$ limit the matrices in Eq. (66) simplify to,

$$\lim_{m\rightarrow n_e} Z^1 = \begin{bmatrix} 1 & 0 \\ \eta_0 & 1 \end{bmatrix}; \qquad \lim_{m\rightarrow n_e} Z^0 = \begin{bmatrix} 1 & -\eta_0 \\ 0 & 1 \end{bmatrix}. \tag{B.19}$$

The parameter η_0 in this expression reads $\eta_0 = \frac{2}{\pi}\arctan\left(\frac{\sin(\pi n_e)}{u}\right)$ and thus has limiting behaviors,

$$\begin{aligned} \eta_0 &= 1\,, \qquad u \rightarrow 0\,, \\ &= \frac{2}{\pi\, u}\sin(\pi n_e)\,, \qquad u \gg 1\,. \end{aligned} \tag{B.20}$$

References

[1] M.C. Gutzwiller, Phys. Rev. Lett. 10 (1963) 159.
[2] J. Hubbard, Proc. R. Soc. Lond. Ser. A 276 (1963) 238.
[3] E.H. Lieb, F.Y. Wu, Phys. Rev. Lett. 20 (1968) 1445.
[4] E.H. Lieb, F.Y. Wu, Physica A 321 (2003) 1.
[5] C.N. Yang, Phys. Rev. Lett. 19 (1967) 1312.
[6] M.J. Martins, P.B. Ramos, Nucl. Phys. B 522 (1998) 413.
[7] M. Takahashi, Prog. Theor. Phys. 47 (1972) 69.
[8] B.S. Shastry, B. Sutherland, Phys. Rev. Lett. 65 (1990) 243.
[9] J.M.P. Carmelo, N.M.R. Peres, D.K. Campbell, A.W. Sandvik, Z. Phys. B 103 (1997) 217; N.M.R. Peres, R.G. Dias, P.D. Sacramento, J.M.P. Carmelo, Phys. Rev. B 61 (2000) 5169.
[10] S. Tomonaga, Prog. Theor. Phys. 5 (1950) 544.
[11] J.M. Luttinger, J. Math. Phys. 4 (1963) 1154.
[12] J. Sólyom, Adv. Phys. 28 (1979) 201.
[13] J. Voit, Rep. Prog. Phys. 57 (1994) 977.
[14] F. Woynarovich, H.P. Eckle, T.T. Truong, J. Phys. A 22 (1989) 4027.
[15] H. Frahm, V.E. Korepin, Phys. Rev. B 42 (1990) 10553.
[16] H. Frahm, V.E. Korepin, Phys. Rev. B 43 (1991) 5653.
[17] F.H.L. Essler, H. Frahm, F. Göhmann, A. Klümper, V.E. Korepin, The One-Dimensional Hubbard Model, Cambridge University Press, Cambridge, UK, 2005, Chapter 9.
[18] K.-V. Pham, M. Gabay, P. Lederer, Phys. Rev. B 61 (16) (2000) 397.

[19] M. Karowski, P. Weisz, Nucl. Phys. B 139 (1978) 455;
B. Berg, M. Karowski, P. Weisz, Phys. Rev. D 19 (1979) 2477.
[20] F.A. Smirnov, Form Factors in Completely Integrable Models of Quantum Field Theory, Advanced Series in Mathematical Physics, vol. 14, World Scientific, Singapore, 1992.
[21] J.L. Cardy, G. Mussardo, Nucl. Phys. B 340 (1990) 387;
A. Fring, G. Mussardo, P. Simonetti, Nucl. Phys. B 393 (1993) 413.
[22] V.P. Yurov, Al.B. Zamolodchikov, Int. J. Mod. Phys. A 6 (1991) 3419;
S. Lukyanov, Commun. Math. Phys. 167 (1995) 183;
S. Lukyanov, A.B. Zamolodchikov, Nucl. Phys. B 493 (1997) 2541;
S. Lukyanov, Mod. Phys. Lett. A 12 (1990) 2543.
[23] F.H.L. Essler, A.M. Tsvelik, G. Delfino, Phys. Rev. B 56 (1997) 11001;
F.H.L. Essler, A.M. Tsvelik, Phys. Rev. B 57 (1998) 10592.
[24] B.L. Altshuler, R.M. Konik, A.M. Tsvelik, Nucl. Phys. B 739 (2006) 311.
[25] F.H.L. Essler, R.M. Konik, J. Stat. Mech. (2009) P09018.
[26] M. Jimbo, T. Miwa, Algebraic Analysis of Solvable Lattice Models, American Mathematical Society, Providence, 1994.
[27] A.H. Bougourzi, M. Couture, M. Kacir, Phys. Rev. B 54 (2006) 12669;
A. Abada, A.H. Bougourzi, B. Si-Lakhal, Nucl. Phys. B 497 (1997) 733;
M. Karbach, G. Müller, A.H. Bougourzi, A. Fledderjohann, K.H. Mütter, Phys. Rev. B 55 (1997) 12510.
[28] D. Biegel, M. Karbach, G. Müller, Europhys. Lett. 59 (2002) 882.
[29] N. Kitanine, J.M. Maillet, V. Tetras, Nucl. Phys. B 554 (1999) 647.
[30] J.-S. Caux, J.M. Maillet, Phys. Rev. Lett. 95 (2005) 077201.
[31] J.-S. Caux, H. Konno, M. Sorrell, R. Weston, Phys. Rev. Lett. 106 (2011) 217203.
[32] M. Ogata, T. Sugiyama, H. Shiba, Phys. Rev. B 43 (1991) 8401.
[33] K. Penc, K. Hallberg, F. Mila, H. Shiba, Phys. Rev. Lett. 77 (1996) 1390.
[34] K. Penc, K. Hallberg, F. Mila, H. Shiba, Phys. Rev. B 55 (15) (1997) 475.
[35] F. Woynarovich, J. Phys. C, Solid State Phys. 15 (1982) 85.
[36] F. Woynarovich, J. Phys. C, Solid State Phys. 15 (1982) 97.
[37] M. Ogata, H. Shiba, Phys. Rev. B 41 (1990) 2326.
[38] H.V. Kruis, I.P. McCulloch, Z. Nussinov, J. Zaanen, Phys. Rev. B 70 (2004) 075109.
[39] J.M.P. Carmelo, K. Penc, D. Bozi, Nucl. Phys. B 725 (2005) 421, Nucl. Phys. B 737 (2006) 351 (Erratum).
[40] J.M.P. Carmelo, L.M. Martelo, K. Penc, Nucl. Phys. B 737 (2006) 237.
[41] J.M.P. Carmelo, J.M. Román, K. Penc, Nucl. Phys. B 683 (2004) 387.
[42] J.M.P. Carmelo, T. Čadež, Nucl. Phys. B 904 (2016) 39.
[43] A. Imambekov, T.L. Schmidt, L.I. Glazman, Rev. Mod. Phys. 84 (2012) 1253.
[44] F.H.L. Essler, Phys. Rev. B 81 (2010) 205120.
[45] L. Seabra, F.H.L. Essler, F. Pollmann, I. Schneider, T. Veness, Phys. Rev. B 90 (2014) 245127.
[46] J.M.P. Carmelo, D. Bozi, K. Penc, J. Phys. Condens. Matter 20 (2008) 415103.
[47] M. Sing, U. Schwingenschlögl, R. Claessen, P. Blaha, J.M.P. Carmelo, L.M. Martelo, P.D. Sacramento, M. Dressel, C.S. Jacobsen, Phys. Rev. B 68 (2003) 125111.
[48] J.M.P. Carmelo, K. Penc, L.M. Martelo, P.D. Sacramento, J.M.B. Lopes dos Santos, R. Claessen, M. Sing, U. Schwingenschlögl, Europhys. Lett. 67 (2004) 233.
[49] J.M.P. Carmelo, K. Penc, P.D. Sacramento, M. Sing, R. Claessen, J. Phys. Condens. Matter 18 (2006) 5191.
[50] M. Kohno, Phys. Rev. Lett. 105 (2010) 106402.
[51] H. Benthien, F. Gebhard, E. Jeckelmann, Phys. Rev. Lett. 92 (2004) 256401.
[52] A.E. Feiguin, D.A. Huse, Phys. Rev. B 79 (2009) 100507(R).
[53] F.H.L. Essler, V.E. Korepin, K. Schoutens, Phys. Rev. Lett. 67 (1991) 3848.
[54] D. Braak, N. Andrei, Nucl. Phys. B 542 (1999) 551.
[55] R.G. Pereira, K. Penc, S.R. White, P.D. Sacramento, J.M.P. Carmelo, Phys. Rev. B 85 (2012) 165132.
[56] A.A. Ovchinnikov, Sov. Phys. JETP 30 (1970) 1160.
[57] J.M.P. Carmelo, P. Horsch, P.A. Bares, A.A. Ovchinnikov, Phys. Rev. B 44 (1991) 9967;
J.M.P. Carmelo, P. Horsch, A.A. Ovchinnikov, Phys. Rev. B 45 (1992) 7899.
[58] J.M.P. Carmelo, P.D. Sacramento, Phys. Rev. B 68 (2003) 085104.
[59] C.N. Yang, Phys. Rev. Lett. 63 (1989) 2144.
[60] C.N. Yang, S.C. Zhang, Mod. Phys. Lett. B 4 (1990) 759.
[61] E.H. Lieb, Phys. Rev. Lett. 62 (1989) 1201.

[62] J.M.P. Carmelo, S. Östlund, M.J. Sampaio, Ann. Phys. 325 (2010) 1550.
[63] L.D. Faddeev, L.A. Takhtajan, Phys. Lett. A 85 (1981) 375.
[64] F.H.L. Essler, V.E. Korepin, Phys. Rev. Lett. 72 (1994) 908;
F.H.L. Essler, V.E. Korepin, Nucl. Phys. B 426 (1994) 505 (Section 5).
[65] F.D.M. Haldane, Phys. Rev. Lett. 67 (1991) 937.
[66] Y.R. Wang, Phys. Rev. B 46 (1992) 151.
[67] P.W. Anderson, Phys. Rev. Lett. 18 (1967) 1049.
[68] J.M.P. Carmelo, K. Penc, J. Phys. Condens. Matter 18 (2006) 2881.
[69] V.L. Campo Jr., K. Capelle, J. Quintanilla, C. Hooley, Phys. Rev. Lett. 99 (2007) 240403.
[70] D. Greif, G. Jotzu, M. Messer, R. Desbuquois, T. Esslinger, Phys. Rev. Lett. 115 (2015) 260401.
[71] V.L. Campo Jr., K. Capelle, J. Quintanilla, C. Hooley, Phys. Rev. Lett. 115 (2015) 215301.